

# **New Homogenous and Heterogenised Catalysts for Bioethanol Upgrading to Advanced Biofuels.**



**Folasade Josephine Sama**

A dissertation submitted to the Cardiff University in accordance with the requirements for award of the degree of Doctor of Philosophy in the Faculty of Science.

School of Chemistry

**2021**

*Dedicated to my family*

*To my husband who made this possible*

*To my beloved children Tofunmi and Bukunmi*

## Abstract

Biofuels obtained from biomass sources have attracted increasing attention due to their economic and environmental benefits. Shifting society's dependence away from gasoline to biofuels is an important contributor to sustainable development and effective management of greenhouse gas emissions. Particular attention has been given to bioethanol as an alternative to gasoline in past few decades. With the limitations of bioethanol as fuel and the sought for better substitutes for gasoline, the focus of this work is geared towards upgrading bioethanol to 1-butanol and *iso*-butanol whose fuel properties are similar to that of gasoline and, are thus termed "advanced biofuels". Such transformation processes require the employment of suitable catalysts for acceptable productivity and selectivity. Ruthenium complexes have shown great catalytic activity in borrowed hydrogen chemistry which is advantageous to this system. In this study, special interest is given to the design of Ru-catalysts with combined homogeneous and heterogeneous properties in order to preclude the degradation of metal complexes and promote the recoverability and reusability of the catalysts.

A two distinct classes of ruthenium-diphosphine has been synthesised and employed in the upgrading of ethanol to advanced biofuels. The first class, ruthenium-PNP with remote functionalities, displayed reasonable activity in the conversion of ethanol to 1-butanol and *iso*-butanol. With this baseline activity, the heterogenisation of the ruthenium-PNP catalysts was performed and variety of characterisation techniques confirmed the process was successful. The utilisation of the heterogeneous catalysts for ethanol-methanol upgrading to *iso*-butanol gave moderate yield and selectivity of *iso*-butanol with good recoverability. The other class of catalysts, ruthenium-PP, showed remarkable activity towards ethanol-methanol upgrading to *iso*-butanol with good productivity and excellent selectivity.

## **Acknowledgements**

First and foremost, my profound gratitude goes to Almighty God for the gift of life to start and complete this work. Special thanks to the Federal Government of Nigeria through Petroleum Technology Development Fund (**PTDF**) for sponsorship of my PhD study in the UK. Also, I am grateful to RSC Community Fund for the hardship fund during Covid-19 Phase I, UK national lockdown.

My thanks to all my family and friends for their supports, encouragements, and prayers during the period of my study. My heartfelt gratitude goes to my husband without whose support, I would have quitted this study. I must specially thank you for absorbing those funny behaviour of mine when the pressure of study overwhelmed me! I am also thankful to all my friends (Bibian, Uwaila, Idowu etc) who always believe in my potentials. Those “you can do it” words from you were powerful ingredients that made me stayed focus during the period of my PhD study.

I am deeply indebted to my project supervisor Professor Duncan Wass whose support, advice, guidance and supervision made this work come to a successful end. Your patience, tolerance, understanding and commitment have been essential factors to the success of this work. I am incredible grateful to you. Many thanks to Dr. Richard Wingad for your guidance and unrelenting support throughout my PhD programme. Your exceptional proofreading skills are invaluable in the productivity of this thesis. I thank all past and present members of the Wass group for their support in one way or the other (Katy, Matt, Hugh, Alex Riley, Hope, Krishna, Kanakon, Malsarah, Ashley, Sam, Andres, Taha, Jamie, Alex Adshead, Kennedy and co). It is really nice meeting you all. My thanks to everyone that contributed to the completion of this project (Nia Richards, Greg shaw, Thomas Davies, Simon Waller and Benson Kariuki, Hazel Sparkes).

Special thanks to all Redeemed Christian Church of God (RCCG) members (Bristol and Cardiff) for your incredible support to my family and study. You all have demonstrated the true love of our Lord Jesus Christ to my family and I during our period of stay in the United Kingdom. The acknowledgement page is limited to list all your names.

*“It always seems impossible until it's done.”*

*Nelson Mandela*

# Table of Contents

<b>Abstract</b> .....	<b>i</b>
<b>Acknowledgements</b> .....	<b>ii</b>
<b>Table of Contents</b> .....	<b>iv</b>
<b>List of Figures</b> .....	<b>x</b>
<b>List of Schemes</b> .....	<b>xiv</b>
<b>List of Tables</b> .....	<b>xvi</b>
<b>List of Equations</b> .....	<b>xviii</b>
<b>Chapter 1: Literature Review</b> .....	<b>1</b>
<b>1.1 Fossil Fuels</b> .....	<b>1</b>
<b>1.2 Bioethanol</b> .....	<b>1</b>
<b>1.3 Advanced Biofuels</b> .....	<b>3</b>
<b>1.4 Traditional Methods of manufacturing butanols</b> .....	<b>4</b>
1.4.1 Chemical Synthesis .....	4
1.4.2 Biological Synthesis .....	5
<b>1.5 Ethanol Upgrading</b> .....	<b>6</b>
<b>1.6 Mechanism of Guerbet Reaction</b> .....	<b>6</b>
<b>1.7 Mechanism of Other By-Products Formed</b> .....	<b>8</b>
<b>1.8 Previous Work</b> .....	<b>10</b>
1.8.1 Homogeneous and Mixed Homo/Heterogeneous Catalysis .....	10
1.8.2 Heterogeneous Catalysis .....	19
<b>1.9 Thesis Scope</b> .....	<b>27</b>
<b>1.10 References</b> .....	<b>28</b>

<b>Chapter 2: Alkoxysilyl-functionalised Bidentate Phosphine-based Ruthenium(II) Complexes for Ethanol Upgrading to Advanced Biofuels .....</b>	<b>31</b>
<b>2.1 Introduction .....</b>	<b>31</b>
<b>2.2 Aims and Objectives.....</b>	<b>32</b>
<b>2.3 Results and Discussion .....</b>	<b>33</b>
2.3.1 Synthesis and Characterization of Complex Precursors .....	33
2.3.2 Synthesis of (Ph <sub>2</sub> P) <sub>2</sub> N(CH <sub>2</sub> ) <sub>3</sub> Si(OMe) <sub>3</sub> (L2.1).....	33
2.3.3 Synthesis of trans-[RuCl <sub>2</sub> {(PPh <sub>2</sub> ) <sub>2</sub> N(CH <sub>2</sub> ) <sub>3</sub> Si(OCH <sub>3</sub> ) <sub>3</sub> } <sub>2</sub> ] ([Ru]-2.1) .....	33
2.3.4 Reaction of L2.1 with dichloro(η <sup>6</sup> -p-cymene)ruthenium(II) dimer.....	40
2.3.5 Reaction of L2.1 with dichloro(η <sup>6</sup> -p-cymene)ruthenium(II) dimer in varied ratios.....	45
2.3.6 Synthesis of related Complexes.....	45
2.3.6.1 Reaction of L2.1 and [RuCl <sub>2</sub> (Ph <sub>3</sub> P) <sub>3</sub> ] in equimolar ratio .....	46
2.3.6.2 Reaction of L2.2 with [RuCl <sub>2</sub> (PPh <sub>3</sub> ) <sub>3</sub> ] and [RuCl <sub>2</sub> {(PPh <sub>2</sub> ) <sub>2</sub> C=CH <sub>2</sub> } <sub>2</sub> ].....	46
2.3.7 Catalytic Activity .....	47
2.3.7.1 Ethanol/methanol Upgrading to Iso-butanol.....	48
2.3.7.2 Ethanol Upgrading to 1-butanol.....	51
<b>2.4 Conclusion .....</b>	<b>53</b>
<b>2.5 Future work .....</b>	<b>53</b>
<b>2.6 References.....</b>	<b>55</b>

<b>Chapter 3: Fumed silica/MCM-41-supported Alkoxysilyl-functionalised Bidentate Phosphine-based Ruthenium(II) Complexes for Ethanol Upgrading to Advanced Biofuels.....</b>	<b>58</b>
<b>3.1 Introduction .....</b>	<b>58</b>
3.1.1 Nature of silica.....	58
3.1.2 Modification of silica surface by organosilanes .....	63
3.1.3 Types of silica Supports.....	63
<b>3.2 Aims and objectives .....</b>	<b>65</b>
<b>3.3 Results and Discussion .....</b>	<b>66</b>
3.3.1 Immobilisation methods .....	66

3.3.2	Synthesis of fumed silica/MCM-41-supported [Ru]-2.1 and [Ru]-2.2.....	67
3.3.3	Characterisation of unfunctionalised and functionalised silica .....	68
3.3.3.1	Fourier-transform infra-red (FTIR) method.....	69
3.3.3.2	Thermal analysis .....	71
3.3.3.3	X-ray diffraction (XRD) studies .....	73
3.3.3.4	N <sub>2</sub> adsorption/desorption studies.....	74
3.3.3.5	Electron microscopy studies .....	77
3.3.3.6	Solid-State NMR spectroscopy .....	79
3.3.3.6.1	<sup>31</sup> P CP/MAS NMR spectroscopy .....	79
3.3.3.6.2	<sup>13</sup> C CP/MAS NMR spectroscopy.....	82
3.3.3.6.3	<sup>29</sup> Si CP/MAS NMR spectroscopy .....	85
3.3.3.7	Inductively Coupled Plasma-Mass Spectrometry (ICP-MS) .....	87
3.3.4	Catalytic activity .....	88
3.3.4.1	Ethanol/methanol upgrading to iso-butanol.....	88
3.3.4.2	Recyclability studies .....	91
3.3.4.3	Leachability test .....	93
3.3.4.4	Water tolerance .....	94
3.3.4.5	Reactor size effect.....	96
<b>3.4</b>	<b>Conclusion and Future work.....</b>	<b>96</b>
<b>3.5</b>	<b>References.....</b>	<b>97</b>

<b>Chapter 4: Alumina-supported Alkoxysilyl-functionalised Bidentate Phosphine-based Ruthenium (II) Complexes for Ethanol Upgrading to Advanced Biofuels .....</b>	<b>101</b>
<b>4.1 Introduction .....</b>	<b>101</b>
<b>4.2 Aims and Objectives.....</b>	<b>103</b>
<b>4.3 Results and Discussion .....</b>	<b>104</b>
4.3.1 Immobilisation method .....	104
4.3.2 Characterisation of unmodified and modified alumina .....	105
4.3.2.1 Fourier-transform infra-red (FTIR) method.....	105
4.3.2.2 Thermal analysis .....	106
4.3.2.3 X-ray diffraction (XRD) studies .....	111
4.3.2.4 Surface Area and Porosity (N <sub>2</sub> Adsorption/Desorption measurements) .....	112
4.3.2.5 TEM/STEM/EDS.....	114

4.3.2.6 Solid-State NMR spectroscopy .....	116
4.3.2.6.1 <sup>31</sup> P CP/MAS NMR spectroscopy .....	116
4.3.2.6.2 <sup>13</sup> C CP/MAS NMR spectroscopy .....	116
4.3.2.6.3 <sup>29</sup> Si CP/MAS NMR spectroscopy .....	121
4.3.2.6.4 <sup>27</sup> Al CP/MAS NMR spectroscopy .....	123
4.3.2.7 Inductively Coupled Plasma-Mass Spectrometry (ICP-MS) .....	123
4.3.3 Catalytic activity .....	124
<b>4.4 Conclusion and Future work.....</b>	<b>126</b>
<b>4.5 References.....</b>	<b>128</b>

## **Chapter 5: Nucleophilic Addition to a Vinylidene Diphosphine Ru(II) Complex - Synthesis, Characterisation and Catalytic Activity towards Ethanol Upgrading to Advanced Biofuels ..... 130**

<b>5.1 Introduction .....</b>	<b>130</b>
<b>5.2 Aim and objectives .....</b>	<b>131</b>
<b>5.3 Results and Discussion .....</b>	<b>131</b>
5.3.1 Synthesis of [RuCl <sub>2</sub> {(PPh <sub>2</sub> ) <sub>2</sub> CH=CH <sub>2</sub> } <sub>2</sub> ] ([Ru]-5.1) .....	131
5.3.2 Functionalization of [Ru]-5.1 with Amines .....	132
5.3.3 Crystal Structures.....	134
5.3.4 Catalytic Activity .....	140
5.3.4.1 Base Screening with Complex Precursor .....	144
5.3.4.2 Functionalised Complex Screening.....	146
<b>5.4 Conclusion/Future Work.....</b>	<b>150</b>
<b>5.5 References.....</b>	<b>152</b>

## **Chapter 6: Experimental ..... 154**

<b>6.1. General Experimental Information.....</b>	<b>154</b>
6.1.1 General Experimental Considerations .....	154
6.1.2 General Catalytic Procedure .....	154
6.1.3 GC Calibration Methods and Calculation of Conversion, Yield and Selectivity. ....	155
<b>6.2 Chapter 2 Experimental.....</b>	<b>160</b>
6.2.1 Ligand Synthesis.....	160

6.2.1.1 Synthesis of $(\text{Ph}_2\text{P})_2\text{N}(\text{CH}_2)_3\text{Si}(\text{OMe})_3$ (L2.1) .....	160
6.2.2 Catalysts Synthesis.....	160
6.2.2.1 Synthesis of dichlorotris(triphenylphosphine)ruthenium(II) - $[\text{RuCl}_2(\text{PPh}_3)_3]$ ([Ru]-1.5) .....	160
6.2.2.2 Dichloro(p-cymene)ruthenium(II) dimer - $[\text{RuCl}_2(\text{p-cymene})]_2$ ([Ru]-1.7). 161	
6.2.2.3 Synthesis of trans- $[\text{RuCl}_2\{(\text{PPh}_2)_2\text{N}(\text{CH}_2)_3\text{Si}(\text{OCH}_3)_3\}_2]$ ([Ru]-2.1) .....	161
6.2.2.4 Synthesis of $[(\eta^6\text{-p-cymene})\text{Ru}(\mu\text{-Cl})_3\text{RuCl}\{(\text{PPh}_2)_2\text{N}(\text{CH}_2)_3\text{Si}(\text{OMe})_3\}]\text{Cl}$ ([Ru]-2.2) .....	162
6.2.2.5 Synthesis of $[\text{RuCl}_2(\text{PPh}_3)_2\{\text{NH}_2(\text{CH}_2)_2\text{NH}(\text{CH}_2)_3\text{Si}(\text{OCH}_3)_3\}_2]$ ([Ru]-2.5) 162	
<b>6.3 Chapter 3 and 4 Experimental .....</b>	<b>164</b>
6.3.1 Experimental Procedure .....	164
6.3.1.1 Chemicals.....	164
6.3.1.2 Pre-treatment procedure for alumina and silica .....	164
6.3.1.3 Immobilisation method .....	164
6.3.2 Instrument Methods .....	165
6.3.2.1 Thermal analysis .....	165
6.3.2.2 Fourier-transform infra-red (FTIR) method.....	165
6.3.2.3 X-ray diffraction (XRD) .....	165
6.3.2.4 Electron microscopy.....	165
6.3.2.5 Nitrogen adsorption and desorption measurement.....	165
6.3.2.6 NMR spectroscopy.....	166
6.3.2.7 Inductively coupled plasma-mass spectroscopy (ICP-MS).....	166
6.3.3 Catalyst Compositions Weight % based on Loadings (Chapter 3).....	167
6.3.3.1 Weight % $\text{PPh}_2$ for fumed silica-supported [Ru]-2.1 .....	167
6.3.3.2 Weight % $\text{PPh}_2$ for MCM-41-supported [Ru]-2.1 .....	167
6.3.3.3 Weight % Cl for fumed silica-supported [Ru]-2.2.....	168
6.3.3.4 Weight % Cl for MCM-41-supported [Ru]-2.2 .....	168
6.3.3.5 Weight % Ph for fumed silica-supported [Ru]-2.2 .....	169
6.3.3.6 Weight % Ph for MCM-41-supported [Ru]-2.2.....	169
6.3.3.7 Weight % Cy for fumed silica-supported [Ru]-2.2.....	169
6.3.3.8 Weight % Cy for MCM-41-supported [Ru]-2.2.....	170
6.3.4 Catalyst Compositions Weight % based on Loadings (Chapter 4).....	171
6.3.4.1 Weight % $\text{PPh}_2$ for acidic alumina-supported [Ru]-2.1 .....	171
6.3.4.2 Weight % $\text{PPh}_2$ for basic alumina-supported [Ru]-2.1.....	171
6.3.4.3 Weight % $\text{PPh}_2$ for neutral alumina-supported [Ru]-2.1.....	172
6.3.4.4 Weight % Cy for acidic alumina-supported [Ru]-2.2 .....	172
6.3.4.5 Weight % Cl for acidic alumina-supported [Ru]-2.2 .....	173

6.3.4.6 Weight % Ph for acidic alumina-supported [Ru]-2.2.....	173
6.3.4.7 Weight % Cy for basic alumina-supported [Ru]-2.2.....	174
6.3.4.8 Weight % Cl for basic-supported [Ru]-2.2 .....	174
6.3.4.9 Weight % Ph for basic alumina-supported [Ru]-2.2 .....	174
<b>6.5 Chapter 5 Experimental.....</b>	<b>176</b>
6.5.1 Catalysts Synthesis.....	176
6.5.1.1 Synthesis of $\text{RuCl}_2\{(\text{PPh}_2)_2\text{CH}=\text{CH}_2\}_2$ ([Ru]-5.1).....	176
6.5.1.2 Synthesis of $[\text{RuCl}_2\{(\text{Ph}_2\text{P})_2\text{CHCH}_2\text{NH}(\text{CH}_2)_2\text{PPh}_2\}_2]$ ([Ru]-5.2) .....	176
6.5.1.3 Synthesis of $[\text{RuCl}_2\{(\text{Ph}_2\text{P})_2\text{CHCH}_2\text{NH}(\text{CH}_2)_2\text{NH}_2\}_2]$ ([Ru]-5.3).....	177
6.5.1.4 Synthesis of $[\text{RuCl}_2\{(\text{Ph}_2\text{P})_2\text{CHCH}_2\text{NH}(\text{CH}_2)_3\text{NH}_2\}_2]$ ([Ru]-5.4).....	177
6.5.1.5 Synthesis of $[\text{RuCl}_2\{(\text{Ph}_2\text{P})_2\text{CHCH}_2\text{NH}(\text{CH}_2)_3\text{Si}(\text{OEt})_3\}_2]$ ([Ru]-5.5) .....	178
6.5.1.6 Synthesis of $[\text{RuCl}_2\{(\text{Ph}_2\text{P})_2\text{CHCH}_2\text{NH}(\text{CH}_2)_2\text{C}_6\text{H}_5\}_2]$ ([Ru]-5.6) .....	178
6.5.1.7 Synthesis of $[\text{RuCl}_2\{(\text{Ph}_2\text{P})_2\text{CHCH}_2\text{NH}(\text{CH}_2)_2\text{SH}\}]$ ([Ru]-5.7) .....	179
6.5.1.8 Synthesis of $[\text{RuCl}_2\{(\text{Ph}_2\text{P})_2\text{CHCH}_2\text{NH}(\text{CH}_2)_2\text{OH}\}_2]$ ([Ru]-5.8) .....	179
6.5.1.9 Synthesis of $[\text{RuCl}_2\{(\text{Ph}_2\text{P})_2\text{CHCH}_2\text{NH}(\text{CH}_2)_2\text{NH}(\text{CH}_2)_3\text{Si}(\text{OMe})_3\}_2]$ ([Ru]-5.9).....	179
<b>6.6 Appendix.....</b>	<b>181</b>
6.6.1 Chapter 2 Crystallographic data .....	181
6.6.1.1 Crystallographic data of cis-[Ru]-2.1 .....	181
6.6.1.2 Crystallographic data of dinuclear complex [Ru]-2.2 .....	182
6.6.2 Chapter 5 Crystallographic data .....	183
6.6.2.1 Crystallographic data of trans-[Ru]-5.3 .....	183
6.6.2.2 Crystallographic data of trans-[Ru]-5.5 .....	184
6.6.2.3 Crystallographic data of trans-[Ru]-5.6 .....	185
6.6.2.4 Crystallographic data of trans-[Ru]-5.8 .....	186
6.6.3 Mass Spectrum of [Ru]-2.1 .....	187
<b>6.7 References.....</b>	<b>188</b>

## List of Figures

<b>Figure 1.1:</b> Schematic processes of manufacturing ethanol from corn in the U.S.....	2
<b>Figure 1.2:</b> Ruthenium precursors used in Mitsubishi patent.....	11
<b>Figure 2.1:</b> $^{31}\text{P}\{^1\text{H}\}$ NMR spectrum ( $\text{CDCl}_3$ , 202 MHz) of <b>[Ru]-2.1</b> , Full NMR spectrum, 50 80 ppm region.....	30
<b>Figure 2.2:</b> Single Crystal of <i>cis</i> - <b>[Ru]-2.1</b> , $P2_1/n$ monoclinic space group.....	37
<b>Figure 2.3:</b> Single Crystal of <i>trans</i> - <b>[Ru]-2.1</b> , $P-1$ triclinic space group.....	38
<b>Figure 2.4:</b> Trigonal distortion of octahedral complex.....	39
<b>Figure 2.5:</b> $^{31}\text{P}\{^1\text{H}\}$ NMR spectrum (unlocked, 162 MHz) obtained after 1h of reaction between <b>L2.1</b> and dichloro( $\eta^6$ - <i>p</i> -cymene)ruthenium(II) dimer.....	41
<b>Figure 2.6:</b> $^{31}\text{P}\{^1\text{H}\}$ NMR spectrum ( $\text{CDCl}_3$ , 162 MHz) of isolated product <b>[Ru]-2.2</b> .....	42
<b>Figure 2.7:</b> $^{31}\text{P}\{^1\text{H}\}$ NMR spectrum ( $\text{CDCl}_3$ , 162 MHz) of the filtrate solution from the reaction of <b>L2.1</b> with dichloro( $\eta^6$ - <i>p</i> -cymene)ruthenium(II) dimer.....	43
<b>Figure 2.8:</b> Single crystal of complex <b>[Ru]-2.2</b> with $P-1$ space group.....	44
<b>Figure 2.9:</b> $^{31}\text{P}\{^1\text{H}\}$ NMR spectrum (unlocked, 202 MHz) of <b>L2.1</b> and $[\text{RuCl}_2(\textit{p}\text{-cymene})]_2$ reaction mixture.....	45
<b>Figure 2.10:</b> $^{31}\text{P}\{^1\text{H}\}$ NMR spectrum ( $\text{CDCl}_3$ , 202 MHz) of <b>L2.1</b> and $[\text{RuCl}_2(\textit{p}\text{-cymene})]_2$ reaction mixture.....	46
<b>Figure 3.1:</b> Simplified silica surface.....	58
<b>Figure 3.2:</b> Different types of silanol on silica surfaces.....	59
<b>Figure 3.3:</b> $^{29}\text{Si}$ CP-MAS NMR spectrum of an amorphous porous silica.....	61
<b>Figure 3.4:</b> Different silicon environments.....	61
<b>Figure 3.5:</b> M41S family structures: MCM-41 (hexagonal), MCM-48 (cubic) and MCM-50 (lamellar) with corresponding XRD diffraction pattern.....	64
<b>Figure 3.6:</b> Synthetic route to MCM-41.....	64
<b>Figure 3.7:</b> FTIR analysis of unmodified fumed silica and MCM-41, supported and unsupported <b>[Ru]-2.1</b> , supported and unsupported <b>[Ru]-2.2</b> .....	70
<b>Figure 3.8:</b> TG/DTG analysis of unmodified fumed silica, unmodified MCM-41, fumed silica-supported <b>[Ru]-2.1</b> , MCM-41-supported <b>[Ru]-2.1</b> , fumed silica-supported <b>[Ru]-2.2</b> , MCM-41-supported <b>[Ru]-2.2</b> .....	72

<b>Figure 3.9:</b> XRD patterns of unmodified fumed silica/MCM-41 and fumed silica/MCM-41-supported <b>[Ru]-2.1</b> and fumed silica/MCM-41 supported <b>[Ru]-2.2</b> .....	73
<b>Figure 3.10:</b> N <sub>2</sub> adsorption/desorption isotherms of unmodified fumed silica /MCM-41 and fumed silica/MCM-41-supported <b>[Ru]-2.1/[Ru]-2.2</b> .....	76
<b>Figure 3.11:</b> Pore size distribution curves of bare fumed silica/fumed silica-supported <b>[Ru]-2.1/[Ru]-2.2</b> and MCM-41/MCM-41-supported <b>[Ru]-2.1/[Ru]-2.2</b> .....	77
<b>Figure 3.12:</b> Representative TEM, STEM and EDS of bare fumed silica/MCM-41 and fumed silica/MCM-41-supported <b>[Ru]-2.1/[Ru]-2.2</b> .....	78
<b>Figure 3.13:</b> <sup>31</sup> P CP/MAS NMR spectra (162 MHz, 10 kHz spinning speed) of fumed silica/MCM-41-supported <b>[Ru]-2.1</b> and <b>[Ru]-2.2</b> .....	80
<b>Figure 3.14:</b> Side products observed by Posset <i>et al.</i> .....	81
<b>Figure 3.15:</b> Liquid state <sup>13</sup> C{ <sup>1</sup> H} NMR spectra (CDCl <sub>3</sub> , 126 MHz) of complexes <b>[Ru]-2.1</b> and <b>[Ru]-2.2</b> .....	83
<b>Figure 3.16:</b> <sup>13</sup> C CP/MAS NMR spectra (101 MHz, 10 kHz spinning speed) of fumed silica/MCM-41-supported <b>[Ru]-2.1</b> and <b>[Ru]-2.2</b> .....	84
<b>Figure 3.17:</b> <sup>29</sup> Si CP/MAS NMR spectra (80 MHz, 10 kHz spinning speed) of bare fumed silica/MCM-41 and fumed silica/MCM-41-supported <b>[Ru]-2.1</b> and <b>[Ru]-2.2</b> .....	86
<b>Figure 3.18:</b> Yield of liquid products and ethanol conversion obtained from fumed silica/MCM-41-supported <b>[Ru]-2.1/2.2</b> .....	90
<b>Figure 3.19:</b> Selectivity of liquid products and ethanol conversion obtained from fumed silica/MCM-41-supported <b>[Ru]-2.1/2.2</b> .....	90
<b>Figure 3.20:</b> Recycling test using 0.1 mol% fumed silica-supported <b>[Ru]-2.1</b> .....	93
<b>Figure 3.20:</b> Leachability test using 0.1 mol% fumed silica-supported <b>[Ru]-2.1</b> .....	93
<b>Figure 4.1:</b> The five possible types of surface hydroxyl groups on the surface of γ-, η- and higher surface area aluminas.....	101
<b>Figure 4.2:</b> <sup>31</sup> P{ <sup>1</sup> H} NMR spectra (unlocked, 162 MHz) of filtrate and washings after refluxing complex <b>[Ru]-2.1</b> and neutral alumina in toluene.....	105
<b>Figure 4.3:</b> FTIR analysis of unmodified aluminas, supported and unsupported <b>[Ru]-2.1</b> , supported and unsupported <b>[Ru]-2.2</b> .....	107
<b>Figure 4.4:</b> Thermal analysis of unmodified neutral, acidic, and basic.....	109
<b>Figure 4.5:</b> Thermal analysis of aluminas-supported <b>[Ru]-2.1</b> and <b>[Ru]-2.2</b> .....	110

<b>Figure 4.6:</b> XRD patterns of pure alumina and alumina-supported catalysts <b>[Ru]-2.1</b> and <b>[Ru]-2.2</b> .....	111
<b>Figure 4.7:</b> N <sub>2</sub> adsorption/desorption isotherms and pore distribution curve of pure pre-heated Al <sub>2</sub> O <sub>3</sub> and supported catalysts.....	113
<b>Figure 4.8:</b> Representative TEM, STEM and EDS of acidic, basic and neutral Al <sub>2</sub> O <sub>3</sub> -supported <b>[Ru]-2.1/[Ru]-2.2</b> .....	115
<b>Figure 4.9:</b> <sup>31</sup> P CP/MAS NMR spectra (162 MHz, 10 kHz spinning speed) of Al <sub>2</sub> O <sub>3</sub> -supported <b>[Ru]-2.1</b> and <b>[Ru]-2.2</b> .....	117
Figure <b>4.10:</b> Liquid state <sup>13</sup> C{ <sup>1</sup> H} NMR spectra (CDCl <sub>3</sub> , 126 MHz) of complexes <b>[Ru]-2.1</b> and <b>[Ru]-2.2</b> .....	118
Figure <b>4.11:</b> <sup>13</sup> C CP/MAS NMR spectra (101 MHz, 10 kHz spinning speed) of Al <sub>2</sub> O <sub>3</sub> -supported <b>[Ru]-2.1</b> and <b>[Ru]-2.2</b> .....	119
Figure <b>4.12:</b> <sup>13</sup> C CP/MAS NMR spectrum (101 MHz, 10kHz spinning speed) of unsupported catalyst <b>[Ru]-2.1</b> .....	120
Figure <b>4.13:</b> Exposed and unexposed basic alumina-supported catalyst <b>[Ru]-2.1</b> .....	121
Figure <b>4.14:</b> <sup>29</sup> Si CP/MAS NMR spectra (80 MHz, 10 kHz spinning speed) of Al <sub>2</sub> O <sub>3</sub> -supported <b>[Ru]-2.1</b> and <b>[Ru]-2.2</b> .....	122
Figure <b>4.15:</b> <sup>27</sup> Al CP/MAS NMR spectra (104 MHz, 10kHz spinning speed) of pure Al <sub>2</sub> O <sub>3</sub> and Al <sub>2</sub> O <sub>3</sub> -supported <b>[Ru]-2.1</b> and <b>[Ru]-2.2</b> .....	123
Figure <b>5.1:</b> <sup>31</sup> P{ <sup>1</sup> H} NMR spectrum (CDCl <sub>3</sub> , 162 MHz) of complex <b>[Ru]-5.1</b> .....	132
Figure <b>5.2:</b> <sup>31</sup> P{ <sup>1</sup> H} NMR spectra (CDCl <sub>3</sub> , 162 MHz) of complexes <b>[Ru]-5.2</b> , <b>[Ru]-5.3</b> , and <b>[Ru]-5.8</b> .....	133
Figure <b>5.3:</b> <sup>31</sup> P{ <sup>1</sup> H} NMR spectra (CDCl <sub>3</sub> , 162 MHz) of complexes <b>[Ru]-5.4</b> to <b>[Ru]-5.9</b> .....	134
Figure <b>5.4:</b> X-ray crystal structure of complex <b>[Ru]-5.3</b> .....	136
Figure <b>5.5:</b> X-ray crystal structure of complex <b>[Ru]-5.5</b> .....	137
Figure <b>5.6:</b> X-ray crystal structure of complex <b>[Ru]-5.6</b> .....	138
Figure <b>5.7:</b> X-ray crystal structure of complex <b>[Ru]-5.8</b> .....	139
<b>Figure 5.8:</b> Yield of liquid products and ethanol conversion achieved with pre-catalyst <b>[Ru]-5.1</b> and different bases.....	144
Figure <b>5.9:</b> Selectivity of liquid products and ethanol conversion achieved with pre-catalyst <b>[Ru]-5.1</b> and different bases.....	145

<b>Figure 5.10:</b> Yield of liquid products and ethanol conversion achieved with 0.1 mol% [Ru]-5.2 - 5.9 at 2h.....	148
<b>Figure 5.11:</b> Selectivity of liquid products and ethanol conversion achieved with 0.1 mol% [Ru]-5.2 - 5.9 at 2h .....	148
<b>Figure 5.12:</b> Yield of liquid products and ethanol conversion achieved with 0.1 mol% [Ru]-5.2 - 5.9 at 20h.....	149
<b>Figure 5.13:</b> Selectivity of liquid products and ethanol conversion achieved with 0.1 mol% [Ru]-5.2 - 5.9 at 20 .....	150
<b>Figure 6.1:</b> Ethanol Calibration Curve.....	156
<b>Figure 6.2:</b> 1-butanol Calibration Curve.....	157

## List of Schemes

<b>Scheme 1.1:</b> Petrochemical processes for the production of 1-butanol, Oxo synthesis, Reppe synthesis, Crotonaldehyde hydrogenation-	-	-	-	-	4
<b>Scheme 1.2:</b> ABE fermentation of glucose-	-	-	-	-	5
<b>Scheme 1.3:</b> Mechanism of Bimolecular and Guerbet coupling-	-	-	-	-	6
<b>Scheme 1.4:</b> Catalytic pathway for Guerbet reaction of ethanol to higher alcohols-	-	-	-	-	7
<b>Scheme 1.5:</b> Catalytic pathway for Guerbet reaction of ethanol and methanol to <i>iso</i> -butanol-	-	-	-	-	8
<b>Scheme 1.6:</b> Tishchenko reaction with subsequent saponification reaction--	-	-	-	-	9
<b>Scheme 1.7:</b> Acetate formation by Cannizzaro reaction-	-	-	-	-	10
<b>Scheme 1.8:</b> Reaction conditions, complexes and phosphine ligands tested by Ishii <i>et al</i> -	-	-	-	-	11
<b>Scheme 1.9:</b> Reaction conditions, P-P ligands and complexes tested for 1-butanol by Wass group-	-	-	-	-	12
<b>Scheme 1.10:</b> Reaction conditions, P-N ligands and complexes tested for ethanol upgrading to 1-butanol reported by the Wass group-	-	-	-	-	13
<b>Scheme 1.11:</b> Reaction conditions and complexes reported by Jones <i>et al</i> -	-	-	-	-	14
<b>Scheme 1.12:</b> Reaction conditions and catalysts reported by Szymczak <i>et al</i> -	-	-	-	-	15
<b>Scheme 1.13:</b> Ruthenium pincer complexes studied by Milstein and co-workers-	-	-	-	-	16
<b>Scheme 1.14:</b> Reaction conditions and complexes studied by Liu <i>et al</i> -	-	-	-	-	16
<b>Scheme 1.15:</b> Reaction conditions, P-P and P-N complexes tested for ethanol/methanol upgrading to <i>iso</i> -butanol by Wass group-	-	-	-	-	17
<b>Scheme 1.16:</b> Reaction conditions and complex studied by Newland and co-workers-	-	-	-	-	18
<b>Scheme 1.17:</b> Reaction conditions and Ir-phenanthroline ligand tested by Xu <i>et al</i> -	-	-	-	-	26
<b>Scheme 1.18:</b> Supported Ir-N functionalised complexes tested for ethanol/methanol upgrading to <i>iso</i> -butanol by Xu <i>et al</i> -	-	-	-	-	26
<b>Scheme 2.1:</b> Synthesis of $(\text{Ph}_2\text{P})_2\text{N}(\text{CH}_2)_3\text{Si}(\text{OMe})_3$ -	-	-	-	-	33
<b>Scheme 2.2:</b> Synthesis of complex $[\text{RuCl}_2\{(\text{PPh}_2)_2\text{N}(\text{CH}_2)_3\text{Si}(\text{OCH}_3)_3\}_2]$ -	-	-	-	-	34
<b>Scheme 2.3:</b> Reaction of <b>L2.1</b> with dichloro( $\eta^6$ - <i>p</i> -cymene)ruthenium(II) dimer to form a mixture of complexes--	-	-	-	-	40
<b>Scheme 2.4:</b> Reaction of <b>L2.1</b> and $[\text{RuCl}_2(\text{Ph}_3\text{P})_3]$ in equimolar ratio-	-	-	-	-	46
<b>Scheme 2.5:</b> Synthesis of complexes <b>[Ru]-2.5</b> and <b>[Ru]-2.6</b> -	-	-	-	-	47

<b>Scheme 3.1:</b> Dehydroxylation of silanols to form siloxanes--	-	-	59
<b>Scheme 3.2:</b> Schematic approach for immobilising homogeneous metal complexes incorporating silylating linkers onto support materials-	-	-	66
<b>Scheme 3.3:</b> Schematic approach for immobilising homogeneous metal complexes incorporating silylating linkers onto support materials-	-	-	67
<b>Scheme 3.4:</b> Immobilisation approach for supporting catalysts <b>[Ru]-2.1</b> and <b>[Ru]-2.2</b> on fumed silica and MCM-41-	-	-	68
<b>Scheme 4.1:</b> Immobilisation approach for supporting catalysts <b>[Ru]-2.1</b> and <b>[Ru]-2.2</b> on alumina-	-	-	104
<b>Scheme 5.1:</b> Synthesis of complex <b>[Ru]-5.1-</b>	-	-	131
<b>Scheme 5.2:</b> Synthesis of complexes <b>[Ru]-5.2 to [Ru]-5.9-</b>	-	-	132
<b>Scheme 5.3:</b> Catalytic pathway for 2-methyl-1-butanol formation via 1-butanol/methanol coupling and 1-butanol to higher alcohols-	-	-	141
<b>Scheme 5.4:</b> Catalytic pathway for 2-methyl-1-butanol formation via propanol/ethanol coupling-	-	-	141
<b>Scheme 5.5:</b> Catalytic dehydrogenation and decarbonylation of primary alcohols-	-	-	142

## List of Tables

<b>Table 1.1:</b> Comparison of alcohol fuels and gasoline-	-	-	-	3
<b>Table 1.2:</b> Chronological order of heterogeneous systems employed for ethanol upgrading to <i>n</i> -butanol-	-	-	-	20
<b>Table 2.1:</b> Ruthenium catalysed conversion of ethanol and methanol to <i>iso</i> -butanol-	-	-	-	49
<b>Table 2.2:</b> Ruthenium catalysed conversion of ethanol to 1-butanol-	-	-	-	52
<b>Table 3.1:</b> Selected IR vibration bands of silica and modified silica-	-	-	-	60
<b>Table 3.2:</b> <sup>29</sup> Si CP/MAS NMR spectroscopic peak positions of immobilised aminosilanes-	-	-	-	62
<b>Table 3.3:</b> <sup>29</sup> Si CP/MAS NMR spectroscopic peak positions of immobilised aminosilanes-	-	-	-	62
<b>Table 3.4:</b> BET surface area, BJH pore volume, and pore diameter of bare fumed silica and MCM-41, fumed silica and MCM-41-supported [Ru]- <b>2.1</b> and fumed silica and MCM-41-supported [Ru]- <b>2.2</b> -	-	-	-	75
<b>Table 3.5:</b> Ru amount in immobilised complexes determined by ICP-MS-	-	-	-	87
<b>Table 3.6:</b> Ruthenium catalysed conversion of ethanol and methanol to <i>iso</i> -butanol-	-	-	-	89
<b>Table 3.7:</b> Recyclability studies with fumed silica and MCM-41-supported [Ru]- <b>2.1</b> -	-	-	-	92
<b>Table 3.8:</b> Leachability Test (Hot filtration) with fumed silica-supported [Ru]- <b>2.1</b> -	-	-	-	92
<b>Table 3.9:</b> Effect of water on catalytic activity of fumed silica-supported [Ru]- <b>2.1</b>	-	-	-	95
<b>Table 3.10:</b> Effect of reactor size on catalytic activity of fumed silica-supported [Ru]- <b>2.1</b> -	-	-	-	95
<b>Table 4.1:</b> BET surface area, BJH pore volume, and pore diameter of pre-heated pure aluminas and alumina-supported [Ru]- <b>2.1</b> and [Ru]- <b>2.2</b> -	-	-	-	112
<b>Table 4.2:</b> Ru amount in supported catalysts determined by ICP-	-	-	-	124
<b>Table 4.3:</b> Ruthenium catalysed conversion of ethanol and methanol to <i>iso</i> -butanol	-	-	-	125
<b>Table 5.1:</b> Ruthenium catalysed conversion of ethanol and methanol to <i>iso</i> -butanol different bases -	-	-	-	143

<b>Table 5.2:</b> Ruthenium catalysed conversion of ethanol and methanol to <i>iso</i> -butanol	-	-	-	-	-	-	-	-	-	147
<b>Table 6.1:</b> GC Calibration Data for Ethanol-	-	-	-	-	-	-	-	-	-	156
<b>Table 6.2:</b> GC Calibration Data for 1-butanol-	-	-	-	-	-	-	-	-	-	156
<b>Table 6.3:</b> Ru amount in immobilised complexes determined by ICP-MS-	-	-	-	-	-	-	-	-	-	167
<b>Table 6.4:</b> Ru amount in immobilised complexes determined by ICP-MS-	-	-	-	-	-	-	-	-	-	171

## List of Equations

<b>Equation 1.1</b>	-	-	-	-	-	-	-	-	-	8
<b>Equation 6.1</b>	-	-	-	-	-	-	-	-	-	157
<b>Equation 6.2</b>	-	-	-	-	-	-	-	-	-	157
<b>Equation 6.3</b>	-	-	-	-	-	-	-	-	-	157
<b>Equation 6.4</b>	-	-	-	-	-	-	-	-	-	158
<b>Equation 6.5</b>	-	-	-	-	-	-	-	-	-	159

## **Chapter 1: Literature Review**

### **1.1 Fossil Fuels**

The ever-increasing demand for fuel to meet energy need continues to destabilise the supply chain for fossil fuels in the global market, leading to fluctuations in crude oil prices, as demands are usually more than global supplies. The world's passenger transportation relies on crude oil for an adequate supply of gasoline.<sup>1</sup> The gasoline shortages of the 1970s due to the OPEC oil export embargo (in 1973) and the Iranian Revolution (in 1979) affected the economies of major industrial countries including the United States, Canada, Western Europe, Japan, and Australia.<sup>1</sup> This occurred because of the increasing demand for gasoline over limited supplies of geological reserves. Likewise, the fuel price panic after Hurricane Katrina cannot be forgotten.<sup>2</sup> The demand for energy is likely to increase by more than 50% by 2025, with much of this increase emerging from several rapidly developing nations.<sup>2</sup> Also, it has been predicted that the supply of crude oil will only last for another 45 years at the current consumption rate.<sup>1</sup> Thus, the decline in crude oil reserves, price fluctuation, unsustainability and environmental/health problems associated with the use of fossil fuels gave rise to the idea of seeking alternative fuels that can alleviate these problems. It is therefore necessary to develop renewable sources of gasoline substitutes that fit the existing liquid fuel supply systems. Shifting society's dependence away from petroleum to renewable biomass resources is generally viewed as an important contributor to the development of a sustainable industrial society and effective management of greenhouse gas emissions.<sup>2</sup> As part of this drive towards sustainability, deriving biofuels for transportation from renewable biomass sources remains an important component of future energy supply.<sup>2-4</sup>

### **1.2 Bioethanol**

In the past few decades, bioethanol derived from biomass feedstock has been used as an alternative to gasoline either directly or in the form of a blend of the two.<sup>5-7</sup> The advantages of such a fuel include higher octane number and minimal greenhouse gas emissions.<sup>7</sup> As a solution to the problem of diminishing oil reserves, a Scientific American issue dated back as far as 1918 commended the effectiveness of a fuel blend of 25% gasoline, 25% benzole (mixture of benzene and toluene), and 50% alcohol.<sup>1</sup> For instance, bioethanol obtained mainly from corn fermentation in the United States

contributes ~ 20% to the total transportation fuels mix while another ~0.01% is based on biodiesel.<sup>2</sup> The common procedure for producing bioethanol from corn is depicted in Figure 1.1.<sup>1</sup> The U.S. Department of Energy has set a goal to replace 30% of the liquid petroleum transportation fuel with biofuels and to substitute 25% of petroleum based chemicals with biomass-derived chemicals by 2025.<sup>2</sup>

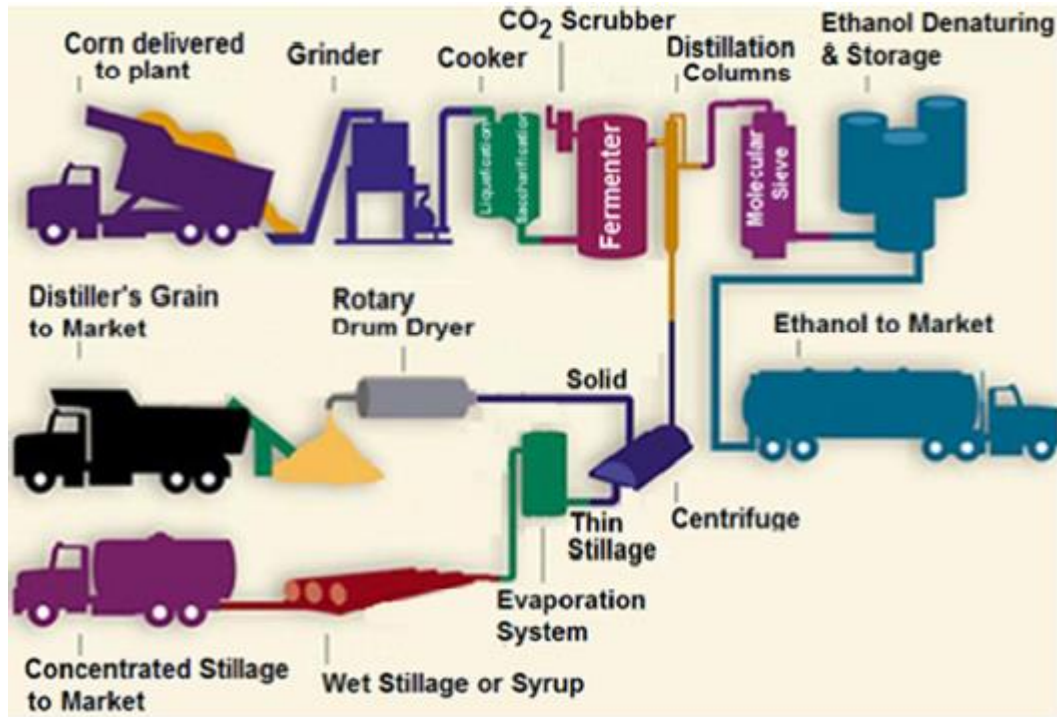


**Figure 1.1:** Schematic processes of manufacturing ethanol from corn in the U.S.

Extracted from reference 1.

Most of the feedstock used for bioethanol production are animal and human food crops (first-generation). In order not to interfere with food production, attention has been shifted to the production of bioethanol using non-food lignocellulosic plant sources (second-generation), e.g. forest slashes, crop residues, yard trimmings, food processing waste, and municipal organic refuse. Special biomass crops such as switch grass, miscanthus, giant reed, energy cane, Napier grass, grain sorghum, shrub willow, and hybrid poplar can be grown for this purpose.<sup>8</sup> Likewise, algae (third generation) have been used as feedstock for bioethanol production.<sup>9</sup>

Unfortunately, there are some drawbacks associated with the use of bioethanol as a fuel in relation to gasoline. Its energy density is low (70% of gasoline), it is corrosive to current engine technology and fuel pipelines, and it forms an azeotrope with water

which, over time, separates from the gasoline blend resulting in storage problems (Table 1.1).<sup>1, 3-5, 7, 10, 11</sup> Based on these limitations, biomass based products that meet liquid fuel specification have attracted significant attention. Higher alcohols, such as 1-butanol, have fuel properties that more closely resemble those of gasoline.<sup>5, 7</sup>

Biomass	Bioethanol	Biobutanol/Isobutanol	Gasoline	
				
Energy density (MJ/L)	19.6	29.2	29	32
Octane number	102	78	112	81-89
Miscibility with water	High	Low	Low	Low
Corrosivity	High	Low	Low	Low
Heat of vaporisation (MJ/Kg)	0.92	0.43	-	0.36
Compatibility	No	Yes	Yes	n/a
Air-to-fuel ratio	9.0	11.1	-	14.7
Blend ratio*	5-10%	16-100%	100%	n/a

\*Maximum blend without engine modification.

**Table 1.1:** Comparison of alcohol fuels and gasoline.<sup>12-14</sup>

### 1.3 Advanced Biofuels

1-Butanol is superior to bioethanol in several ways. Its number of carbon atoms is double that of ethanol leading to better performance as a biofuel. It is often termed an “advanced biofuel”. Because its fuel properties are much closer to that of standard gasoline. It has an energy density closer to gasoline (90%), it is immiscible with water and far less corrosive than ethanol, which provides support for better storage and handling capabilities. 1-Butanol can also be blended with gasoline at higher concentrations than ethanol.<sup>7, 13</sup> The air to fuel ratio for 1-butanol is closer to that of gasoline which is compatible with existing vehicle engines. These properties make 1-butanol compatible with OEM (Original Equipment Manufacturer) gasoline engines without any modification to existing fuel pipeline infrastructure. The cold starting problem associated with ethanol-gasoline blends is eliminated in 1-butanol-gasoline blends due to its heat of vaporisation being slightly above that of gasoline (Table 1.1). Also, the low solubility of butanol in water reduces the potential for groundwater contamination.<sup>13</sup> Most importantly, butanol is safer to handle than gasoline, it is less flammable (lower pressure and higher flash point), proves an overall low order of

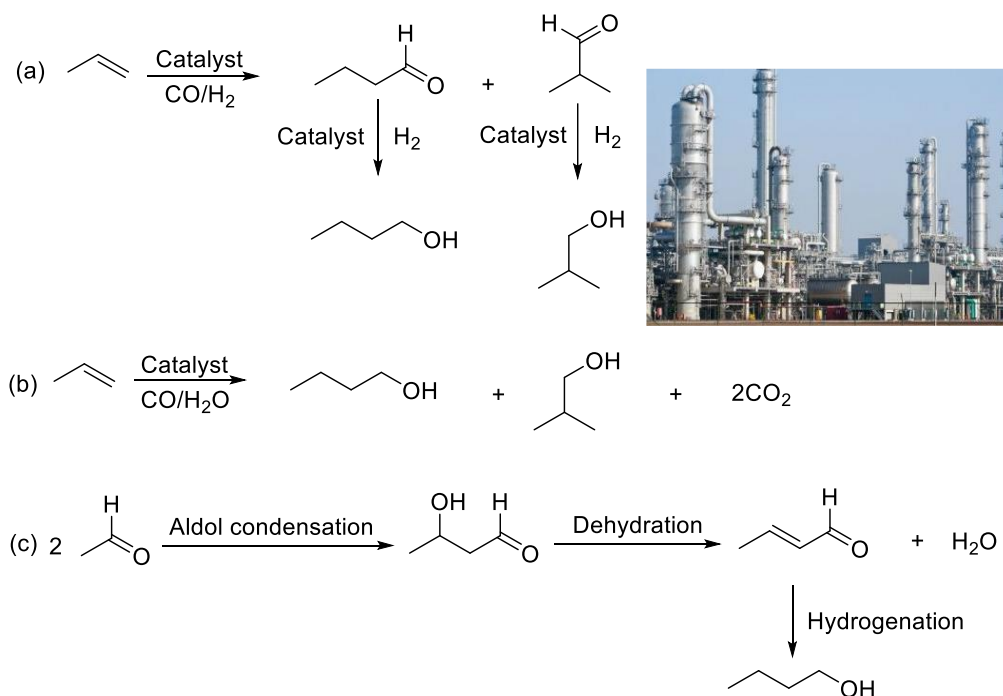
toxicity, and can be blended with gasoline at any ratio.<sup>13</sup> With increasing interest in using *n*-butanol as an advanced biofuel, research has been directed to the development of processes based on alternative feedstock for biofuel production.<sup>7</sup> The branched isomer, *iso*-butanol obtained from biomass-based materials has even more desirable fuel properties (Table 1.1).<sup>3, 10</sup>

#### 1.4 Traditional Methods of manufacturing butanols

Traditionally, 1-butanol has been manufactured by chemical (Oxo synthesis, Reppe synthesis and Crotonaldehyde hydrogenation) and biological means (ABE-fermentation by microorganisms).<sup>13</sup>

##### 1.4.1 Chemical Synthesis

In the oxo process (Scheme 1.1a), propylene from petroleum feedstocks, is hydroformylated with CO and H<sub>2</sub> over homogeneous Fe, Co, Rh, or Ru hydrocarbonyl substituted catalysts to form butyraldehydes which can be hydrogenated to form 1-butanol or *iso*-butanol depending on the reactor or ligand design.<sup>12, 13, 15, 16</sup> This process requires a high-energy input, has relatively high capital costs and the price of 1-butanol fluctuates with propylene prices.<sup>8</sup>

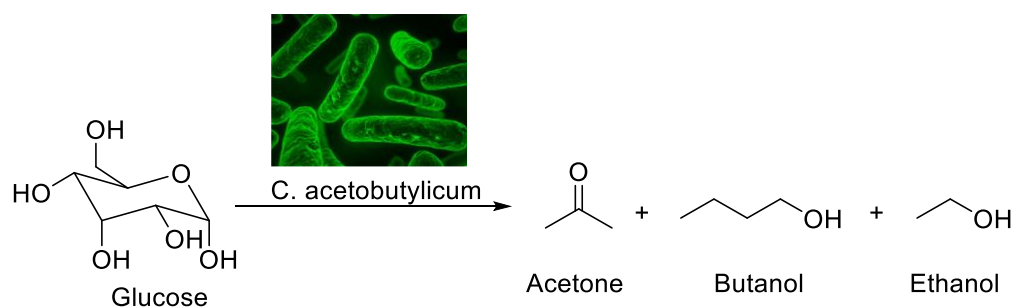


**Scheme 1.1:** Petrochemical processes for the production of 1-butanol (a) Oxo synthesis (b) Reppe synthesis (c) Crotonaldehyde hydrogenation.<sup>16</sup>

In the Reppe process (Scheme 1.1b) propylene, CO and H<sub>2</sub>O are reacted in the presence of a catalyst (tertiary ammonium salt or polynuclear iron carbonylhydrides) to produce 1-butanol and *iso*-butanol at low temperature and pressure.<sup>13, 16</sup> Compared to the oxo process, Reppe chemistry was found to be less successful with the Co catalyst despite the more favourable ratio of 1-butanol to *iso*-butanol and the milder reaction conditions. This is due to more expensive process technology.<sup>16</sup> Again, non-renewable feedstocks are used.

Crotonaldehyde hydrogenation consists of aldol condensation of acetaldehydes, dehydration, and hydrogenation (Scheme 1.1c).<sup>13, 16</sup> The first stage (i.e. aldol condensation) in this third process occurs in the presence of alkaline catalysts at ambient temperature and pressure. To induce the dehydration step, acetic or phosphoric acid is added, followed by distillation. Finally, the hydrogenation step is performed in the gas or liquid phase with a Cu catalyst.

#### 1.4.2 Biological Synthesis



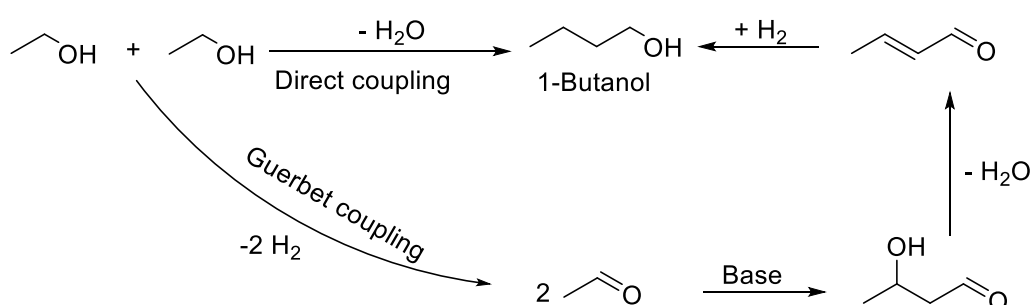
**Scheme 1.2:** ABE fermentation of glucose

1-Butanol is produced by microbial fermentation using solventogenic clostridial strains (e.g., *Clostridium acetobutylicum* etc) that convert biomass-derived sugars to mixtures of acetone, 1-butanol, and ethanol (ABE fermentation) (Scheme 1.2).<sup>1, 17, 18</sup> This fermentation process was first reported by Louis Pasteur in around 1861-1862.<sup>19, 20</sup> The process has been applied industrially since 1915.<sup>16, 20</sup> A typical ABE process with starting substrates of 60 g L<sup>-1</sup> between 36-72 h produced less than 20 g L<sup>-1</sup> product mixture of acetone, 1-butanol and ethanol in the ratio of 3:6:1 respectively. The low productivity (0.5–0.6 g L<sup>-1</sup>h<sup>-1</sup>) and yield (0.30 %) in this system was reported to have resulted from the toxic effects of 1-butanol on the bacterial strains.<sup>20</sup> Until recently, there was a decline in biofuel production using biological approaches due to the high cost of fermentation substrates (molasses), low productivity and low crude oil prices,

leading to cheaper petrochemical products.<sup>7, 16</sup> However, the ABE fermentation has gained renewed interest with the invention of metabolic and genetic engineering techniques, although the bulk synthesis of 1-butanol from bio-sustainable feedstocks remains a challenge for the biorefinery industry as it competes with food production.<sup>5,7,16</sup> Additionally, separation of 1-butanol from the product mixture of ABE fermentation via distillation is expensive and energy-demanding.

### 1.5 Ethanol Upgrading

To date, the synthesis of biofuels from biomass feedstocks have been faced with low conversions and poor selectivity.<sup>5, 11</sup> To address the shortcomings of ABE fermentation shortcomings, research has been geared towards upgrading bioethanol to butanol and other higher alcohols at higher selectivity and productivity.<sup>7</sup> This can be achieved through bimolecular (direct coupling) and aldol coupling (Guerbet) mechanisms (Scheme 1.3). The bimolecular mechanism, popularly known as direct coupling is the reaction of two ethanol molecules via a one-step concerted water elimination.<sup>7</sup> The Guerbet mechanism remains the most widely accepted pathway.<sup>7</sup> Detailed discussion follows in the next section.

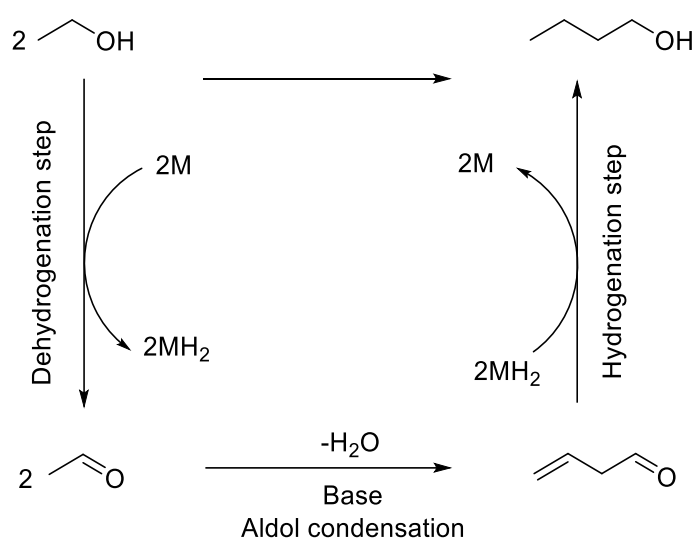


**Scheme 1.3:** Mechanism of Bimolecular and Guerbet coupling.<sup>7</sup>

### 1.6 Mechanism of Guerbet Reaction

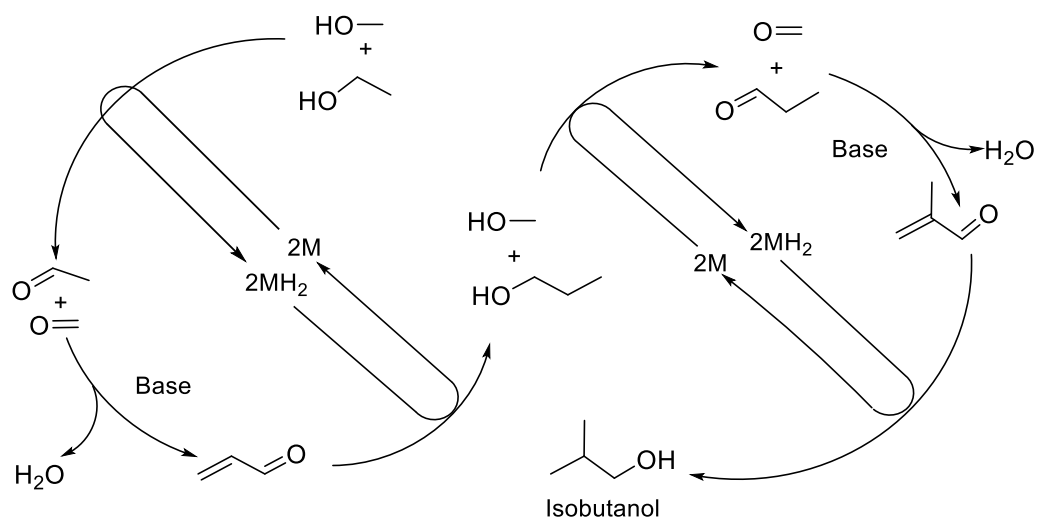
The Guerbet reaction was named after its inventor Marcel Guerbet.<sup>21, 22</sup> It specifically involves the coupling of primary alcohols to form higher alcohols with the elimination of a water molecule. A primary or secondary alcohol with a methylene group attached to the carbinol may condense with itself (self-condensation) or with another alcohol (cross-condensation) resulting in the formation of higher alcohols. The Guerbet reaction requires a catalyst that can initiate the oxidation of unreactive alcohol

substrates through borrowed hydrogen chemistry, the presence of a base to facilitate the aldol condensation step and an elevated temperature.<sup>3-5, 7, 10, 12</sup> The accepted catalytic reaction scheme for this conversion was first reported by Veibel and Neilsen in 1967.<sup>23</sup> The reaction begins with the dehydrogenation of the alcohol substrate to form an aldehyde capable of undergoing aldol condensation to give an allylic aldehyde after loss of water which is then re-hydrogenated to give higher chain alcohols (Scheme 1.4). One molecule of water is formed for every molecule of product formed.<sup>7, 12</sup> The 1-butanol product formed can further react either with itself or another ethanol to form 1-hexanol, 2-ethyl-1-butanol, 2-ethyl-1-hexanol, and octanol.



**Scheme 1.4:** Catalytic pathway for Guerbet reaction of ethanol to higher alcohols

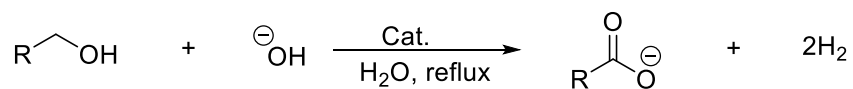
The direct conversion of ethanol alone to *iso*-butanol is unlikely given this mechanism. However, with the addition of methanol, which can also be derived from biomass, *iso*-butanol can be obtained via a co-condensation reaction.<sup>3, 10</sup> The catalytic pathway proceeds with dehydrogenation of methanol and ethanol to give formaldehyde and acetaldehyde respectively, which then undergo aldol coupling and re-hydrogenation to produce 1-propanol. The desired product (*iso*-butanol) can be obtained by the reaction of the propanol intermediate with another equivalent amount of methanol via repeated dehydrogenation, aldol coupling and re-hydrogenation steps (Scheme 1.5). This proposed mechanism for *iso*-butanol was supported by the Wass and co-workers who identified intermediate propanol as a minor product of the reaction and through isotope labelling detected that the methyl substituent on the *iso*-butanol product was from labelled <sup>13</sup>CH<sub>3</sub>OH.<sup>3, 10</sup>



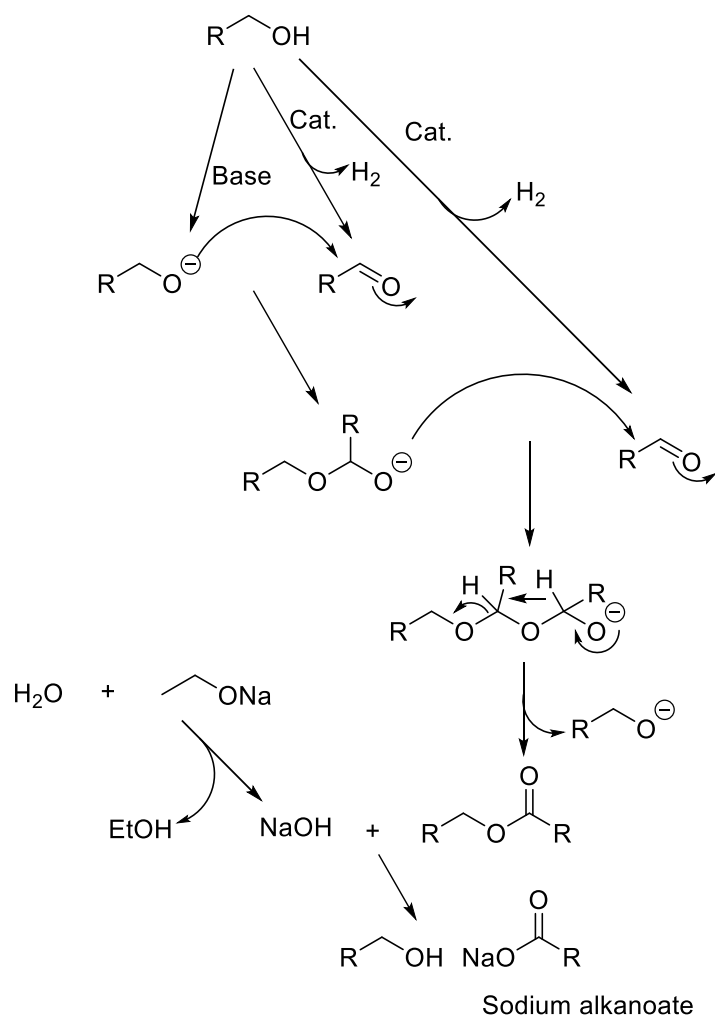
**Scheme 1.5:** Catalytic pathway for Guerbet reaction of ethanol and methanol to isobutanol

### 1.7 Mechanism of Other By-Products Formed

Guerbet-type catalytic systems produce water as a by-product. The presence of water in such catalytic systems has been found to reduce catalyst activity or deactivate the alkoxide base co-catalyst by forming inactive hydroxide.<sup>4, 11, 14, 24-26</sup> Carboxylate salts and esters can also be produced by the reaction of an alcohol with water and base resulting in hydrogen gas evolution (Equation 1.1).<sup>27</sup>

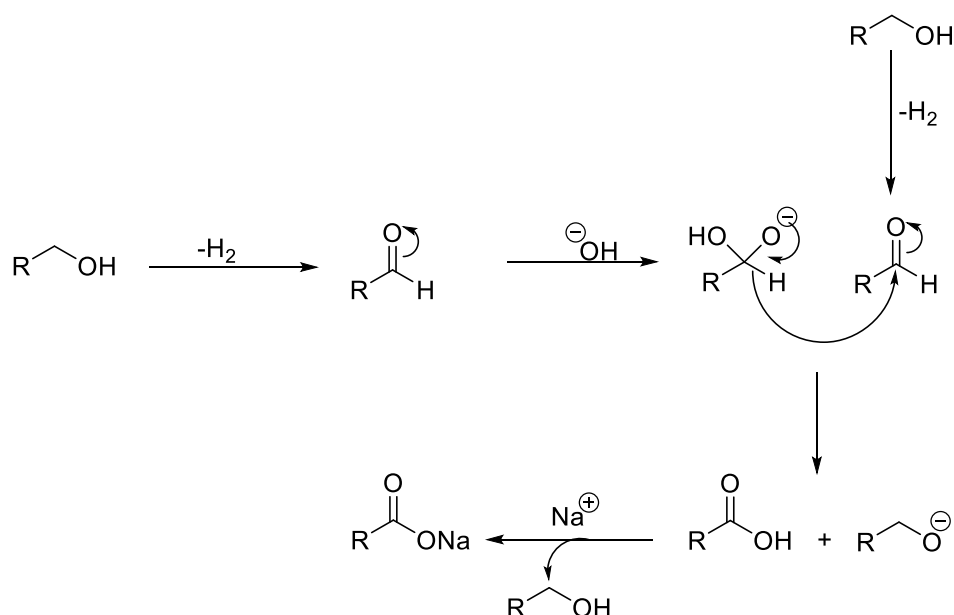


**Equation (1.1)**



**Scheme 1.6:** Tishchenko reaction with subsequent saponification reaction.

Other unwanted side reactions competing with this catalytic system are Tishchenko or Cannizzaro reaction pathways leading to acetate formation.<sup>4</sup> Presumably, the ethyl acetate formed via Tishchenko reaction undergoes saponification reaction with the sodium hydroxide generated from the reaction of water and sodium ethoxide (Scheme 1.6).<sup>28</sup> This can occur even in the absence of alkoxide base because an alkoxide base can be generated in situ from the reaction of mineral base with the alcohol substrates promoting acetate formation. On the other hand, the Cannizzaro reaction can take place through the disproportionation of the aldehyde intermediate with a base (Scheme 1.7).<sup>29</sup> These two reaction pathways are related as both involve the disproportionation of an aldehyde with a base but are different in terms of product formed. The products of the Cannizzaro reaction are alcohol and carboxylic acid while that of the Tishchenko reaction is the corresponding ester.



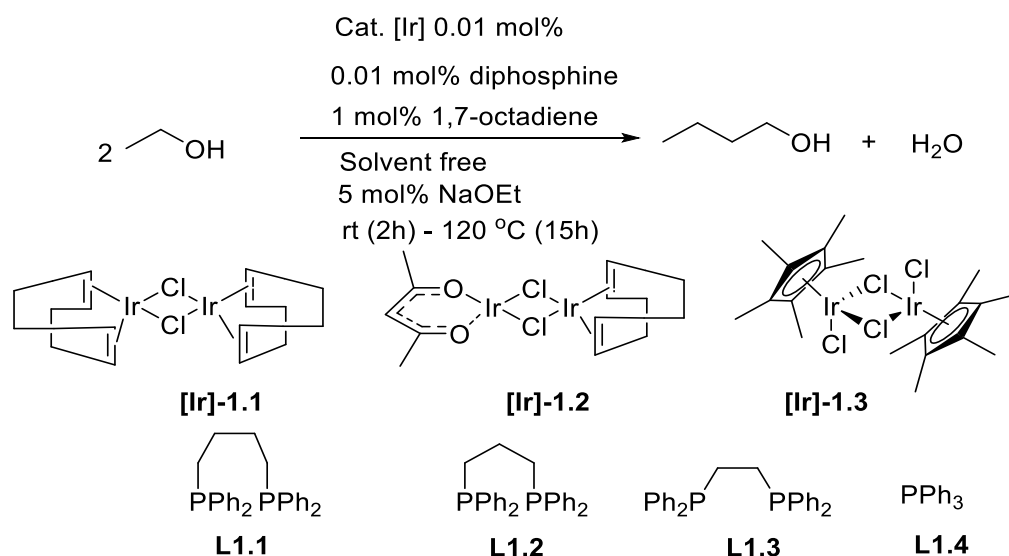
**Scheme 1.7:** Acetate formation by Cannizzaro reaction.

## 1.8 Previous Work

The transformation of bioethanol to advanced biofuels with homogeneous, heterogeneous or mixed heterogeneous and homogeneous catalysts via the Guerbet reaction has been reported, but these are often challenged by low conversion and/or poor selectivity.<sup>9-11,30</sup> The following sections give a brief overview of some key papers published to date. The Guerbet coupling of alcohols has been extensively reviewed in recent years.<sup>9, 10, 31-34</sup>

### 1.8.1 Homogeneous and Mixed Homo/Heterogeneous Catalysis

A series of homogeneous catalysts for the synthesis of higher molecular weight alcohols via the Guerbet mechanism were first discovered by Ugo *et al* in 1972. These authors reported the condensation of alcohols (C<sub>4</sub>+) catalysed by tertiary phosphine complexes of Group VIII transition metals and observed metal deposition with all the catalysts used suggesting that the true catalytic system may have been heterogeneous. Catalyst activity decreased with time, however, the Ru and Rh catalysts proved to be most stable.<sup>35</sup> Ishii and co-workers made some progress in ethanol coupling to 1-butanol using homogeneous iridium precursor complexes, in the presence of a phosphine ligand, 1,7-octadiene additive and an alkoxide base (Scheme 1.8). 1,7-octadiene was proposed to serve as a hydrogen acceptor in the ethanol dehydrogenation step.<sup>36</sup>



**Scheme 1.8:** Reaction conditions, complexes and phosphine ligands tested by Ishii *et al.*

Using a combination of complex **[Ir]-1.1** and phosphine **L1.2**, these authors achieved 22% yields of 1-butanol with 58% selectivity. When the iridium precursor was changed to **[Ir]-1.2**, selectivity dropped to 51% with no significant change in yield (21%). Selectivity was stepped up to 67% with ligand **L1.1** however at the detriment of conversion (12%). Poor selectivity and reduced yields were obtained with ligands **L1.3** and **L1.4**.<sup>36</sup> In 2005, Fujita *et al* reported an excellent yield of  $\beta$ -alkylated higher alcohols from the reaction between different secondary alcohols and primary alcohols in the presence of **[Ir]-1.3** and a base. However, substrates other than ethanol were used in this system. Unlike Ishii and co-workers, no hydrogen acceptor or donor was used. According to these authors, the Ir catalyst acted as the hydrogen acceptor due to electronic and steric effects of the Cp\* ligand.<sup>9, 37</sup>

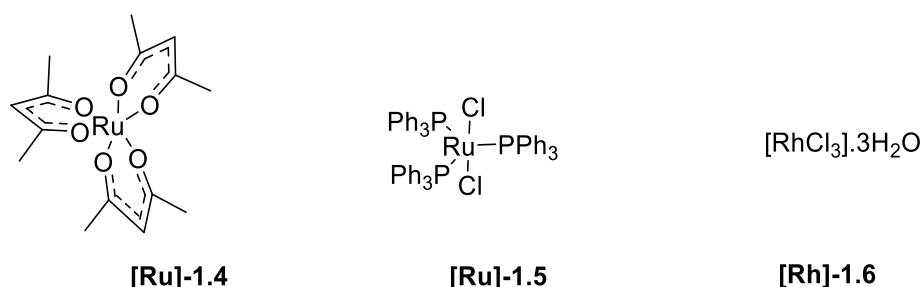
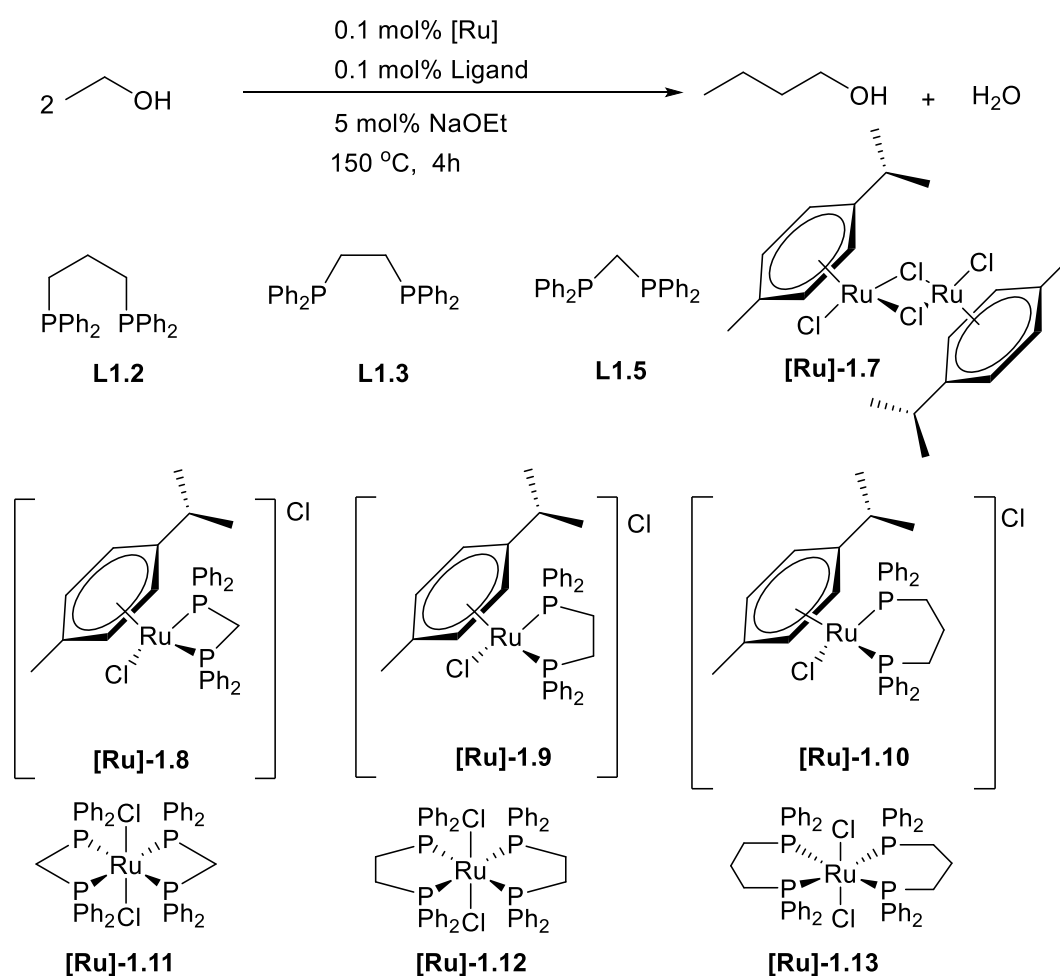


**Figure 1.2:** Ruthenium precursors used in Mitsubishi patent.

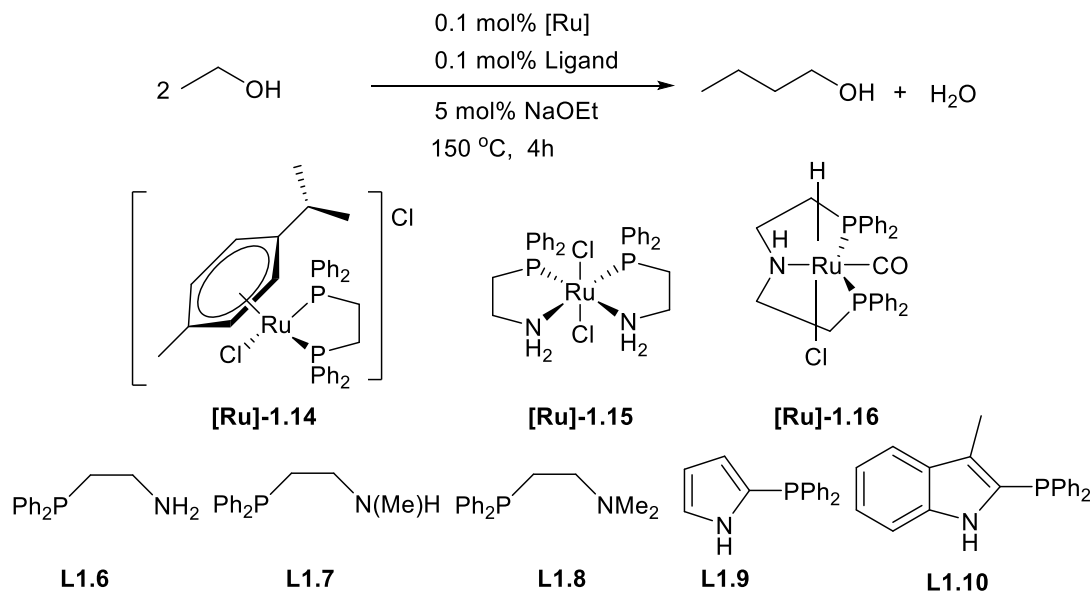
A patent from Mitsubishi Chemical Corporation in 2010 used combinations of **[Ru]-1.4**, **[Ru]-1.5**, or **[Rh]-1.6** with excess triphenylphosphine **L1.4**, and KO<sup>t</sup>Bu base under hydrogen pressures to convert ethanol to 1-butanol (Figure 1.2).<sup>38</sup> Yields up to 21% with 93% selectivity to 1-butanol were reported when 0.5 mol% of **[Ru]-1.5**, 3.5 mol% of **L1.4**, and 3.5 mol% of KO<sup>t</sup>Bu were used at 180 °C and 2 MPa hydrogen for 3 h. When the reaction was performed in the absence of a hydrogen atmosphere lower 1-butanol yield (18%) and selectivity (59%) was achieved. The catalytic reaction was favoured by addition of *o*-xylene as a solvent or with the use of neat substrate. Similar to the Ru system, Rh catalyst **[Rh]-1.60**, produced 20% yield and 93% selectivity to 1-butanol.<sup>38</sup>



**Scheme 1.9:** Reaction conditions, P-P ligands and complexes tested for 1-butanol by Wass group.

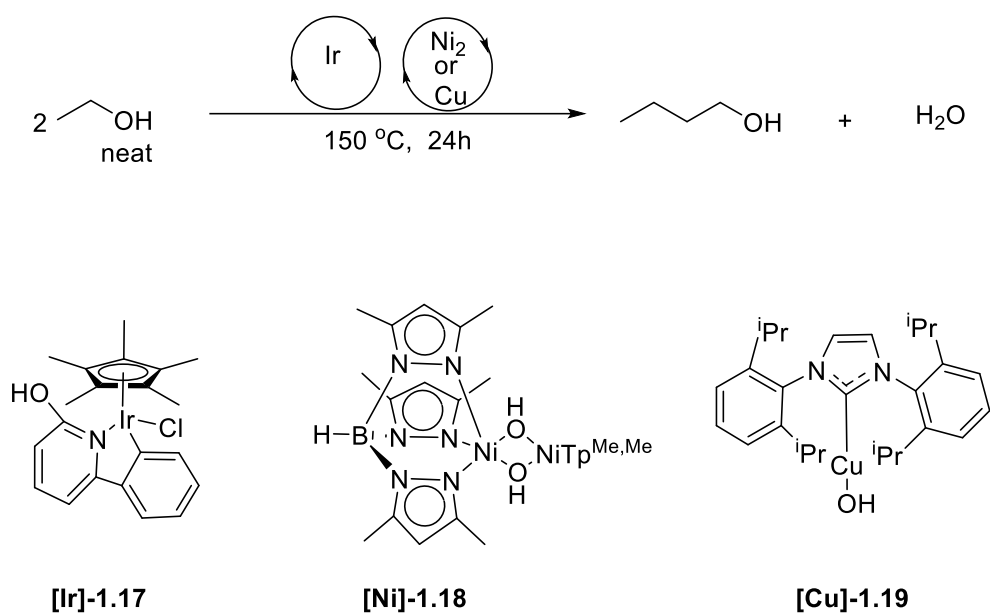
Wass and co-workers reported homogeneous and mixed heterogeneous-homogeneous phosphine based ruthenium(II) catalysts for the upgrading of ethanol to 1-butanol via

Guerbet chemistry (Scheme 1.9).<sup>4, 5</sup> They utilised 5 mol% NaOEt base, 0.1 mol% ligand (**L1.2-1.3**, **L1.5**) and 0.1 mol%  $[\text{RuCl}_2(\text{p-cymene})]_2$  (**[Ru]-1.7**) loading (relative to ethanol) at 150°C for 4 h (Scheme 1.10). Hydrogen acceptors such as 1,7-octadiene and 2 h catalyst pre-activation reported by Ishii *et al* were not required in this process. In contrast to other ligands employed for this system, the combination of ligand **L1.5** with pre-catalyst **[Ru]-1.7** gave the highest ethanol conversion (20%), 1-butanol yield (17.5%) and selectivity (90%) at 4 h. Of the three preformed mono-chelated catalysts (**[Ru]-1.8**, **[Ru]-1.9**, **[Ru]-1.10**) used, **[Ru]-1.8** gave the best result; 1-butanol yield (20%) with selectivity as high as 94% at 22% conversion for over 4 h. The key factor to this enhanced selectivity was the presence of the small bite angle ligand **L1.5** (1,1-bis(diphenylphosphino)methane, dppm). All the catalysts showed signs of decomposition with precipitation of ruthenium metal. However, using bis-chelate complex **[Ru]-1.11** provided a more robust catalyst, which showed no sign of decomposition. Increased yield (35.5%) and ethanol conversions (46%) could be achieved with longer reaction time (24 h) albeit with a decrease in selectivity (85%). Analogous complexes with wider bite angle diphosphines 1,2-bis(diphenylphosphino)ethane, dppe (**[Ru]-1.12**) and 1,3-bis(diphenylphosphino)propane (**[Ru]-1.13**), dppp gave very low conversions (3% and 2% respectively).



**Scheme 1.10:** Reaction conditions, P-N ligands and complexes tested for ethanol upgrading to 1-butanol reported by the Wass group.

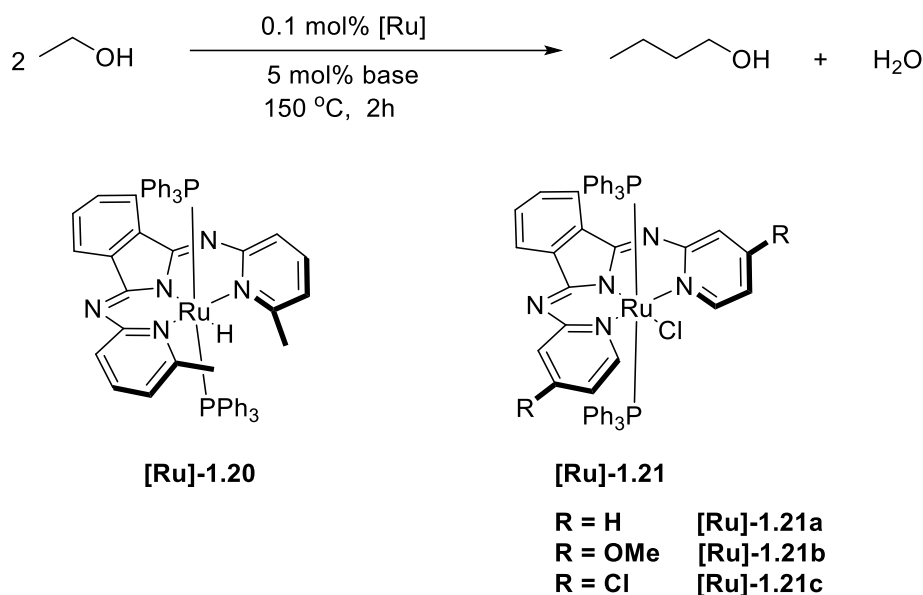
Further advances were made by the group by utilising P-N ligands (**L1.6-1.10**), which also gave promising 1-butanol yields and selectivity (Scheme 1.10).<sup>4</sup> These ligands generally perform similarly to the dppm system under the same reaction conditions. When 2 equivalents of **L1.6** was used in combination with **[Ru]-1.7** as the catalyst precursor, selectivity as high as 94% at 21% conversion was achieved after 4 h in contrast to the dppm system. Surprisingly, while maintaining the same catalyst precursor, ligand **L1.10** performed even better than the dppm system in terms of selectivity (93%) and conversion (31%). Catalyst **[Ru]-1.16**, which has previously been reported by Beller *et al* to give ethyl acetate from ethanol in excellent selectivity<sup>39, 40</sup>, gave extremely low 1-butanol yield (2%) and selectivity (12%). Preformed complex **[Ru]-1.14** and **[Ru]-1.15** gave similar results compared with the in situ runs. Notably, the P-N systems showcased an improved water tolerance compared to the P-P systems.



**Scheme 1.11:** Reaction conditions and complexes reported by Jones *et al*.

In 2015, Jones and co-workers reported highly selective tandem complexes for upgrading ethanol to 1-butanol through the Guerbet process.<sup>41</sup> Ethanol conversion up to 37% and excellent selectivity (>99%) to 1-butanol were achieved using a combination of complex **[Ir]-1.17** with **[Ni]-1.18** or **[Cu]-1.19** (Scheme 1.11). In their work, sterically crowded **[Ni]-1.18** and **[Cu]-1.19** hydroxides acted as the base co-

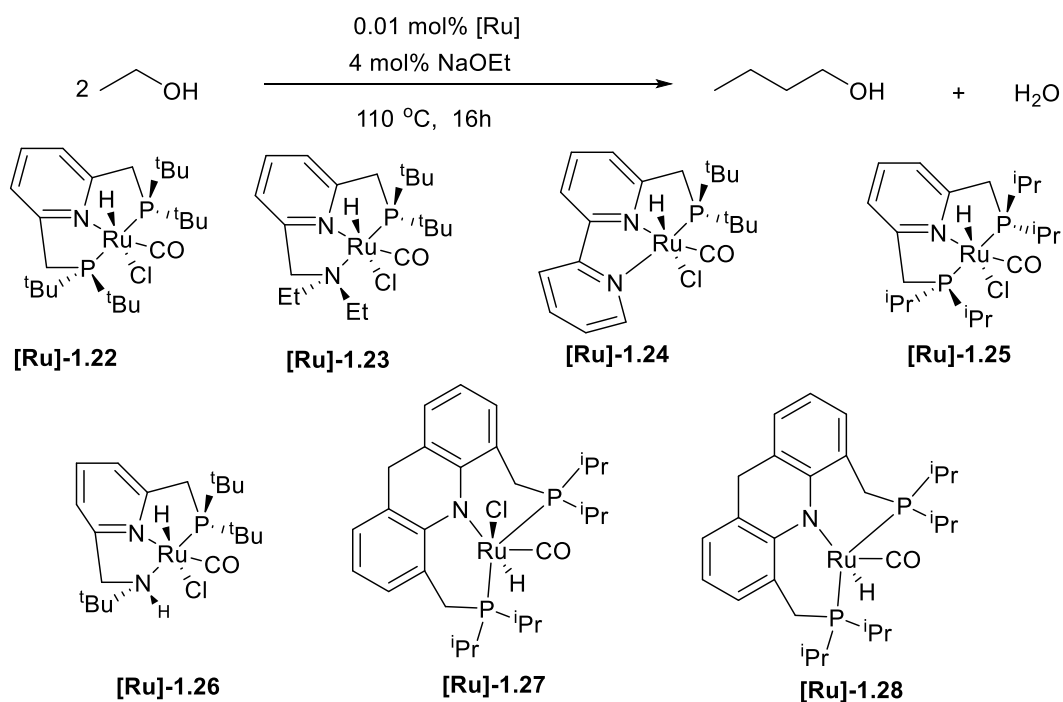
catalyst. Through control experiments and mechanistic studies, these authors unravelled the origin of the high selectivity associated with this system. To have an in-depth knowledge on this surprisingly high selectivity, attention was focused on the base-catalysed aldol coupling step of the Guerbet reaction which usually controls the selectivity of products formed. Both complexes **[Ni]-1.18** and **[Cu]-1.19** catalysed the aldol coupling reaction of acetaldehyde to give only the desired C<sub>4</sub> coupling product, crotonaldehyde in the Guerbet reaction. Comparative studies with KOH base yielded only 23% selectivity to crotonaldehyde, under the same reaction conditions. Further tests with these hydroxides confirmed their absence in the dehydrogenation and hydrogenation steps of the Guerbet reaction, again supporting the hypothesis that they were only involved in the aldol condensation step.



**Scheme 1.12:** Reaction conditions and catalysts reported by Szymczak *et al.*

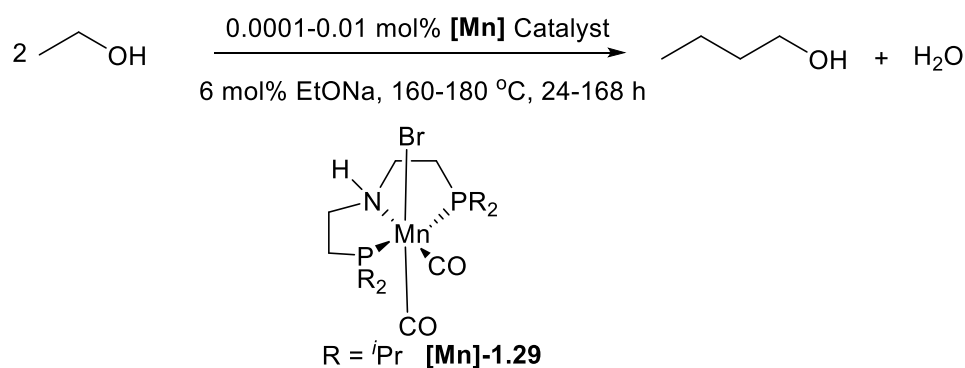
Work by Szymczak *et al* with an *N,N,N*-bMepi Ru(II) hydride complex **[Ru]-1.20** (bMepi = 1,3-bis(6'-methyl-2'-pyridylimino)isoindolate) showed that it was able to mediate reversible transformations between ketones and alcohols via hydrogenation-dehydrogenation reactions.<sup>42, 43</sup> From the mechanistic knowledge gained, they postulated that complexes of this type may be suitable for alcohol upgrading. In 2016, these authors reported air stable amide-derived *N,N,N*-Ru(II) complexes **[Ru]-1.21a-c** for the conversion of ethanol to 1-butanol with high activity (Scheme 1.12).<sup>11</sup> Of the three complexes used, **[Ru]-1.21a** performed better with 30% conversion and 91% selectivity to 1-butanol. Complex **[Ru]-1.21a** was also found to be active when the

catalysis was carried out in the presence of oxygen but at the detriment of selectivity (34% conversion and 83% selectivity). Conversion was enhanced (53%) on the addition of 1-4 equivalents of extra PPh<sub>3</sub> at the sacrifice of selectivity (~80%). PPh<sub>3</sub> was added to prevent phosphine dissociation thereby reducing the chances of a decarbonylation deactivation pathway occurring.



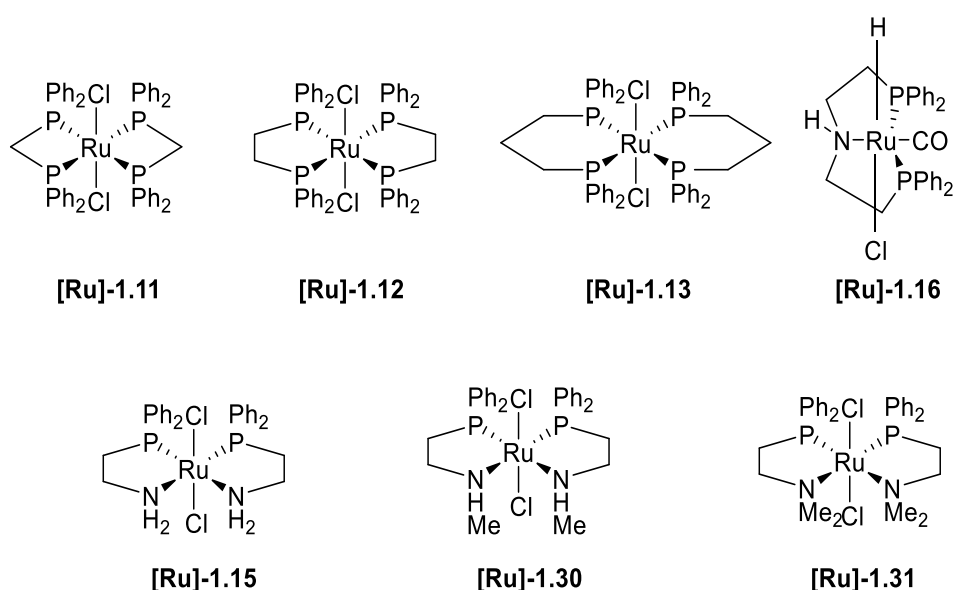
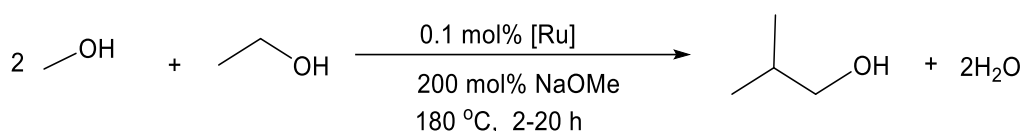
**Scheme 1.13:** Ruthenium pincer complexes studied by Milstein and co-workers.

Recently, Milstein and co-workers reported ruthenium pincer complexes (Scheme 1.13) for the Guerbet- type process of ethanol to advanced biofuel.<sup>30</sup> Among the complexes examined **[Ru]-1.21-1.28**, the acridine-based catalyst **[Ru]-1.27** performed best giving a remarkable turnover (18209 TON) at low catalyst loading (0.001 mol%). Complex **[Ru]-1.27** also produced good ethanol conversion (73%) and 1-butanol yield (36%) with C<sub>6</sub> and C<sub>8</sub> alcohols present as side products.



**Scheme 1.14:** Reaction conditions and complexes studied by Liu *et al.*

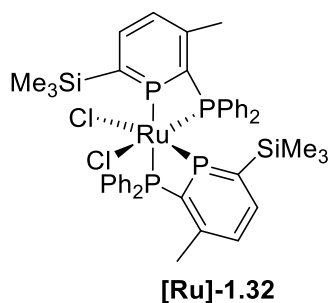
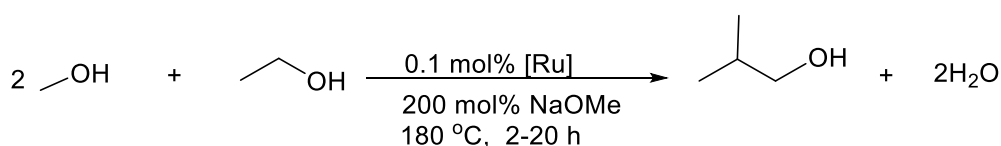
Most recently, Liu *et al.* explored the upgrading of ethanol to 1-butanol using homogeneous non-noble-manganese complexes (Scheme 1.14). A range of complexes were studied in this system. The most effective and easily prepared manganese pincer complex **[Mn]-1.29**, gave record turnover number (up to 114120) and turnover frequency ( $3078 \text{ h}^{-1}$ ) with 92% selectivity to 1-butanol after 7 days at part per million catalyst loading.<sup>44</sup>



**Scheme 1.15:** Reaction conditions, P-P and P-N complexes tested for ethanol/methanol upgrading to *iso*-butanol by Wass group.

The Wass group also explored the upgrading of bioethanol to *iso*-butanol with phosphine based ruthenium(II) catalysts via Guerbet chemistry.<sup>3, 24</sup> *iso*-butanol was obtained by the cross-condensation of methanol and ethanol (Scheme 1.15). Catalyst **[Ru]-1.11** with small bite angle diphosphine ligands gave the highest ethanol conversion (75%), *iso*-butanol yield (75%) and selectivity (99.8%) under the reaction conditions after 20 h at 180°C. Sodium methoxide was used as the base. Excess methanol was employed to discourage ethanol homocoupling. Even at shorter reaction times (2 h), **[Ru]-1.11** was found to be very active (66% conversion, 65% yield and 98% selectivity). Analogues with wider bite angle diphosphines (**[Ru]-1.12** and **[Ru]-**

**1.13**) gave extremely low conversion (3% and 5% respectively).<sup>3</sup> The mixed phosphine amine ligand catalysts (**[Ru]-1.15**, **[Ru]-1.30**, and **[Ru]-1.31**) were less successful for *iso*-butanol than complex **[Ru]-1.11**. However, with increased reaction times (20 h), moderate conversions (31-56%) and good selectivity (90-95%) were achieved.<sup>3</sup> At 2 h, complex **[Ru]-1.16** gave similar results compared with **[Ru]-1.15**.<sup>24</sup> In contrast to other Guerbet systems, complex **[Ru]-1.11** performed excellently with sodium hydroxide as a base even at lower base loading (150 mol%). The introduction of sodium hydroxide as a co-catalyst with complex **[Ru]-1.15** led to decrease in conversion, selectivity and yield compared to when the alkoxide base was used. Sodium hydroxide in conjunction with complex **[Ru]-1.16** gave 1-propanol as the sole product of catalysis. Water formation during this catalysis has a negative impact on catalyst activity. Complex **[Ru]-1.11** maintained excellent results with sodium hydroxide even with extra water added into the catalytic system. Addition of water to this system has a detrimental effect on the performance of complex **[Ru]-1.15**<sup>24</sup> in contrast to the *in-situ* run performed by the Wass group discussed under 1-butanol chemistry above.<sup>4</sup> Complex **[Ru]-1.11** still maintained good results in the presence of air-saturated solvent and extra water. The use of commercial alcoholic drinks as surrogates for ethanolic fermentation broth were also investigated.<sup>24</sup> The improved water tolerance of complex **[Ru]-1.11** was also maintained with these ethanol sources. Despite the amount of water and biogenic impurities present in these alternative ethanol sources, reasonable conversion, yield and selectivity were still obtained with complex **[Ru]-1.11**.



**Scheme 1.16:** Reaction conditions and complex studied by Newland and co-workers.

Using the standard reaction conditions developed by Wass *et al*, Newland and co-workers reported 38% *iso*-butanol yield with 88% selectivity after 2 h with catalyst [Ru]-1.32. Yield (50%) and selectivity (96%) were enhanced with increased reaction time (20 h) (Scheme 1.16).<sup>45</sup>

### 1.8.2 Heterogeneous Catalysis

Recently, comprehensive reviews on upgrading bioethanol to advanced biofuels with heterogeneous catalysts have been published.<sup>7, 9, 10, 31, 33, 46, 47</sup> In summary, Table 1.2 below gives an outline of several heterogeneous systems employed in literature for the upgrading of ethanol to *n*-butanol via Guerbet chemistry in chronological order. As shown in Table 1.2, previous heterogeneous systems comprise of basic metal oxides, solid acids, mixture of both, hydrotalcite and hydroxyapatite derived mixed metal oxide catalysts. In the heterogeneous systems with only basic metal oxides as catalysts for ethanol upgrading to higher alcohols, MgO remains the most efficient catalyst towards 1-butanol (18% 1-butanol yield, 33% selectivity and 56% ethanol conversion)<sup>48</sup> and *iso*-butanol (60% selectivity and 46% ethanol conversion)<sup>49</sup> production. Noteworthily, the addition of metal oxide (SiO<sub>2</sub>), basic metal ion (Ca, Ba), transition metal ion (Zn etc.) and even acids (HCl, H<sub>2</sub>SO<sub>4</sub>, acetic acid etc.) to enhance the surface area and basicity of MgO, unfortunately, gave no improvement on the reactivity MgO towards the desired products.<sup>48, 49</sup> Additionally, heterogeneous systems involving mixture of MgO with transition metal oxides with or without solid acids such as Al<sub>2</sub>O<sub>3</sub> for 1-butanol synthesis from ethanol were patented since 1930s. Ethanol conversion around 30-66% and 1-butanol yield above 6% were achieved from such systems.<sup>50, 51</sup> Other heterogeneous systems are those comprising of one heterogeneous catalyst for the dehydrogenation-hydrogenation step and one homogeneous base catalyst for the aldol condensation step of the Guerbet reaction of ethanol to *n*-butanol. Typical homogeneous bases used are alkali or alkali earth metal hydroxides, carbonate and alkoxides. This system is generally referred to as mixed homogeneous-heterogeneous catalytic system. Scott reported relatively high ethanol conversion (>90%) with the application of this system.<sup>52, 53</sup> Similarly, when this system was applied to *iso*-butanol synthesis with a combination of ethanol/methanol as substrates, 61% ethanol conversion and 98% selectivity were obtained by Carlini *et al*.<sup>54</sup> Another interesting heterogeneous systems found in the open literature are those

**Table 1.2:** Chronological order of heterogeneous systems employed for ethanol upgrading to *n*-butanol (NG = Not Given).

Catalysts	Surface Area (m <sup>2</sup> /g)	Base	Temp. (°C)	Time (h)	Pressure (atm)	Ethanol Conversion (%)	1-Butanol Yields (%)	1-butanol Selectivity (%)	Year (Ref)
MgO, BeO, CaO, CuO, ZnO, NiO and mixture of these	NG	-	240-400	2-48	60-300	30-34	6-34	NG	1933 <sup>50</sup>
MgO + oxides of Cu, Ni, Pb, Th, Ag, Cr, Cd, Sn, Mn, Zn, Fe, Co, U + Al <sub>2</sub> O <sub>3</sub> , Al(OH) <sub>3</sub> , stannic acid gel, silica gel and charcoal	NG	-	200-400	6-160	+ H <sub>2</sub>	52-66	11-20	NG	1935 <sup>51</sup>
Copper/nickel supported alumina gel (reduced in H <sub>2</sub> ) or copper chromite catalyst.	NG	K <sub>2</sub> CO <sub>3</sub> , Ce <sub>2</sub> CO <sub>3</sub> , KOH, K <sub>2</sub> SiO <sub>3</sub> , NaOH	>150	4-22	10-68 (+H <sub>2</sub> )	>90	36-58	NG	1935 <sup>52</sup>
Cu or Ni compound supported on alumina gel (reduced in H <sub>2</sub> ) or copper chromite catalyst.	NG	K <sub>2</sub> CO <sub>3</sub> , Ce <sub>2</sub> CO <sub>3</sub> , KOH, K <sub>2</sub> SiO <sub>3</sub> , NaOH	150-550	4-22	10-68 (+H <sub>2</sub> )	>90	<3	NG	1939 <sup>53</sup>
K <sub>2</sub> CO <sub>3</sub> , MgO, 2CuO.Cr <sub>2</sub> O <sub>3</sub>	NG	-	225-230	4-10	61-68	13	47	NG	1961 <sup>59</sup>

MgO [other catalysts used: ZnO, CaO, ZrO <sub>2</sub> , Mn-MgO, Cr-MgO, Zn-MgO, Al-MgO, Na-MgO, Cs-MgO]	137	-	390	20	1	60	NG	1 (46) <sup>a</sup>	1990 <sup>49</sup>
Pt-ZnMnZr [other catalyst used: Pd-ZnMnZr, Ag-ZnMnZr. Pt-ZnMnCr, Pd-ZnMnCr, Pt-ZnMnCe]	NG	-	350	16	3	99	NG	14 <sup>a</sup>	1996 <sup>60</sup>
Na/NaX [other catalysts used: Na <sub>2</sub> CO <sub>3</sub> supported NaY/SiO <sub>2</sub> -Al <sub>2</sub> O <sub>3</sub> /kaolinite/active carbon/MgO]	-	-	300	20	1	25	NG	42 <sup>a</sup>	2000 <sup>61</sup>
Cu-1955P [other catalyst used: Cu-Raney and BO 134]	-	MeONa	200	6	30 (+N <sub>2</sub> )	61	NG	98 <sup>a</sup>	2003 <sup>54</sup>
MgO [other catalysts used: CaO, BaO, $\gamma$ -Al <sub>2</sub> O <sub>3</sub> , Na/Al <sub>2</sub> O <sub>3</sub> , K/Al <sub>2</sub> O <sub>3</sub> , Cs/Al <sub>2</sub> O <sub>3</sub> , Mg/SiO <sub>2</sub> , Ba/MgO, Ca/MgO, Zn/MgO, Ce/MgO, Zr/MgO, Pb/MgO, Sn/MgO, Cu/MgO, HCl/MgO, H <sub>2</sub> PO <sub>4</sub> /MgO, Acetic/MgO, H <sub>2</sub> SO <sub>4</sub> /MgO, H <sub>2</sub> SO <sub>4</sub> /MgO, H <sub>2</sub> SO <sub>4</sub> /MgO, H <sub>2</sub> SO <sub>4</sub> /MgO]	38	-	450		1	56	18	33	2003 <sup>48</sup>
Hydroxyapatite (Ca/P ratio of 1.64) [other catalyst used: MgO, Mg(OH) <sub>2</sub> , Mg <sub>3</sub> (PO <sub>4</sub> ) <sub>2</sub> ·8H <sub>2</sub> O,	30-50	-	300	2 <sup>b</sup>	Autogenous pressure	15	NG	76.3	2006 <sup>62</sup>

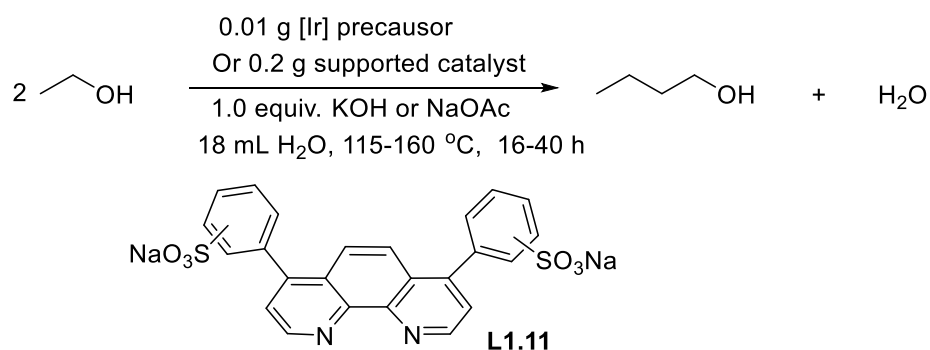
CaO, Ca(OH) <sub>2</sub> , CaF <sub>2</sub> , CaSiO <sub>3</sub> , CaSO <sub>4</sub> ·2H <sub>2</sub> O, Li <sub>3</sub> PO <sub>4</sub> , AlPO <sub>4</sub> , Hydroxyapatite (HAP; Ca/P varied ratio), Ca <sub>10</sub> /(PO <sub>4</sub> ) <sub>6</sub> F <sub>2</sub> (FAP), Ca <sub>4</sub> /(PO <sub>4</sub> ) <sub>2</sub> O (TTCP), hydrotalcite, sepiolite, talc, kaolin]									
HAP-4 [other catalyst used: HAP-(1-3), CaO, MgO, β-TCP]	38	-	272		Atmospheric pressure	10	NG	71	2008 <sup>63</sup>
HAP (Ca/P Ratio at 1.64)	33	-	400		Atmospheric pressure	NG	NG	29	2008 <sup>64</sup>
Cu <sub>5</sub> MgAl <sub>5</sub> O [other catalysts used: Cu <sub>1</sub> MgAl <sub>3</sub> O, MgAl <sub>3</sub> O, Cu <sub>5</sub> MgAl <sub>3</sub> O, Cu <sub>10</sub> MgAl <sub>3</sub> O, Cu <sub>20</sub> MgAl <sub>3</sub> O, CuO]	182	-	260	2	Atmospheric pressure	9	NG	80	2009 <sup>55</sup>
Hydrotalcite/metal carbonate	NG	-	300	1	Atmospheric pressure	77	NG	8	2009 <sup>56</sup>
Hydrotalcite containing the anion of Ethylenediaminetetraacetic acid	NG	-	300	1	1	13	8	63	2010 <sup>57</sup>
Sr <sub>10</sub> (PO <sub>4</sub> ) <sub>6</sub> (OH) <sub>2</sub> [other catalysts used: Ca <sub>10</sub> (PO <sub>4</sub> ) <sub>6</sub> (OH) <sub>2</sub> , Ca <sub>10</sub> (VO <sub>4</sub> ) <sub>6</sub> (OH) <sub>2</sub> , Sr <sub>10</sub> (VO <sub>4</sub> ) <sub>6</sub> (OH) <sub>2</sub> ]	26	-	300		Atmospheric pressure	1-24	NG	81	2011 <sup>65</sup>
Sr-HAP (1.70) [other catalyst used: Sr-HAP (1.58), Sr-HAP (1.64), Sr-HAP (1.67), Sr-HAP-NH <sub>3</sub> (1.71)]	38	-	300		Atmospheric pressure	11	NG	86	2012 <sup>66</sup>

Commercial 20%Ni/Al <sub>2</sub> O <sub>3</sub> [other supported catalysts used: Ru, Rh, Pd, Pt, Ag, Au/Al <sub>2</sub> O <sub>3</sub> with varied catalyst loadings]	NG	-	250	72	70	25	NG	80	2012 <sup>4</sup>
Pd <sub>5</sub> MgAlO [other catalysts used: Ag <sub>5</sub> MgAlO, Mn <sub>5</sub> MgAlO, Fe <sub>5</sub> MgAlO, Cu <sub>5</sub> MgAlO, Sm <sub>5</sub> MgAlO, Yb <sub>5</sub> MgAlO]	187	-	200	5	Autogenous pressure	4	3	72	2013 <sup>58</sup>
8%Ni/γ-Al <sub>2</sub> O <sub>3</sub> [other catalysts used: 17%-27%Ni/γ-Al <sub>2</sub> O <sub>3</sub> , Mn <sub>2</sub> O <sub>3</sub> /γ-Al <sub>2</sub> O <sub>3</sub> + 27%Ni/γ-Al <sub>2</sub> O <sub>3</sub> , Mn <sub>2</sub> O <sub>3</sub> + 27%Ni/γ-Al <sub>2</sub> O <sub>3</sub> ]	128	-	250	18	176	35	22	64	2013 <sup>67</sup>
Co [other catalysts used: Ni, Raney Cu, Fe, copper chromite, CoCO <sub>3</sub> , Co <sub>2</sub> O <sub>3</sub> ]	1	NaHCO <sub>3</sub>	200	72	Autogenous pressure	NG	3	69	2013 <sup>68</sup>
1wt% Na/ZrO <sub>2</sub> [ZrO <sub>2</sub> and 0.11wt% Na/ZrO <sub>2</sub> ]	11	-	400		Autogenous pressure	8	NG	12	2013 <sup>69</sup>
20%Ni/γ-Al <sub>2</sub> O <sub>3</sub> [other catalysts used: 8%Ni/γ-Al <sub>2</sub> O <sub>3</sub> , 5%Pd-8%Fe/Al <sub>2</sub> O <sub>3</sub> ]	NG	-	330	50	120	51	13	26	2015 <sup>70</sup>
8wt%Ni/9wt%La <sub>2</sub> O <sub>3</sub> -γ-Al <sub>2</sub> O <sub>3</sub> , [other catalysts used: 8-10wt%Ni/γ-Al <sub>2</sub> O <sub>3</sub> , 8wt%Ni/7wt%La <sub>2</sub> O <sub>3</sub> -γ-	124	-	230	10	Autogenous pressure	55	39	71	2015 <sup>12</sup>

Al <sub>2</sub> O <sub>3</sub> , 14wt%La <sub>2</sub> O <sub>3</sub> - $\gamma$ -Al <sub>2</sub> O <sub>3</sub> , and 8wt%Ni/10wt%CeO <sub>2</sub> - $\gamma$ Al <sub>2</sub> O <sub>3</sub> ]										
Cu/ HSACeO <sub>2</sub> [other catalysts used: Cu/Al <sub>2</sub> O <sub>3</sub> , Cu/ZSM-5, Cu/CeO <sub>2</sub> , Cu/TiO <sub>2</sub> , Cu/Si/Al]	178	-	260	-	High pressure CO <sub>2</sub>	67	30	45	2015 <sup>71</sup>	
19%Ni/Al <sub>2</sub> O <sub>3</sub> [other catalyst used: Co/Al <sub>2</sub> O <sub>3</sub> , Cu/Al <sub>2</sub> O <sub>3</sub> ]	NG	-	240	17-100	70	25	NG	60-65	2015 <sup>72</sup>	
Hydroxyapatite	82	-	400		1	<30	NG	55	2015 <sup>73</sup>	
Calcined MgO–Al <sub>2</sub> O <sub>3</sub> mixed oxides derived from hydrotalcite	200	-	600	-	NG	44	NG	50	2016 <sup>74</sup>	
MgO–Al <sub>2</sub> O <sub>3</sub> [other catalyst used: MgO, Al <sub>2</sub> O <sub>3</sub> ]	NG	-	350	24	NG	62	NG	42	2016 <sup>75</sup>	
Cu <sub>10</sub> Ni <sub>10</sub> -PMO [other catalyst used: MgAl-PMO, Cu <sub>20</sub> -PMO, Ni <sub>20</sub> -PMO, Cu <sub>13</sub> Ni <sub>7</sub> -PMO, Cu <sub>7</sub> Ni <sub>13</sub> -PMO, Cu <sub>10</sub> Ni <sub>10</sub> -PMO, Cu <sub>10</sub> Ni <sub>10</sub> -HTC]	256	-	320	6	Autogenous pressure	56	22	70	2017 <sup>76</sup>	
CuMgAl [other catalyst used: Pd-CuMgAl, In-CuMgAl]	127	-	300	5	1	47	15	62	2018 <sup>77</sup>	
CuNi-PMO [other catalyst used: Cu-PMO, Ni-PMO]	256	-	320	60-170	1	14	3	71	2020 <sup>78</sup>	
[Ir(OAc) <sub>3</sub> ] - (L1.11) on activated carbon		KOH	160		Atmospheric pressure	45	25	76	<sup>26</sup>	

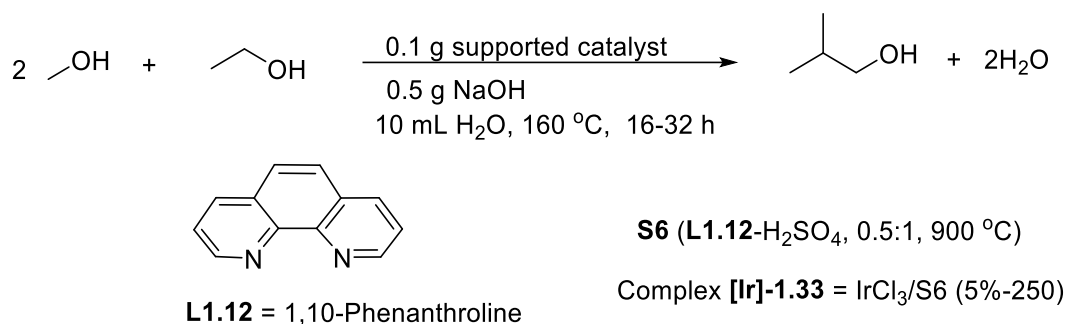
<sup>a</sup>*iso*-butanol (Substrate ethanol + methanol), <sup>b</sup>Contact time in seconds

consisting varied ratios of hydrotalcite-derived Mg/Al mixed oxides and varied ratios of Ca/P hydroxyapatites (HAP). The application of hydrotalcite and hydroxyapatites relies on the presence of both acids and basic sites in the materials, which play pivotal roles in the Guerbet coupling of primary alcohols to higher alcohols. To direct the reactivity of these materials towards dehydrogenation-hydrogenation and aldol condensation steps of Guerbet reaction, the acid and basic properties of hydrotalcite and hydroxyapatites are tuned by varying the Mg/Al and Ca/P ratios, respectively. The acids sites are required for the dehydrogenation of alcohol to aldehyde and hydrogenation of the intermediate aldol condensation product to higher alcohol. However, higher acid sites promote dehydration of alcohol instead, leading to undesired products. In other words, increasing basic sites is selective towards alcohol condensation products minimising unwanted side products. Interestingly, the introduction of transition metals into Mg/Al mixed oxide catalysts increased the catalytic activity of hydrotalcite towards ethanol conversion to *n*-butanol.<sup>55-58</sup> Particularly, Cu-doped Mg/Al mixed oxide catalyst has shown impressive performance with the most efficient Cu loadings reported in Marcu *et al.*<sup>55</sup> Further investigation by this author also showed Pd-Mg/Al mixed oxides as catalyst for enhanced 1-butanol yield.<sup>58</sup> Contrary to the hydrotalcite, the HAP performed well in the transformation of ethanol to *n*-butanol in the absence of any transition metals incorporated into the catalyst matrix. Many authors have demonstrated the effective activity of HAP towards ethanol upgrading to 1-butanol.<sup>62-66, 73</sup> Other categories of heterogeneous catalyst systems used can be seen in Table 1.2 with corresponding catalytic results and reaction conditions.<sup>12, 14, 59-61, 67, 68, 70</sup> It important to note that, majority of heterogeneous systems reported are metal oxides, mixed metals and transition metals supported metal oxides. None of these systems involved the heterogenisation of homogeneous metal-phosphine complexes for Guerbet reaction. The only heterogeneous systems that adopted the heterogenisation of metal complexes for Guerbet chemistry are discussed in the last paragraphs of this section. To the best of our knowledge, the present study is the first to adopt and explore the heterogenisation of alkoxy functionalised transition metal-phosphine complexes for *n*-butanol production.



**Scheme 1.17:** Reaction conditions and Ir-phenanthroline ligand tested by Xu *et al.* for 1-butanol chemistry.

Xu *et al.* explored the activity of water soluble ligand **L1.11** with  $[\text{IrCl}_3]$  and  $[\text{Ir}(\text{OAc})_3]$  for ethanol transformation to 1-butanol in both homogeneous and heterogeneous systems<sup>26</sup> (Scheme 1.17). In situ generated complexes  $[\text{Ir}(\text{OAc})_3]$ -**L1.11** and  $[\text{IrCl}_3]$ -**L1.11** gave similar results with more condensation products resulting from the former. Increasing the molar ratio of ligand to Ir and addition of NaOAc gave slightly higher results. This system was heterogenized by immobilising the *in-situ* generated complex of **L1.11** and  $[\text{Ir}(\text{OAc})_3]$  on activated carbon and was thereafter pyrolyzed. The supported catalyst gave up to 25% 1-butanol yield with more than 50% selectivity under these reaction conditions. Notably, the Ir-phenanthroline catalysts are stable, reusable and exhibit good water tolerance.



**Scheme 1.18:** Supported Ir-N functionalised complexes tested for ethanol/methanol upgrading to *iso*-butanol by Xu *et al.*

Xu *et al.*, also explored the reactivity of N-functionalised carbon supports for the cross-condensation of ethanol and methanol to *iso*-butanol (Scheme 1.18).<sup>79</sup> The previously utilized supported complex of **L1.11** gave up to 39% conversion and 29%

selectivity. With further optimization of the reaction conditions, **[Ir]-1.33** gave high *iso*-butanol selectivity (>90%) with good ethanol conversion (>50%).

## 1.9 Thesis Scope

Despite the impressive work of previous authors in catalytic conversion of bioethanol to advanced biofuels as highlighted in this chapter, the need for better performing catalysts is imperative in this area of research to improve the yield and selectivity of 1-butanol and *iso*-butanol. Homogenous catalysts have shown good activity and excellent selectivity; however, catalyst stability under what are harsh conditions for a homogeneous catalyst is often poor. At the large production volumes required for manufacture of a fuel, homogeneous catalysts are also typically more difficult to engineer into a process. Heterogenising homogeneous catalysts on solid support materials serves a better approach of introducing stability and recyclability in the catalytic system.

Thus, the main aim of the present study is to develop efficient heterogenised catalysts for the upgrading of small alcohols (methanol/ethanol) to advanced biofuels. Specific objectives are:

- To synthesise new homogeneous catalyst with remote functionalities capable of covalently attaching unto support materials.
- To support such complexes on a range of solid supports and characterise the materials formed.
- To test these catalysts (homogeneous and heterogeneous) as Guerbet catalysts for bioethanol upgrading.

## 1.10 References

1. M. Guo, W. Song and J. Buhain, *Renewable and Sustainable Energy Rev.*, 2015, **42**, 712-725.
2. A. J. Ragauskas, C. K. Williams, B. H. Davison, G. Britovsek, J. Cairney, C. A. Eckert, W. J. Frederick, J. P. Hallett, D. J. Leak, C. L. Liotta, J. R. Mielenz, R. Murphy, R. Templer and T. Tschaplinski, *Science*, 2006, **311**, 484-489.
3. R. L. Wingad, E. J. E. Bergstrom, M. Everett, K. J. Pellow and D. F. Wass, *Chem. Commun.*, 2016, **52**, 5202-5204.
4. R. L. Wingad, P. J. Gates, S. T. G. Street and D. F. Wass, *ACS Catal.*, 2015, **5**, 5822-5826.
5. G. R. M. Dowson, M. F. Haddow, J. Lee, R. L. Wingad and D. F. Wass, *Angew. Chem. Int. Ed.*, 2013, **52**, 9005-9008.
6. L. Wu, T. Moteki, A. A. Gokhale, D. W. Flaherty and F. D. Toste, *Chem*, 2016, **1**, 32-58.
7. Q. Zhang, J. Dong, Y. Liu, Y. Wang and Y. Cao, *J. Energy Chem.*, 2016, **25**, 907-910.
8. M. Al-Noaimi, I. Warad, O. S. Abdel-Rahman, F. F. Awwadi, S. F. Haddad and T. B. Hadda, *Polyhedron*, 2013, **62**, 110-119.
9. D. Gabriëls, W. Y. Hernández, B. Sels, P. Van Der Voort and A. Verberckmoes, *Catal. Sci. Technol.*, 2015, **5**, 3876-3902.
10. H. Aitchison, R. L. Wingad and D. F. Wass, *ACS Catal.*, 2016, **6**, 7125-7132.
11. K.-N. T. Tseng, S. Lin, J. W. Kampf and N. K. Szymczak, *Chem. Commun.*, 2016, **52**, 2901-2904.
12. T. L. Jordison, C. T. Lira and D. J. Miller, *Ind. Eng. Chem. Res.*, 2015, **54**, 10991-11000.
13. S. B. Bankar, S. A. Survase, H. Ojamo and T. Granstrom, *RSC Adv.*, 2013, **3**, 24734-24757.
14. T. Riittonen, E. Toukoniitty, D. K. Madnani, A.-R. Leino, K. Kordas, M. Szabo, A. Sapi, K. Arve, J. Wärnä and J.-P. Mikkola, *Catalysts*, 2012, **2**, 68-84.
15. F. E. Paulik, *Catal. Rev.*, 1972, **6**, 49-84.
16. M. Uyttebroek, W. Van Hecke and K. Vanbroekhoven, *Catal. Today*, 2015, **239**, 7-10.
17. P. Dürre, *Curr. Opin. Biotechnol.*, 2011, **22**, 331-336.
18. E. M. Green, *Curr. Opin. Biotechnol.*, 2011, **22**, 337-343.
19. P. Dürre, *Appl. Microbiol. Biotechnol.*, 1998, **49**, 639-648.
20. N. Qureshi, in *Encyclopedia of Microbiology (Third Edition)*, ed. M. Schaechter, Academic Press, Oxford, 2009, pp. 512-528.
21. M. C. Guerbet, *Acad. Sci. Paris* 1988, **128**, 1002-1004.
22. M. C. Guerbet, *Acad. Sci. Paris* 1906, **149**, 129-132.
23. S. Veibel and J. I. Nielsen, *Tetrahedron*, 1967, **23**, 1723-1733.
24. K. J. Pellow, R. L. Wingad and D. F. Wass, *Catal. Sci. Technol.*, 2017, **7**, 5128-5134.
25. T. L. Jordison, L. Peereboom and D. J. Miller, *Ind. Eng. Chem. Res.*, 2016, **55**, 6579-6585.
26. G. Xu, T. Lammens, Q. Liu, X. Wang, L. Dong, A. Caiazzo, N. Ashraf, J. Guan and X. Mu, *Green Chem.*, 2014, **16**, 3971-3977.
27. E. Balaraman, E. Khaskin, G. Leitius and D. Milstein, *Nature Chem.*, 2013, **5**, 122-125.
28. V. Tishchenko, *J. Russ. Phys. Chem. Soc.*, 1906, **38**, 482-540.
29. S. Cannizzaro, *J. Liebigs Ann. Chem.*, 1853, **88**, 129-130
30. Y. Xie, Y. Ben-David, L. J. W. Shimon and D. Milstein, *J. Am. Chem. Soc.*, 2016, **138**, 9077-9080.

31. J. T. Kozlowski and R. J. Davis, *ACS Catal.*, 2013, **3**, 1588-1600.
32. W. R. d. S. Trindade and R. G. d. Santos, *Renewable and Sustainable Energy Rev.*, 2017, **69**, 642-651.
33. X. Wu, G. Fang, Y. Tong, D. Jiang, Z. Liang, W. Leng, L. Liu, P. Tu, H. Wang and J. Ni, *ChemSusChem*, 2018, **11**, 71-85.
34. N. M. Eagan, M. D. Kumbhalkar, J. S. Buchanan, J. A. Dumesic and G. W. Huber, *Nat. Rev. Chem.*, 2019, **3**, 223-249.
35. G. Gregorio, G. F. Pregaglia and R. Ugo, *J. Organomet. Chem.*, 1972, **37**, 385-387.
36. K. Koda, T. Matsu-ura, Y. Obora and Y. Ishii, *Chem. Lett.*, 2009, **38**, 838-839.
37. K.-i. Fujita, C. Asai, T. Yamaguchi, F. Hanasaka and R. Yamaguchi, *Org. Lett.*, 2005, **7**, 4017-4019.
38. Y. Tanaka and M. Utsunomiya, *US Patent 8318990B2*, 2010.
39. M. Nielsen, A. Kammer, D. Cozzula, H. Junge, S. Gladiali and M. Beller, *Angew. Chem. Int. Ed.*, 2011, **50**, 9593-9597.
40. M. Nielsen, H. Junge, A. Kammer and M. Beller, *Angew. Chem. Int. Ed.*, 2012, **51**, 5711-5713.
41. S. Chakraborty, P. E. Pizsel, C. E. Hayes, R. T. Baker and W. D. Jones, *J. Am. Chem. Soc.*, 2015, **137**, 14264-14267.
42. K.-N. T. Tseng, J. W. Kampf and N. K. Szymczak, *Organometallics*, 2013, **32**, 2046-2049.
43. K.-N. T. Tseng, J. W. Kampf and N. K. Szymczak, *ACS Catal.*, 2015, **5**, 5468-5485.
44. Y. Liu, Z. Shao, Y. Wang, L. Xu, Z. Yu and Q. Liu, *ChemSusChem*, 2019, **12**, 3069-3072.
45. R. J. Newland, M. F. Wyatt, R. L. Wingad and S. M. Mansell, *Dalton Trans.*, 2017, **46**, 6172-6176.
46. A. Galadima and O. Muraza, *Ind. Eng. Chem. Res.*, 2015, **54**, 7181-7194.
47. J. Sun and Y. Wang, *ACS Catal.*, 2014, **4**, 1078-1090.
48. A. S. Ndou, N. Plint and N. J. Coville, *Appl. Catal., A*, 2003, **251**, 337-345.
49. W. Ueda, T. Kuwabara, T. Ohshida and Y. Morikawa, *Chem. Comm.*, 1990, 1558-1559.
50. J. P. Wibaut, *US Patent 1910582*, 1933.
51. O. Fuchs and Q. Wilhelm, *US Patent 1992480*, 1935.
52. N. D. Scott, *US Patent 2004350*, 1935.
53. N. D. Scott, *US Patent 2145097*, 1939.
54. C. Carlini, M. Di Girolamo, A. Macinai, M. Marchionna, M. Noviello, A. M. Raspolti Galletti and G. Sbrana, *J. Mol. Catal. A: Chem.*, 2003, **200**, 137-146.
55. I.-C. Marcu, D. Tichit, F. Fajula and N. Tanchoux, *Catal. Today*, 2009, **147**, 231-238.
56. K. Kourtakis, M. B. D'Amore and L. E. Manzer, *WO 2009/026501* 2009.
57. K. Kourtakis, M. B. D'Amore and L. E. Manzer, *US Patent 7700812*, 2010.
58. I.-C. Marcu, N. Tanchoux, F. Fajula and D. Tichit, *Catal Lett.*, 2013, **143**, 23-30.
59. M. W. Farrar, *US Patent 2971033*, 1961.
60. P. T. Barger, *US Patent 5559275*, 1996.
61. K. Gotoh, S. Nakamura, T. Mori and Y. Morikawa, in *Studies in Surface Science and Catalysis*, eds. A. Corma, F. V. Melo, S. Mendioroz and J. L. G. Fierro, Elsevier, 2000, **130**, 2669-2674.
62. T. Tsuchida, S. Sakuma, T. Takeguchi and W. Ueda, *Ind. Eng. Chem. Res.*, 2006, **45**, 8634-8642.
63. T. Tsuchida, J. Kubo, T. Yoshioka, S. Sakuma, T. Takeguchi and W. Ueda, *J. Catal.*, 2008, **259**, 183-189.

64. T. Tsuchida, T. Yoshioka, S. Sakuma, T. Takeguchi and W. Ueda, *Ind. Eng. Chem. Res.*, 2008, **47**, 1443-1452.
65. S. Ogo, A. Onda and K. Yanagisawa, *Appl. Catal., A*, 2011, **402**, 188-195.
66. S. Ogo, A. Onda, Y. Iwasa, K. Hara, A. Fukuoka and K. Yanagisawa, *J. Catal.*, 2012, **296**, 24-30.
67. H. S. Ghaziaskar and C. Xu, *RSC Adv.*, 2013, **3**, 4271-4280.
68. X. Zhang, Z. Liu, X. Xu, H. Yue, G. Tian and S. Feng, *ACS Sustainable Chem. Eng.*, 2013, **1**, 1493-1497.
69. J. T. Kozlowski and R. J. Davis, *J. Energy Chem.*, 2013, **22**, 58-64.
70. P. Dziugan, K. G. Jastrzabek, M. Binczarski, S. Karski, I. A. Witonska, B. Kolesinska and Z. J. Kaminski, *Fuel*, 2015, **158**, 81-90.
71. J. H. Earley, R. A. Bourne, M. J. Watson and M. Poliakoff, *Green Chem.*, 2015, **17**, 3018-3025.
72. T. Riittonen, K. Eränen, P. Mäki-Arvela, A. Shchukarev, A.-R. Rautio, K. Kordas, N. Kumar, T. Salmi and J.-P. Mikkola, *Renewable Energy*, 2015, **74**, 369-378.
73. F. C. Meunier, J. Scalbert and F. Thibault-Starzyk, *C. R. Chim.*, 2015, **18**, 345-350.
74. K. K. Ramasamy, M. Gray, H. Job, D. Santosa, X. S. Li, A. Devaraj, A. Karkamkar and Y. Wang, *Top Catal* 2016, **59**, 46-54.
75. K. K. Ramasamy, M. Gray, H. Job, C. Smith and Y. Wang, *Catal. Today*, 2016, **269**, 82-87.
76. Z. Sun, A. Couto Vasconcelos, G. Bottari, M. C. A. Stuart, G. Bonura, C. Cannilla, F. Frusteri and K. Barta, *ACS Sustain. Chem. Eng.* , 2017, **5**, 1738-1746.
77. O. M. Perrone, F. Lobefaro, M. Aresta, F. Nocito, M. Boscolo and A. Dibenedetto, *Fuel Process. Technol.*, 2018, **177**, 353-357.
78. X.-Y. Xi, Z.-H. Sun, H.-T. Cao, Y.-T. Pei, G. H. ten Brink, P. J. Deuss, K. Barta and H. J. Heeres, *Catalysts*, 2020, **10**, 996.
79. Q. Liu, G. Xu, X. Wang and X. Mu, *Green Chem.*, 2016, **18**, 2811-2818.

## Chapter 2: Alkoxysilyl-functionalised Bidentate Phosphine-based Ruthenium(II) Complexes for Ethanol Upgrading to Advanced Biofuels

### 2.1 Introduction

Chelating diaryl- and dialkylphosphines ('diphosphines') are important bidentate chelating agents in coordination and organometallic chemistry.<sup>1, 2</sup> Since the days of Wilkinson's catalysts,<sup>3</sup> a plethora of phosphine ligands have been synthesised and employed in metal complexation and catalysis. Diphosphines have remarkable impact on the reactivity and selectivity of a catalyst;<sup>2</sup> the exceptional catalytic properties of diphosphine ligands have led to them finding wide use in many applications. The development of new bidentate phosphine incorporating heteroatoms in the bridging backbone rather than carbon has led to the emergence of N-groups connecting the two phosphine nuclei to give small bite angle P-N-P ligands. Considerable interest is given to phosphines with P-N-P bonds due to the possibility of the transfer of electronic properties from the nitrogen atom to the phosphorus atom.<sup>4, 5</sup> Additionally, the introduction of N-groups to diphosphines during ligand design do not necessarily make one phosphine react independently of the other. Therefore, diphosphinoamines react in a similar way to traditional diphosphines.<sup>1</sup> For example, *N,N*-bis(diphenylphosphino)amine, Ph<sub>2</sub>PNHPPH<sub>2</sub> (dppa), which is isoelectronic with 1,1-bis(diphenylphosphino)methane, Ph<sub>2</sub>PCH<sub>2</sub>PPh<sub>2</sub>, (dppm), shows relative coordinative mode to the CH<sub>2</sub>-ligand, either in its neutral or anionic [Ph<sub>2</sub>PNPPH<sub>2</sub>]<sup>-</sup> state.<sup>6</sup> The scope and versatility of diphosphinoamine (phosphazane) ligands is extensive as the substituents on the N and P atoms can be easily varied, with concomitant alterations in the P-N-P angle and arrangement around the phosphorus centres.<sup>7-10</sup> They exhibit bidentate coordination modes like normal diphosphines, and thus serve as good stabilising ligands in organometallic complexes and clusters.<sup>11</sup> Furthermore, to modify the structural and electronic properties of (Ph<sub>2</sub>P)<sub>2</sub>NR type ligands and their metal-coordinated complexes in catalysis,<sup>7-9, 12</sup> the R group is tuned by the reaction of chlorodiphenylphosphine with a variety of primary amines.<sup>1, 5</sup> Through this synthetic route, a library of bis(diphenylphosphino)arylamines are reported in literature.<sup>4, 7-10, 12-29</sup> Some of them are sensitive to air and moisture<sup>9, 10, 14</sup> due to the presence of free PPh<sub>2</sub> ends and polar P-N bonds. Lately, there is immense interest in transition-metal complexes of these ligands for several catalytic applications.<sup>5, 30</sup> Special interest in the ruthenium metal complexes arise from the observation that they act as great promoters

in many catalytic reactions.<sup>8-10, 12</sup> Furthermore, ruthenium complexes usually exhibit adequate stability between the electronic and steric properties of most ligand environment.<sup>31</sup> Most importantly, bis(diphenylphosphino)aminoalkyltrialkoxysilanes,  $(\text{Ph}_2\text{P})_2\text{NR}$  ( $\text{R} = (\text{CH}_2)_3\text{Si}(\text{OR}')_3$ ,  $\text{R}' = \text{methyl, ethyl etc}$ ) are receiving increasing attention in recent years due to their unique potential as linkers for metal anchorage.<sup>11, 32, 33</sup> Since, good catalytic activity was achieved by Wass and co-workers with ruthenium complexes, the present study expands on the existing work through the investigation of new bis(diphenylphosphino)aminopropyltrimethoxysilane-ruthenium(II) complexes for upgrading ethanol to advanced biofuels. Additionally, the afore-mentioned complexes possess the possibility of being anchored onto support materials to potentially access the benefits of heterogeneous catalytic systems such as stability and ease of recyclability.

## 2.2 Aims and Objectives

In the Wass previous studies, a range of ruthenium complexes with P-P and P-N ligands were explored for *n*-butanol and *iso*-butanol synthesis from ethanol substrate (chapter 1, Section 1.8.1, Scheme 1.9-1.10, 1.15). The complex carbonylchlorohydrido{bis[2-(diphenylphosphino)ethyl]amino} ruthenium(II), Ru-MACHO<sup>®</sup>, remains the only ruthenium catalyst with a supporting P-N-P ligand utilised by the group for this chemistry in the open literature. Other P-N-P ruthenium catalysts have been used by other authors for ethanol upgrading (Chapter 1, Section 1.8.1, Scheme 1.13-1.14). However, none of these ruthenium P-N-P catalysts are isoelectronic with the most efficient ruthenium-dppm ( $(\text{Ph}_2\text{P})_2\text{CH}_2$ ) catalyst for upgrading ethanol to *n*-butanol and *iso*-butanol.<sup>34-37</sup> Hence, the aims of the present chapter are to synthesise and characterise a *N,N*-bis(diphenylphosphino)amine,  $(\text{Ph}_2\text{P})_2\text{NR}$  (where  $\text{R} = (\text{CH}_2)_3\text{Si}(\text{OMe})_3$ ), ligand and its respective ruthenium complexes. Incorporating siloxymethyl groups should allow these catalysts to be heterogenised by covalent bonding to the surface of a support material. Unpublished results from the Wass group investigating bidentate PNP ligands in ethanol upgrading have generally yielded low activity catalysts.<sup>38</sup> Therefore, before heterogenisation, it was important to gauge the efficiency of catalysts incorporating the  $\text{PN}((\text{CH}_2)_3\text{Si}(\text{OMe})_3)\text{P}$  motif under homogeneous catalytic conditions.

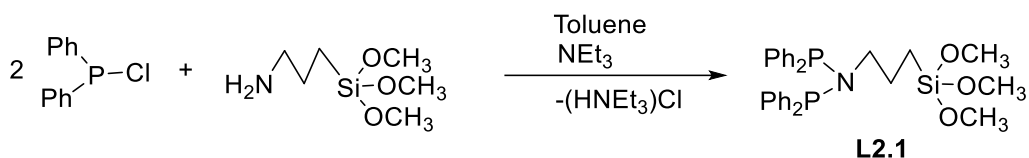
## 2.3 Results and Discussion

### 2.3.1 Synthesis and Characterization of Complex Precursors

According to literature procedures  $[\text{RuCl}_3(\text{PPh}_3)_3]$ , **[Ru]-1.5**<sup>10, 39-43</sup> and  $[\text{RuCl}_2(p\text{-cymene})_2]$ , **[Ru]-1.7**<sup>34, 35</sup> were synthesised and characterised.  $^1\text{H}$  and  $^{31}\text{P}\{^1\text{H}\}$  NMR spectra of the complexes formed matched exactly what has been reported.<sup>44-48</sup>

### 2.3.2 Synthesis of $(\text{Ph}_2\text{P})_2\text{N}(\text{CH}_2)_3\text{Si}(\text{OMe})_3$ (**L2.1**)

Using a literature method,<sup>11</sup> ligand **L2.1** was prepared by dropwise addition of two equivalents of chlorodiphenylphosphine to one equivalent of 3-aminopropyltrimethoxysilane in toluene in the presence of triethylamine at  $-40^\circ\text{C}$  and left to stir for 2 h (Scheme 2.1).



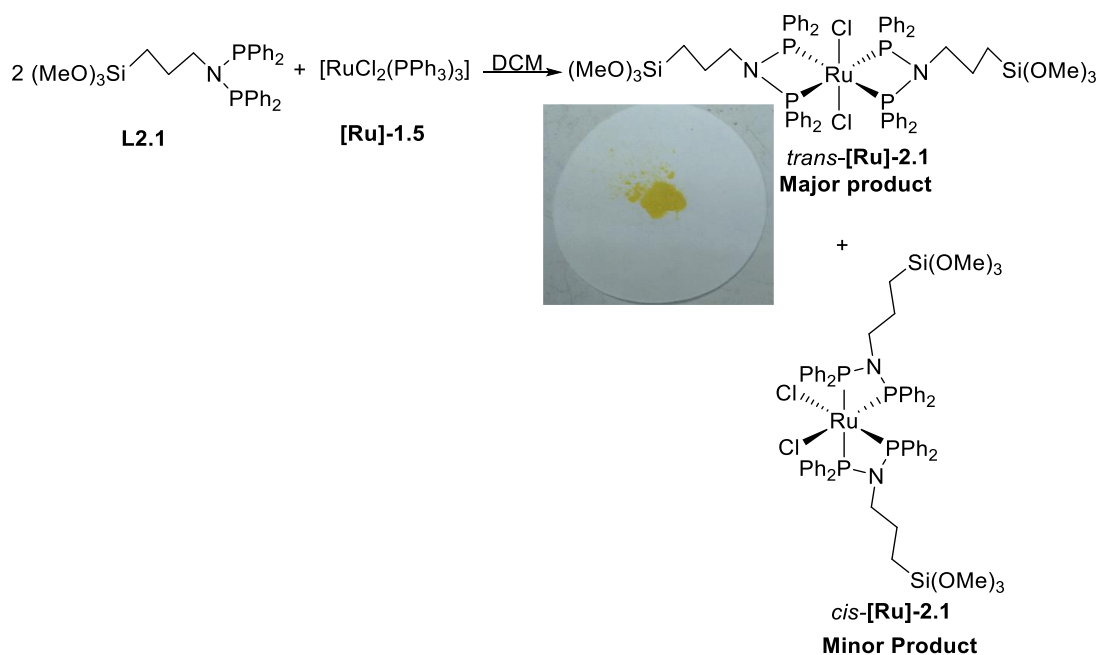
**Scheme 2.1:** Synthesis of  $(\text{Ph}_2\text{P})_2\text{N}(\text{CH}_2)_3\text{Si}(\text{OMe})_3$

A yellow oily product was obtained in 74% yield. The  $^{31}\text{P}\{^1\text{H}\}$  NMR spectrum of this ligand showed a singlet at  $\delta$  62.2 as reported in reference 11, so similar to the peaks of related P-N-P ligands.<sup>14, 21, 24</sup> This chemical shift is at low field compared to that of *N,N*-bis(diphenylphosphino)amine, dppa ( $\delta$  43.5)<sup>11</sup> and at higher field in comparison to *N,N*-bis(diphenylphosphino)methylamine ( $\delta$  74.2).<sup>18, 49</sup> “Downfield shifts of about 20 ppm is typical for a derivatised dppa ligand and is also similar to that observed on going from coordinated dppa to coordinated dppaMe (dppaMe =  $(\text{Ph}_2\text{P})_2\text{NMe}$ )”.<sup>11</sup>  $^1\text{H}$  NMR spectroscopy of the ligand in  $\text{CDCl}_3$  showed resonances that matched exactly those reported.<sup>11</sup> IR data showed a typical absorption band for a P-N-P ligand found within  $900 - 700\text{ cm}^{-1}$  literature range.<sup>21</sup> The ligand gave a characteristic vibration of  $861\text{ cm}^{-1}$  which is attributed to P-N stretching frequencies, providing an evidence for the successful synthesis of this ligand.<sup>25</sup>

### 2.3.3 Synthesis of $\text{trans-}[\text{RuCl}_2\{(\text{PPh}_2)_2\text{N}(\text{CH}_2)_3\text{Si}(\text{OCH}_3)_3\}_2]$ (**[Ru]-2.1**)

Using a modified literature procedure,<sup>10</sup> complex **[Ru]-2.1** was synthesised by the reaction of one equivalent of **[Ru]-1.5** and two equivalents of **L2.1** in dichloromethane solution at room temperature with the elimination of  $\text{PPh}_3$  to give a yellow crystalline powder in 77% yield (Scheme 2.2). The yellow complex was characterised by  $^1\text{H}$  /  $^{31}\text{P}\{^1\text{H}\}$  NMR spectroscopy, IR spectroscopy, ESI mass spectrometry and X-ray

crystallography. The  $^{31}\text{P}\{^1\text{H}\}$  NMR spectrum showed a very sharp singlet at  $\delta$  76.5 (Figure 2.1) corresponding to that of similar literature complexes<sup>9, 10, 12</sup> indicating that **L2.1** is, as expected, acting as a bidentate ligand with the two chlorine atoms *trans* to each other. The geometry of the complex with regards to single sharp phosphorus peak is assigned *trans*-**[Ru]-2.1** (Major product, Scheme 2.2).



**Scheme 2.2:** Synthesis of complex  $[\text{RuCl}_2\{(\text{PPh}_2)_2\text{N}(\text{CH}_2)_3\text{Si}(\text{OCH}_3)_3\}_2]$

A downfield shift of about 14.3 ppm relative to the free ligand peak ( $\delta$  62.2) is observed in this complex (Section 4.2.1). A similar chemical shift difference (13.6 ppm) was reported for *trans*- $[\text{RuCl}_2\{(\text{PPh}_2)_2\text{N}^n\text{Pr}\}_2]$  and corresponding free ligand ( $^n\text{Pr} = \text{propyl}$ ).<sup>12</sup> On closer inspection, two triplets were noticed which represent the isomer *cis*-**[Ru]-2.1** (minor product, Scheme 2.2, Figure 2.1(bottom)).  $^1\text{H}$  NMR peaks of complex **[Ru]-2.1** lie in the same expected region as those of the free ligand. The integration of  $\text{OCH}_3$  ligand peak of **[Ru]-2.1** gave exactly 18 protons. It is not unusual for P-N-P ligands to react with complex precursors in a 2:1 ratio to give both the *cis* and *trans* products. Some authors have reported as such and obtained the crystals of both isomers.<sup>10</sup> Separation of such *cis* and *trans* complexes can be very challenging due to similar solubilities of the isomers. IR spectroscopy is a very useful technique for determining the P-N bands of aminophosphines and their coordination compounds. The IR spectrum of **[Ru]-2.1** disclosed similar stretching frequencies to those observed for the ligand **L2.1**, suggesting its coordination. Most importantly, the P-N

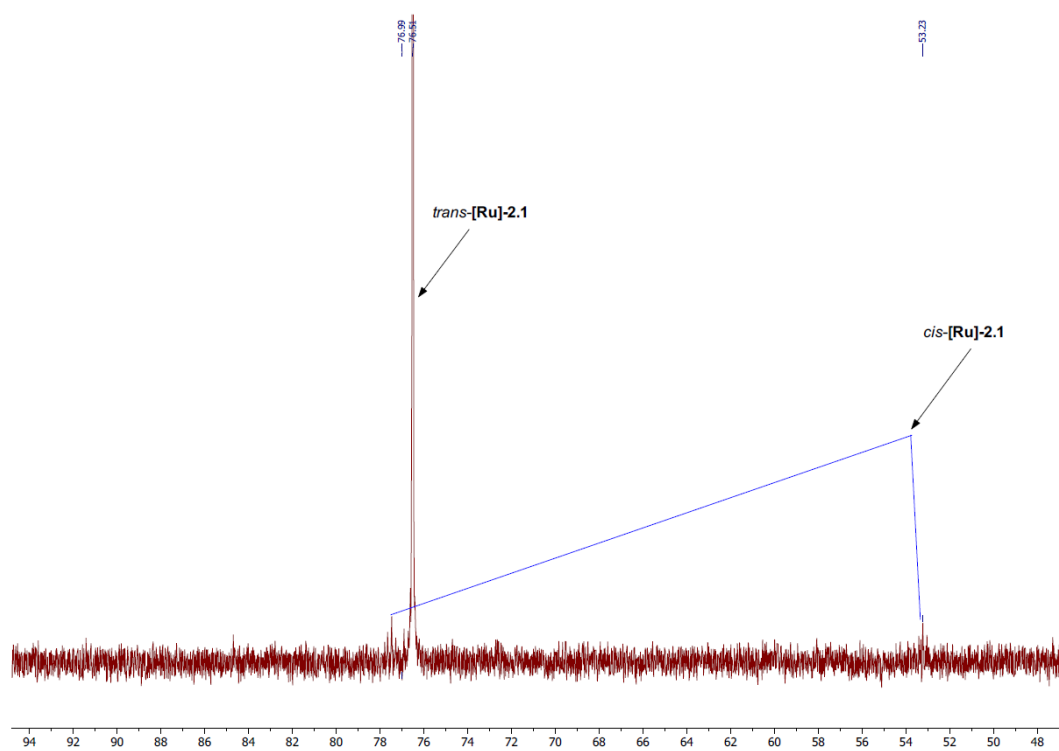
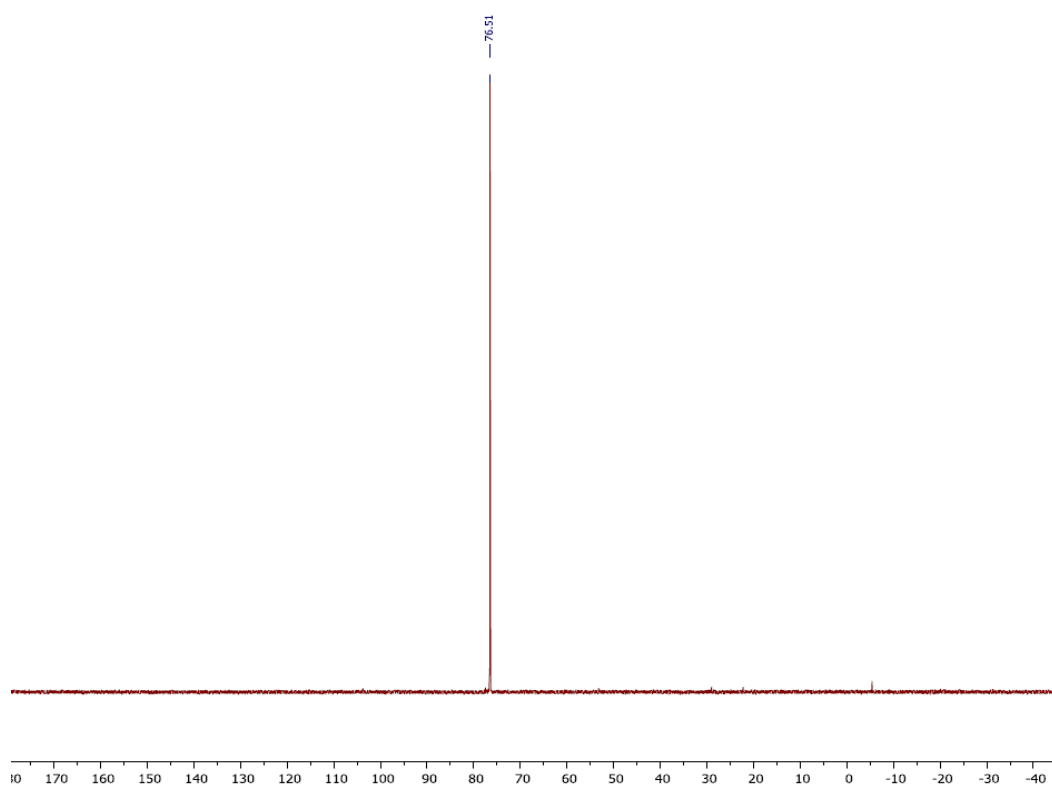


**Figure 2.1:**  $^{31}\text{P}\{^1\text{H}\}$  NMR spectrum ( $\text{CDCl}_3$ , 202 MHz) of **[Ru]-2.1**, Full NMR spectrum (Top), 50-80 ppm region (Bottom).

stretching vibration frequency of this complex appears at  $854\text{ cm}^{-1}$  close to the values reported for other similar P-N-P complexes.<sup>25</sup> As expected, complex **[Ru]-2.1**

displayed a lower P-N frequency ( $854\text{ cm}^{-1}$ ) relative to that of ligand **L2.1** ( $861\text{ cm}^{-1}$ ), providing evidence of complexation. ESI mass spectrometry gave  $m/z$  values of 1231.2449  $[\text{M} - \text{Cl}]^+$ , and 721.1249  $[\text{M} - 1\text{L2.1}]^+$  (See Appendix for mass spectrum). A yellow crystal of **[Ru]-2.1** was obtained by slow diffusion of pentane into a concentrated benzene solution which was suitable for X-ray diffraction studies. This single crystal features *cis*-**[Ru]-2.1** complex as revealed by X-ray crystallography. The crystal of *cis*-**[Ru]-2.1** is showcased in Figure 2.2 with selected bond lengths and angles (see Appendix for crystallographic data). Single crystals of *trans*-**[Ru]-2.1** were obtained but were of poor diffraction, therefore, challenging to refine. A typical one of such is displayed in Figure 2.3. It grew as twin structures with very high R-value (only one displayed). Nevertheless, the *trans* nature of complex is unequivocally confirmed. The space group is *P*-1 triclinic and it has an octahedra geometry around the ruthenium centre.

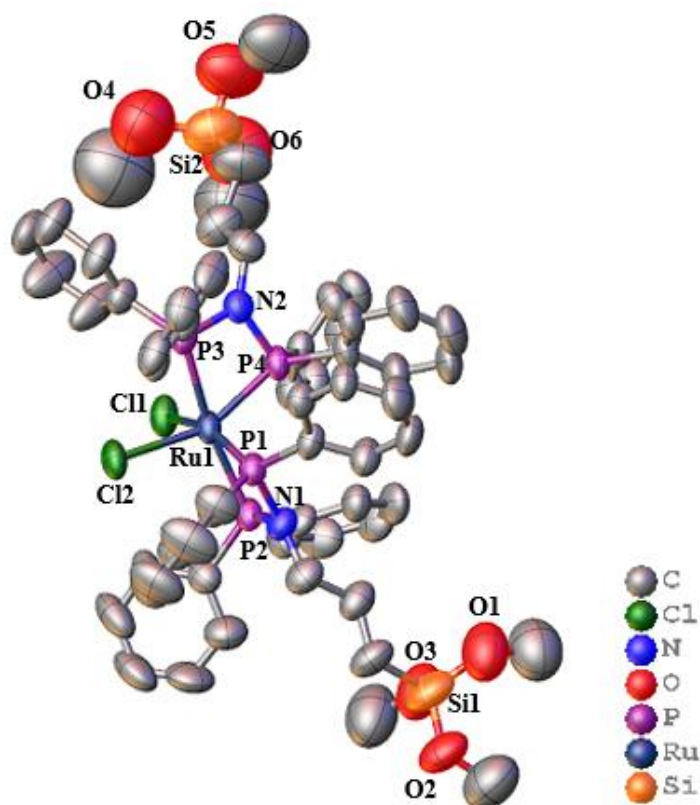


**Figure 2.2:** Single Crystal of **[Ru]-2.1** (All hydrogen atoms are omitted for clarity). **Selected bond lengths** (Å): Ru(1)-P(1) = 2.289(2), Ru(1)-P(2) = 2.3429(19), Ru(1)-P(3) = 2.3217(18), Ru(1)-P(4) = 2.3078(19), Ru(1)-Cl(1) = 2.4564(18), Ru(1)-Cl(2) = 2.4821(17), N(1)-P(1) = 1.735(6), N(1)-P(2) = 1.690(6), N(2)-P(3) = 1.689(6), N(2)-P(4) = 1.716(6), P(1)...P(2) = 2.636(2), P(3)...P(4) = 2.654(2), Si(1)-O(1) = 1.604(12), Si(1)-O(2) = 1.632(8), Si(1)-O(3) = 1.534(10), Si(2)-O(4) = 1.680(17), Si(2)-O(5) = 1.515(14), Si(2)-O(6) = 1.438(14). **Selected bond angles** (°): P(1)-Ru(1)-P(2) = 69.37(7), P(4)-Ru(1)-P(3) = 69.96(6), Cl(1)-Ru(1)-Cl(2) = 85.43(7), P(1)-Ru(1)-Cl(1) = 160.25(7), P(1)-Ru(1)-Cl(2) = 92.16(7), P(2)-Ru(1)-Cl(2) = 99.98(7), P(1)-Ru(1)-P(4) = 99.83(7), P(3)-Ru(1)-Cl(1) = 94.20(7), P(4)-Ru(1)-P(2) = 103.13(6), P(3)-Ru(1)-P(2) = 170.86(7), P(4)-Ru(1)-Cl(2) = 156.51(7), P(2)-N(1)-P(1) = 100.6(3), P(3)-N(2)-P(4) = 102.4(3).

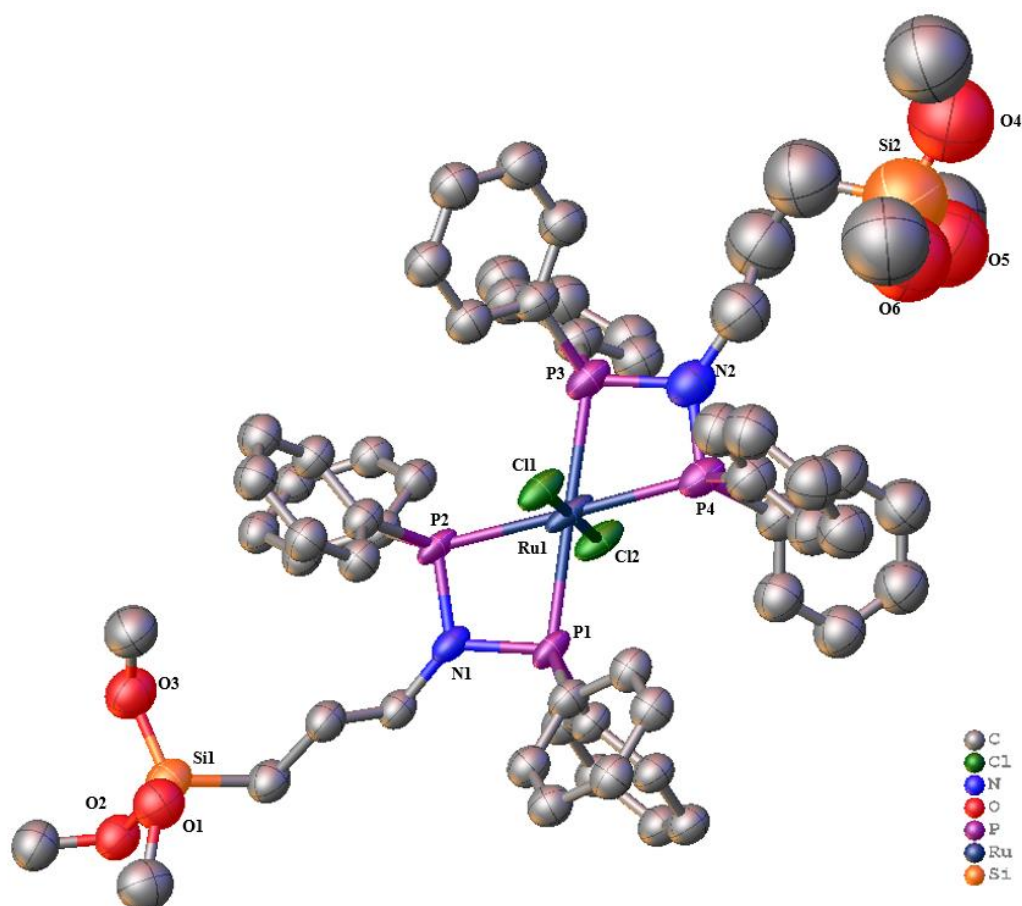


**Figure 2.3:** Single Crystal of *trans*-[Ru]-2.1 *P*-1 triclinic space group. (All hydrogen atoms are omitted for clarity).

The crystal system of *cis*-[Ru]-2.1 is monoclinic with  $P2_1/n$  space group (see Chapter 6, Appendix for crystallographic data). The structure displays a distorted octahedral arrangement around the ruthenium centre of [Ru]-2.1 in its coordination with the two *cis*-chlorido ligands, and a pair of bidentate phosphine ligands. The ruthenium atom in this complex has coordination spheres intermediate between an octahedral ( $O_h$ ) and trigonal prismatic ( $D_{3h}$ ). Such an effect is known as trigonal distortion ( $D_{3d}$ ), a condition when the two opposite faces of an octahedron move away from their original positions due to an intrinsic effect called Jahn-Teller distortion to produce a series of structures that are in between normal octahedral and trigonal-prismatic. In particular, the presence of small bite angle chelating ligand in six-coordinate complexes causes distortion from octahedral towards trigonal-prismatic geometry (Figure 2.4).<sup>50</sup>

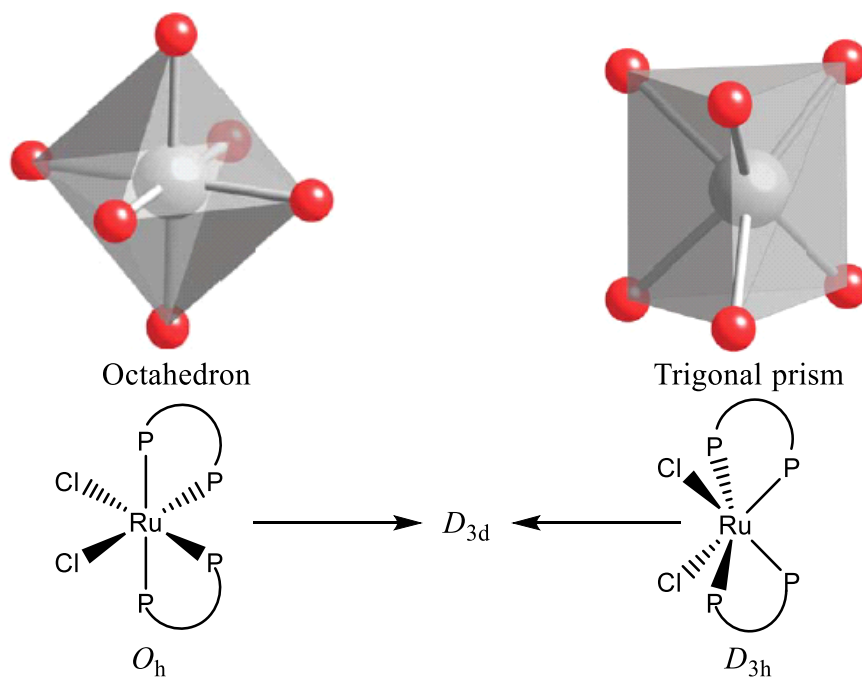


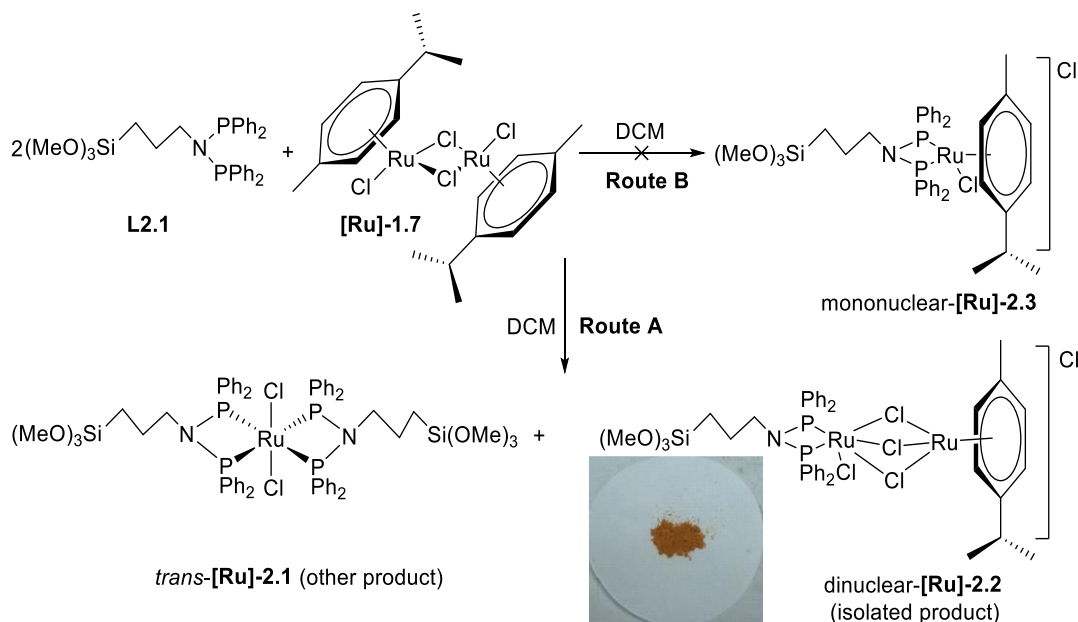
**Figure 2.4:** Trigonal distortion of octahedral complex.<sup>50</sup>

The distortion in *cis*-[Ru]-2.1 can be clearly seen in the bond lengths and angles displayed in Figure 2.1. Ru(1)-Cl(1) and Ru(1)-Cl(2) are 2.4564(18) Å and 2.4821(17) Å respectively. Ru(1)-P(1), Ru(1)-P(2), Ru(1)-P(3), Ru(1)-P(4) are 2.289(2) Å, 2.3429(19) Å, 2.3217(18) Å and 2.3078(19) Å respectively. From this data, the Ru-Cl and Ru-P bond lengths are all comparable with other reported [RuCl<sub>2</sub>(P-N-P)<sub>2</sub>] complexes.<sup>12, 14, 51</sup> All the bonds angles around the ruthenium centre deviate significantly from the usual 90° for octahedral complexes. The two chlorido ligands are pushed closer together as a result of the bite angle imposed by the chelating **L2.1** ligands to metal centre giving a Cl(1)-Ru(1)-Cl(2) bond angle equal to 85.43° (<90°). The two chlorine atoms, therefore, adopt a *cis* geometry. Additionally, each of two bidentate ligands coordinates with the ruthenium centre to form a four-membered metallacycle Ru-P-N-P ring. The inherent strain in the four-membered chelate ring causes the P(1)-Ru(1)-P(2) and P(4)-Ru(1)-P(3) bond angles to be approximately 70° each, far less than 90°. Apparently, the P-Ru-P angles are greatly influenced by the metalacyclic Ru-P-N-P ring.<sup>12, 51</sup> Furthermore, the trigonal distortion experienced by complex *cis*-[Ru]-2.1 makes one of the two trigonal faces occupied by the two bidentate ligands to be twisted (Figure 2.2). This effect led to a reduction of the P(1)-P(2) interatom distance. Consequently, the homoatomic P(1)-P(2) and P(3)-P(4) bond distances differ slightly (2.636(2) Å and 2.654(2) Å respectively). In agreement

with this, the Ru(1)-P(1) bond length (2.289(2) Å) is significantly shorter than that observed for Ru(1)-P(2) (2.3429(19) Å). Also, the P-atoms *trans* disposed to each other (Ru(1)-P(2) and Ru(1)-P(3)) display larger bond lengths (2.3429(19) Å and 2.3217(18) Å respectively) than those (Ru(1)-P(2) and Ru(1)-P(3)) *cis* to one another/*trans* to chlorine atoms (2.289(2) Å and 2.3078(19) Å respectively). Moreover, the P(2)-N(1)-P(1) and P(3)-N(2)-P(4) bond angles are 100.6(3) and 102.4(3) respectively. In chelated P-N-P complexes, as revealed by crystallographic and computational studies, the small bite angle of this type of ligand tends to compress the P-N-P bond angles to around 100° due to formation of strained four-membered ring with higher angle-strain energy as compared with dppm ligand-type.<sup>52</sup> Correspondingly, the P-N-P angle (~100°) of complex *cis*-[Ru]-2.1 is significantly less than the values obtained from crystallographically characterised uncoordinated P-N-P ligands (>112°).<sup>4, 26</sup> Interestingly, the P-N-P angles (~100°) and P-N single bond lengths (~1.7 Å) from crystallographic data of *cis*-[Ru]-2.1 agree with literature values of related Ru-complexes.<sup>12, 14, 25</sup>

### 2.3.4 Reaction of L2.1 with dichloro( $\eta^6$ -*p*-cymene)ruthenium(II) dimer

Using a method adapted from the literature,<sup>10, 11</sup> two equivalents of ligand L2.1 were treated with one equivalent of complex [Ru]-1.7 in DCM at room temperature with continuous stirring (Scheme 2.3).



**Scheme 2.3:** Reaction of L2.1 with dichloro( $\eta^6$ -*p*-cymene)ruthenium(II) dimer to form a mixture of complexes

The expectation was that bridge splitting of the dimer would occur to form complex **[Ru]-2.3**, however, after 1 h,  $^{31}\text{P}\{^1\text{H}\}$  NMR spectroscopy of the crude sample exhibited three peaks at  $\delta$  84.3, 77.4 and 76.2 (Figure 2.5), indicating that three complexes were present. After recrystallisation from dichloromethane/ether, an orange crystalline powder was obtained in 51% yield which gave a single  $^{31}\text{P}\{^1\text{H}\}$  NMR peak at  $\delta$  85.1 ppm (Figure 2.6).  $^{31}\text{P}\{^1\text{H}\}$  NMR spectroscopy of the dichloromethane/ether filtrate was recorded and showed a prominent peak at  $\delta$  77.7 with a trace of isolated product at  $\delta$  85.1 (Figure 2.7). The prominent chemical shift in the filtrate ( $\delta$  77.7) closely resembled that of the *trans*-complex **[Ru]-2.1** obtained in the previous section (Section 2.4.2, Scheme 2.2, Figure 2.1) and the peak at  $\delta$  85.1 is assigned to cationic dinuclear complex **[Ru]-2.2** based on the crystal structure and information obtained from X-ray diffraction studies of the isolated product.

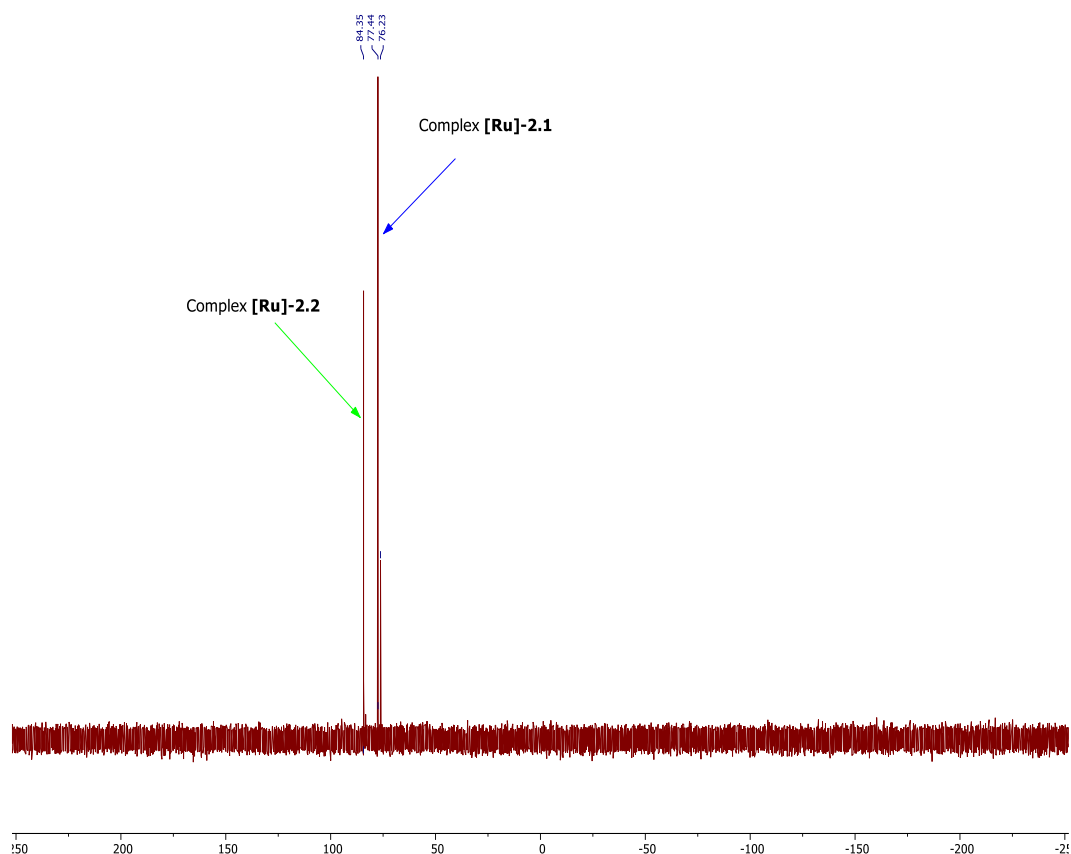


**Figure 2.5:**  $^{31}\text{P}\{^1\text{H}\}$  NMR spectrum (unlocked, 162 MHz) obtained after 1h of reaction between **L2.1** and dichloro( $\eta^6$ -*p*-cymene)ruthenium(II) dimer

The  $^1\text{H}$  NMR spectrum of **[Ru]-2.2** reveals the presence of  $\eta^6$ -*p*-cymene and coordinated **L2.1**. In contrast to the result obtained for *trans*-**[Ru]-2.1** in Section 2.4.2, the integration of the  $\text{OCH}_3$  proton peak gave 9, evidence of only one bidentate **L2.1**

coordination. Also, ESI mass spectrometry gave a result consistent with the mass of isolated dinuclear complex **[Ru]-2.2**. The IR spectrum of **[Ru]-2.2** exhibits similar stretching frequencies to those observed for the ligand **L2.1**, again suggesting its coordination. Substantially, the P-N stretching vibration frequency of this complex appears at  $842\text{ cm}^{-1}$  close to the values reported for other similar P-N-P complexes.<sup>25</sup> As expected, complex **[Ru]-2.2** displayed a lower P-N frequency ( $842\text{ cm}^{-1}$ ) relative to the ligand **L2.1** ( $861\text{ cm}^{-1}$ ), another evidence of complexation.

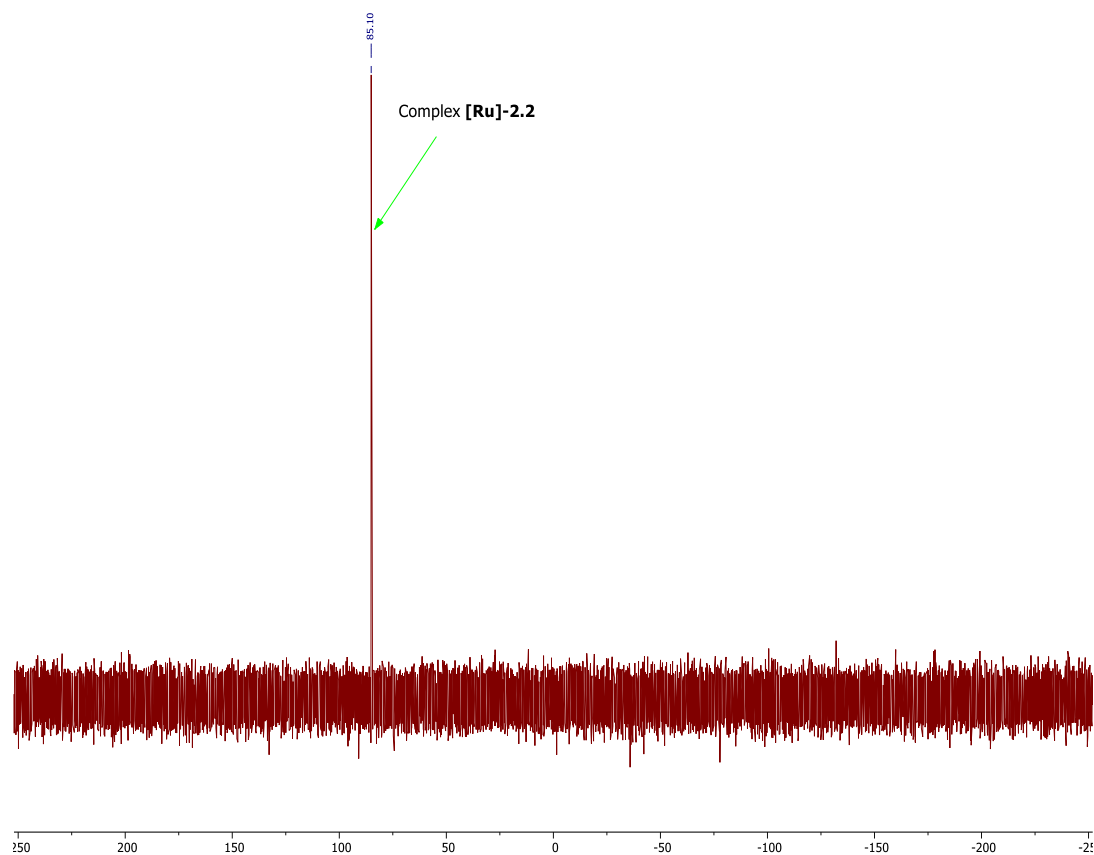


**Figure 2.6:**  $^{31}\text{P}\{^1\text{H}\}$  NMR spectrum ( $\text{CDCl}_3$ , 162 MHz) of isolated product **[Ru]-2.2**

Good quality single-crystals of **[Ru]-2.2** suitable for X-ray diffraction were successfully obtained by layering pentane on a dichloromethane/toluene solution of the complex. Complex **[Ru]-2.2** crystallised as **[Ru]-2.2.CH<sub>2</sub>Cl<sub>2</sub>**. The molecular structure is shown in Figure 2.8 with selected bond lengths and angles (see Appendix for crystallographic data). The crystal system of **[Ru]-2.2** is triclinic with *P*-1 space group (see Appendix). The two ruthenium atoms (Ru1 and Ru2) in this complex exhibit an octahedral ( $O_h$ ) coordination geometry with three bridging chlorine atoms.

Ligand **L2.1** occupies the coordination spheres of one of the ruthenium centres (Ru2) in a monochelating fashion in conjunction with four chlorine atoms. There is a little

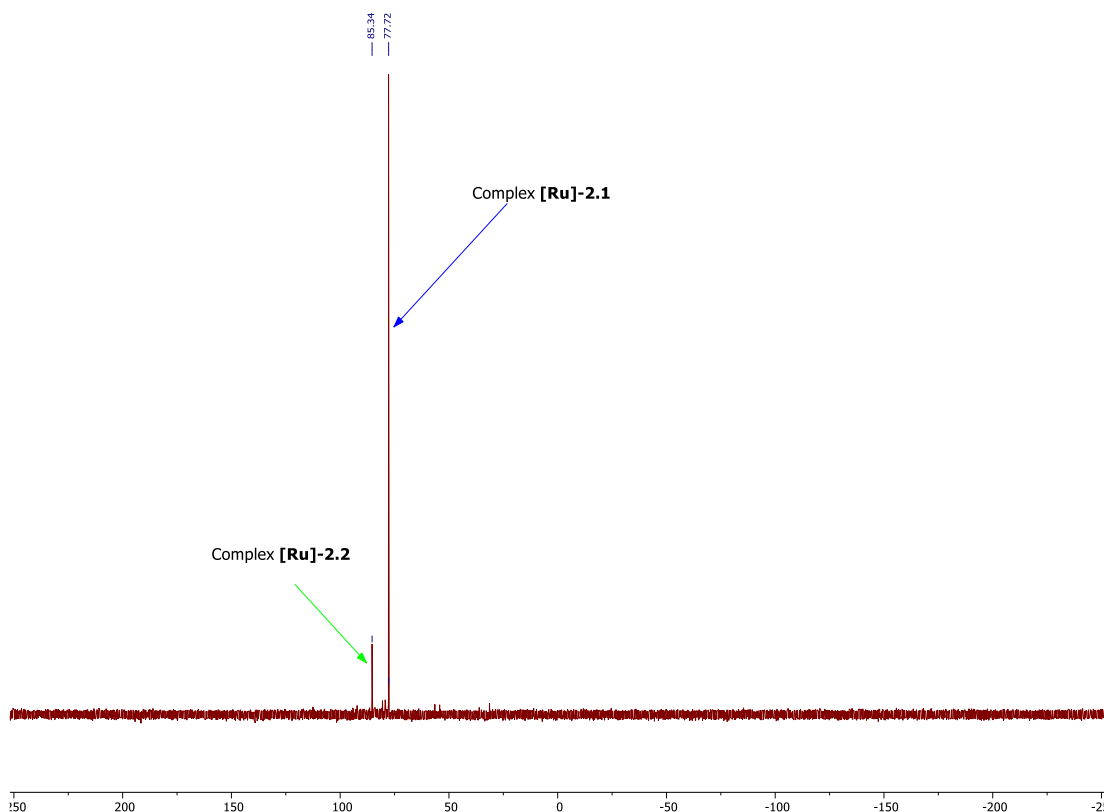


**Figure 2.7:**  $^{31}\text{P}\{^1\text{H}\}$  NMR spectrum ( $\text{CDCl}_3$ , 162 MHz) of the filtrate solution from the reaction of **L2.1** with dichloro( $\eta^6$ -*p*-cymene)ruthenium(II) dimer distortion in the octahedral arrangement around this ruthenium centre (Ru2) with bond angles of  $70.76(4)^\circ$  for P(1)-Ru(2)-P(2) (strained four-membered ring),  $167.07(3)^\circ$  for Cl(4)-Ru(2)-Cl(1) (two *trans* chlorido), and  $79.91(3)^\circ$  for Cl(3)-Ru(2)-Cl(2) (two *cis* chlorido). Here, the P-N-P bond angle ( $97.26(17)^\circ$ ) of complex **[Ru]-2.2** is significantly smaller than the normal trigonal angle if the nitrogen atom is  $\text{sp}^2$ -hybridised.<sup>12</sup> Also, the P-N bond lengths ( $1.714(3)$  Å and  $1.712(3)$  Å for P(1)-N(1) and P(2)-N(1) respectively) of complex **[Ru]-2.2** is in general agreement with literature values of associated Ru-complexes.<sup>5, 51</sup> However, the P-N bond lengths in this complex are slightly less than the standard acceptable P-N lengths ( $1.77$  Å), revealing some degree of P-N  $\pi$ -bonding.<sup>12</sup> In harmony with this, the total bond angles around the nitrogen atom are  $356.96^\circ$ , almost planar ( $360^\circ$ ). Consistently, the sum of bond angles of the metalacyclic Ru-P-N-P ring is  $359.92^\circ$ , indicating a planar ring system.<sup>12, 51</sup> Furthermore, the other ruthenium centre (Ru1) manifests a typical three legged piano-stool distorted octahedral geometry, in which *p*-cymene and three

bridging chlorido ligands are coordinated to the metal centre. Complex **[Ru]-2.2** possesses ruthenium-carbon (Ru1-C2 to Ru1-C7) bond lengths within the range of 2.163(4) – 2.184(4) Å which are shorter than typical Ru-C bond lengths (2.190(3) – 2.328(3) Å) in similar mononuclear complexes [RuCl( $\eta^6$ -*p*-cymene)(Ph<sub>2</sub>P)<sub>2</sub>NR)], (R = CH<sub>2</sub>Py, Ph, *p*-tolyl, X = BF<sub>4</sub> or PF<sub>6</sub>).<sup>5</sup> In summary, the two ruthenium centres in complex **[Ru]-2.2** crystal exist in the +3 and +2 oxidation states relative to the chlorides.

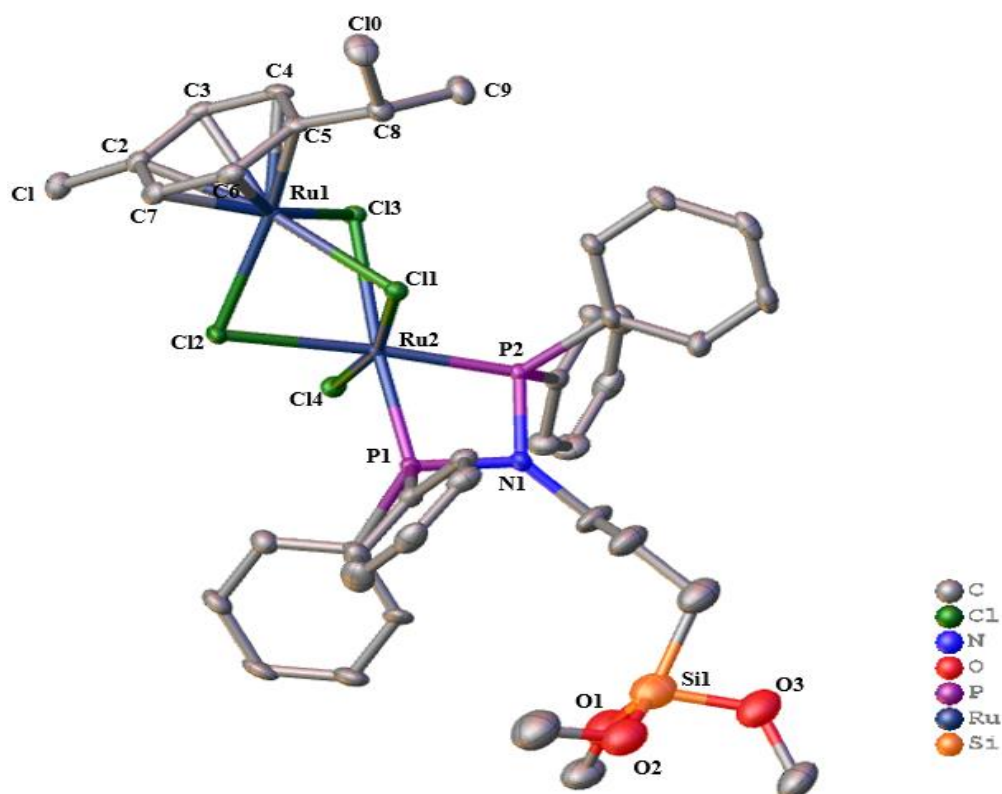


**Figure 2.8:** Single crystal of complex **[Ru]-2.2** with *P*-1 space group. Hydrogen atoms, CH<sub>2</sub>Cl<sub>2</sub> molecules and Cl<sup>-</sup> ion are omitted for clarity. **Selected bond lengths:** Ru(1)-C(2) = 2.184(4), Ru(1)-C(3) = 2.163(4), Ru(1)-C(4) = 2.169(4), Ru(1)-C(5) = 2.177(4), Ru(1)-C(6) = 2.180(4), Ru(1)-C(7) = 2.174(4), Ru(1)-Cl(1) = 2.4545(9), Ru(1)-Cl(2) = 2.4480(9), Ru(1)-Cl(3) = 2.4255(9), Ru(2)-Cl(1) = 2.4315(9), Ru(2)-Cl(2) = 2.5302(9), Ru(2)-Cl(3) = 2.5122(9), Ru(2)-Cl(4) = 2.3769(9), Ru(2)-P(1) = 2.225(10), Ru(2)-P(2) = 2.2185(10), P(1)-N(1) = 1.714(3), P(2)-N(1) = 1.712(3); **Selected bond angles:** Ru(2)-Cl(1)-Ru(1) = 84.72(3), P(1)-Ru(2)-P(2) = 70.76(4), Cl(4)-Ru(2)-Cl(1) = 167.07(3), P(2)-Ru(2)-Cl(1) = 99.11(3), P(2)-N(1)-P(1) = 97.26(17), Cl(1)-Ru(2)-Cl(2) = 79.11(3), Cl(1)-Ru(2)-Cl(3) = 79.10(3), Cl(3)-Ru(2)-Cl(2) = 79.91(3).

It should be noted that Zhang *et al.* have recently reported the crystal structure of **[Ru]-2.2** as **[Ru]-2.2·½H<sub>2</sub>O** with monoclinic *P*2<sub>1</sub>/*n* space group showing a single <sup>31</sup>P NMR peak in CDCl<sub>3</sub> at δ 60.1<sup>53</sup> even though the ligand peak (**L2.1**) has been reported at δ

62.<sup>11</sup> Additionally, the ligand <sup>31</sup>P NMR peak was not reported and compared against that of complex **[Ru]-2.2.½H<sub>2</sub>O**. In the present study, <sup>31</sup>P NMR peak of ligand **L2.1** was confirmed (δ 62) and after complexation with **[RuCl<sub>2</sub>(η<sup>6</sup>-p-cymene)]<sub>2</sub>** in 2:1 ratio gave complex **[Ru]-2.2** at δ 85 with <sup>31</sup>P{<sup>1</sup>H} NMR spectroscopy. The chemical shift of complex **[Ru]-2.2** is at low field compared with that of the free ligand and downfield shift range of 18-25 ppm is typical for dinuclear complexes of similar ligands.<sup>27, 54</sup>

### 2.3.5 Reaction of **L2.1** with dichloro(η<sup>6</sup>-p-cymene)ruthenium(II) dimer in varied ratios

Notably, the targeted cationic mononuclear **[Ru]-2.3** was not formed in the reaction of two equivalents of **L2.1** and one equivalent of **[RuCl<sub>2</sub>(η<sup>6</sup>-p-cymene)]<sub>2</sub>** (Scheme 2.3, Route B). Consequently, varied ratios (1:1, 1:2, 1:4 and 4:1) of **L2.1** and **[RuCl<sub>2</sub>(p-cymene)]<sub>2</sub>** respectively were considered with the aim of obtaining the targeted cationic complex **[Ru]-2.3** but none gave this product. Surprisingly, these ratios still gave mixtures of complexes **[Ru]-2.2** and *trans*-**[Ru]-2.1** with exception of molar ratio 4:1 that gave exclusively complex **[Ru]-2.1** as strictly yellow product. <sup>31</sup>P{<sup>1</sup>H} NMR spectroscopy of the crude samples of the four ratios are shown in Figure 2.9. Uniquely, aside 4:1 ratio, complex **[Ru]-2.2** was isolated as the major products of the reaction irrespective of the reactant's molar ratio.

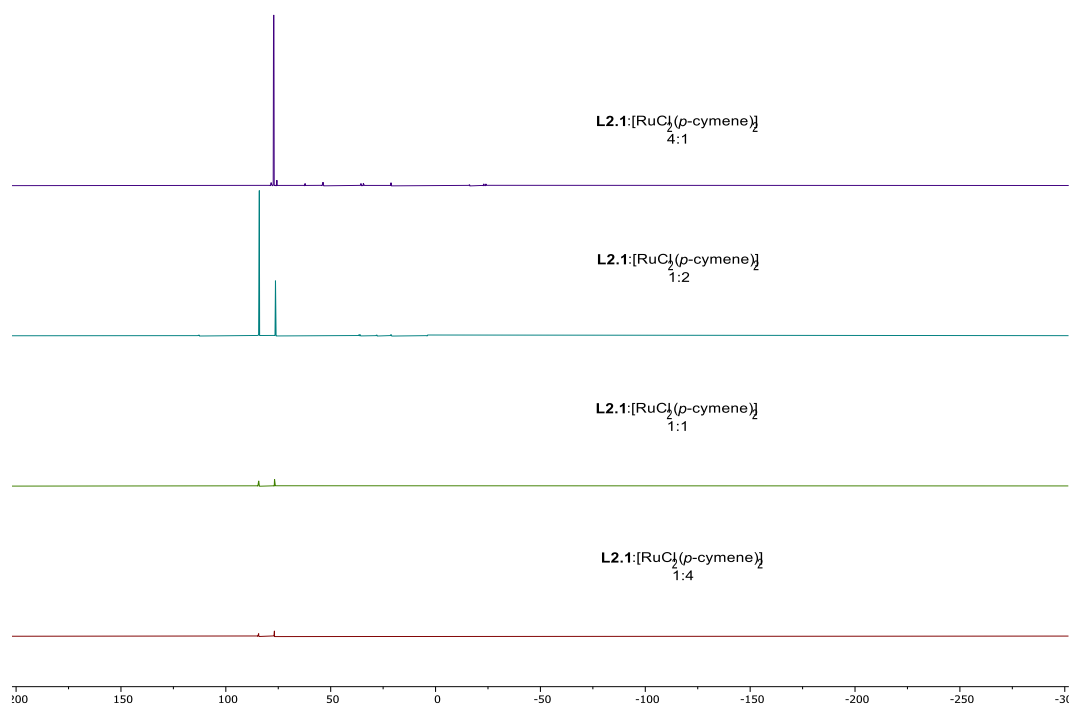
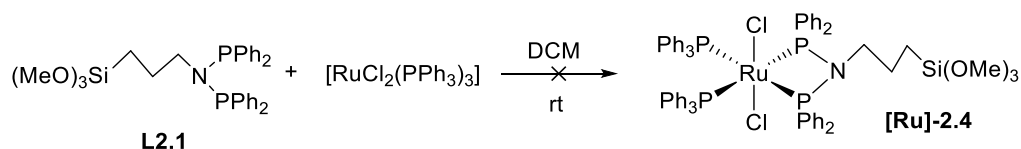


**Figure 2.9:** <sup>31</sup>P{<sup>1</sup>H} NMR spectrum (unlocked, 202 MHz) of **L2.1** and **[RuCl<sub>2</sub>(p-cymene)]<sub>2</sub>** reaction mixture

## 2.3.6 Synthesis of related Complexes.

### 2.3.6.1 Reaction of L2.1 and [RuCl<sub>2</sub>(Ph<sub>3</sub>P)<sub>3</sub>] in equimolar ratio



**Scheme 2.4:** Reaction of L2.1 and [RuCl<sub>2</sub>(Ph<sub>3</sub>P)<sub>3</sub>] in equimolar ratio

A reaction of **L2.1** and [RuCl<sub>2</sub>(PPh<sub>3</sub>)<sub>3</sub>] in an equimolar ratio at room temperature was carried out with the hope of synthesising complex **[Ru]-2.4**; however, the <sup>31</sup>P{<sup>1</sup>H} NMR spectroscopy of the isolated product showed formation of *trans*-**[Ru]-2.1** with a singlet at δ 76.5. Two other characteristic peaks were observed at δ 29.1 and δ -5.5 assigned to free Ph<sub>3</sub>P=O and PPh<sub>3</sub> respectively (Figure 2.10). Balakrishna *et al.*, reported similar observation with non-siloxy PPh<sub>2</sub>N(R)PPh<sub>2</sub> (R=H, Me, Et, <sup>n</sup>Pr, <sup>i</sup>Pr, <sup>n</sup>Bu, Ph) ligands.<sup>12</sup>

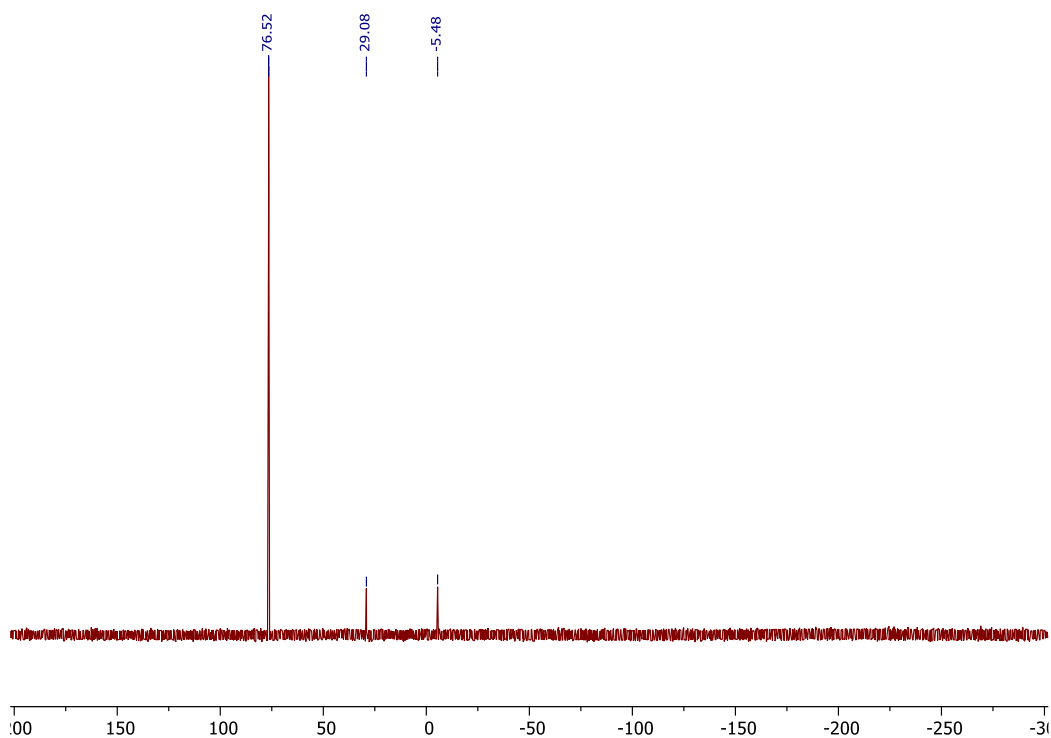
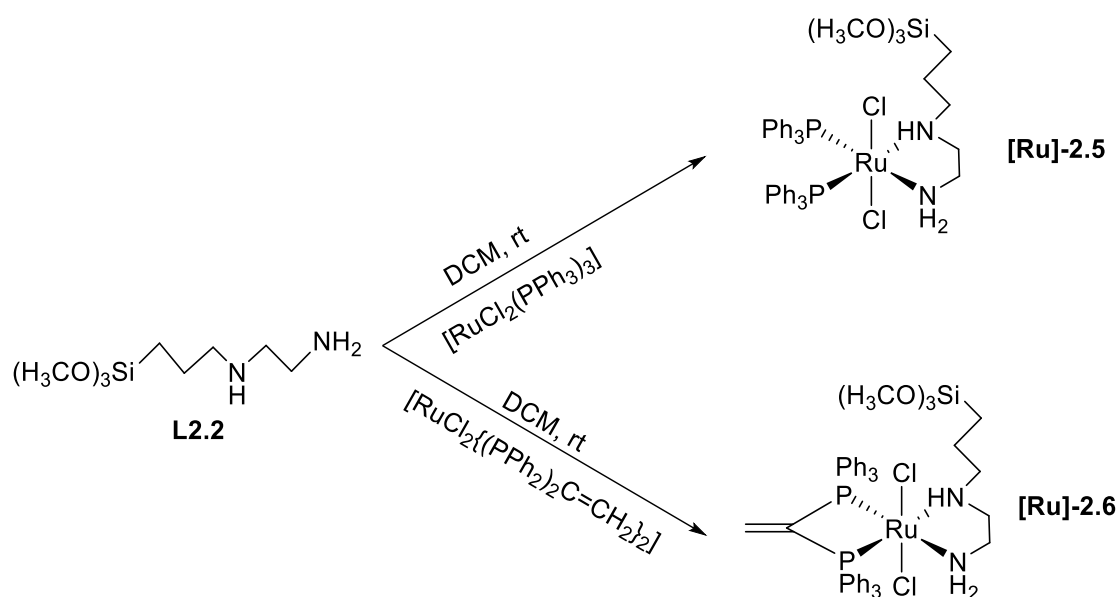


**Figure 2.10:** <sup>31</sup>P{<sup>1</sup>H} NMR spectrum (CDCl<sub>3</sub>, 202 MHz) of **L2.1** and [RuCl<sub>2</sub>(*p*-cymene)]<sub>2</sub> reaction mixture

### 2.3.6.2 Reaction of L2.2 with [RuCl<sub>2</sub>(PPh<sub>3</sub>)<sub>3</sub>] and [RuCl<sub>2</sub>{(PPh<sub>2</sub>)<sub>2</sub>C=CH<sub>2</sub>}<sub>2</sub>]

Adapting a literature method,<sup>55</sup> complex **[Ru]-2.5** was synthesised by the addition of N-[3-(trimethoxysilyl)propyl]ethane-1,2-diamine (**L2.2**) to [RuCl<sub>2</sub>(PPh<sub>3</sub>)<sub>3</sub>] in dichloromethane solution (Scheme 2.5).



**Scheme 2.5:** Synthesis of complexes **[Ru]-2.5** and **[Ru]-2.6**

The silyl amine ligand coordinate to the ruthenium metal centre through the two nitrogen atoms by the loss of two  $\text{PPh}_3$  in  $C_2$  axis of the complex. The  $^{31}\text{P}\{^1\text{H}\}$  NMR of isolated product showed two doublets at 39.4 ppm and 43.5 ppm with coupling constant of 31.95 Hz, implying that the two  $\text{PPh}_3$  ligands in complex **[Ru]-2.5** are *cis* to each other. The  $^1\text{H}$  NMR spectrum matched reported data. Complex **[Ru]-2.6** was prepared in a similar way using  $[\text{RuCl}_2\{(\text{PPh}_2)_2\text{C}=\text{CH}_2\}_2]$  as complex precursor, but the isolated product remains insoluble in all deuterated solvents used (chloroform- $d$ , methanol- $d_4$ , dichloromethane- $d_2$  and dimethyl sulfoxide- $d_6$ ) precluding NMR analysis and stereochemical assignment.

### 2.3.7 Catalytic Activity

In recent years, Wass and co-workers have reported that P–P and P–N Ru(II) complexes are active catalysts for upgrading ethanol to *n*-butanol/*iso*-butanol in the presence of alkoxide bases following the Guerbet mechanism.<sup>34, 37</sup> It was reported that those catalysts function in the dehydrogenation and rehydrogenation steps of the Guerbet mechanism and the base facilitates the aldol-condensation step. The Guerbet mechanism for 1-butanol and *iso*-butanol production can be found in Chapter 1, Section 1.6, Schemes 1.4 and 1.5. The present study is an expansion of this work to investigate the activity *N,N*-bis(diphenylphosphino) aminoalkyltrialkoxysilanes,  $(\text{Ph}_2\text{P})_2\text{NR}$  ( $\text{R} = (\text{CH}_2)_3\text{Si}(\text{OR}')_3$ ,  $\text{R}' = \text{methyl}$ ) Ru(II) complexes for ethanol upgrading. To the best of our knowledge, the application of such catalysts in Guerbet

chemistry remains unknown. Therefore, these P-N-P catalysts were screened for ethanol upgrading to 1-butanol and *iso*-butanol using optimised standard conditions developed by Wass *et al.*<sup>34-36</sup> All reactions were performed in a 100 mL Parr autoclave. The post catalytic liquid products from these systems were analysed and identified by gas chromatography (GC) using hexadecane as internal standard and also, confirmed by <sup>1</sup>H/<sup>13</sup>C{<sup>1</sup>H} NMR spectroscopy. Notably, the ethanol conversion was calculated based on only the liquid products formed with product yield and selectivity determined accordingly. Besides the major liquid alcohols produced in these systems, other solid and gaseous side products were formed concomitantly. Though, analyses of the solid and gaseous products were not carried out in the present study, Wass *et al.*<sup>34, 35, 37, 56</sup> and other authors<sup>57, 58</sup> have identified the presence of sodium acetate, sodium formate and sodium carbonate in the solid products as well as H<sub>2</sub>, CO, CO<sub>2</sub>, O<sub>2</sub> and C<sub>1</sub>-C<sub>4</sub> hydrocarbons as components of the gas phase. Since white solids and pressure built up were observed in the current catalytic systems, it was therefore assumed that similar identified solid and gas components were present in the post catalytic solids and the headspace gases.

### 2.3.7.1 Ethanol/methanol Upgrading to Iso-butanol

Herein, catalyst screening was conducted to evaluate the catalytic activity of complexes **[Ru]-2.1** and **[Ru]-2.2** for ethanol-methanol upgrading to *iso*-butanol using sodium methoxide (NaOMe) as the co-catalyst for 2, 24, and 48 h at 180°C. In addition to this, an *in-situ* reaction was carried out with ligand **L2.1** and pre-catalysts [RuCl<sub>2</sub>(PPh<sub>3</sub>)<sub>3</sub>] (**[Ru]-1.5**) and [RuCl<sub>2</sub>(*p*-cymene)]<sub>2</sub> (**[Ru]-1.7**). Also, the role of the alkoxide base was tested by catalytic reaction with only the base in the absence of a transition metal catalyst. Results are listed in Table 2.1. Good selectivity was observed for all catalytic runs with the exception of runs 15 and 16 in which a transition metal catalyst was absent. Previous studies have shown that a metal centre and a co-catalyst base are required for the Guerbet reaction.<sup>34-36, 59-61</sup> The Wass group previously reported [RuCl<sub>2</sub>(P-P)<sub>2</sub>] (P-P = 1,1-bis(diphenylphosphino)methane) complex (**[Ru]-1.11**) as the most efficient for this conversion among those studied. The group also studied several [RuCl<sub>2</sub>(P-N)<sub>2</sub>] complexes and found **[Ru]-1.12** was the most successful of this class. Complexes **[Ru]-1.11** and **[Ru]-1.12** were the benchmarks for

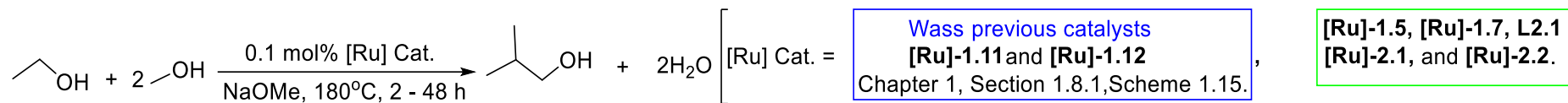


**Table 2.1:** Ruthenium catalysed conversion of ethanol and methanol to *iso*-butanol.

Run <sup>a</sup>	Catalysts	Time (h)	Conversion <sup>b</sup> (%)	Total TON <sup>c</sup>	TON <sup>d</sup> (yield) <sup>e</sup> [selectivity] %				
					<i>iso</i> -butanol	1-Propanol	1-butanol	2-methyl-1-butanol	Hexanol
1 <sup>fg</sup>	[Ru]-1.11	2	66	660	650(65)[98]	10(1)[2]	<1 <sup>h</sup>	-	-
2 <sup>fg</sup>	[Ru]-1.11	20	75	750	750(75)[100]	<1 <sup>h</sup>	<1 <sup>h</sup>	-	-
3 <sup>fg</sup>	[Ru]-1.12	2	42	420	380(38)[92]	30(3)[7]	<1 <sup>h</sup>	-	-
4 <sup>fg</sup>	[Ru]-1.12	20	56	560	510(51)[90]	60(6)[10]	<1 <sup>h</sup>	-	-
5	[Ru]-2.1	2	28	280	90(9)[72]	20(2)[18]	-	20(2)[9]	<1 <sup>h</sup>
6	[Ru]-2.1	24	79	790	440(44)[87]	20(2)[4]	10(1)[1]	-	120(12)[8]
7	[Ru]-2.1	48	77	770	580(58)[91]	30(3)[5]	-	-	90(9)[5]
8	[Ru]-2.2	2	25	250	80(8)[74]	30(3)[26]	-	-	-
9	[Ru]-2.2	24	78	780	170(17)[87]	20(2)[11]	-	-	10(1)[2]
10	[Ru]-2.2	48	86	860	270(27)[89]	20(2)[7]	-	-	30(3)[4]
11	[Ru]-1.5/L2.1	24	62	620	310(31)[91]	30(3)[9]	-	-	-
12	[Ru]-1.7/L2.1	24	69	690	190(19)[85]	30(3)[13]	-	-	10(1)[2]
13	[Ru]-1.5	24	86	860	440(44)[96]	10(1)[2]	-	-	30(3)[2]
14	[Ru]-1.7	24	60	600	150(15)[76]	40(4)[20]	-	-	30(3)[5]
15	L2.1	24	<1 <sup>h</sup>	-	<1 <sup>h</sup>	-	-	-	-
16	-	24	<1 <sup>h</sup>	-	<1 <sup>h</sup>	-	-	-	-
17	[Ru]-2.5	2	14	140	110(11)[96]	10(1)[5]	-	-	-

<sup>a</sup>Conditions: Ethanol (1 mL, 17.13 mmol), methanol (10 mL, 247.13 mmol), [Ru] catalyst (0.01713 mmol, 0.1 mol%), NaOMe base (34.26 mmol, 200 mol%), mol% is based on ethanol substrate, 180 °C. <sup>b</sup>Total conversion of ethanol to liquid product as determined by GC analysis of the liquid phase. <sup>c</sup>Total TON based on mmol of total ethanol converted to products per mmol of [Ru] catalyst (ethanol equivalent relative to mmol of catalysts x conversion = 1000 x conversion). <sup>d</sup>TON based on mmol of any product formed per mmol [Ru] catalyst (ethanol equivalent relative to mmol of catalysts x product yield = 1000 x product yield). <sup>e</sup>Total yield and selectivity of alcohol products in the liquid fraction as determined by GC. <sup>f</sup>Previous work.<sup>36</sup> <sup>g</sup>Ethanol conversion based on just liquid products formed (i.e. *iso*-butanol, propanol and 1-butanol). <sup>h</sup>Conversion, yield or selectivity value below 0.5%.

this study (entries 1-2 and entries 3-4 respectively). The P-N-P complexes **[Ru]-2.1** (entries 5-7) and **[Ru]-2.2** (entries 8-10) under investigation catalysed the reaction of ethanol to *iso*-butanol, however, they were not as effective as catalysts **[Ru]-1.11** and **[Ru]-1.12** (entries 1-10) reported by Wass *et al.* Also, the combinations of 1:2 molar equivalents of metal precursor **[Ru]-1.5** or **[Ru]-1.7** and P-N-P ligand **L2.1** were employed as catalysts for this transformation and in comparison, the preformed catalysts **[Ru]-2.1** showed better activity with improved *iso*-butanol yield and ethanol conversion (entries 6 and 11). Additionally, enhanced *iso*-butanol selectivity was achieved with preformed catalyst **[Ru]-2.1** but both yield and selectivity decreased with preformed catalyst **[Ru]-2.2** (entries 6 and 11, 9 and 12). Contrary to *iso*-butanol results, higher 1-propanol yield and selectivity were obtained from the *in-situ* runs (entries 6 and 11, 9 and 12). For 1-hexanol formation, better yield favoured *in-situ* run with **[Ru]-1.7** while no 1-hexanol was detected in the *in-situ* run with **[Ru]-1.5**. In the pre-catalyst run only, **[Ru]-1.7** performed poorly without the P-N-P ligand resulting in a decrease in ethanol conversion, *iso*-butanol selectivity and yield (entries 12 and 14). Conversely, pre-catalyst **[Ru]-1.5** gave higher ethanol conversion, *iso*-butanol yield and selectivity in the absence of the P-N-P ligand (entries 11 and 13). Subsequent comparison of the activity of the two pre-catalysts were examined for other alcohols with higher production of 1-propanol obtained from pre-catalyst **[Ru]-1.7** run whereas both pre-catalysts gave similar 1-hexanol results (entry 13 and 14). With the P-N-P ligand (**L2.1**) plus the base or only base in the absence of ruthenium metal precursor, the same ethanol conversion values (0.4%) were recorded leaving about 99.6% of the ethanol substrate unchanged (entries 15 and 16). This further supports findings that a metal centre plays vital role in Guerbet chemistry. Consequently, the absence of other Guerbet products were observed in the P-N-P ligand (**L2.1**) plus the base only (entry 15) and the base only (entry 16) runs. Generally, catalyst **[Ru]-2.1** performed better than catalyst **[Ru]-2.2** in the conversion of ethanol-methanol to *iso*-butanol probably due to ligand effect. Notably, the formation of 2-methyl-1-butanol and 1-butanol were only detected with preformed catalyst **[Ru]-2.1** (entries 5 and 6 respectively). Furthermore, the utilisation of complex **[Ru]-2.5** as catalysts in this transformation at 2 h yielded lower conversion (14%) but enhanced *iso*-butanol productivity (11%) and selectivity (96%) compared with preformed catalysts **[Ru]-2.1** and **[Ru]-2.2** results (entries 5, 8 and 17). Like Wass P-N catalysts,<sup>35</sup> catalyst decomposition was observed

in all the runs (asides entries 15 and 16) resulting to very dark post catalytic solution. Leaving the post catalytic solution to settle down for some hours, a dark supernatant liquid resulted with large white solid residue spotted with black precipitates. The black precipitates are assumed to be Ru(0) nanoparticles.

### 2.3.7.2 Ethanol Upgrading to 1-butanol

Similarly, complexes **[Ru]-2.1** and **[Ru]-2.2** were screened for ethanol upgrading to 1-butanol using existing catalytic conditions of 5 mol% sodium ethoxide (NaOEt) for 4 to 20 h at 150°C.<sup>34,35</sup> The results are presented in Table 2.2. Consistent with Guerbet reaction, the major product of this catalytic reaction was 1-butanol along with other higher alcohols (2-ethylbutanol, 1-hexanol, 2-ethylhexanol and 1-octanol) as minor products. Also, 2-butanol was detected in some runs. In addition to the alcohol products formed in the present catalytic system, ethyl acetate (nonalcohol product) was present in considerable yield corroborating with other studies on bidentate P-N and tridentate P-N-P complexes.<sup>35, 58</sup> The formation of ethyl acetate in this system either result from Tishchenko reaction (Chapter 1, Section 1.7, Scheme 1.6) or via dehydrogenative coupling of ethanol by the ruthenium catalysts.<sup>62, 63</sup> Again, previously reported complexes **[Ru]-1.11** and **[Ru]-1.12** were used as benchmarks for this system (entries 1-2 and entry 3 respectively). Similar to *iso*-butanol system, complex **[Ru]-2.1** maintained better catalytic activity over complex **[Ru]-2.2** in ethanol conversion, 1-butanol selectivity and yield (entries 4 and 5, 7 and 8). On the other hand, improved productivity of higher alcohols favoured complex **[Ru]-2.2** (entries 4 and 5, 7 and 8). There did not appear to be any significant differences in the performances of complexes **[Ru]-2.1** and **[Ru]-2.2** in the 4 and 20 h runs (entries 4 and 5, 7 and 8). Similar to Wass *et al.* P-N complex **[Ru]-1.12** (entry 3), complexes **[Ru]-2.1** and **[Ru]-2.2** produced 1-butanol as major product and also gave ethyl acetate product typical with previously reported tridentate P-N-P ruthenium complexes known for producing ethyl acetate as sole product.<sup>35, 63</sup> The replacement of NaOEt with KO<sup>t</sup>Bu at 4 h led to higher ethanol conversion with both complexes **[Ru]-2.1** and **[Ru]-2.2**, however, selectivity and productivity of 1-butanol and other higher alcohols reduced comparatively (entries 4 and 6, 7 and 9). Surprisingly, KO<sup>t</sup>Bu co-catalyst was rather reasonably active and selective towards ethyl acetate formation

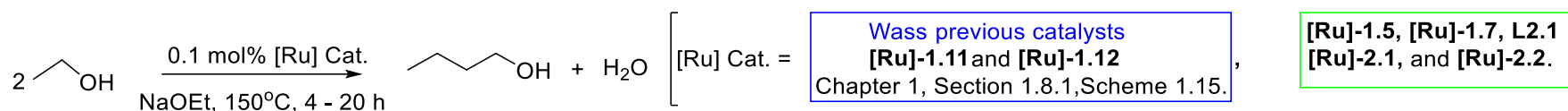


**Table 2.2:** Ruthenium catalysed conversion of ethanol to 1-butanol.

Run <sup>a</sup>	Catalysts	Time (h)	Conv. (%) <sup>b</sup>	Total TON <sup>c</sup>	TON <sup>d</sup> (yield) <sup>e</sup> [selectivity] %					
					1-Butanol	2-Ethyl-1-butanol	1-Hexanol	2-Ethyl-1-Hexanol	1-Octanol	EtOAc <sup>f</sup>
1 <sup>g</sup>	[Ru]-1.11	4	11	110	100(10)[94]	<1 <sup>k</sup>	10(1)[5]	10(1)[1]	-	-
2 <sup>g</sup>	[Ru]-1.11	20	42	420	330(33)[85]	20(2)[3]	50(5)[9]	10(1)[1]	10(1)[1]	-
3 <sup>h</sup>	[Ru]-1.12	4	19	190	170(17)[94]	<1 <sup>k</sup>	10(1)[4]	-	-	<1 <sup>k</sup>
4 <sup>i</sup>	[Ru]-2.1	4	24	240	140(14)[78]	10(1)[2]	20(2)[7]	<1 <sup>k</sup>	<1 <sup>k</sup>	20(2)[10]
5 <sup>i</sup>	[Ru]-2.1	20	25	250	140(14)[77]	10(1)[2]	20(2)[6]	<1 <sup>k</sup>	<1 <sup>k</sup>	20(2)[12]
6 <sup>j</sup>	[Ru]-2.1	4	36	360	130(13)[44]	10(1)[1]	10(1)[3]	<1 <sup>k</sup>	<1 <sup>k</sup>	150(15)[51]
7	[Ru]-2.2	4	16	160	90(9)[73]	10(1)[6]	30(3)[13]	10(1)[2]	10(1)[3]	<1 <sup>k</sup>
8	[Ru]-2.2	20	15	150	100(10)[72]	10(1)[6]	30(3)[13]	10(1)[3]	10(1)[3]	10(1)[4]
9 <sup>j</sup>	[Ru]-2.2	4	26	260	70(7)[31]	10(1)[4]	20(2)[6]	10(1)[1]	10(1)[1]	130(13)[57]
10	[Ru]-1.5/L2.1	20	20	200	100(10)[77]	10(1)[4]	30(3)[13]	<1 <sup>k</sup>	10(1)[2]	<1 <sup>k</sup>
11 <sup>i</sup>	[Ru]-1.7/L2.1	20	9	90	70(7)[63]	<1 <sup>k</sup>	10(1)[6]	<1 <sup>k</sup>	<1 <sup>k</sup>	30(3)[25]

<sup>a</sup>Conditions: Ethanol (10 mL, 171.3 mmol), [Ru] catalyst (0.1713 mmol, 0.1 mol%), NaOEt base (8.57 mmol, 5 mol%), mol% is based on ethanol substrate, 150 °C. <sup>b</sup>Total conversion of ethanol to liquid product as determined by GC analysis of the liquid phase (Conv. = Conversion). <sup>c</sup>Total TON based on mmol of total ethanol converted to products per mmol of [Ru] catalyst (ethanol equivalent relative to mmol of catalysts x conversion = 1000 x conversion). <sup>d</sup>TON based on mmol of any product formed per mmol [Ru] catalyst (ethanol equivalent relative to mmol of catalysts x product yield = 1000 x product yield). <sup>e</sup>Total yield and selectivity of alcohol products in the liquid fraction as determined by GC. <sup>f</sup>EtOAc = Ethyl acetate. <sup>g,h</sup>Previous work.<sup>34, 35</sup> <sup>i</sup>2-Butanol detected in Run 4 Run 5 and Run 11 but yield less than 1%. <sup>j</sup>5 mol% KO<sup>t</sup>Bu, <sup>k</sup>Yield or selectivity value below 0.5%.

than alcohol products (entries 4 and 6, 7 and 9) when used in conjunction with complexes **[Ru]-2.1** and **[Ru]-2.2**. This suggests a real base effect on selectivity and investigating this effect remains part of this study primary future focus. Furthermore, an *in-situ* reaction using two equivalents of P-N-P ligand **L2.1** and one equivalent of pre-catalyst **[Ru]-1.5** or **[Ru]-1.7** gave lower ethanol conversion, 1-butanol yield and selectivity compared to the reaction with preformed complexes **[Ru]-2.1** and **[Ru]-2.2** (entries 5 and 10, 8 and 11). On the overall, as in *iso*-butanol system in the previous section, results from *in-situ* runs revealed that preformed complexes **[Ru]-2.1** and **[Ru]-2.2** exhibited unique features of maintaining better conversion, productivity and selectivity of the desired product (1-butanol and *iso*-butanol). Summarily, all the runs gave dark post catalytic liquid indicating complex degradation and white solid was observed in all the runs after the catalysis apart from KO<sup>t</sup>Bu runs that gave very small little solid.

#### 2.4 Conclusion

In this chapter, bidentate phosphine-based ruthenium(II) (P-N-P) complexes were synthesised, characterised, and utilised for ethanol conversion to *iso*-butanol and 1-butanol. Preformed complexes **[Ru]-2.1** and **[Ru]-2.2** with their corresponding *in-situ* runs produce low *iso*-butanol yield but significantly higher product selectivity. Based on the results from *iso*-butanol system, both a transition metal centre and the presence of a base are necessary to observe appreciable ethanol conversion. Relative to the 1,1-bis(diphenylphosphino)methane (dppm) and bis(2-(diphenylphosphino)ethylamine) ruthenium complexes studied by Wass *et al.*, preformed complexes **[Ru]-2.1** and **[Ru]-2.2** showed good activity in the conversion of ethanol homocoupling to 1-butanol with lower selectivity. Additionally, the effect of base on the selectivity of product was revealed when NaOEt was substituted with KO<sup>t</sup>Bu. In general, although the complexes performances are not as expected but they are sufficiently active. Conclusively, the significant activity of these catalysts serves as foundational basis to proceed with heterogenisation studies. The subject of which is discussed in Chapter 3.

#### 2.5 Future work

Considering the uniqueness of these complexes, catalyst optimisation is necessary to study the effect of reaction time, temperature, catalyst loading, base loading and variety of bases. Additionally, mechanistic studies to reveal the catalytic active species

for better understanding of base effect will be beneficial. Also, the effect of water and co-solvents on the catalytic activity of these complexes worth investigating. Analogous complexes with different non phenyl groups or substituted phenyl groups on the P atoms are catalysts of considerable interest in this catalysis. Finally, the synthesis of ethoxyl/hydroxyl derivatives of complexes **[Ru]-2.1** and **[Ru]-2.2** for ethanol upgrading will receive attention.

## 2.6 References

1. T. Appleby and J. D. Woollins, *Coord. Chem. Rev.*, 2002, **235**, 121-140.
2. P. C. Kamer, P. W. Van Leeuwen and J. N. Reek, *Acc. Chem. Res.*, 2001, **34**, 895-904.
3. J. Young, J. Osborn, F. Jardine and G. Wilkinson, *J. Chem. Soc., Chem. Commun.*, 1965, **131**.
4. Z. Fei, R. Scopelliti and P. J. Dyson, *Dalton Trans.*, 2003, 2772-2779.
5. J. P. da Silva, I. C. Silva, F. R. Pavan, D. F. Back and M. P. de Araujo, *J. Inorg. Biochem.*, 2017, **173**, 134-140.
6. P. Bhattacharyya and J. D. Woollins, *Polyhedron*, 1995, **14**, 3367-3388.
7. M. S. Balakrishna, T. K. Prakasha, S. S. Krishnamurthy, U. Siriwardane and N. S. Hosmane, *J. Organomet. Chem.*, 1990, **390**, 203-216.
8. M. S. Balakrishna, R. Panda, D. C. Smith Jr, A. Klaman and S. P. Nolan, *J. Organomet. Chem.*, 2000, **599**, 159-165.
9. M. Aydemir, A. Baysal, S. Özkar and L. T. Yildirim, *Polyhedron*, 2011, **30**, 796-804.
10. M. Aydemir, A. Baysal, S. Özkar and L. T. Yildirim, *Inorg. Chim. Acta*, 2011, **367**, 166-172.
11. P. Braunstein, H. P. Kormann, W. Meyer-Zaika, R. Pugin and G. Schmid, *Chem. Eur. J.*, 2000, **6**, 4637-4646.
12. M. S. Balakrishna, R. Panda and J. T. Mague, *Polyhedron*, 2003, **22**, 587-593.
13. I. Bachert, I. Bartussek, P. Braunstein, E. Guillon, J. Rosé and G. Kickelbick, *J. Organomet. Chem.*, 1999, **580**, 257-264.
14. K. G. Gaw, M. B. Smith and A. M. Slawin, *New J. Chem.*, 2000, **24**, 429-435.
15. S. J. Dossett, A. Gillon, A. G. Orpen, J. S. Fleming, P. G. Pringle, D. F. Wass and M. D. Jones, *Chem. Commun.*, 2001, 699-700.
16. N. A. Cooley, S. M. Green, D. F. Wass, K. Heslop, A. G. Orpen and P. G. Pringle, *Organometallics*, 2001, **20**, 4769-4771.
17. A. Carter, S. A. Cohen, N. A. Cooley, A. Murphy, J. Scutt and D. F. Wass, *Chem. Commun.*, 2002, 858-859.
18. A. Bollmann, K. Blann, J. T. Dixon, F. M. Hess, E. Killian, H. Maumela, D. S. McGuinness, D. H. Morgan, A. Neveling, S. Otto, M. Overett, A. M. Z. Slawin, P. Wasserscheid and S. Kuhlmann, *J. Am. Chem. Soc.*, 2004, **126**, 14712-14713.
19. F. Majoumo-Mbe, P. Lönnecke, E. V. Novikova, G. P. Belov and E. Hey-Hawkins, *Dalton Trans.*, 2005, 3326-3330.
20. L. E. Bowen and D. F. Wass, *Organometallics*, 2006, **25**, 555-557.
21. N. Biricik, F. Durap, C. Kayan and B. Gümgüm, *Heteroatom Chem.*, 2007, **18**, 613-616.
22. J. Gopalakrishnan, *Appl. Organomet. Chem.*, 2009, **23**, 291-318.
23. M. Aydemir, A. Baysal, N. Gürbüz, I. Oezdemir, B. Gümgüm, S. Özkar, N. Caylak and L. T. Yildirim, *Appl. Organomet. Chem.*, 2010, **24**, 17-24.
24. N. Biricik, C. Kayan, B. Gümgüm, Z. Fei, R. Scopelliti, P. J. Dyson, N. Gürbüz and İ. Özdemir, *Inorg. Chim. Acta*, 2010, **363**, 1039-1047.
25. T. Ogawa, Y. Kajita, Y. Wasada-Tsutsui, H. Wasada and H. Masuda, *Inorg. chem.*, 2013, **52**, 182-195.
26. S. Naik, S. Kumar, J. T. Mague and M. S. Balakrishna, *Dalton Trans.*, 2016, **45**, 18434-18437.
27. L. Broomfield, C. Alonso-Moreno, E. Martin, A. Shafir, I. Posadas, V. Ceña and J. Castro-Osma, *Dalton Trans.*, 2017, **46**, 16113-16125.
28. N. Arslan, *DUFED*, 2020, **9**, 9-16.

29. D. Naicker, P. B. Pansuriya and H. B. Friedrich, *Z. Kristallogr. NCS*, 2016, **231**, 653-656.
30. C. Fliedel, A. Ghisolfi and P. Braunstein, *Chem. Rev.*, 2016, **116**, 9237-9304.
31. A.-Q. Jia, L.-M. Shi, F. Wu, Z.-F. Xin and Q.-F. Zhang, *J. Organomet. Chem.*, 2018, **855**, 33-43.
32. T. Posset, F. Rominger and J. Blümel, *Chem. Mater.*, 2005, **17**, 586-595.
33. J. Blümel, *Coord. Chem. Rev.*, 2008, **252**, 2410-2423.
34. G. R. M. Dowson, M. F. Haddow, J. Lee, R. L. Wingad and D. F. Wass, *Angew. Chem. Int. Ed.*, 2013, **52**, 9005-9008.
35. R. L. Wingad, P. J. Gates, S. T. G. Street and D. F. Wass, *ACS Catal.*, 2015, **5**, 5822-5826.
36. R. L. Wingad, E. J. E. Bergstrom, M. Everett, K. J. Pellow and D. F. Wass, *Chem. Commun.*, 2016, **52**, 5202-5204.
37. K. J. Pellow, R. L. Wingad and D. F. Wass, *Catal. Sci. Technol.*, 2017, **7**, 5128-5134.
38. R. L. Wingad, D. Wise and K. J. Pellow, *Unpublished results*.
39. L. A. Ortiz-Frade, L. Ruiz-Ramírez, I. González, A. Marín-Becerra, M. Alcarazo, J. G. Alvarado-Rodriguez and R. Moreno-Esparza, *Inorg. Chem.*, 2003, **42**, 1825-1834.
40. A. P. Shaw, B. L. Ryland, J. R. Norton, D. Buccella and A. Moscatelli, *Inorg. Chem.*, 2007, **46**, 5805-5812.
41. M. A. Fox, J. E. Harris, S. Heider, V. Pérez-Gregorio, M. E. Zakrzewska, J. D. Farmer, D. S. Yufit, J. A. K. Howard and P. J. Low, *J. Organomet. Chem.*, 2009, **694**, 2350-2358.
42. A. P. Shaw, B. L. Ryland, J. R. Norton, D. Buccella and A. Moscatelli, *Inorg. Chem.*, 2009, **48**, 5048-5048.
43. J. R. Miecznikowski, J. P. Caradonna, K. M. Foley, D. J. Kwiecien, G. P. Lisi and A. M. Martinez, *J. Chem. Educ.*, 2011, **88**, 657-661.
44. M. A. Bennett and A. K. Smith, *J. Chem. Soc., Dalton Trans.*, 1974, 233-241.
45. G. T. Giuffredi, S. Purser, M. Sawicki, A. L. Thompson and V. Gouverneur, *Tetrahedron: Asymmetry*, 2009, **20**, 910-920.
46. A. K. Widaman, N. P. Rath and E. B. Bauer, *New J. Chem.*, 2011, **35**, 2427-2434.
47. R. Mitra, S. Das, S. V. Shinde, S. Sinha, K. Somasundaram and A. G. Samuelson, *Chem. Eur. J.*, 2012, **18**, 12278-12291.
48. R. Sáez, J. Lorenzo, M. J. Prieto, M. Font-Bardia, T. Calvet, N. Omeñaca, M. Vilaseca and V. Moreno, *J. Inorg. Biochem.*, 2014, **136**, 1-12.
49. M. J. Overett, K. Blann, A. Bollmann, J. T. Dixon, F. Hess, E. Killian, H. Maumela, D. H. Morgan, A. Neveling and S. Otto, *Chem. Commun.*, 2005, 622-624.
50. D. Shriver, M. Weller, T. Overton, J. Rourke and F. Armstrong, *Inorganic Chemistry*, W.H Freeman and Company, New York, 6th ed, 2014, ch. 7, pp. 216.
51. J. Geicke, I. P. Lorenz, M. Engel and K. Polborn, *Inorg. Chim. Acta*, 1998, **269**, 157-161.
52. M. Valderrama, V. Arancibia, R. Contreras and C. Soto, *J. Coord. Chem.*, 2001, **54**, 389-400.
53. J. Ji, F. Wu, L.-M. Shi, A.-Q. Jia and Q.-F. Zhang, *J. Organomet. Chem.*, 2019, **885**, 1-6.
54. S. Naik, J. T. Mague and M. S. Balakrishna, *Inorg. Chim. Acta*, 2013, **407**, 139-144.
55. I. Warad, *Molecules*, 2010, **15**, 4652-4669.
56. K. J. Pellow, PhD Thesis, University of Bristol, 2018.
57. E. S. Olson, R. K. Sharma and T. R. Aulich, *Appl. Biochem. Biotechnol.*, 2004, **115**, 913-932.

58. Y. Xie, Y. Ben-David, L. J. W. Shimon and D. Milstein, *J. Am. Chem. Soc.*, 2016, **138**, 9077-9080.
59. T. L. Jordison, C. T. Lira and D. J. Miller, *Ind. Eng. Chem. Res.*, 2015, **54**, 10991-11000.
60. Q. Zhang, J. Dong, Y. Liu, Y. Wang and Y. Cao, *J. Energy Chem.*, 2016, **25**, 907-910.
61. H. Aitchison, R. L. Wingad and D. F. Wass, *ACS Catal.*, 2016, **6**, 7125-7132.
62. S. Chakraborty, P. E. Pizsel, C. E. Hayes, R. T. Baker and W. D. Jones, *J. Am. Chem. Soc.*, 2015, **137**, 14264-14267.
63. M. Nielsen, H. Junge, A. Kammer and M. Beller, *Angew. Chem. Int. Ed.*, 2012, **51**, 5711-5713.

## Chapter 3: Fumed silica/MCM-41-supported Alkoxysilyl-functionalised Bidentate Phosphine-based Ruthenium(II) Complexes for Ethanol Upgrading to Advanced Biofuels

### 3.1 Introduction

Silicas and modified silicas are widely used in chemical separations and heterogeneous catalysis due to their distinctive surface properties and stability, even at elevated temperatures.<sup>1-7</sup> Since such materials are in a different phase to the reaction mixture they can be easily removed by simple separation methods.<sup>8</sup> Considerable attention has been given to the synthesis, characterisation and application of silica-related materials; for example, unmodified silicas can be synthesised in a variety of ways of which the sol-gel approach remains the most commonly used method. The physical and chemical properties of pure silicas control reactivity and applications; these properties include surface area, pore volume, pore size, particle size, and active sites.<sup>9</sup> An overview of the surface properties of silica is discussed in the next section.

#### 3.1.1 Nature of silica

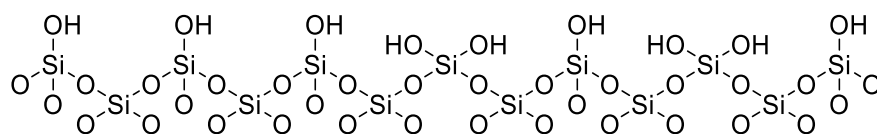


**Figure 3.1:** Simplified silica surface

Silica originates from the class of products with the general formula  $\text{SiO}_2$  or  $\text{SiO}_2 \cdot x\text{H}_2\text{O}$ . It can be formed naturally or synthetically in crystalline or amorphous phase. Synthetic amorphous silica exists in a variety of forms and is used widely in chemical and physical applications. Important physical properties include surface area, pore volume, pore size and particle size which can be varied depending on the methods of preparation or modification of the silica material.<sup>9</sup> For application purposes, porosity, active site, particle size and hardness (i.e. thermal stability) are considered the main features of interest that provide information on what happens on the silica surface. Also, these properties form the basis for making silica an effective support material.<sup>8</sup> For example, the pore size of the silica material according to IUPAC classification also gives an interesting view of its nature. Under this classification, there are microporous (0 - 2 nm pore diameter), mesoporous (2 - 50 nm pore diameter), macroporous (50 - 7500 nm pore diameter) and megaporous silicas (> 7500 nm pore diameter).<sup>10</sup> Additionally, the active sites on the silica surfaces expose the material to

lots of interactions allowing reactivity with other modifying agents. These active species present on silica surfaces play a pivotal role in heterogeneous catalysis.<sup>11</sup> Furthermore, the silica surfaces are dominated by siloxane bridges ( $\equiv\text{Si-O-Si}\equiv$ ) and a variety of silanol groups ( $\equiv\text{Si-OH}$ ).<sup>8</sup> These are the prominent functional groups on the surface of silicas (Figure 3.1). However, these groups are not limited to the surface of silica but also found throughout the particle structure. Internal silanols (intraglobular) for example are inaccessible to water interaction. Nevertheless, internal and external silanols are not distinguishable. Depending on the number of sites, nature and bonding, silanols can be classified as isolated (free), vicinal (bridged) and geminal (Figure 3.2).<sup>12, 13</sup>

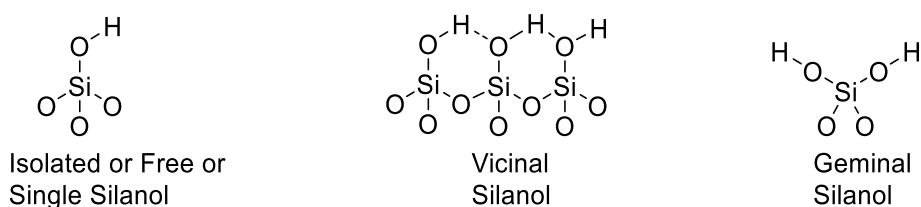
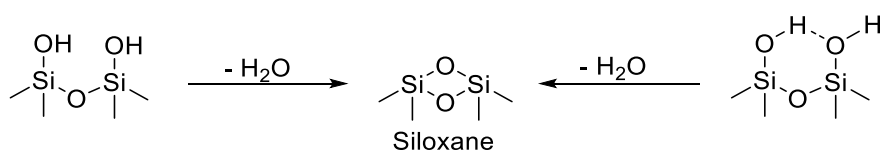


**Figure 3.2:** Different types of silanol on silica surfaces<sup>12, 13</sup>

An isolated, free or single silanol has a free hydroxy group attached to a silicon atom with three oxy bonds into the bulk structure. The hydroxy groups in this type of silanol are so far apart that hydrogen bonding is precluded. Geminal silanols, also known as silanediols, consist of two free hydroxy groups connected to a single silicon atom with two oxy bonds into the bulk structure. In vicinal (bridged) silanols, there are two hydroxy groups attached to two different silicon atoms with three oxy bonds into the bulk structure, however, these hydroxy groups are close enough for hydrogen bonding to occur. Silanetriols are posited in literature but their existence remains a postulate.<sup>12, 14</sup> Different silanols on silica surfaces are distinguishable by IR spectroscopy (Table 3.1).<sup>15</sup> On the other hand, siloxane bridges ( $\equiv\text{Si-O-Si}\equiv$ ) are formed through the condensation of surface or internal silanol groups, a process known as dehydroxylation (Scheme 3.1).<sup>12, 16, 17</sup>



**Scheme 3.1:** Dehydroxylation of silanols to form siloxanes.<sup>12, 16, 17</sup>

**Table 3.1:** Selected IR vibration bands of silica and modified silica<sup>15</sup>

Wavenumber (cm <sup>-1</sup> )	Assignment
3746	Free Si-OH vibration (stretching)*
3742	Geminal Si-OH vibration (stretching)*
3740	Free Si-OH vibration (stretching)
3740-3500	Bridged Si-OH vibration (stretching)
3400-3500	Molecular adsorbed H <sub>2</sub> O
2978	CH <sub>3</sub> vibration (stretching)
2936	CH <sub>2</sub> vibration (stretching)
2869	CH <sub>2</sub> vibration (stretching)
1940-1770	Si-O-Si vibration
1625	Bending O-H (molecular water)*
1597	NH <sub>2</sub> bending
1471	CH <sub>2</sub> bending
1448	CH <sub>3</sub> bending
1413	Si- <u>CH<sub>2</sub></u> bending
1393	CH <sub>3</sub> bending vibration
1250-1020	Si-O-Si asymmetric CH <sub>3</sub> vibration (stretching)
970	Si-O-(H---H <sub>2</sub> O) bending*
800	OH bending

\*unmodified silica

Crucially, <sup>29</sup>Si solid-state NMR spectroscopy is a powerful tool used to identify various silanol and siloxane sites on the surface of silica (Figure 3.3).<sup>18-21</sup> The techniques employed the use of “Q<sup>n</sup>” terminology to specify the particular silicon sites on silica surfaces. Q denotes quaternary,

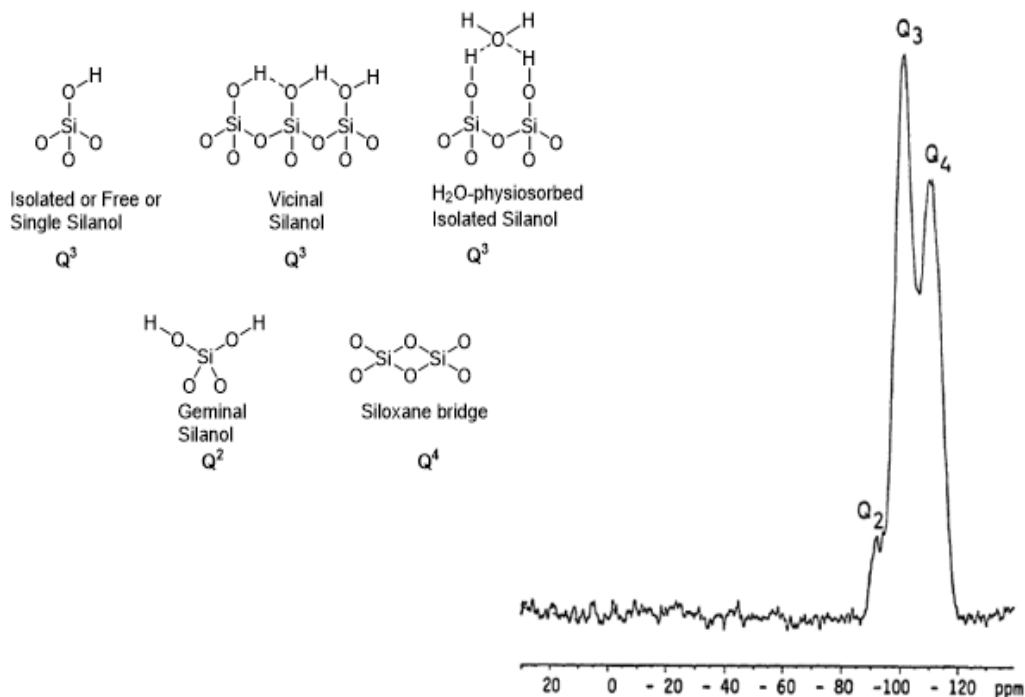


**Figure 3.3:**  $^{29}\text{Si}$  CP-MAS NMR spectrum of an amorphous porous silica (extracted from literature).<sup>20, 21</sup>

meaning the tendency to form four possible siloxane (-Si-O-Si-) bonds, and  $n$  is the number of oxygen-silicon (-O-Si) units (i.e. bridging oxygen) bonded to a central silicon atom ( $n = 0-4$ ).<sup>14, 22</sup> These silicon sites ( $Q^4$ ,  $Q^3$ ,  $Q^2$ ,  $Q^1$  and  $Q^0$ ) give distinct chemical shifts in accordance with the pioneer authors' data whenever the  $^{29}\text{Si}$  CP/MAS NMR technique is used (Figure 3.4).<sup>5, 18, 23-25</sup>

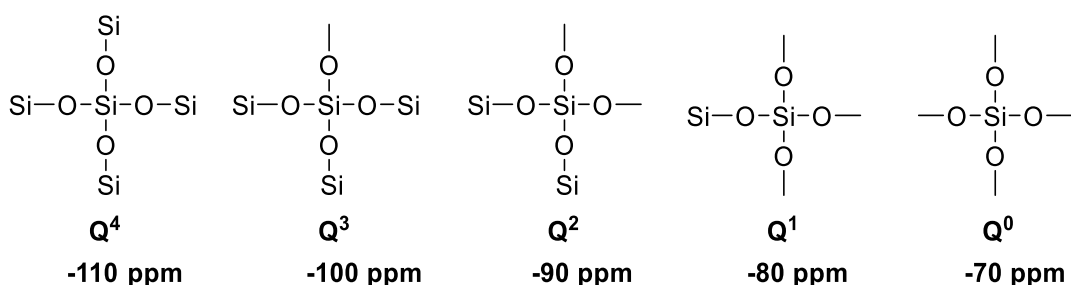


**Figure 3.4:** Different silicon environments. Groups not shown can be  $R = \text{H}$ , alkyl etc.

Other notations such as “ $T^n$ ” (Tri-, tendency to form  $n = 0-3$  siloxane bonds), “ $D^n$ ” (Di-, tendency to form  $n = 0-2$  siloxane bonds) and “ $M^n$ ” (Mono-, tendency to form  $n = 0-1$  siloxane bond) are also used, however, these apply when silica is modified with

functionalised silanes like  $\text{RSi}(\text{OR}')_3$ ,  $\text{R}_2\text{Si}(\text{OR}')_2$  and  $\text{R}_3\text{Si}(\text{OR}')$ , ( $\text{R}' = \text{H}$ , alkyl) respectively (Table 3.2 and 3.3).<sup>22, 26-32</sup>

**Table 3.2:**  $^{29}\text{Si}$  CP/MAS NMR spectroscopic peak positions of immobilised aminosilanes (APTS).<sup>30, 33, 34</sup>

Hydrolysed monodentate	monodentate	bidentate	tridentate
$\begin{array}{c} \text{R} \\   \\ \text{HO}-\text{Si}-\text{OH} \\   \\ \text{O} \\   \\ \text{O}^*-\text{Si}-\text{O} \\   \\ \text{O} \end{array}$	$\begin{array}{c} \text{R} \\   \\ \text{EtO}-\text{Si}-\text{OEt} \\   \\ \text{O} \\   \\ \text{O}^*-\text{Si}-\text{O} \\   \\ \text{O} \end{array}$	$\begin{array}{c} \text{R} \quad \text{OR}' \\ \diagdown \quad / \\ \text{Si} \\ / \quad \diagdown \\ \text{O} \quad \text{O} \\   \quad   \\ \text{O}^*-\text{Si}-\text{O}^*-\text{Si}-\text{O} \\   \quad   \\ \text{O} \quad \text{O} \end{array}$	$\begin{array}{c} \text{R} \quad \text{O}-\text{Si} \\ \diagdown \quad / \\ \text{Si} \\ / \quad \diagdown \\ \text{O} \quad \text{O} \\   \quad   \\ \text{O}^*-\text{Si}-\text{O}^*-\text{Si}-\text{O} \\   \quad   \\ \text{O} \quad \text{O} \end{array}$
T <sup>1</sup>	T <sup>1</sup>	T <sup>2</sup>	T <sup>3</sup>
-43 ppm	-53 ppm	-59 ppm	-67 ppm

$\equiv\text{Si}-\text{O}$  (T environment) and  $-\text{*Si}\equiv$  (Q environment) represent silicon sites of aminosilane and surface silanols respectively, ( $\text{R} = \text{CH}_2\text{CH}_2\text{CH}_2\text{NH}_2$ ,  $\text{R}' = \text{H}$ ,  $\text{CH}_2\text{CH}_3$ ).

**Table 3.3:**  $^{29}\text{Si}$  CP/MAS NMR spectroscopic peak positions of immobilised aminosilanes (APDMS)<sup>28, 30</sup>

Hydrolysed monodentate	bidentate	bidentate	monodentate
$\begin{array}{c} \text{R} \\   \\ \text{H}_3\text{C}-\text{Si}-\text{OH} \\   \\ \text{O} \\   \\ \text{O}^*-\text{Si}-\text{O} \\   \\ \text{O} \end{array}$	$\begin{array}{c} \text{R} \quad \text{CH}_3 \\ \diagdown \quad / \\ \text{Si} \\ / \quad \diagdown \\ \text{O} \quad \text{O} \\   \quad   \\ \text{O}^*-\text{Si}-\text{O} \\   \\ \text{O} \end{array}$	$\begin{array}{c} \text{R} \quad \text{R} \\   \quad   \\ \text{H}_3\text{C}-\text{Si}-\text{O}-\text{Si}-\text{CH}_3 \\   \quad   \\ \text{O} \quad \text{O} \\   \quad   \\ \text{O}^*-\text{Si}-\text{O}^*-\text{Si}-\text{O} \\   \quad   \\ \text{O} \quad \text{O} \end{array}$	$\begin{array}{c} \text{CH}_3 \\   \\ \text{H}_3\text{C}-\text{Si}-\text{CH}_3 \\   \\ \text{O} \\   \\ \text{O}^*-\text{Si}-\text{O} \\   \\ \text{O} \end{array}$
D <sup>1</sup>	D <sup>2</sup>	D <sup>2</sup>	M
-12.4 ppm	-19.7 ppm	-19.7 ppm	12.5 ppm

$\equiv\text{Si}-\text{O}$  (D or M environment) and  $-\text{*Si}\equiv$  (Q environment) represent silicon sites of aminosilane and surface silanols respectively, ( $\text{R} = \text{CH}_2\text{CH}_2\text{CH}_2\text{NH}_2$ ).

### 3.1.2 Modification of silica surface by organosilanes

The versatile surface reactivity of silicas allows different modifying agents (alkoxy-, halo-, aminosilanes and organosilazanes etc.) to be bonded to the surface through chemical and physical processes.<sup>26</sup> Chemical surface modification may be defined as the chemical bonding of molecules or molecule fragments to a surface in order to change its chemical or physical properties in a controlled way.<sup>9</sup> When the surface of silica is modified, it results in a material with the combined properties of silica and those of the interacting species. On that note, the binding of organofunctional silanes onto silica surfaces has gained considerable interest in heterogeneous catalysis.<sup>35</sup> Also, organofunctional silanes have the capacity to form Si-O-Si units (bond angle 143°) with silica surfaces resulting in polymers with exceptional structural features compared to carbon-based polymers with C-C-C units (bond angle 109°).<sup>26</sup> The cleavage of Si-O-Si bonds occurs under more stringent conditions compared to C-O-C bonds.<sup>36</sup> Additionally, the dual functionalities of organofunctional silanes are key to their broad usage as silylating agents, the hydrolysable alkoxyl functional end being anchored onto the silica surface while the other end coordinates to a metal centre as a ligand.<sup>37</sup> This field of chemical science takes advantage of the combined inorganic properties of the silica material and the metal complexes in this catalyst-type and the design of such catalysts has received much attention since the 1970s.<sup>38</sup> Despite the advantages offered by the silica-supported metal complexes,<sup>8</sup> their use in advanced biofuels synthesis via Guerbet catalysis remained unknown at the commencement of this study. Previous studies on the conversion of bioethanol to C<sub>4-8</sub> alcohols have almost exclusively been based on either admixtures of metal oxides or homogeneous metal complexes.<sup>39</sup>

### 3.1.3 Types of silica Supports

Several types of silica materials are employed as supports in heterogeneous catalysis and have likewise received application in other fields of chemistry such as chemical separation, adsorption process, enzyme immobilisation, drug delivery systems, advance composite material design, etc.<sup>40-42</sup> The various types of silica obtained are based on the method of preparation, surface area, pore volume, pore size and particle size.<sup>9</sup> These include silica gel, fused silica, fumed silica, colloidal silica, precipitated silica, Santa Barbara Amorphous (SBA-15), molecular 41 sieves (M41S) family and others.<sup>13, 43, 44</sup>

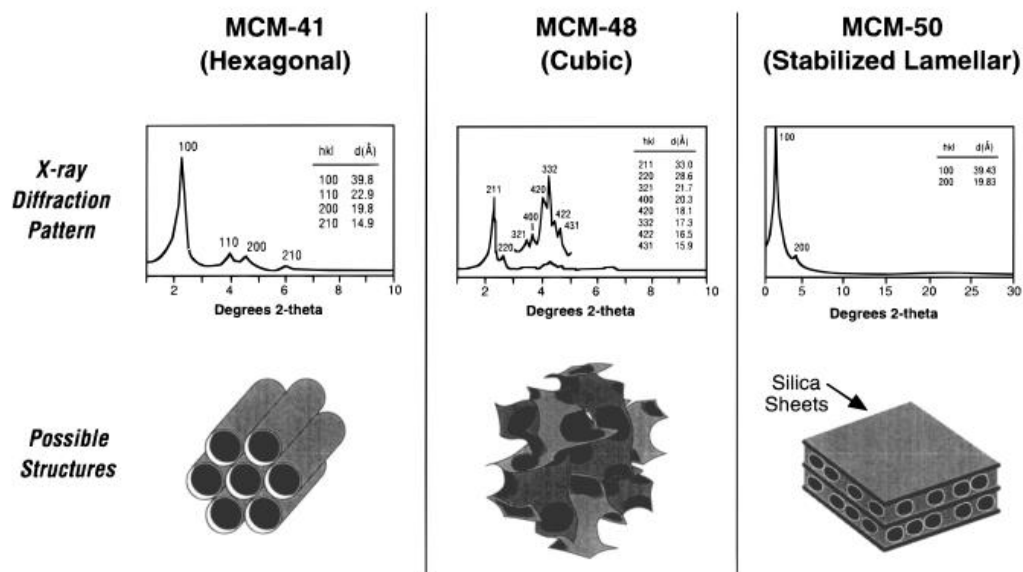


**Figure 3.5:** M41S family structures: MCM-41 (hexagonal), MCM-48 (cubic) and MCM-50 (lamellar) with corresponding XRD diffraction pattern<sup>13</sup>

The M41S family comprises of mesoporous silica with unique pore structures. So, three different mesoporous silica constitute the M41S family based on geometric structures: MCM-41 (hexagonal structure), MCM-48 (3D cubic pore structure) and MCM-50 (lamellar structure)<sup>13, 44, 45</sup> as depicted in Figure 3.5. The hexagonal structure, named as Mobil Composition of Matter No. 41 (MCM-41), was produced by researchers at Mobil Corporation laboratories in 1992.<sup>46</sup> It has highly ordered hexagonal channels ranging from 15–100 Å in diameters. MCM-41 is the most widely used among the M41S family,<sup>13</sup> due to its exceptional surface properties and surface reactivity, making the material find many applications in catalysis.<sup>40, 44</sup>

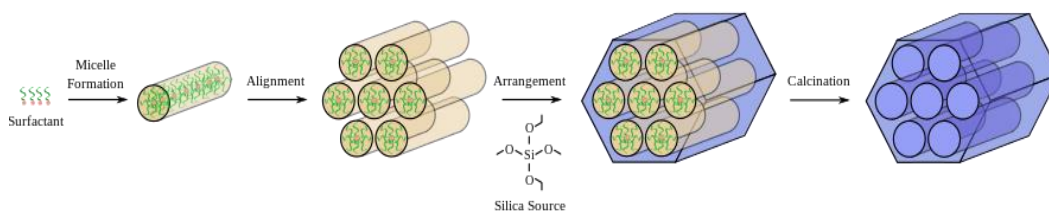


**Figure 3.6:** Synthetic route to MCM-41 (Extracted from Wikipedia).<sup>47</sup>

In a typical synthesis of MCM-41, an anionic surfactant (commonly cationic cetyltrimethylammonium bromide, CTAB) initially form rod-like micelles capable of undergoing self-alignment into hexagonal arrays that interact with silica species under hydrothermal conditions to produce mesostructured composite. The composite material is subjected to thermal treatment (calcination) where the silanols groups of

the silica species condense to form siloxane bridges (-Si-O-Si-) and the surfactant template disappears by oxidation process to give hexagonally ordered mesoporous material known as MCM-41 (Figure 3.6).<sup>13, 41, 45, 47</sup> Herein, MCM-41 and fumed silica are the two silica supports employed in this study.

### 3.2 Aims and objectives

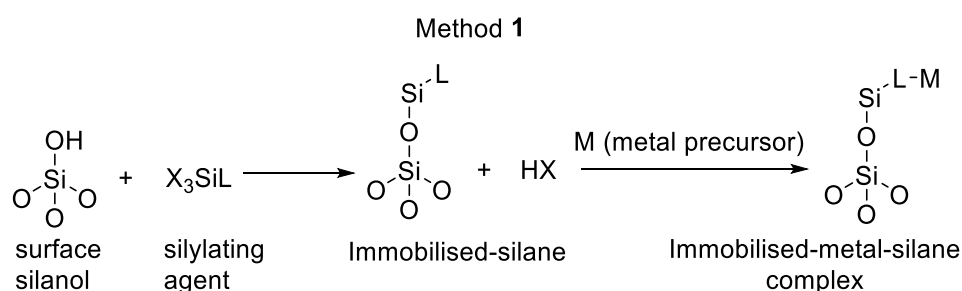
The present study focuses on anchoring metal complexes of bisphosphine-aminopropylalkoxysilanes onto silica surfaces for the catalytic conversion of bioethanol to advanced biofuels. The design of these materials is based on the following considerations. Firstly, silicas as support materials meet the required specifications such as surface hydrophilicity, insolubility in most solvents (easy to remove), porosity with mechanical stability (allows diffusion of substrates) and chemical inertness yet easily modified, wide surface for accessibility of active sites and better dispersibility.<sup>8, 9, 26, 48</sup> On a second note, hydrolysable alkoxy groups have the capacity to bond onto silica surfaces via different modes including cross-linking depending on the number of alkoxy groups present.<sup>7, 8</sup> A strong bond is formed when alkoxy groups condense onto the silica<sup>35</sup> preventing the leaching of catalysts by disconnection of the linker from the surface.<sup>49</sup> Thirdly, the diphosphine aminoalkoxysilane coordinates to a metal centre<sup>50</sup> through the phosphine groups to retain the metal sites required in our catalytic reaction.<sup>51-54</sup> Such a chelation-type helps hold the metal in place during immobilisation processes thereby precluding metal leaching during catalysis.<sup>7</sup> Thus, resulting in viable silica-supported metal complexes for heterogeneous catalysis. The most explored metal centre within the Wass group is ruthenium metal.<sup>54</sup> This remains the metal centre in the present work for easy comparison with the homogeneous counterparts. Additionally, there is need for improvement in the catalytic activity and lifetime of these homogeneous catalysts. So, the target catalysts hopefully combine the effectiveness and selectivity of the homogeneous catalysts with the stability, recoverability, and recyclability of the heterogenised analogues. Furthermore, since water is a by-product in our closed catalytic reactor, the hydrophobic surface properties of the obtained heterogeneous catalysts will help enhance the water resistance of moisture-sensitive homogeneous complexes. Therefore, the overall aim of the study described in this chapter is to synthesise, characterise and utilise silica-supported ruthenium complexes for the conversion of bioethanol to advanced biofuels to improve selectivity and yield. The

primary focus of the chapter is (1) elucidating the surface properties of the silica support before and after modification using a variety of spectroscopic tools; (2) investigating the degree of condensation and hydrolysis of the alkoxy groups; (3) evaluating the activity of the immobilised catalysts for bioethanol upgrading in comparison to homogeneous analogues; (4) examining the hydrophobicity of heterogeneous catalysts in the presence of external water introduced into the catalytic system.

### 3.3 Results and Discussion

#### 3.3.1 Immobilisation methods

The silylating agent used in this work is 3-aminopropyltrimethoxysilane (APTMS). Our choice of this specific organosilane is centred on the following reasons: the Si(OMe)<sub>3</sub> groups condense more rapidly with surface hydroxyl groups than the Si(OEt)<sub>3</sub> moiety; the amino end group can be easily phosphinated with two equivalents of Ph<sub>2</sub>PCl to give the bidentate phosphine analogue of this silylating agent capable of coordinating to transition metal centres.<sup>55</sup> There are two general methods for immobilising homogeneous metal complexes onto support materials by using silylating agents as linkers. The first method (Method 1, Scheme 3.2) involves the anchorage of the silylating agent onto the silica surface via the hydrolysable alkoxy groups followed by coordination with a metal complex precursor through the ligand ends.

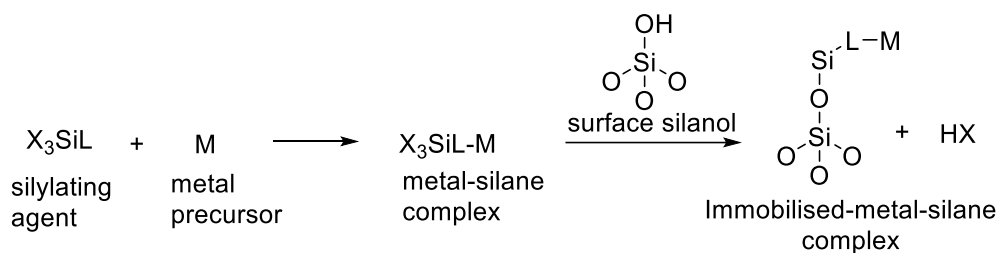


\*where X can be any hydrolysable group such as chloride, alkoxy etc.

**Scheme 3.2:** Schematic approach for immobilising homogeneous metal complexes incorporating silylating linkers onto support materials (Method 1)

In the second method (Method 2, Scheme 3.3), coordination of the silylating agents with complex precursors precedes the anchorage step.<sup>7, 38, 50, 55, 56</sup> There is still controversy on which route is best for incorporating metal complexes onto a support.

### Method 2



\*where X can be any hydrolysable group such as chloride, alkoxy etc.

### Scheme 3.3: Schematic approach for immobilising homogeneous metal complexes incorporating silylating linkers onto support materials (Method 2)

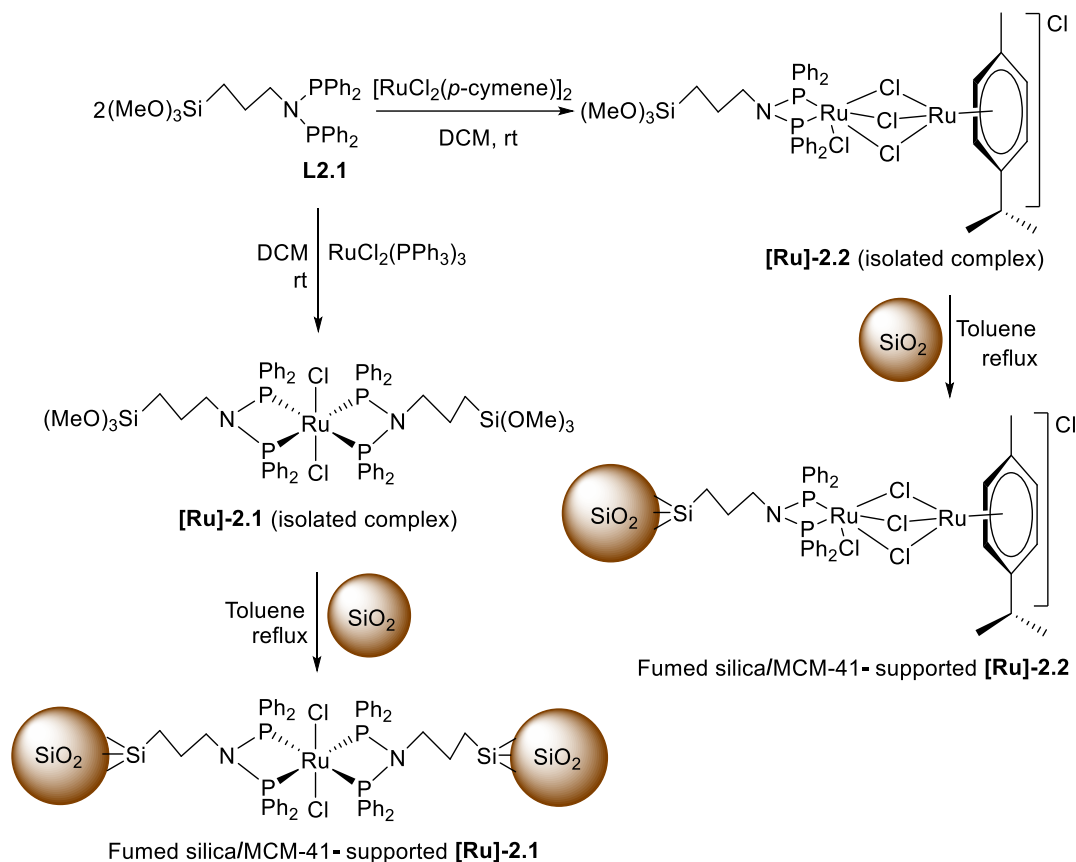
Method 2 was adapted for this study based on the following considerations:

- Method 2 allows easy characterisation of the metal complexes prior to anchorage onto support materials.
- Method 1 involves longer refluxing conditions, uneven dispersion of metal complexes on support materials, double usage of solid-state techniques to assess the support for individual atom incorporation after silanation and complexation steps, and excessive use of silylating agents.<sup>48</sup>
- Another disadvantage of method 1 is that the free end of immobilised-phosphine ligands can undergo oxidation to phosphine oxides if exposed to any traces of O<sub>2</sub> or reaction with the support material to form undesired P(V) species.<sup>38</sup>
- Finally, with method 2, it is feasible to compare the catalytic activity of homogeneous complexes before and after immobilisation.

#### 3.3.2 Synthesis of fumed silica/MCM-41-supported [Ru]-2.1 and [Ru]-2.2

Following method 2, phosphinated-APTMS, **L2.1**, (experimental detail found in Chapters 2 and 6) was complexed to a ruthenium centre using two metal precursors [RuCl<sub>2</sub>(PPh<sub>3</sub>)<sub>3</sub>] and [RuCl<sub>2</sub>(*p*-cymene)]<sub>2</sub> to form complexes **[Ru]-2.1** and **[Ru]-2.2** respectively which were first tested as homogeneous catalysts in ethanol upgrading to 1-butanol and *iso*-butanol (Chapter 2). These complexes were thereafter immobilised on two pre-treated silica materials (i.e. fumed silica and MCM-41) according to Scheme 3.4. Pre-treated here means fumed silica and MCM-41 subjected to heating

under vacuum to remove any adsorbed water molecule and stored under inert (argon) atmosphere prior to use (detail procedure in Chapter 6).



**Scheme 3.4:** Immobilisation approach for supporting catalysts **[Ru]-2.1** and **[Ru]-2.2** on fumed silica and MCM-41

### 3.3.3 Characterisation of unfunctionalised and functionalised silica

In addition to IR and  $^{29}\text{Si}$  CP/MAS NMR spectroscopy mentioned in the introductory section for identifying active sites on silica, other techniques such as nitrogen adsorption/desorption measurement, thermogravimetry analysis (TGA), X-ray diffraction (XRD) studies, electron microscopy (TEM/STEM/EDS),  $^{13}\text{C}$  CP/MAS NMR spectroscopy, atomic absorption spectroscopy (AAS) and inductively coupled plasma-mass spectrometry (ICP-MS) are useful in characterising pure silica and modified silica in order to elucidate its physical and chemical properties. The aforementioned techniques were applied in the characterisation of bare pre-treated fumed silica/MCM-41 and fumed silica/MCM-41-supported complexes **[Ru]-2.1** and **[Ru]-2.2**. The results from these characterisation methods are discussed accordingly.

### 3.3.3.1 Fourier-transform infra-red (FTIR) method

The surface-active species on pre-treated unmodified fumed silica and MCM-41 were assessed using FTIR spectroscopy before the functionalisation process. The spectra obtained are shown in Figure 3.7a. The broad peak between 3000 - 3884  $\text{cm}^{-1}$  is attributed to the presence of hydroxyl groups (isolated, geminal and vicinal silanols) and unremoved water molecules (Table 3.1).<sup>57</sup> The second sharp broad band from 1300 – 871  $\text{cm}^{-1}$  corresponds to siloxane bonds (-Si-O-Si-). Other peaks at 1633 and 804  $\text{cm}^{-1}$  are attributed to OH groups of water (Table 3.1). There are two possibilities for the presence of water OH peaks on these pre-treated silica materials. They could either result from incomplete elimination of adsorbed water molecules at the chosen activation temperature or the adsorption of atmospheric water molecule during analysis as it was carried out outside an inert atmosphere. Also, fumed silica and MCM-41 can experience both effects. Similarly, fumed silica and MCM-41-supported **[Ru]-2.1** and **[Ru]-2.2** were examined by infra-red for possible anchorage of the complexes to fumed silica and MCM-41. The spectra obtained are shown in Figure 3.7b and c. For both, the  $\text{CH}_3$  vibration of the methoxy groups ( $\text{OCH}_3$ ) seen in the spectra of the complexes at 3052, 2938 – 2964 and 2837 – 2873  $\text{cm}^{-1}$  were no longer present in fumed silica and MCM-41-supported **[Ru]-2.1** and **[Ru]-2.2**. This indicated that a condensation reaction between the methoxy groups of the complexes and the silanol groups of the silica to form siloxane bonds with methanol as a by-product had occurred. Furthermore, the characteristic C-H bending of Si- $\text{CH}_2$  observed in complex **[Ru]-2.1** at 1433  $\text{cm}^{-1}$  appeared at 1436  $\text{cm}^{-1}$  in fumed silica and MCM-41-supported **[Ru]-2.1** (Figure 3.7b, Table 3.1). Additionally, the bands at 743 and 691  $\text{cm}^{-1}$  due to C-H stretching of the monosubstituted aromatic ring<sup>58</sup> in complex **[Ru]-2.1** were observed at 747 and 696  $\text{cm}^{-1}$  in fumed silica and MCM-41-supported **[Ru]-2.1**. However, only the monosubstituted phenyl C-H stretching of complex **[Ru]-2.2** at 696  $\text{cm}^{-1}$  was noticeable in fumed silica and MCM-41-supported **[Ru]-2.2** (Figure 3.7c). In short, the retention of these functional group peaks in the spectra of the supported catalysts implied successful incorporation of the complexes onto fumed silica and MCM-41.

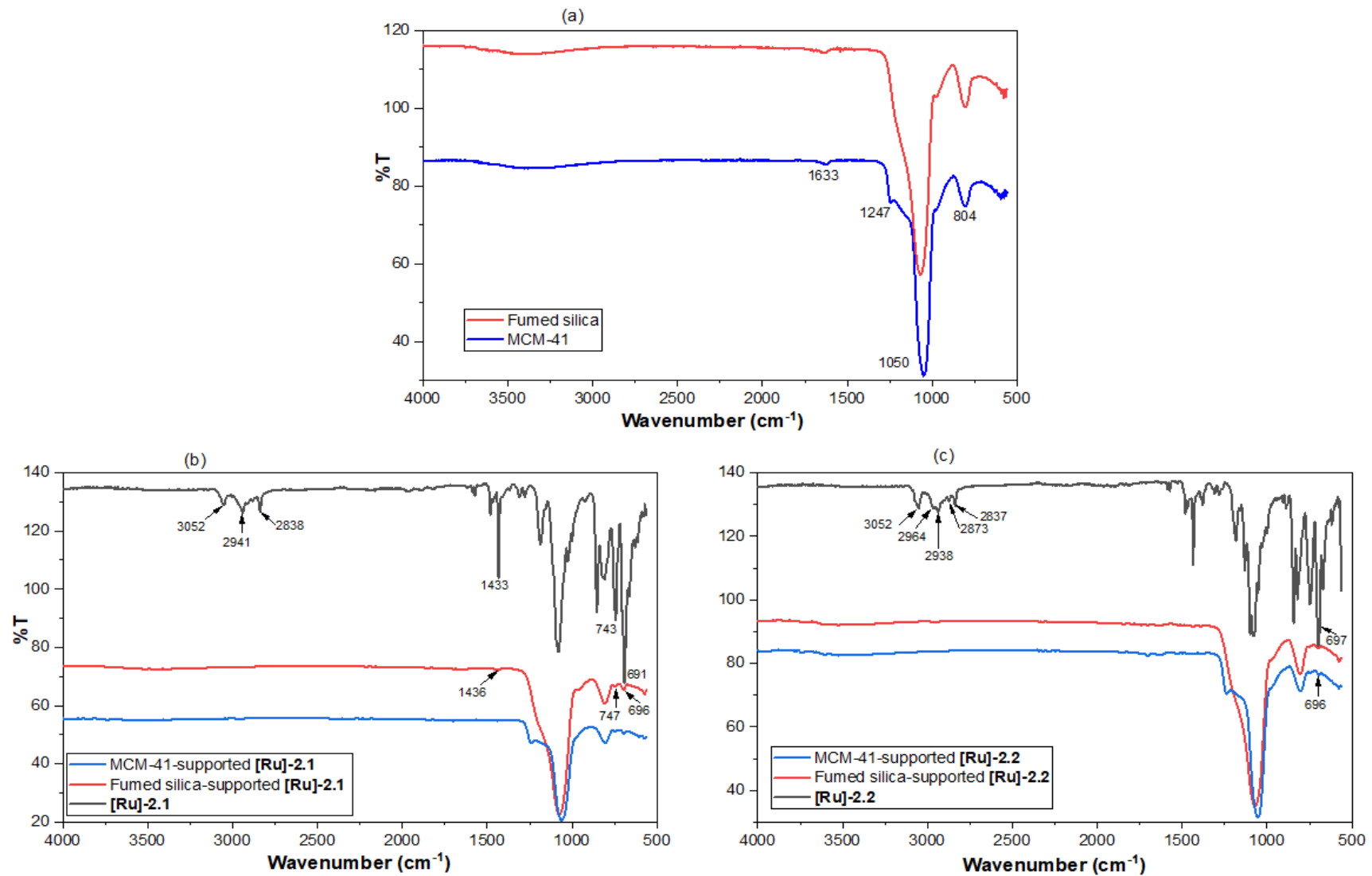
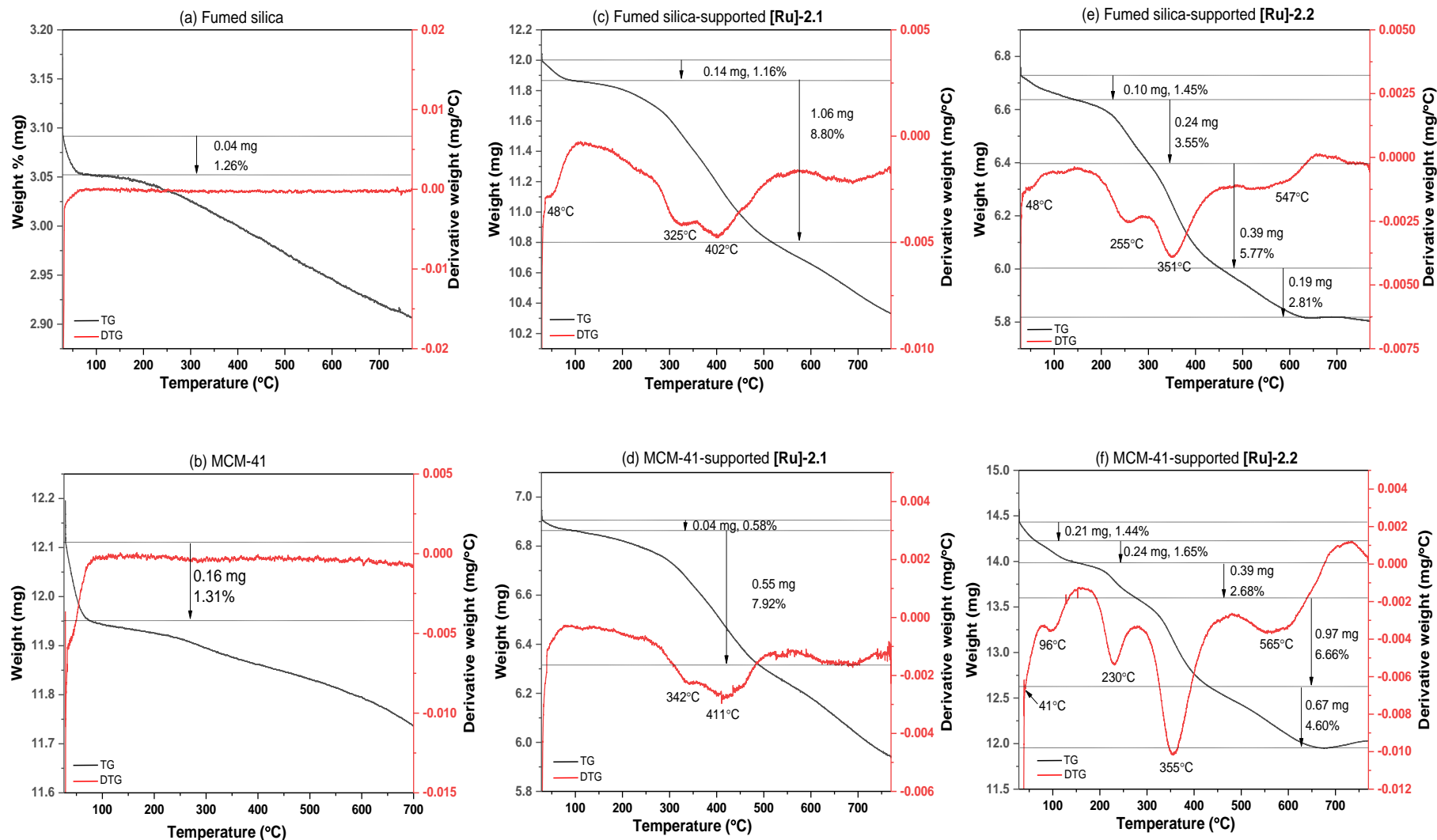


Figure 3.7: FTIR analysis of (a) unmodified fumed silica and MCM-41 (b) supported and unsupported [Ru]-2.1 (c) supported and unsupported [Ru]-2.2

### 3.3.3.2 Thermal analysis

To verify the tethering of organofunctional silane complexes **[Ru]-2.1** and **[Ru]-2.2** on fumed silica and MCM-41, thermal decomposition studies via thermogravimetry (TG) application was carried out on the silica materials under investigation. The result of the thermal stability tests performed on bare fumed silica/MCM-41 and fumed silica/MCM-41-supported **[Ru]-2.1** and **[Ru]-2.2** are shown in Figure 3.8a-f. The thermogravimetry (TG) and differential thermogravimetry (DTG) curves provide information on weight loss stages that occur in these materials from 30-800°C in nitrogen atmosphere at 5 °C /min heating rate. Both fumed silica and MCM-41 exhibited a small weight loss (1.3%) below 100°C, corresponding to the loss of physisorbed water from the surface (Figure 3.8a-b).<sup>59</sup> Typically, adsorbed water weight loss from silica ranges between 1-5%.<sup>60</sup> This is consistent with the IR results showing adsorbed water in pre-treated fumed silica and MCM-41. For fumed silica-supported **[Ru]-2.1** and MCM-41-supported **[Ru]-2.1**, a similar two stage decomposition occurred on the TG curves (Figure 3.8c-d). The initial weight losses within 30-110°C experienced by these functionalised silicas were 1.2 and 0.6%, respectively attributed to the elimination of surface-bound water. However, the weight loss percentage of water in MCM-41-supported **[Ru]-2.1** (0.6%) is relatively low compared to bare MCM-41. The second weight losses on the TG curves within the range of 8-9% corresponded to the loss of organic species, precisely PPh<sub>2</sub>.<sup>40, 59, 61-63</sup> Relatively, these percent weight loss values agree with the percentage theoretical weight loss calculation based on loadings (See experimental sections 6.3.3.1 and 6.3.3.2). Correspondingly, the DTG curves of fumed silica-supported **[Ru]-2.1** and MCM-41-supported **[Ru]-2.1** gave similar doublet peaks at ca. 300 and ca. 400 associated with the loss of phosphines. Furthermore, TG curves of fumed silica-supported **[Ru]-2.2** and MCM-41-supported **[Ru]-2.2** demonstrated four and five stages of degradation, respectively (Figure 3.8e-f). The first stage weight loss for fumed silica-supported **[Ru]-2.2** (1.5%) and the first two stages of weight loss for MCM-41-supported **[Ru]-2.2** (1.4% and 1.7%) corresponded to the loss of weakly bound water. The DTG curve for MCM-41-supported **[Ru]-2.2** with an endothermic peak at 96°C (below 100°C) confirmed the second percentage weight loss of 1.7% was due to the release of physically bound water (Figure 3.8e-f). The second and third decomposition stage on the TG curves of fumed silica-supported **[Ru]-2.2** and MCM-



**Figure 3.8:** TG/DTG analysis of (a) unmodified fumed silica (b) unmodified MCM-41 (c) fumed silica-supported [Ru]-2.1 (d) MCM-41-supported [Ru]-2.1 (e) fumed silica-supported [Ru]-2.2 (f) MCM-41-supported [Ru]-2.2.

41-supported **[Ru]-2.2** respectively corresponded to the loss of chlorides (3-4%). The weight loss percentage of about 3-4% obtained at these stages correlates with the theoretical percentage weight loss of chlorides based on catalyst loadings (See experimental sections 6.3.3.3 and 6.3.3.4). The DTG curves revealed that the release of chlorine atoms from MCM-41-supported **[Ru]-2.2** and fumed silica-supported **[Ru]-2.2** occurred specifically at 230°C and 255°C, respectively. Additionally, the TG curves showed further decomposition fragments of 6-8% for both supported catalysts corresponding to the loss of phenyl groups based on catalyst loadings (See experimental sections 6.3.3.5 and 6.3.3.6). On the DTG curves, the loss of these phenyl groups occurred at ca. 350°C. The last stage of decomposition of both supported catalysts occurred between 476-704°C, closely related to the loss of *p*-cymene based on catalyst loadings (See experimental sections 6.3.3.7 and 6.3.3.8). Notably, due to the nature of organic species in complex **[Ru]-2.2**, the detachment of chlorine atoms, phenyl groups and *p*-cymene can easily occur in the fumed silica-supported **[Ru]-2.2** and MCM-41-supported **[Ru]-2.2** upon decomposition. In summary, the loss of complex **[Ru]-2.2** fragments in the supported catalysts suggested successful incorporation of the complex on the fumed silica and MCM-41.

### 3.3.3.3 X-ray diffraction (XRD) studies

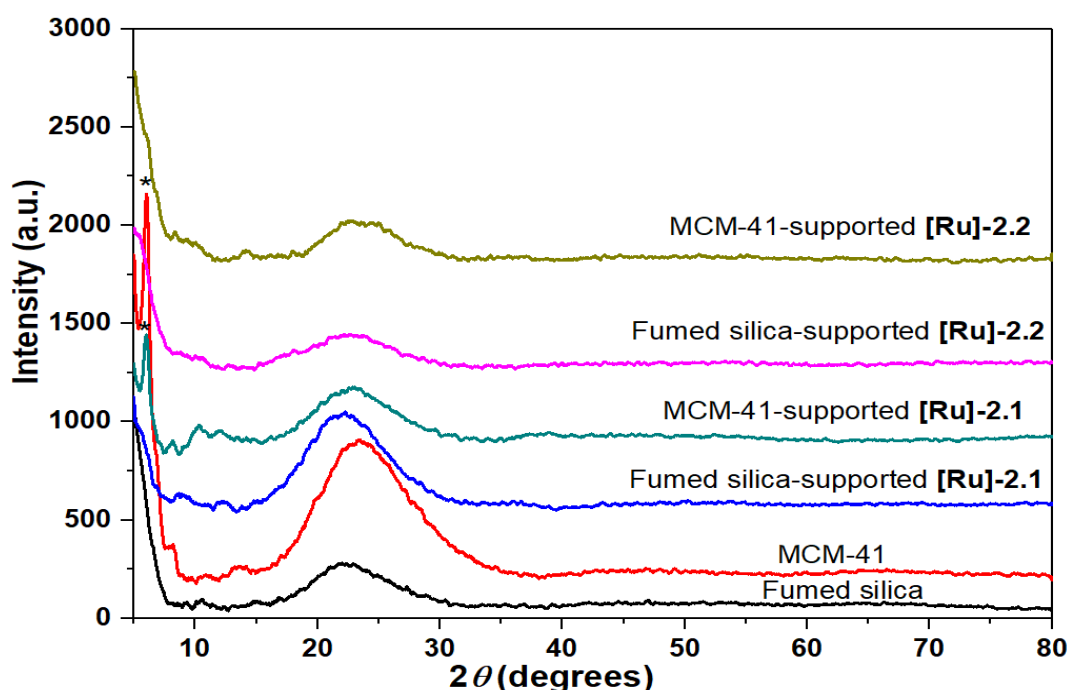


**Figure 3.9:** XRD patterns of unmodified fumed silica/MCM-41 and fumed silica/MCM-41-supported **[Ru]-2.1** and fumed silica/MCM-41-supported **[Ru]-2.2**

To elucidate the structure of fumed silica/MCM-41 and the impact of functionalisation on the crystal structure of these silica materials, XRD studies were conducted and the results are displayed in Figure 3.9.

The XRD patterns of bare fumed silica and MCM-41 exhibited a broad peak at  $2\theta = 21.62^\circ$ , typical of amorphous silica.<sup>64</sup> An additional peak at  $2\theta = 6.01^\circ$  (asterisked) was observed in bare MCM-41 (red line) corresponding to (210) plane<sup>13, 41, 46</sup> as earlier shown in section 3.1.3, Figure 3.5. However, it should be noted that the characteristic MCM-41 peaks between  $2\theta = 0-5^\circ$  were not captured due to the operating conditions ( $2\theta = 5-80^\circ$ ) of the XRD diffractometer used. A lower angle XRD diffractometer is required to capture these peaks. Pleasingly, fumed silica/MCM-41-supported **[Ru]-2.1** and fumed silica/MCM-41-supported **[Ru]-2.2** demonstrated XRD patterns similar to that of bare fumed silica and MCM-41, an indication that the binding of the catalysts to the silica materials occurred primarily inside the mesoporous channels without any alteration to the crystallographic phase.<sup>61, 65</sup> In short, the unaltered XRD pattern displayed by functionalised fumed silica and MCM-41 with respect to bare fumed silica and MCM-41 illustrated that the crystal structures of the silica materials were preserved after the silylation process.

#### 3.3.3.4 N<sub>2</sub> adsorption/desorption studies

The pore structure of unmodified fumed silica/MCM-41 and modified fumed silica/MCM-41 were examined by low pressure N<sub>2</sub> adsorption/desorption measurements. Surface areas, total pore volumes, and average pore radius of unfunctionalised fumed silica/MCM-41, fumed silica/MCM-41-supported **[Ru]-2.1** and fumed silica/MCM-41-supported **[Ru]-2.2** are listed in Table 3.4. The surface areas and pore volume/radius were calculated using Brunauer-Emmett-Teller (BET)<sup>66-68</sup> and Barret-Joyner-Halenda (BJH)<sup>69</sup> methods, respectively. The BET surface areas for bare fumed silica, fumed silica-supported **[Ru]-2.1** and fumed silica-supported **[Ru]-2.2** are 348 m<sup>2</sup>/g, 257 m<sup>2</sup>/g and 168 m<sup>2</sup>/g respectively. As expected, the surface areas of fumed silica decreased after functionalisation with the organofunctional silane complexes. A significant decrease in surface areas of supported complexes in relation to unmodified fumed silica suggested the occupancy of the complexes in the mesoporous channels of fumed silica. On the other hand, the pore volumes and pore

radii of fumed silica- supported complexes were higher than that of bare fumed silica. This could be due to the existence of interparticle mesoporosity in fumed silica.<sup>48</sup>

**Table 3.4:** BET surface area, BJH pore volume, and pore diameter of bare fumed silica/MCM-41, fumed silica/MCM-41-supported [Ru]-2.1 and fumed silica/MCM-41-supported [Ru]-2.2.

<b>Samples</b>	<b>BET Surface Area (m<sup>2</sup>/g)</b>	<b>Pore Volume (cm<sup>3</sup>/g)</b>	<b>Pore Radius (Å)</b>
Fumed silica	348	0.69	16
MCM-41	986	0.27	15
Fumed silica-supported [Ru]-2.1	257	1.74 <sup>Er</sup>	249 <sup>Er</sup>
MCM-41-supported [Ru]-2.1	1083	0.19	20
Fumed silica-supported [Ru]-2.2	168	1.06	16
MCM-41-supported [Ru]-2.2	1016	0.19	20

Er = Error in BJH methods

In the case of MCM-41 and MCM-41-supported complexes [Ru]-2.1 and [Ru]-2.2, an increase in surface area and pore radius was observed post functionalisation whereas a decrease in pore volume was recorded. The surface areas of some silica materials have been reported to be unaffected or even higher than the original values after being functionalised with organofunctional silane transition-metal complexes due to interparticular mesoporosity.<sup>48</sup> Additionally, Cimino and co-workers observed an increase in MgO surface area when impregnated with both nickel and ruthenium metal.<sup>70</sup> Accordingly, all samples studied displayed type IV isotherms with H1 hysteresis according to IUPAC classification,<sup>67</sup> typical for mesoporous silica materials (Figure 3.10a-f).<sup>40, 48, 59, 61, 71, 72</sup> The existence of H1 hysteresis in these materials implied the arrangement of spherical particles in a fairly uniform way with the presence of cylindrical pore geometry indicating relatively high pore size uniformity and facile pore connectivity. Similarly, Ji *et al.* observed type IV isotherms with H1 hysteresis for SBA-supported complex [Ru]-2.2.<sup>73</sup> Using t-plot method, bare fumed

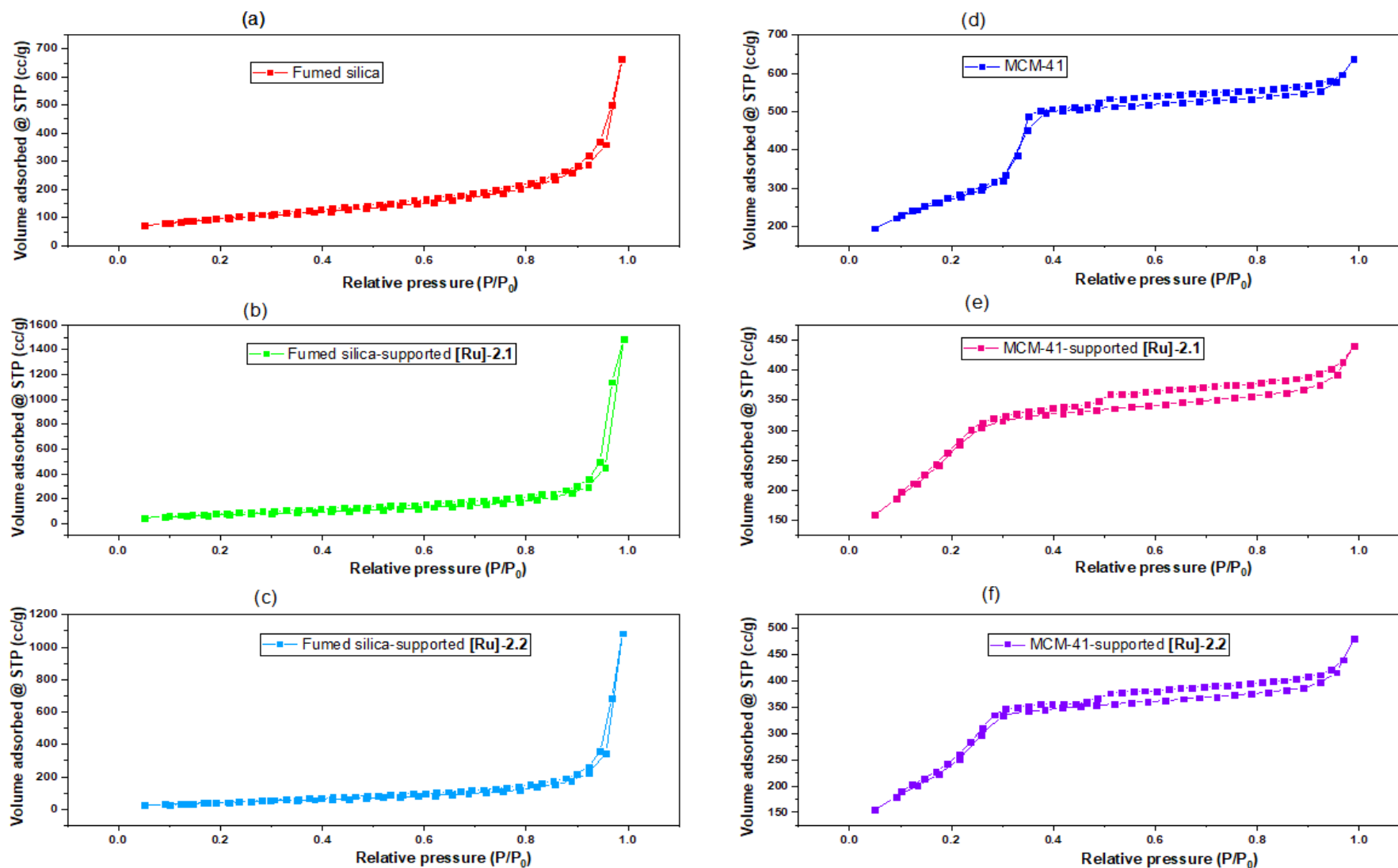


**Figure 3.10:**  $N_2$  adsorption/desorption isotherms of unmodified fumed silica/MCM-41 and fumed silica/MCM-41-supported [Ru]-2.1/[Ru]-2.2

silica and MCM-41-supported **[Ru]-2.1** gave micropore volumes of 0.02 cm<sup>3</sup>/g and 0.14 cm<sup>3</sup>/g respectively while zero micropore volume was recorded for others.

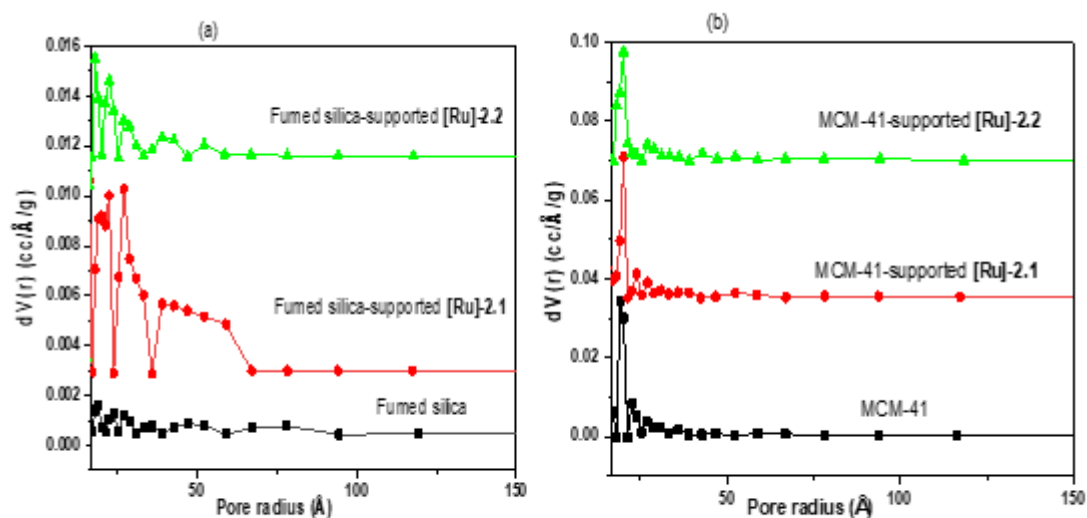


**Figure 3.11:** Pore size distribution curves of (a) bare fumed silica/fumed silica-supported **[Ru]-2.1/[Ru]-2.2** and (b) MCM-41/MCM-41-supported **[Ru]-2.1/[Ru]-2.2**

With the application of BJH method, the particle size distribution curve was obtained by plotting desorption cumulative volume against pore radius. The results for bare fumed silica/MCM-41 and fumed silica/MCM-41-supported **[Ru]-2.1/[Ru]-2.2** are shown in Figure 3.11a-b. Similarly, there was no observable shift in the pore distribution curves of both fumed silica and MCM-41 and their corresponding functionalised analogues, probably due to the slight decrease/increase in pore size post functionalisation. Furthermore, while bare fumed silica/fumed-supported **[Ru]-2.1/[Ru]-2.2** showed an almost trimodal curve, a unimodal pore size distribution curve was observed for bare MCM-41/MCM-41-supported **[Ru]-2.1/[Ru]-2.2**.

### 3.3.3.5 Electron microscopy studies

The morphology of pre-treated bare fumed silica/MCM-41 and functionalised fumed silica/MCM-41 was examined by TEM/STEM/EDS techniques. As can be seen on TEM micrographs displayed in Figure 3.12a-b and c-e (inset), fumed silica samples demonstrated non-ordered mesoporous structures whereas MCM-41 samples exhibited long-range ordered mesoporous structures. The unimodal porosity of MCM-41/MCM-41-supported **[Ru]-2.1/[Ru]-2.2** was also supported by TEM micrographs which showed just small interparticle mesopores (Figure 3.12b, d-e (inset)).

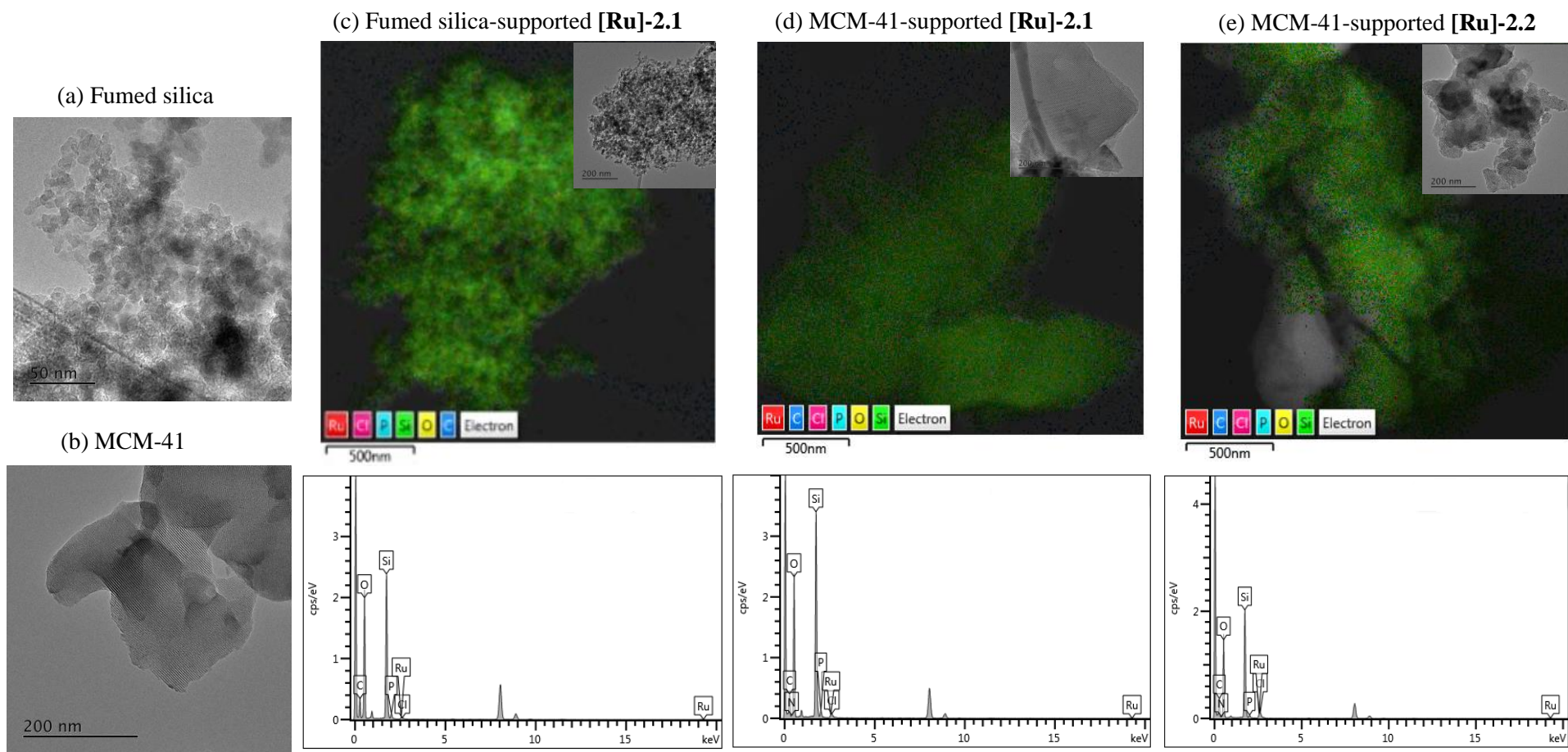


**Figure 3.12:** Representative TEM (grey micrographs including inset), STEM (coloured micrographs) and EDS (spectra) of bare fumed silica/MCM-41 and fumed silica/MCM-41-supported **[Ru]-2.1/ [Ru]-2.2**

Interestingly, the morphologies of the functionalised fumed silica and MCM-41 were quite similar to that of the original materials (Figure 3.12a and c; b, d and e), indicating that the mesostructures of the parent materials were unaffected by the immobilisation process. Fortunately, TEM micrographs of the functionalised fumed silica and MCM-41 showed no visible Ru(0) nanoparticles, implying that Ru(II) was atomically distributed without the formation of agglomeration during the functionalisation process. This observation was further supported by STEM-EDS results. Using a combination of STEM-EDS techniques, the electron mapping of fumed silica and MCM-41-supported **[Ru]-2.1**/**[Ru]-2.2** was performed by using colour to indicate the presence of specific atoms (Ru, P, Si, C, O, Cl) in supported catalysts. Figures 3.12c-e (coloured micrographs) showed the different atoms of the supported catalysts well dispersed over fumed silica and MCM-41 surfaces. As noticed, the homogeneous catalyst moieties were atomically dispersed over the silica materials maintaining the shape of the supports. Interestingly, this result is in harmony with XRD patterns and BJH pore distribution curves which demonstrated unaltered crystal structures of the fumed silica and MCM-41 post functionalisation. In fact, STEM micrographs revealed that these atoms were uniform in their sizes and distinct from each other. Furthermore, EDS spectra of the fumed silica/MCM-41-supported **[Ru]-2.1**/**[Ru]-2.2** was obtained which showed the presence of individual atoms of these complexes. Overall, results from these analyses confirmed the presence of complexes **[Ru]-2.1** and **[Ru]-2.2** on fumed silica and MCM-41.

### 3.3.3.6 Solid-State NMR spectroscopy

The silylation of fumed silica and MCM-41 with organofunctional-silane complexes **[Ru]-2.1** and **[Ru]-2.2** was investigated by  $^{31}\text{P}$ ,  $^{29}\text{Si}$ ,  $^{13}\text{C}$  CP/MAS NMR spectroscopy.

#### 3.3.3.6.1 $^{31}\text{P}$ CP/MAS NMR spectroscopy

In Chapter two, the liquid state  $^{31}\text{P}\{^1\text{H}\}$  NMR chemical shifts of homogeneous complexes **[Ru]-2.1** and **[Ru]-2.2** were reported as ca. 77 and 85 ppm respectively. Figure 3.13 shows the  $^{31}\text{P}$  CP/MAS NMR spectra of fumed silica/MCM-41-supported **[Ru]-2.1** and fumed silica/MCM-41-supported **[Ru]-2.2**. The spectrum of fumed silica-supported catalyst **[Ru]-2.1** showed the complex characteristic peak at ca. 77 ppm (Figure 3.13a), indicating the anchorage of complex **[Ru]-2.1** to fumed silica. Also, two other unknown phosphorus species at 57 and 66 ppm were observed.

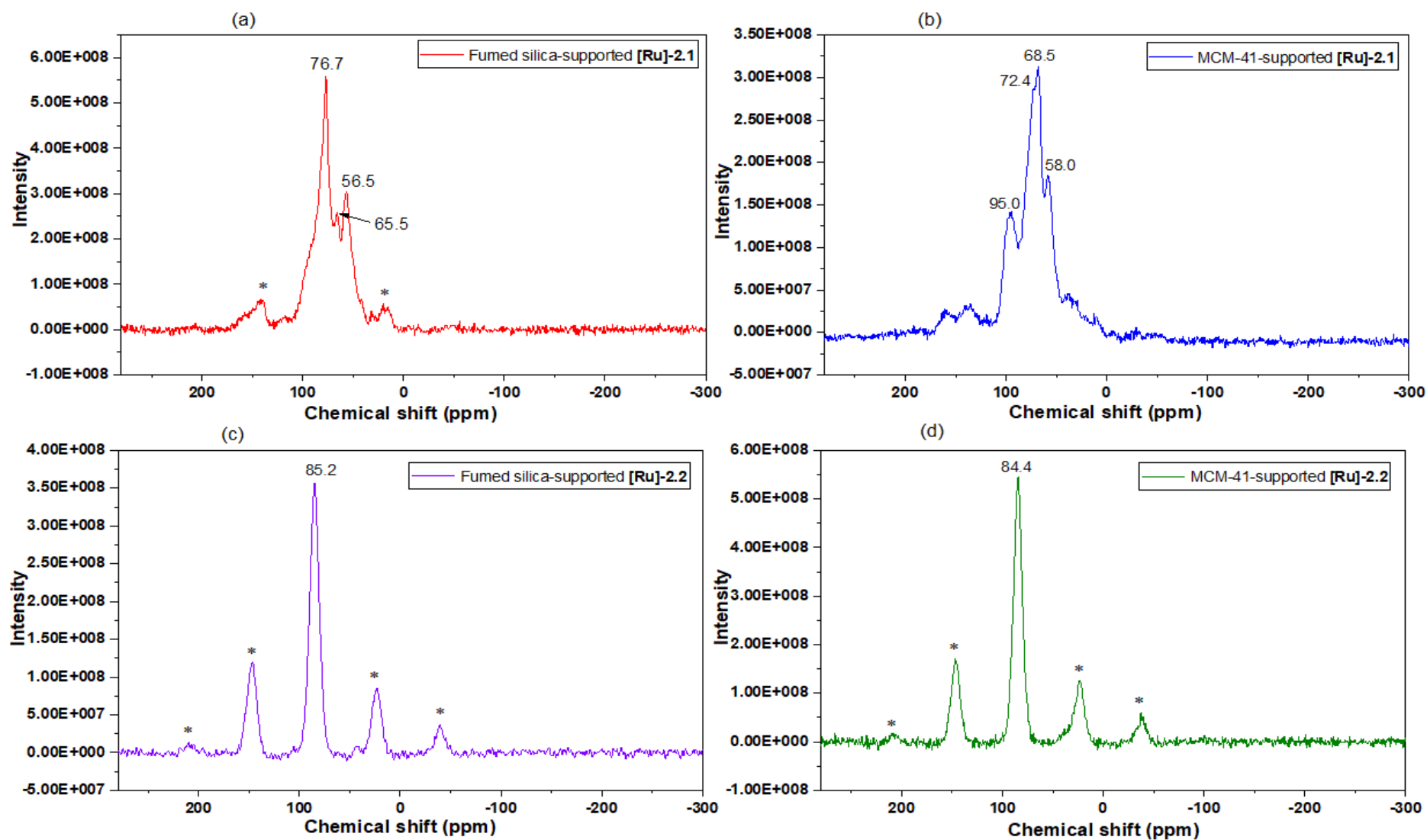
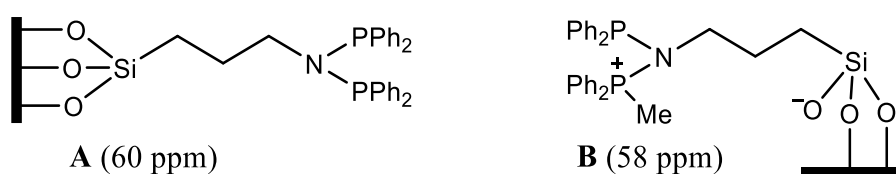


Figure 3.13:  $^{31}\text{P}$  CP/MAS NMR spectra (162 MHz, 10 kHz spinning speed) of fumed silica/MCM-41-supported [Ru]-2.1 and [Ru]-2.2 (\*spinning sidebands)

However, these chemical shifts are very close to those observed in the  $^{31}\text{P}$  NMR (liquid-state) spectrum for the diphenylaminopropyltrimethoxysilane ligand (62 ppm, Chapter 2, Section 2.3.2). Notably, the presence of a few side products was emphasised in the work of Posset *et al* on similar nickel catalysts with silica as a support. However, identification of side products was only achieved by investigating  $\text{SiO}_2$ -bound ligand without metal complexation.<sup>49</sup> Therefore, the peaks at 66 and 57 ppm are similar to the values of  $\text{SiO}_2$ -ligand species **A** and **B** below observed by Posset *et al* and likely originate from traces of uncoordinated ligand bound to the surface of fumed silica (Figure 3.14). It is assumed that it is unlikely that the ligand detached from the ruthenium centre due to the presence of the isotropic complex peak at 77 ppm, therefore, these peaks result from excess ligand from the complex synthesis.



**Figure 3.14:** Side products observed by Posset *et al*

A similar nickel complex by Stamatopoulos *et al* gave just one peak at -42 ppm with SBA-15 as the support.<sup>74</sup> Interestingly, the nature of the support material may thus influence the reactivity of this complex-type as suggested by Posset and co-authors.<sup>49</sup> Another possibility for the appearance of peaks at 57 ppm and 66 ppm may be ascribed to complex anchorage to fumed silica through only one bidentate phosphine with the  $\text{Si}(\text{OMe})_3$  group of the second bidentate remaining unbound, thus, introducing inequivalence in the phosphorus chemical environments.<sup>7</sup>  $^{29}\text{Si}$  and  $^{13}\text{C}$  NMR spectroscopy will reveal further insight into the nature of the immobilised complex. On the other hand, the spectrum of MCM-41-supported **[Ru]-2.1** gave three distinctive phosphorus-31 peaks at 95, 69 and 58 ppm (Figure 3.13b). The characteristic peak for complex **[Ru]-2.1** at 77 ppm was unobservable in this spectrum due to peak broadening of the isotropic line at 69 ppm. However, a shoulder peak at ca. 73 ppm (closer to complex peak) was observed on the isotropic peak at 69 ppm. Comparative examination of fumed silica and MCM-41-supported **[Ru]-2.1** spectra (Figure 3.13a-b) showed some degree of similarity in the peaks position (66/69 and 57/58 ppm) and

difference in peak intensities of the similar peaks at 66/69 ppm as well as the new peak at 95 ppm. From this observed similarity coupled with the shoulder peak at ca. 73 ppm, it can be inferred that the characteristic peak of complex **[Ru]-2.1** is present in MCM-41-supported **[Ru]-2.1** spectrum but overlapped by the line broadening and increasing intensity of the peak at 69 ppm. As discussed earlier, the peaks at 69 and 59 ppm may result from SiO<sub>2</sub>-bound uncoordinated ligand or unbound ligand ends of complex **[Ru]-2.1**.

In contrast to fumed silica and MCM-41-supported **[Ru]-2.1** (Figure 3.13a-b), a well resolved characteristic peaks of complex **[Ru]-2.2** was seen in the spectra of fumed silica and MCM-41-supported **[Ru]-2.2** (Figure 3.13c-d) without any other phosphorus species, signifying a clean immobilisation process. Notably, spinning sidebands were observed in all the spectra of the supported complexes. In summary, the presence of characteristic peaks of complexes **[Ru]-2.1** and **[Ru]-2.2** in functionalised fumed silica and MCM-41 suggested the integrity of the complexes was preserved inside the mesoporous channels of the support without disintegration. Thus, successful immobilisation of the complexes was achieved.

#### 3.3.3.6.2 <sup>13</sup>C CP/MAS NMR spectroscopy

The comparison of the liquid-state <sup>13</sup>C{<sup>1</sup>H} NMR spectra of complexes **[Ru]-2.1** and **[Ru]-2.2** (Figure 3.15) and the <sup>13</sup>C CP/MAS NMR spectra of fumed silica/MCM-41-supported **[Ru]-2.1** and **[Ru]-2.2** (Figure 3.16) revealed the presence of the complexes carbon peaks in the spectra of the functionalised fumed silica and MCM-41. The PPh<sub>2</sub> carbon peaks displayed broad peak between 100 – 150 ppm evidenced in all supported complexes (Figure 3.16a-d). In addition to this, the spectra of fumed silica/MCM-41-supported **[Ru]-2.2** showed the presence of *p*-cymene phenyl carbon peaks around 100 ppm and 77 ppm. The propyl linker methylene peaks were also observed in the spectra of all supported complexes at approximately 30 ppm, 20 ppm, and 6-10 ppm for -NCH<sub>2</sub>-, -CH<sub>2</sub>- and -CH<sub>2</sub>Si- respectively. Most importantly, the presence of these peaks confirmed that complexes **[Ru]-2.1** and **[Ru]-2.2** were successfully anchored onto the fumed silica and MCM-41 surfaces. However, complete condensation of the methoxy groups (OCH<sub>3</sub>) was not achieved in fumed silica/MCM-41-supported **[Ru]-2.1** due to the retention of OCH<sub>3</sub> characteristic peak at ca. 50 ppm in both spectra (Figure 3.16a-b), signifying the existence of free siloxyl (Si(OCH<sub>3</sub>)) group(s) in the supported catalyst.<sup>61, 75</sup>

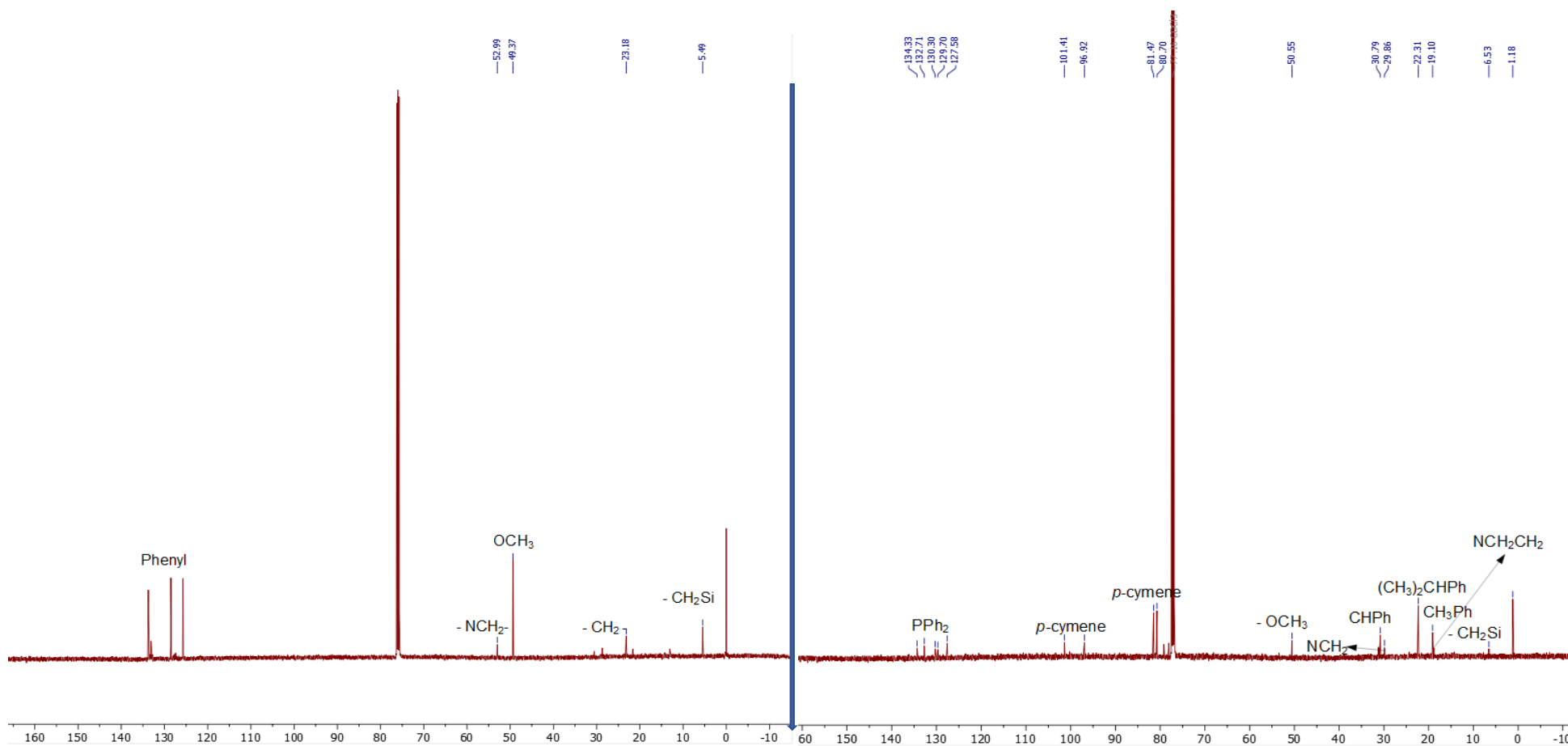


**Figure 3.15:** Liquid-state  $^{13}\text{C}\{^1\text{H}\}$  NMR ( $\text{CDCl}_3$ , 126 MHz) of complex [Ru]-2.1 (left) and [Ru]-2.2 (right)

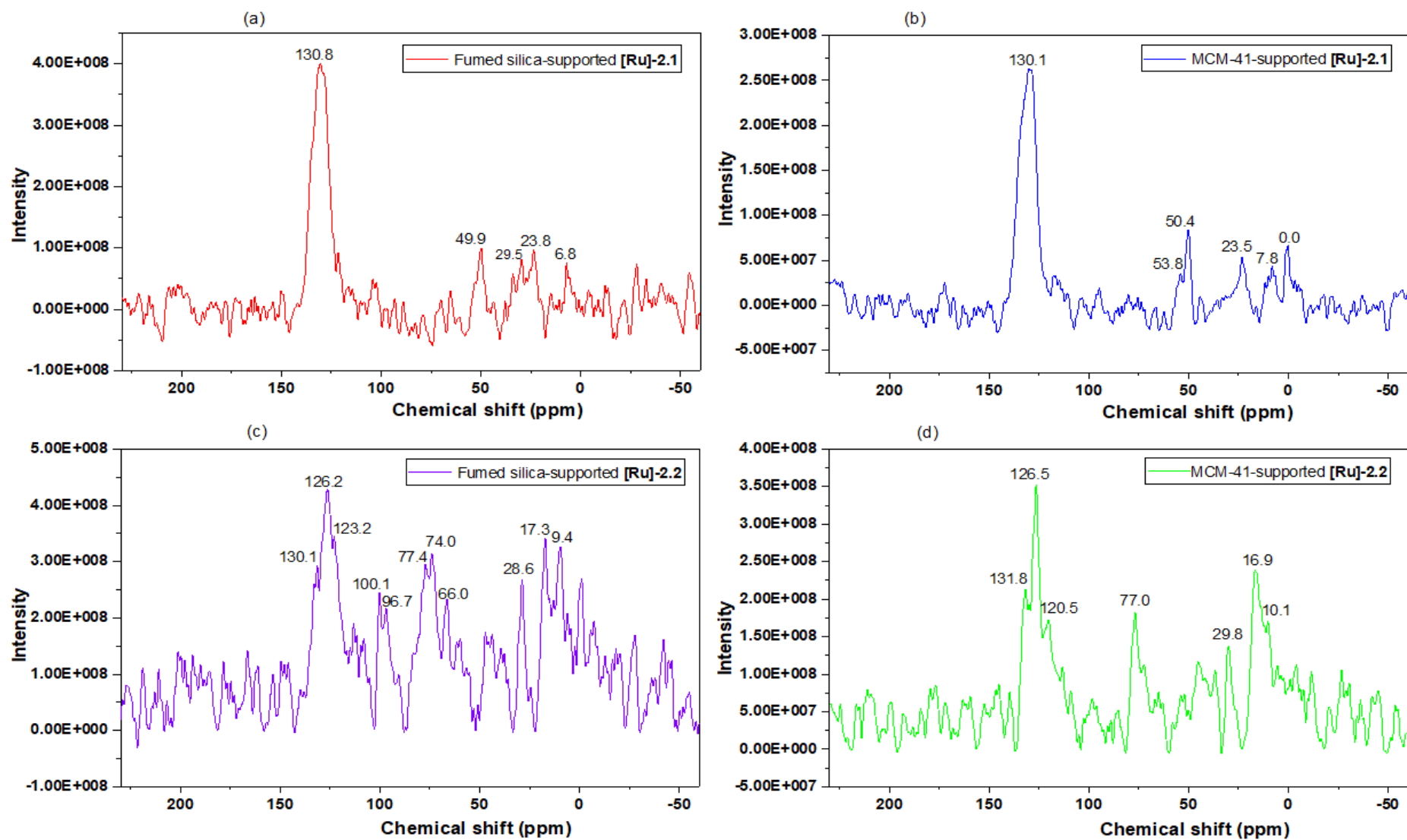


Figure 3.16:  $^{13}\text{C}$  CP/MAS NMR spectra (101 MHz, 10 kHz spinning speed) of fumed silica/MCM-41-supported [Ru]-2.1 and [Ru]-2.2

Contrastingly, no methoxy peak was noticed in the spectra of fumed silica/MCM-41-supported **[Ru]-2.2** (Figure 3.16c-d), an indication of complete condensation process. This result harmonises with the result of  $^{31}\text{P}$  CP/MAS NMR which showed the presence of additional phosphorus species in the spectra for supported **[Ru]-2.1** and a single characteristic peak in supported **[Ru]-2.2**. Summarily, the presence of complexes **[Ru]-2.1** and **[Ru]-2.2** characteristic carbon peaks on the functionalised fumed silica and MCM-41 implied the immobilisation process was successful. It is also important to note here that the  $^{13}\text{C}$  CP/MAS NMR spectra of these complexes showed poor signal-to-noise ratio (S/N), probably due to low catalyst loadings on the support materials (ICP results) coupled with naturally low abundance of  $^{13}\text{C}$  (1.1%). For instance, in Figure 3.16c-d, the signal peaks are barely visible above the noise peaks. Though cross-polarisation (CP) is applied, the efficiency of CP relies on the magnitude of the C-H dipolar interactions such that only those carbons close to protons are magnetised, thus, making some carbons undetectable (e.g., quaternary carbon, aryl-substituted, etc.).<sup>76</sup> S/N is calculated by measuring the height of the peak in relation to the height of the baseline noise, considering the most positive and most negative noise peaks. From the S/N point of view, a higher number of scans (greater than 128 used) is required to improve the signal-to-noise ratio to obtain better spectra because signal-to-noise of a given signal increases proportionally as the square root of the number of scans. That is, for signal-to-noise to double, four times the number of scans is required.<sup>77</sup>

### 3.3.3.6.3 $^{29}\text{Si}$ CP/MAS NMR spectroscopy

The  $^{29}\text{Si}$  CP/MAS NMR spectra of bare fumed silica and fumed silica/MCM-41-supported **[Ru]-2.1** and **[Ru]-2.2** are shown in Figure 3.17. The spectra of bare fumed silica and MCM-41 displayed characteristic peaks of  $\text{Q}^4$ ,  $\text{Q}^3$  and  $\text{Q}^2$  silica surface active sites at - (107-108) ppm, -100 ppm, and - 90 ppm respectively (Figure 3.17a-b) representing siloxane bonds, germinal silanol and isolated silanol accordingly (Figures 3.3 and 3.4). In addition to fumed silica and MCM-41 parent peaks, all supported catalysts gave a single peak at approximately -20 ppm (Figure 3.17c-f) attributed to  $\text{D}^2$  ( $\text{R}_2\text{SiO}_{2/2}$ ) silicon sites according to literature data (Table 3.3). However, the formation of  $\text{D}^n$  (0-2) sites ( $\text{R}_2\text{SiO}_{n/2}$ ) with two R linkers from a T silylating agent ( $\text{RSi}(\text{OR}')_3$ ) with one R linker is uncommon after condensation processes. Even with potential  $-\text{H}_2\text{C}-\text{Si}$  scission during functionalisation,<sup>61, 78</sup> it is unlikely for  $\text{D}^n$  species to

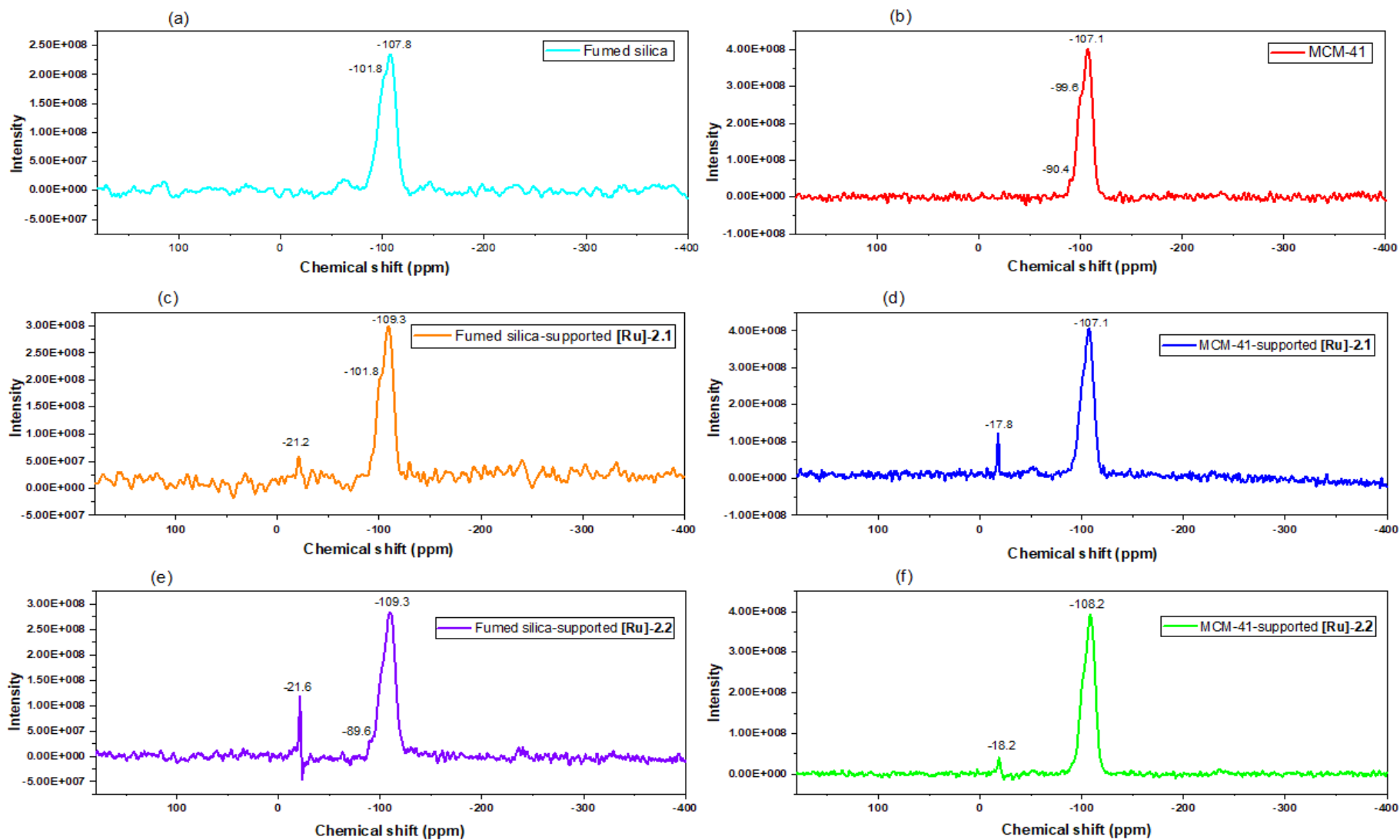


Figure 3.17:  $^{29}\text{Si}$  CP/MAS NMR spectra (80 MHz, 10 kHz spinning speed) of bare fumed silica/MCM-41 and fumed silica/MCM-41-supported [Ru]-2.1 and [Ru]-2.2

result. Similarly, a singlet at -44.6 ppm was reported for a related nickel catalyst.<sup>49</sup> Noteworthy, the alumina-supported **[Ru]-2.1** and **[Ru]-2.2** reported in Chapter four gave two singlet peaks at around -20 ppm and -45 ppm in which the latter matched that of the nickel catalyst reported by Posset *et al.*<sup>79</sup> Thus, since it has been suggested that the nature of the support impacts the reactivity of the silylating complexes, the peak at ca. - 20 ppm present in all supported complexes investigated may be due to due to terminal groups that are only coordinated to a single neighbouring siloxane.<sup>59</sup>

80

### 3.3.3.7 Inductively Coupled Plasma-Mass Spectrometry (ICP-MS)

The amount of Ru in fumed silica/MCM-41 **[Ru]-2.1** and **[Ru]-2.2** was analysed by atomic absorption spectroscopy (AAS) but a relatively low concentration of ruthenium was recorded as a result of undigested supported complexes in aqua regia despite heating on a hot plate in a closed fumehood. Consequently, the application of microwave-assisted digestion was applied through ICP-MS techniques to determine the actual Ru content in the supported catalysts. Ruthenium content was presumed to be 2 wt% assuming complete loading of the homogeneous catalyst relative to fumed silica and MCM-41. The results are shown in Table 3.5.

**Table 3.5:** Ru amount in immobilised complexes determined by ICP-MS

<b>Samples</b>	<b>Amounts of samples taken for ICP (g)</b>	<b>ICP Average Ru Conc. (ppb)</b>	<b>ICP Amount of Ru (mg/g)</b>	<b>ICP Actual Loading (wt %)</b>
Fumed silica-supported <b>[Ru]-2.1</b>	0.05077	12091.95	11.91	1.19
MCM-41-supported <b>[Ru]-2.1</b>	0.05057	11878.16	11.74	1.17
Fumed silica-supported <b>[Ru]-2.2</b>	0.04880	39391.35	40.36	4.04 <sup>a</sup>
MCM-41-supported <b>[Ru]-2.2</b>	0.05070	50717.43	50.02	5.00 <sup>a</sup>

<sup>a</sup>Initial 4 wt% catalyst loading based on two atoms of Ru in catalysts **[Ru]-2.2**

As expected, the final catalyst loadings of 1.17 and 1.19 wt% for MCM-41-supported **[Ru]-2.1** and fumed silica-supported **[Ru]-2.1** respectively were lower than the initial 2 wt% purported. The actual complex **[Ru]-2.2** loading on fumed silica/MCM-41 was 4 wt% not 2 wt% intended to be loaded on the supports based on the presence of two Ru atoms in the complex as revealed by X-ray crystallography. However, the results from ICP gave 4.04 wt% and 5.00 wt% for fumed silica-supported **[Ru]-2.2** and MCM-41-supported **[Ru]-2.2** respectively, higher than the actual 4 wt%. The reason for this additional weight percentage remains unclear.

### 3.3.4 Catalytic activity

#### 3.3.4.1 Ethanol/methanol upgrading to iso-butanol

Fumed silica/MCM-41-supported **[Ru]-2.1** and **[Ru]-2.2** were tested as heterogeneous catalysts in ethanol-methanol upgrading to *iso*-butanol under the standard catalytic conditions used for the homogeneous catalyst; 1 mL ethanol (17.13 mmol), 10 mL methanol (246.88 mmol), 0.1 mol% catalyst loading (0.01713 mmol), 200 mol% NaOMe (34.26 mmol), 2 or 20 h at 180°C in a 100 mL Parr autoclave (mol% relative to ethanol). For consistency and easy comparison, the 0.1 mol% used for homogeneous catalysts is adopted and the calculation for heterogeneous catalysts is based on the ruthenium loading as determined by ICP. Table 3.6 and Figures 3.18 - 3.19 showed the results of the catalysis. Ethanol, *iso*-butanol, 1-propanol, 2-methyl-1-butanol and 1-hexanol are abbreviated as EtOH, *i*BuOH, PrOH and HeOH, respectively in all figures showing catalytic results. Notably, results of the homogeneous catalysts **[Ru]-2.1** and **[Ru]-2.2** reported in Chapter two are included in Table 3.6 for the purpose of comparison (Runs 1-3). As can be seen in Table 3.6 and Figures 3.18 - 3.19, all supported catalysts produced *iso*-butanol as the major product along with other liquid alcohol side products like 1-propanol, 2-methyl-1-butanol and 1-hexanol. Similar to other catalysts reported in this thesis, white solid and gaseous products were observed in all catalytic reactions which have been identified in previous work.<sup>54 81</sup> The utilisation of fumed silica-supported catalyst **[Ru]-2.1** at 2 h gave lower conversion (41%) but higher *iso*-butanol yield (12%) when compared with the results of the unsupported catalyst (compare Runs 1 and 4). Additionally, fumed silica-supported **[Ru]-2.1** gave higher 1-propanol, 2-methyl-1-butanol and 1-hexanol production (Figure 3.18). Though homogeneous **[Ru]-2.1** was

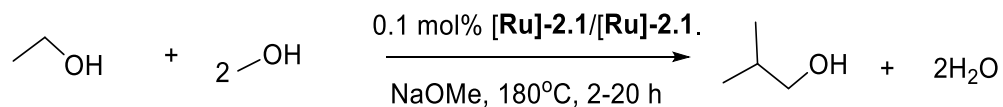


**Table 3.6:** Ruthenium catalysed conversion of ethanol and methanol to *iso*-butanol.

Run <sup>a</sup>	Catalyst	Time (h)	Base	Conversion <sup>b</sup> (%)	Total TON <sup>c</sup>	<i>iso</i> -Butanol	TON <sup>d</sup> (yield) <sup>e</sup> [selectivity] %		
							1-Propanol	2-Methyl-1-butanol	Hexanol
1 <sup>f</sup>	Hom[Ru]-2.1	2	NaOMe	28	280	90(9)[72]	20(2)[18]	20(2)[9]	<5(*)[1]
2 <sup>f</sup>	Hom[Ru]-2.1	24	NaOMe	79	790	440(44)[87]	20(2)[4]	-	120(12)[8]
3 <sup>f</sup>	Hom[Ru]-2.2	24	NaOMe	78	780	170(17)[87]	20(2)[11]	-	10(1)[2]
4	FS[Ru]-2.1	2	NaOMe	41	410	120(12)[73]	20(2)[13]	40(4)[11]	20(2)[4]
5	FS[Ru]-2.1	20	NaOMe	63	630	210(21)[81]	30(3)[10]	30(3)[5]	30(3)[3]
6	M41[Ru]-2.1	20	NaOMe	63	630	240(24)[84]	30(3)[10]	20(2)[4]	20(2)[2]
7	FS[Ru]-2.2	20	NaOMe	65	650	220(22)[85]	30(3)[12]	-	20(2)[3]
8	M41[Ru]-2.2	20	NaOMe	63	630	210(21)[85]	30(3)[12]	-	20(2)[3]

<sup>a</sup>Conditions: Ethanol (1 mL, 17.13 mmol), methanol (10 mL, 247.13 mmol), [Ru] catalyst (0.01713 mmol, 0.1 mol%), Base (34.26 mmol, 200 mol% ), mol% is based on ethanol substrate, 180 °C. <sup>b</sup>Total conversion of ethanol to liquid products as determined by GC analysis of the liquid phase. <sup>c</sup>Total TON based on mmol of total ethanol converted to products per mmol of [Ru] catalyst (ethanol equivalent relative to mmol of catalysts x conversion = 1000 x conversion). <sup>d</sup>TON based on mmol of any product formed per mmol [Ru] catalyst (ethanol equivalent relative to mmol of catalysts x product yield = 1000 x product yield). <sup>e</sup>Total yield and selectivity of alcohol products in the liquid fraction as determined by GC. <sup>f</sup>From Chapter 2, \*Yield less than 0.5%. (Hom = homogeneous, FS = Fumed silica, M41 = MCM-41).

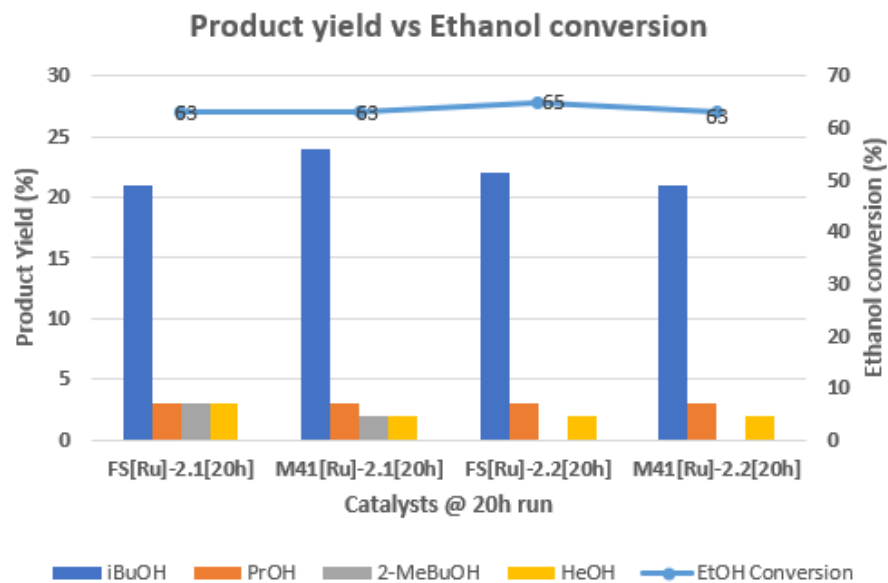


**Figure 3.18:** Yield of liquid products and ethanol conversion obtained from fumed silica/MCM-41-supported [Ru]-2.1/2.2

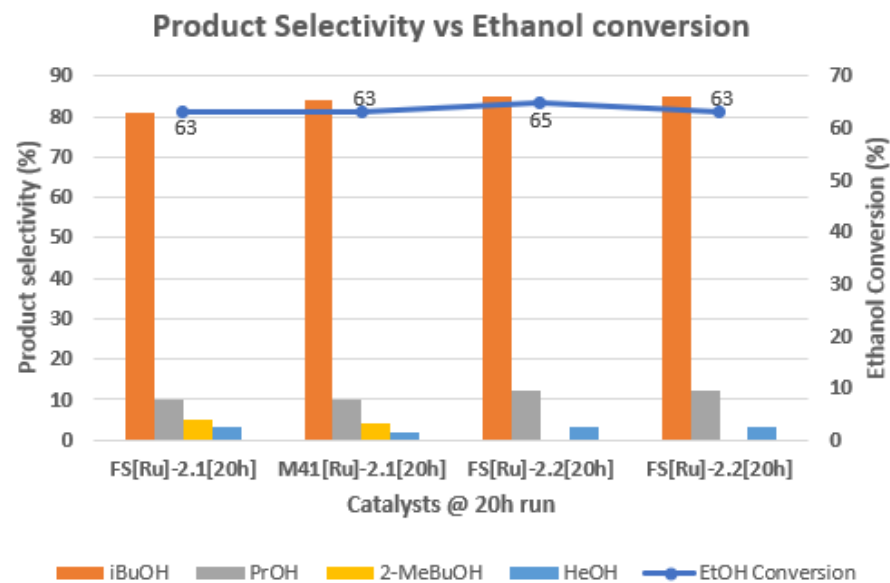


**Figure 3.19:** Selectivity of liquid products and ethanol conversion obtained from fumed silica/MCM-41-supported [Ru]-2.1/2.2

not tested at exactly 20 h, the use of fumed silica and MCM-41-supported catalysts [Ru]-2.1 at 20 h (Runs 5 and 6) compare against 24 h homogeneous run (Run 2) showed that heterogeneous catalysts are less effective at longer reaction times. Presumably, this is due to the limited access of the substrates to metal site in mesoporous channels of the supports coupled with a slow dehydrogenation step due to mobility of the catalyst. In the case of catalyst [Ru]-2.2, higher *iso*-butanol yield (and other alcohols), and selectivity were obtained with the heterogeneous catalysts, however, at the expense of ethanol conversion (Runs 3, 7 and 8). Interestingly, the better performance of fumed silica and MCM-41-supported [Ru]-2.2 over homogeneous [Ru]-2.2 may be ascribed to the high accessibility of substrates to the ruthenium active site via the free ligand end coupled with the stability of the catalysts on the support surface and hydrophobicity of the catalyst (-Si-O-Si- formation). Furthermore, the mobility of the supported catalyst might have affected the rate of ethanol conversion to catalytic products. This result revealed that fumed silica performed better than MCM-41 as a support material (Runs 7 and 8) for catalyst [Ru]-2.2 immobilisation. Generally, these supported catalysts produced clearer post catalytic liquid than the homogeneous counterparts, suggesting some degree of stability in the supported catalysts. The supported catalysts are therefore assumed to be heterogeneous in nature. Next, recyclability studies were conducted with the addition of fresh base and substrates to the recovered immobilised metal catalysts. To further reveal the heterogeneous nature of these catalysts at longer reaction time (20 h), experiments to gauge metal leaching were conducted. Furthermore, the impact of water on the supported catalyst was investigated. All results obtained from these studies are discussed in subsequent sections.

#### 3.3.4.2 Recyclability studies

The result of the recyclability study conducted with fumed silica-supported catalyst [Ru]-2.1 as presented in Table 3.7 (Runs 1-5) and Figure 3.20 illustrated that the catalyst was active up to the fifth cycle, though, inconsistent results were observed in ethanol conversion, productivity and selectivity. The irregularities in these results stemmed from the filtration method adopted for the recovery of fumed silica-supported catalyst [Ru]-2.1 after each 20 h catalytic reaction. Because of the inefficient filtration method, some of the catalysts were filtered off into the filtrate and

**Table 3.7:** Recyclability studies with fumed silica and MCM-41-supported [Ru]-2.1.

Run <sup>a</sup>	Catalyst	Time (h)	Base	Conversion <sup>b</sup> (%)	Total TON <sup>c</sup>	<i>iso</i> -Butanol	TON <sup>d</sup> (yield) <sup>e</sup> [selectivity] %		
							1-Propanol	2-Methyl-1-butanol	Hexanol
1	FS[Ru]-2.1 <sup>B1</sup>	20	NaOMe	63	630	210(21)[81]	30(3)[10]	30(3)[5]	30(3)[3]
2	FS[Ru]-2.1 <sup>B2</sup>	20	NaOMe	6	60	40(4)[49]	30(3)[29]	30(3)[16]	20(2)[6]
3	FS[Ru]-2.1 <sup>B3</sup>	20	NaOMe	4	40	60(6)[51]	30(3)[30]	30(3)[13]	20(2)[6]
4	FS[Ru]-2.1 <sup>B4</sup>	20	NaOMe	18	180	60(6)[47]	40(4)[34]	30(3)[12]	30(3)[7]
5	FS[Ru]-2.1 <sup>B5</sup>	20	NaOMe	23	230	80(8)[56]	40(4)[27]	30(3)[12]	30(3)[6]
6	M41[Ru]-2.1 <sup>B1</sup>	20	NaOMe	63	630	240(24)[84]	30(3)[10]	20(2)[4]	20(2)[2]
7	M41[Ru]-2.1 <sup>B2</sup>	20	NaOMe	7	70	30(3)[47]	20(2)[27]	20(2)[16]	20(2)[10]

<sup>a</sup>Conditions: Ethanol (1 mL, 17.13 mmol), methanol (10 mL, 247.13 mmol), [Ru] catalyst (0.01713 mmol, 0.1 mol%), Base (34.26 mmol, 200 mol% ), mol% is based on ethanol substrate, 180 °C. <sup>b</sup>Total conversion of ethanol to liquid products as determined by GC analysis of the liquid phase. <sup>c</sup>Total TON based on mmol of total ethanol converted to products per mmol of [Ru] catalyst (ethanol equivalent relative to mmol of catalysts x conversion = 1000 x conversion). <sup>d</sup>TON based on mmol of any product formed per mmol [Ru] catalyst (ethanol equivalent relative to mmol of catalysts x product yield = 1000 x product yield). <sup>e</sup>Total yield and selectivity of alcohol products in the liquid fraction as determined by GC. (FS = Fumed silica, M41 = MCM-41 and B1-5 = Batch runs).

**Table 3.8:** Leachability Test (Hot filtration) with fumed silica-supported [Ru]-2.1.

Run <sup>a</sup>	Catalyst	Time (h)	Base	Conversion <sup>b</sup> (%)	Total TON <sup>c</sup>	<i>iso</i> -Butanol	TON <sup>d</sup> (yield) <sup>e</sup> [selectivity] %		
							1-Propanol	2-Methyl-1-butanol	Hexanol
1 <sup>f</sup>	FS[Ru]-2.1	2	NaOMe	43	430	80(8)[85]	10(1)[15]	30(3)[12]	-
2 <sup>f</sup>	FS[Ru]-2.1	4	-	46	460	80(8)[85]	10(1)[15]	-	-
3 <sup>f</sup>	FS[Ru]-2.1	6	-	45	450	90(9)[86]	20(2)[14]	-	-
4 <sup>f</sup>	FS[Ru]-2.1	20	-	62	620	120(12)[89]	10(1)[11]	-	-
5	FS[Ru]-2.1	20	NaOMe	63	630	210(21)[81]	30(3)[10]	30(3)[5]	30(3)[3]

<sup>a</sup>Conditions: Ethanol (1 mL, 17.13 mmol), methanol (10 mL, 247.13 mmol), [Ru] catalyst (0.01713 mmol, 0.1 mol%), Base (34.26 mmol, 200 mol% ), mol% is based on ethanol substrate, 180 °C. <sup>b</sup>Total conversion of ethanol to liquid products as determined by GC analysis of the liquid phase. <sup>c</sup>Total TON based on mmol of total ethanol converted to products per mmol of [Ru] catalyst (ethanol equivalent relative to mmol of catalysts x conversion = 1000 x conversion). <sup>d</sup>TON based on mmol of any product formed per mmol [Ru] catalyst (ethanol equivalent relative to mmol of catalysts x product yield = 1000 x product yield). <sup>e</sup>Total yield and selectivity of alcohol products in the liquid fraction as determined by GC. <sup>f</sup>Hot filtration (FS = Fumed silica).

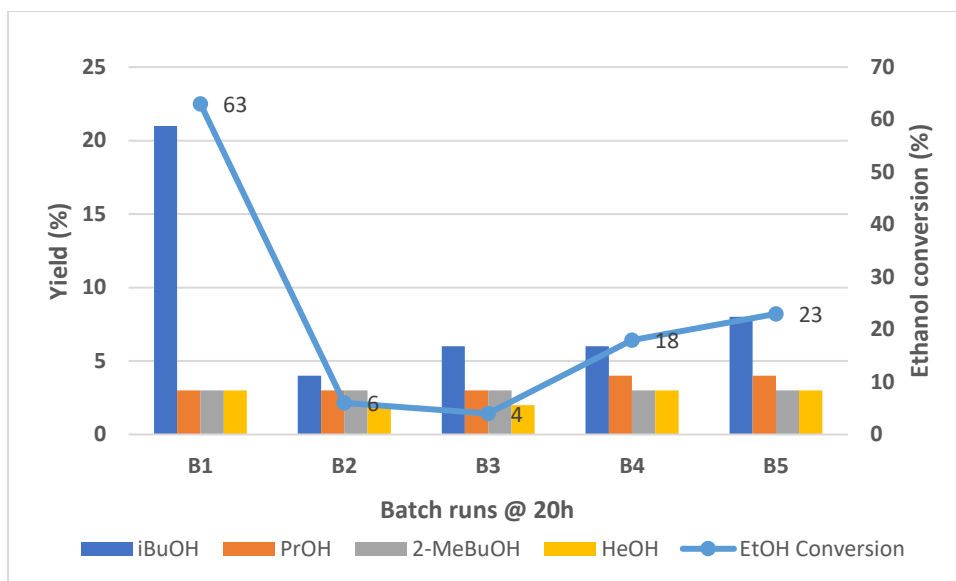


**Figure 3.20:** Recycling test using 0.1 mol% fumed silica-supported **[Ru]-2.1** at 20 h with fresh 200 mol% NaOMe, 1 mL ethanol, 10 mL methanol for every batch run thereafter recovered which were added to subsequent recyclability runs, resulting in increased conversion, yield and selectivity in the subsequent run. Nevertheless, this method demonstrates that the recoverability of the supported catalyst can be achieved. Moreover, to know whether the supported catalyst was left after the 5<sup>th</sup> cycle, the post catalytic solid was analysed with ICP-MS. The result gave 2.33 ppm of ruthenium. Due to time constraints, only one recyclability test was carried out on MCM-41-supported catalyst **[Ru]-2.1**, which still showed some activity towards ethanol-methanol upgrading to *iso*-butanol (Table 3.7, Runs 6-7).

### 3.3.4.3 Leachability test

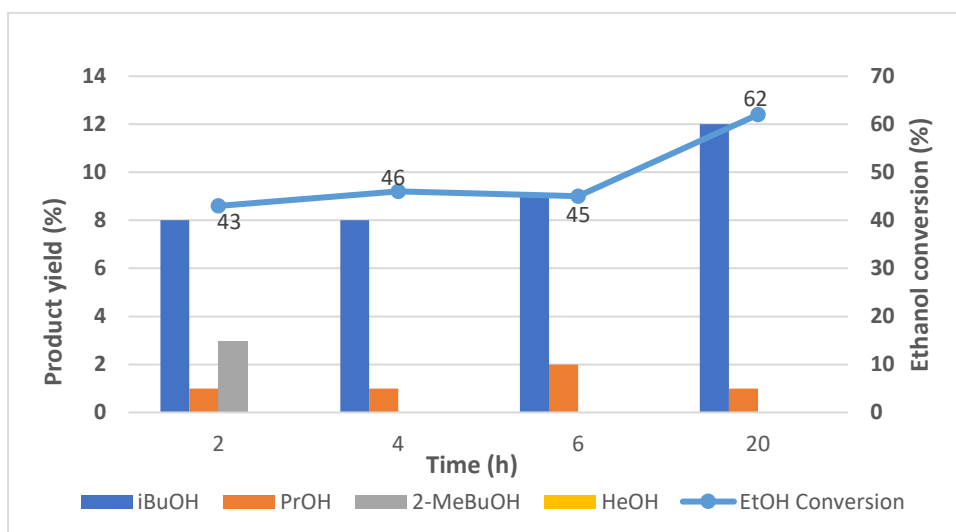


**Figure 3.21:** Leaching test using 0.1 mol% fumed silica-supported **[Ru]-2.1**, 200 mol% NaOMe, 1 mL ethanol, 10 mL methanol for a period of 20 h

Ruthenium leaching from fumed silica-supported catalyst **[Ru]-2.1** was investigated through hot filtration method and ICP-MS. The first leaching test was performed by adding fresh base and substrates to the filtered liquid products from a 20 h catalytic run and allowed to run for another 20 h under the standard catalytic conditions. No pressure build-up was generated throughout the catalytic period and thus, no activity was recorded, suggesting no ruthenium leaching in the liquid product employed in this catalytic reaction. Another leaching test was performed using hot filtration. In this method, a 20 h run was set up and a sample of liquid products was taken every 2 h in the first six hours and thereafter allowed to carry until the end of the catalytic period after which the last sample was collected. Results from analysis of these samples by GC are presented in Table 3.8 (Runs 1 and 4) and Figure 3.21. The results showed increasing yield and selectivity of *iso*-butanol despite an interruption to the closed catalytic system. However, the consecutive release of the generated hydrogen gas essential for this catalytic system during the sample collection process significantly lowered the *iso*-butanol and 1-propanol yield to half the results obtained in an uninterrupted closed system (Table 3.8, Runs 4 and 5). Lastly, analysis of the post catalytic liquid from the hot filtration run was analysed by ICP-MS to further examine the leachability of the supported catalyst. The result gave 0.01 ppm. A less than 10 ppm ruthenium content obtained from this study implied a negligible leaching of Ru(II) species from fumed silica-supported catalyst **[Ru]-2.1**.<sup>40, 61</sup> Various tests performed here illustrated the heterogenous behaviour of fumed silica-supported catalyst **[Ru]-2.1**. The results further confirmed that the integrity of the catalyst **[Ru]-2.1** was preserved in the mesoporous channels of the fumed silica.

#### 3.3.4.4 Water tolerance

The water tolerance of fumed silica-supported catalyst **[Ru]-2.1** was examined with the introduction of 1 mL degassed water into the catalytic system. As shown in Table 3.9, a drastic decrease in activity was observed resulting in lower ethanol conversion (27%), *iso*-butanol yield (5.4%) and selectivity (64%) compared with results from the run without water addition (Runs 1 and 2). A similar effect was reported with previous homogeneous P-N catalysts employed in ethanol conversion to *iso*-butanol using sodium hydroxide as base.<sup>54</sup>

**Table 3.9:** Effect of water on catalytic activity of fumed silica-supported [Ru]-2.1.

Run <sup>a</sup>	Catalyst	Time (h)	Base	Conversion <sup>b</sup> (%)	Total TON <sup>c</sup>	<i>iso</i> -Butanol	TON <sup>d</sup> (yield) <sup>e</sup> [selectivity] %		
							1-Propanol	2-Methyl-1-butanol	Hexanol
1	<sup>FS</sup> [Ru]-2.1	20	NaOMe	63	630	210(21)[81]	30(3)[10]	30(3)[5]	30(3)[3]
2 <sup>f</sup>	<sup>FS</sup> [Ru]-2.1	20	NaOMe	27	270	50(5)[64]	30(3)[36]	-	-

<sup>a</sup>Conditions: Ethanol (1 mL, 17.13 mmol), methanol (10 mL, 247.13 mmol), [Ru] catalyst (0.01713 mmol, 0.1 mol%), Base (34.26 mmol, 200 mol% ), mol% is based on ethanol substrate, 180 °C. <sup>b</sup>Total conversion of ethanol to liquid products as determined by GC analysis of the liquid phase. <sup>c</sup>Total TON based on mmol of total ethanol converted to products per mmol of [Ru] catalyst (ethanol equivalent relative to mmol of catalysts x conversion = 1000 x conversion). <sup>d</sup>TON based on mmol of any product formed per mmol [Ru] catalyst (ethanol equivalent relative to mmol of catalysts x product yield = 1000 x product yield). <sup>e</sup>Total yield and selectivity of alcohol products in the liquid fraction as determined by GC. <sup>f</sup>Water added (1 mL) (FS = Fumed silica).

**Table 3.10:** Effect of reactor size on catalytic activity of MCM-1-supported [Ru]-2.1.

Run <sup>a</sup>	Catalyst	Time (h)	Base	Conversion <sup>b</sup> (%)	Total TON <sup>c</sup>	<i>iso</i> -Butanol	TON <sup>d</sup> (yield) <sup>e</sup> [selectivity] %		
							1-Propanol	2-Methyl-1-butanol	Hexanol
1 <sup>f</sup>	<sup>M41</sup> [Ru]-2.1	2	NaOMe	5	50	70(7)[70]	10(1)[14]	20(2)[11]	20(2)[6]
2 <sup>f</sup>	<sup>M41</sup> [Ru]-2.1	20	NaOMe	36	360	150(15)[77]	20(2)[13]	30(3)[7]	20(2)[3]
3	<sup>M41</sup> [Ru]-2.1	20	NaOMe	63	630	240(24)[84]	30(3)[10]	20(2)[4]	20(2)[2]

<sup>a</sup>Conditions: Ethanol (1 mL, 17.13 mmol), methanol (10 mL, 247.13 mmol), [Ru] catalyst (0.01713 mmol, 0.1 mol%), Base (34.26 mmol, 200 mol% ), mol% is based on ethanol substrate, 180 °C. <sup>b</sup>Total conversion of ethanol to liquid products as determined by GC analysis of the liquid phase. <sup>c</sup>Total TON based on mmol of total ethanol converted to products per mmol of [Ru] catalyst (ethanol equivalent relative to mmol of catalysts x conversion = 1000 x conversion). <sup>d</sup>TON based on mmol of any product formed per mmol [Ru] catalyst (ethanol equivalent relative to mmol of catalysts x product yield = 1000 x product yield). <sup>e</sup>Total yield and selectivity of alcohol products in the liquid fraction as determined by GC. <sup>f</sup>300 mL autoclave used (M41 = MCM-41).

### 3.3.4.5 Reactor size effect

Initially, catalytic experiments with MCM-41-supported catalyst **[Ru]-2.1** were conducted in a 300 mL autoclave to enable concurrent catalytic testing with fumed silica-supported catalyst **[Ru]-2.1**. However, it was noticed that the size of this reactor influenced the pressure generated in the system and as a consequence affected the yield of product formed when compared with the results obtained from a 100 mL autoclave run (Table 3.10, Runs 2 and 3). For correct comparative studies, all subsequent catalytic reactions were carried out in the 100 mL autoclave.

### 3.4 Conclusion and Future work

In conclusion, homogeneous complexes **[Ru]-2.1** and **[Ru]-2.2** were successfully immobilised on fumed silica and MCM-41. Full characterisation of the heterogenised catalysts was accomplished with the use of several characterisation techniques, evidencing the silylation of fumed silica and MCM-41 with the organofunctional silane complexes. Additionally, the heterogeneous catalysts showed reasonable activity towards ethanol-methanol upgrading to *iso*-butanol and the integrity of Ru(II) sites was maintained inside the support channels even under the harsh catalytic conditions. Even, in the presence of water, fumed silica-supported catalyst **[Ru]-2.1** gave acceptable activity. Finally, the supported catalysts demonstrated the possibility of being recyclable if a better separation technique is applied.

Based on the results of this chapter, the following future work are beneficial to the present work.

- Stability and recyclability studies on fumed silica and MCM-41-supported catalyst **[Ru]-2.2**
- Water tolerance of other heterogeneous catalysts.
- Kinetic studies of homogeneous and heterogeneous catalysts.

### 3.5 References

1. C. E. Bronnimann, R. C. Zeigler and G. E. Maciel, *J. Am. Chem. Soc.*, 1988, **110**, 2023-2026.
2. I. S. Chuang, D. R. Kinney and G. E. Maciel, *J. Am. Chem. Soc.*, 1993, **115**, 8695-8705.
3. D. R. Kinney, I. S. Chuang and G. E. Maciel, *J. Am. Chem. Soc.*, 1993, **115**, 6786-6794.
4. I. S. Chuang and G. E. Maciel, *J. Phys. Chem. B*, 1997, **101**, 3052-3064.
5. I.-S. Chuang and G. E. Maciel, *J. Am. Chem. Soc.*, 1996, **118**, 401-406.
6. R. C. Zeigler and G. E. Maciel, *J. Am. Chem. Soc.*, 1991, **113**, 6349-6358.
7. K. D. Behringer and J. Blümel, *Chem. Commun.*, 1996, 653-654.
8. P. M. Price, J. H. Clark and D. J. Macquarrie, *J. Chem. Soc., Dalton Trans.*, 2000, 101-110.
9. E. E. Vansant, P. Van Der Voort and K. C. Vrancken, in *Studies in Surface Science and Catalysis*, Ed. B. Delmon and J.T. Yates, Amsterdam, The Netherlands, 1995, **93**, ch. 1, pp. 3-4.
10. E. E. Vansant, P. Van Der Voort and K. C. Vrancken, in *Studies in Surface Science and Catalysis*, Ed. B. Delmon and J.T. Yates, Amsterdam, The Netherlands, 1995, **93**, ch. 2, pp. 31-46.
11. P. Hoffmann and E. Knözinger, *Surf. Sci.*, 1987, **188**, 181-198.
12. E. E. Vansant, P. Van Der Voort and K. C. Vrancken, in *Studies in Surface Science and Catalysis*, Ed. B. Delmon and J.T. Yates, Amsterdam, The Netherlands, 1995, **93**, ch. 3, pp. 59-66.
13. S. Alahmad, *Orient. J. Chem.*, 2012, **28**, 1.
14. A. V. Blaaderen and A. Vrij, in *The Colloid Chemistry of Silica*, ed. Horacio E. Bergna, Dupot, American Chemical Society, Washington, DC, 1994, **Advances in chemistry series, 234**, ch. 1, pp. 22-23, 28-37.
15. E. E. Vansant, P. Van Der Voort and K. C. Vrancken, in *Studies in Surface Science and Catalysis*, Ed. B. Delmon and J.T. Yates, Amsterdam, The Netherlands, 1995, **93**, ch. 3, pp. 65-68, ch. 69, pp. 201.
16. A. V. Blaaderen and A. Vrij, in *The Colloid Chemistry of Silica*, ed. Horacio E. Bergna, Dupot, American Chemical Society, Washington, DC, 1994, **Advances in chemistry series, 234**, ch. 10, pp. 218.
17. B. Humbert, C. Carteret, A. Burneau and J. P. Gallas, in *Colloidal Silica: Fundamentals and Applications*, ed. Horacio E. Bergna and William O. Roberts, CRC Press, Taylor & Francis Group, Boca Raton, FL, 2006, **Surfactant Science Series, 131**, ch. 25-26, pp. 287-310.
18. G. E. Maciel and D. W. Sindorf, *J. Am. Chem. Soc.*, 1980, **102**, 7606-7607.
19. D. W. Sindorf and G. E. Maciel, *J. Am. Chem. Soc.*, 1983, **105**, 1487-1493.
20. K. K. Unger, in *The Colloid Chemistry of Silica*, ed. Horacio E. Bergna, Dupot, American Chemical Society, Washington, DC, 1994, **Advances in chemistry series, 234**, ch. 8, pp. 174.
21. K. K. Unger, in *Colloidal Silica: Fundamentals and Applications*, ed. Horacio E. Bergna and William O. Roberts, CRC Press, Taylor & Francis Group, Boca Raton, FL, 2006, **Surfactant Science Series, 131**, ch. 23, pp. 272.
22. A. V. Blaaderen and A. Vrij, in *Colloidal Silica: Fundamentals and Applications*, ed. Horacio E. Bergna and William O. Roberts, CRC Press, Taylor & Francis Group, Boca Raton, FL, 2006, **Surfactant Science Series, 131**, ch. 8, pp. 65-80.
23. E. G. Maciel, W. D. Sindorf and J. V. Bartuska, *J. Chromatogr. A*, 1981, **205**, 438-443.

24. D. W. Sindorf and G. E. Maciel, *J. Am. Chem. Soc.*, 1981, **103**, 4263-4265.
25. D. W. Sindorf and G. E. Maciel, *J. Phys. Chem.*, 1982, **86**, 5208-5219.
26. I. S. Protsak, Y. M. Morozov, W. Dong, Z. Le, D. Zhang and I. M. Henderson, *Nanoscale Res. Lett.*, 2019, **14**, 160.
27. A. V. Blaaderen and A. Vrij, in *The Colloid Chemistry of Silica*, ed. Horacio E. Bergna, Dupot, American Chemical Society, Washington, DC, 1994, **Advances in chemistry series, 234**, ch. 4, pp. 83-111.
28. G. Engelhardt, H. Jancke, E. Lippmaa and A. Samoson, *J. Organomet. Chem.*, 1981, **210**, 295-301.
29. M. Itoh, F. Oka, M. Suto, S. D. Cook and N. Auner, *Int. J. Polym. Sci.*, 2012, **2012**, 1-17.
30. E. E. Vansant, P. V. D. Voort and K. C. Vrancken, in *Studies in Surface Science and Catalysis*, Ed. B. Delmon and J.T. Yates, Amsterdam, The Netherlands, 1995, **93**, ch. 9, pp. 203, 230, 258.
31. E. Lindner, R. Schreiber, M. Kemmler, T. Schneller and H. A. Mayer, *Chem. Mater.*, 1995, **7**, 951-960.
32. H.-J. Egelhaaf, E. Holder, P. Herman, H. A. Mayer, D. Oelkrug and E. Lindner, *J. Mater. Chem.*, 2001, **11**, 2445-2452.
33. G. E. Maciel, C. E. Bronnimann, R. C. Zeigler, I.-S. Chuang, D. R. Kinney and E. A. Keiter, in *The Colloid Chemistry of Silica*, ed. Horacio E. Bergna, Dupot, American Chemical Society, Washington, DC, 1994, **Advances in chemistry series, 234**, ch. 14, pp. 278.
34. G. E. Maciel and I.-S. Chuang, in *Colloidal Silica: Fundamentals and Applications*, ed. Horacio E. Bergna and William O. Roberts, CRC Press, Taylor & Francis Group, Boca Raton, FL, 2006, **Surfactant Science Series, 131**, ch. 34, 445.
35. J. Bluemel, *J. Am. Chem. Soc.*, 1995, **117**, 2112-2113.
36. E. E. Vansant, P. Van Der Voort and K. C. Vrancken, in *Studies in Surface Science and Catalysis*, Ed. B. Delmon and J.T. Yates, Amsterdam, The Netherlands, 1995, **93**, ch. 9, pp. 290-291.
37. E. E. Vansant, P. Van Der Voort and K. C. Vrancken, in *Studies in Surface Science and Catalysis*, Ed. B. Delmon and J.T. Yates, Amsterdam, The Netherlands, 1995, **93**, ch. 8, pp. 160-161.
38. D. Brunel, N. Bellocq, P. Sutra, A. Cauvel, M. Laspéras, P. Moreau, F. Di Renzo, A. Galarneau and F. Fajula, *Coord. Chem. Rev.*, 1998, **178-180**, 1085-1108.
39. H. Aitchison, R. L. Wingad and D. F. Wass, *ACS Catal.*, 2016, **6**, 7125-7132.
40. A. Ghorbani-Choghamarani, B. Tahmasbi, R. H. E. Hudson and A. Heidari, *Microporous Mesoporous Mater.*, 2019, **284**, 366-377.
41. F. Raji and M. Pakizeh, *Appl. Surf. Sci.*, 2013, **282**, 415-424.
42. B. G. Trewyn, I. I. Slowing, S. Giri, H.-T. Chen and V. S. Y. Lin, *Acc. Chem. Res.*, 2007, **40**, 846-853.
43. S. M. Bulatovic, in *Handbook of Flotation Reagents: Chemistry, Theory and Practice*, ed. S. M. Bulatovic, Elsevier, Amsterdam, 2015, pp. 121-127.
44. M. Ghaferi, M. Koochi Moftakhari Esfahani, A. Raza, S. Al Harthi, H. Ebrahimi Shahmabadi and S. E. Alavi, *J. Drug Targeting*, 2021, **29**, 131-154.
45. S. Bhattacharyya, G. Lelong and M.-L. Saboungi, *J. Exp. Nanosci.*, 2006, **1**, 375-395.
46. J. S. Beck, J. C. Vartuli, W. J. Roth, M. E. Leonowicz, C. Kresge, K. Schmitt, C. Chu, D. H. Olson, E. Sheppard and S. McCullen, *J. Am. Chem. Soc.*, 1992, **114**, 10834-10843.

47. Wikipedia, The Wikipedia Online, <https://en.wikipedia.org/wiki/MCM-41> (Accessed on May 2021).
48. N. Linares, A. E. Sepulveda, M. C. Pacheco, J. R. Berenguer, E. Lalinde, C. Nájera and J. Garcia-Martinez, *New J. Chem.*, 2011, **35**, 225-234.
49. T. Posset, F. Rominger and J. Blümel, *Chem. Mater.*, 2005, **17**, 586-595.
50. E. E. Vansant, P. Van Der Voort and K. C. Vrancken, in *Studies in Surface Science and Catalysis*, Ed. B. Delmon and J.T. Yates, Amsterdam, The Netherlands, 1995, **93**, ch. 8, pp. 149-192.
51. G. R. M. Dowson, M. F. Haddow, J. Lee, R. L. Wingad and D. F. Wass, *Angew. Chem. Int. Ed.*, 2013, **52**, 9005-9008.
52. R. L. Wingad, P. J. Gates, S. T. G. Street and D. F. Wass, *ACS Catal.*, 2015, **5**, 5822-5826.
53. R. L. Wingad, E. J. E. Bergstrom, M. Everett, K. J. Pellow and D. F. Wass, *Chem. Commun.*, 2016, **52**, 5202-5204.
54. K. J. Pellow, R. L. Wingad and D. F. Wass, *Catal. Sci. Technol.*, 2017, **7**, 5128-5134.
55. P. Braunstein, H. P. Kormann, W. Meyer-Zaika, R. Pugin and G. Schmid, *Chem. Eur. J.*, 2000, **6**, 4637-4646.
56. J. Blümel, *Coord. Chem. Rev.*, 2008, **252**, 2410-2423.
57. S. Prasertsri, F. Lagarde, N. Rattanasom, C. Sirisinha and P. Daniel, *Polymer Testing*, 2013, **32**, 852-861.
58. M. L. Shoji and H. B. Friedrich, *S. Afr. J. Chem.*, 2012, **65**, 214-222.
59. S. Shylesh, S. Sharma, S. P. Mirajkar and A. P. Singh, *J. Mol. Catal. A: Chem.*, 2004, **212**, 219-228.
60. F. Kunc, V. Balhara, Y. Sun, M. Daroszewska, Z. J. Jakubek, M. Hill, A. Brinkmann and L. J. Johnston, *Analyst*, 2019, **144**, 5589-5599.
61. C. Kang, J. Huang, W. He and F. Zhang, *J. Organomet. Chem.*, 2010, **695**, 120-127.
62. B. Tahmasbi and A. Ghorbani-Choghamarani, *Catal. Lett.*, 2017, **147**, 649-662.
63. H. W. Darwish, A. Barakat, A. Nafady, M. Suleiman, M. Al-Noaimi, B. Hammouti, S. Radi, T. B. Hadda, A. Abu-Obaid and M. S. Mubarak, *Molecules*, 2014, **19**, 5965-5980.
64. C. Huo, J. Ouyang and H. Yang, *Sci. Rep.*, 2014, **4**, 3682.
65. S. O. Akiri and S. O. Ojwach, *Catalysts*, 2019, **9**, 143.
66. S. Brunauer, P. H. Emmett and E. Teller, *J. Am. Chem. Soc.*, 1938, **60**, 309-319.
67. K. S. Sing, *Pure Appl. Chem.*, 1985, **57**, 603-619.
68. N. Hwang and A. R. Barron, *The Connexions project*, 2011, 1-11.
69. E. P. Barrett, L. G. Joyner and P. P. Halenda, *J. Am. Chem. Soc.*, 1951, **73**, 373-380.
70. S. Cimino, L. Lisi and S. Romanucci, *Catal. Today*, 2018, **304**, 58-63.
71. M. Waseem, S. Mustafa, A. Naeem, K. H. Shah and I. Shah, *Chem. Eng. J.*, 2011, **169**, 78-83.
72. R.-Q. Meng, B. Wang, H.-M. Sui, B. Li, W. Song, L.-X. Wu, B. Zhao and L.-H. Bi, *Eur. J. Inorg. Chem.*, 2013, **2013**, 1935-1942.
73. J. Ji, F. Wu, L.-M. Shi, A.-Q. Jia and Q.-F. Zhang, *J. Organomet. Chem.*, 2019, **885**, 1-6.
74. I. Stamatopoulos, D. Giannitsios, V. Psycharis, C. P. Raptopoulou, H. Balcar, A. Zukal, J. Svoboda, P. Kyritsis and J. Vohlidal, *Eur. J. Inorg. Chem.*, 2015, **2015**, 3038-3044.
75. K. D. Behringer and J. Blümel, *J. Liq. Chromatogr. Relat. Technol.*, 1996, **19**, 2753-2765.
76. J. C. Freitas, T. J. Bonagamba and F. G. Emmerich, *Energy & Fuels*, 1999, **13**, 53-59.

77. T. Ikeya and Y. Ito, in *Experimental Approaches of NMR Spectroscopy*, Springer, 2018, pp. 63-90.
78. D. Jiang, J. Gao, Q. Yang, J. Yang and C. Li, *Chem. Mater.*, 2006, **18**, 6012-6018.
79. J. J. Calvin, M. Asplund, Y. Zhang, B. Huang and B. F. Woodfield, *J. Chem. Thermodyn.*, 2017, **112**, 77-85.
80. X. Feng, G. E. Fryxell, L.-Q. Wang, A. Y. Kim, J. Liu and K. M. Kemner, *Science*, 1997, **276**, 923-926.
81. K. J. Pellow, PhD Thesis, University of Bristol, 2018.

## Chapter 4: Alumina-supported Alkoxysilyl-functionalised Bidentate Phosphine-based Ruthenium (II) Complexes for Ethanol Upgrading to Advanced Biofuels

### 4.1 Introduction

In recent years, there is increasing attention in immobilising homogeneous catalysts on oxidic inorganic supports via functional ligands.<sup>1</sup> Of the metal oxides available as supports, alumina is particularly interesting. For several reasons, the structure of alumina possesses vital frameworks through which linkers can easily bind. A brief overview of the surface properties of alumina is discussed.

The surface of alumina has been studied extensively for nearly six decades.<sup>2-5</sup> Aluminas are mainly composed of  $\text{Al}(\text{-O-})_4$  tetrahedra and  $\text{Al}(\text{-O-})_6$  octahedra with many hydroxyl groups terminating at the surface (Figure 4.1).<sup>6</sup>

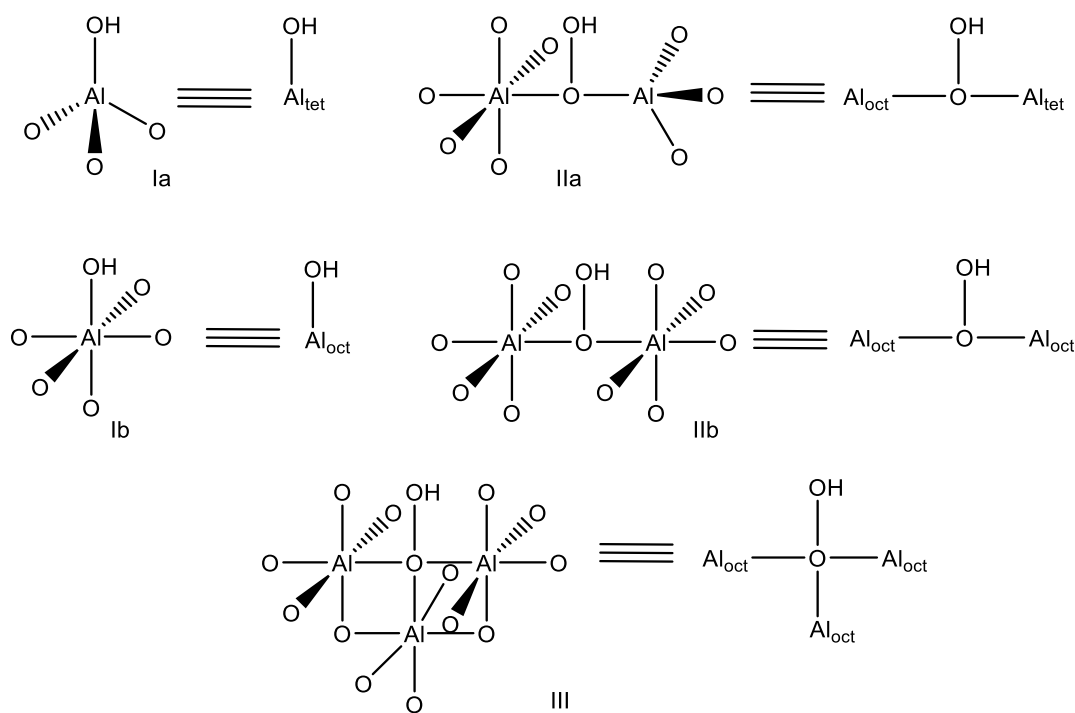


**Figure 4.1:** The five possible types of surface hydroxyl groups on the surface of  $\gamma$ -,  $\eta$ - and higher surface area aluminas (Extracted from reference 6)

For example,  $\gamma$ -alumina, has a tetragonal distorted defect spinel lattice structure described as (110) and (111) planes indicating a combination of octahedral ( $\text{Al}_{\text{oct}}$ ) and tetrahedral ( $\text{Al}_{\text{tet}}$ ) alumina sites. This is the transition alumina most popularly used in surface chemistry and catalysis.<sup>4,7</sup> There are around 32 oxygen atoms,  $21\frac{1}{3}$  aluminum atoms and  $2\frac{2}{3}$  vacant cation positions per unit cell of  $\gamma$ -alumina. Three species ( $-\text{OH}$ ,

$O^{2-}$ , and  $Al^{3+}$ ) exist on the surface of aluminas. Each hydroxyl group acts as a Brønsted acid as well as base/nucleophile,  $O^{2-}$  as a strong base/nucleophile and  $Al^{3+}$  as a Lewis acid. Furthermore, the existence of both Brønsted acid (hydroxyl groups) and Lewis acid (anionic vacancies) sites on the surface of high surface area aluminas, like  $\gamma$ -alumina, are responsible for its reactivity. However, the Brønsted and Lewis acid site reactivities are controlled by the alumina activation temperature.

Additionally, alumina adsorbs water at room temperature and the water is considered to exist as both “physisorbed” and chemically bound water. During the pre-treatment process of alumina by heating, physisorbed water is lost. At higher elevated temperatures, hydroxyl groups are lost as they begin to react with each other via proton transfer to give anionic vacant sites,  $O^{2-}$ , and water, which is eliminated at such temperatures.<sup>8</sup>

In contrast to  $\alpha$ -alumina ( $2 \text{ m}^2/\text{g}$ ),  $\gamma$ -aluminas are very reactive with surface area ranges between  $100 - 300 \text{ m}^2/\text{g}$ .<sup>6, 7</sup> For example, Kabalka and Pagni estimated there are  $3.2 \text{ mmol}$  of hydroxyl groups per gram of an alumina with a surface area of  $155 \text{ m}^2/\text{g}$  based on information that there are 12.5 hydroxyl groups on the surface per  $100 \text{ \AA}^2$ .<sup>7</sup>

Moreover, alumina can be basic, neutral and acidic. Inactivated  $\gamma$ -alumina is generally basic, when water is added to it, the pH of the water becomes basic. Neutral and acidic  $\gamma$ -alumina are obtained by addition of ethyl acetate, hydrochloric acid, and acetic acid. These three forms of alumina are available commercially from various suppliers. Ideally, specifying the type of alumina employed in synthetic reactions is essential as each type impacts the reaction differently.<sup>7</sup>

Most importantly, the hydroxyl groups on alumina surfaces serve as channels for anchoring catalytic centres that have shown significant activity in homogeneous catalysis but are thermally unstable under harsh catalytic conditions. Thus, the immobilised catalyst exhibits both homogeneous and heterogeneous properties<sup>1</sup> desirable in present day catalysis. Advantageously, the experimental techniques (IR, TGA, BET, XRD, TEM/STEM, NMR etc) applicable for characterising silicas and adsorbed species are likewise useful for alumina characterisation.<sup>6, 9</sup> Silylation reactions between surface hydroxyl groups of alumina and trialkoxysilyl phosphine linkers of metal catalysts via condensation, have been studied by Blümel and co-workers.<sup>1, 10, 11</sup> However, the tethering of active homogeneous phosphine-based

ruthenium centres on alumina has not been reported in the literature. Therefore, the present chapter centres on supporting homogeneous ruthenium catalysts obtained in Chapter two on three types of alumina.

## 4.2 Aims and Objectives

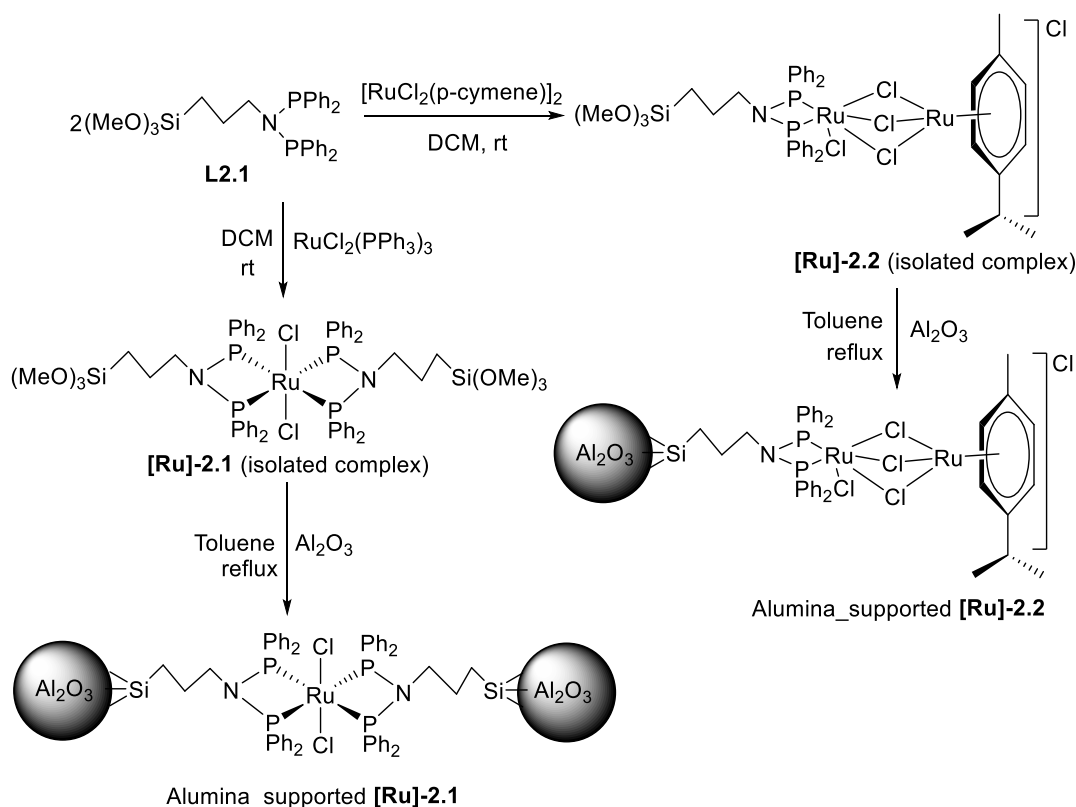
Experiments carried out with catalysts **[Ru]-2.1** and **[Ru]-2.2** on fumed silica and MCM-41 (Chapter 3) confirmed successful binding of these catalysts with the surface hydroxyl groups of the supports. Additionally, significant activity was achieved with the supported catalysts when employed in ethanol-methanol upgrading to *iso*-butanol. Moreover, the supported catalysts were potentially reusable with right separation techniques. Since alumina and silica have similar hydroxyl groups, it is expedient to explore the alumina analogues of these homogeneous catalysts in the same catalysis process to examine the most compactable and efficient supports as well as the influence of alumina pH on the catalytic activity of supported catalysts. So, the overall aims and objectives of this chapter are outlined below:

- To immobilise catalysts **[Ru]-2.1** and **[Ru]-2.2** on three different types of alumina (neutral, acidic and basic)
- To fully characterise the immobilised catalysts with several surface experimental techniques.
- To explore characterised supported catalysts in ethanol-methanol upgrading to *iso*-butanol.
- To study the influence of alumina pH (neutral, acidic and basic) on the catalytic reaction.
- To investigate the recyclability and leachability potential of the supported catalysts.

## 4.3 Results and Discussion

### 4.3.1 Immobilisation method

Catalysts **[Ru]-2.1** and **[Ru]-2.2** (2 wt% per gram of support) were supported on pre-treated alumina supports (heated under vacuum at 180-250°C for 24 h) by wet impregnation method.<sup>10</sup> Three pH ranges of alumina were used in this research (neutral, basic and acidic). The highly reactive hydroxyl groups on the surface of alumina are responsible for the selective retention of adsorbed materials. The mechanism involves a one-step condensation of alkoxyisilyl functional groups present in the complex and hydroxyl groups on the surface of alumina. In all types studied, the colour of the alumina changed from white to brown upon adsorption (Scheme 4.1) and the uncoordinated complex on the support was removed by washings until no phosphorus peak was detected in the wash by <sup>31</sup>P NMR spectroscopy (Figure 4.2).



**Scheme 4.1:** Immobilisation approach for supporting catalysts **[Ru]-2.1** and **[Ru]-2.2** on alumina

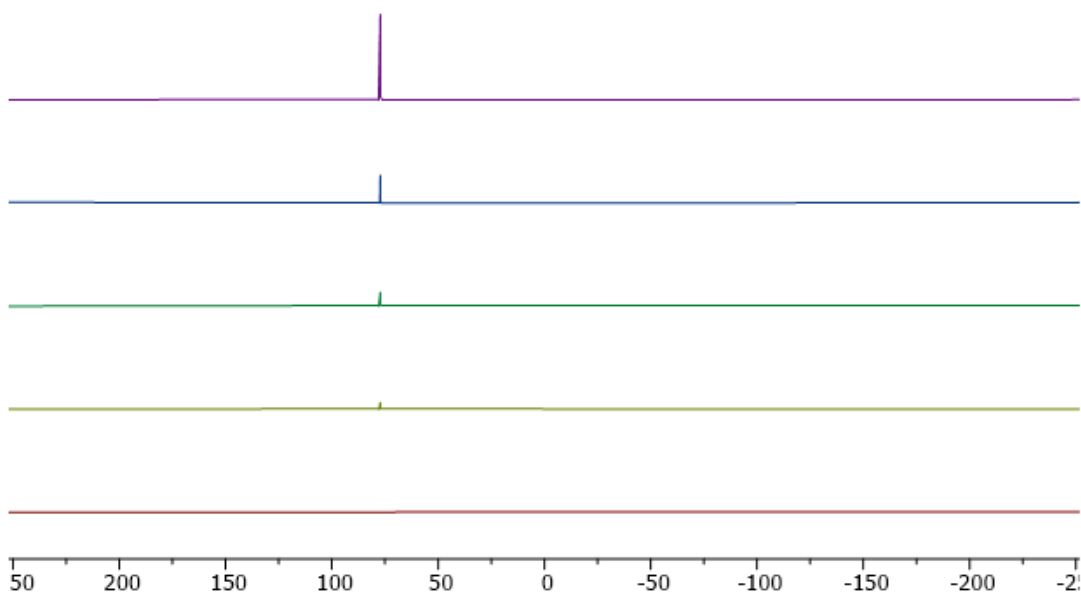


**Figure 4.2.**  $^{31}\text{P}\{^1\text{H}\}$  NMR spectra (unlocked, 162 MHz) of filtrate and washings after refluxing complex **[Ru]-2.1** and neutral alumina in toluene.

### 4.3.2 Characterisation of unmodified and modified alumina

Different experimental techniques were employed in the characterisation of bare neutral, acidic, and basic alumina and the corresponding modified alumina (i.e. supported catalyst). Since the present chapter deals with these three alumina types, for clarity, the use of “aluminas” here denotes all of the three types of alumina used in this work. It is also important to note that immobilisation of catalyst **[Ru]-2.2** on neutral alumina was not examined due to the project time frame. All characterisation methodologies utilised are discussed accordingly.

#### 4.3.2.1 Fourier-transform infra-red (FTIR) method

Pre-treated neutral, basic and acidic alumina were initially examined for surface hydroxyl groups by FTIR analysis and the results are shown in Figure 4.3a. The frequency band from  $3058 - 3758 \text{ cm}^{-1}$  corresponds to free hydroxyl groups on alumina typical for  $\gamma\text{-Al}_2\text{O}_3$  samples dried at medium temperatures. The peak at  $1644 \text{ cm}^{-1}$  is likely due to OH of water.<sup>2</sup> This implies at the activation temperature chosen for the present study, complete removal of adsorbed water molecules was not achieved. Likewise, supported **[Ru]-2.1** and **[Ru]-2.2** on the three types of alumina were analysed by infra-red for possible coordination to alumina and the results are shown in Figure 4.3b and c. The characteristic C-H bands of methoxy groups ( $\text{OCH}_3$ ) observed in the unsupported catalysts at  $3052$ ,  $2938\text{-}2964$  and  $2837\text{-}2873 \text{ cm}^{-1}$  were

no longer present in the spectra of the supported catalysts. Additionally, the CH<sub>2</sub> characteristic peak of propyl linker at 1433 and 1435 cm<sup>-1</sup> became present on supported **[Ru]-2.1** and **[Ru]-2.2** respectively. Also, the formation of new aluminosiloxane bonds (Al-O-Si)<sup>12</sup> with frequency relatively similar to that of the Si-O-C band of the silanes (1105-1080 cm<sup>-1</sup>)<sup>13</sup> was suspected to be associated with the peak at 1080 cm<sup>-1</sup> observed in both supported catalysts suggesting the involvement of surface OH groups with OCH<sub>3</sub> of the catalysts.

#### 4.3.2.2 Thermal analysis

The thermal stability of pre-treated pure alumina and modified alumina (supported catalysts) were examined over a 30-800°C temperature range in nitrogen flow at a heating rate of 5°C/min. The thermogravimetry (TG) and differential thermogravimetry (DTG) curves obtained are shown in Figure 4.4 and 4.5. For unmodified alumina types (Figure 4.4a-c), loss of weight occurred in the 30-200°C range with approximately 4% weight loss. The loss experienced at this temperature range corresponded to the evaporation and dehydration of adsorbed surface water from the alumina.<sup>14</sup> This agrees with the IR results that show the presence of water in the pre-treated aluminas. The DTG curves for the three alumina types showed one endothermic peak at 70, 72 and 80°C for acidic, neutral and basic alumina respectively. A single peak in the DTG curve implies the removal of water without any decomposition or de-hydroxylation processes occurring. For the supported catalysts, neutral, acidic and basic alumina-supported **[Ru]-2.1** underwent similar two stage weight loss (Figure 4.5a-c). The first stage with ~3% weight loss in the 30-200°C range (DTG at ~70°C) corresponds to the elimination of adsorbed water molecules, whereas the 5-6% weight loss in the 200-500°C range at stage two (DTG at ~400°C) correlates to theoretical percentage weight loss (5-7%) of four PPh<sub>2</sub> from the supported catalyst according to loadings (See experimental sections 6.3.4.1 - 6.3.4.3). Thus, the main stage of degradation of alumina-supported **[Ru]-2.1** involves the loss of phosphines taking place within 200-500°C with an endothermic peak at around 400°C. Therefore, neutral, acidic and basic alumina-supported **[Ru]-2.1** are thermally stable up to 200°C until the loss of phosphino groups at ~400°C. Furthermore, acidic alumina-supported **[Ru]-2.1** displayed additional degradation stages at 527, 578, 614,

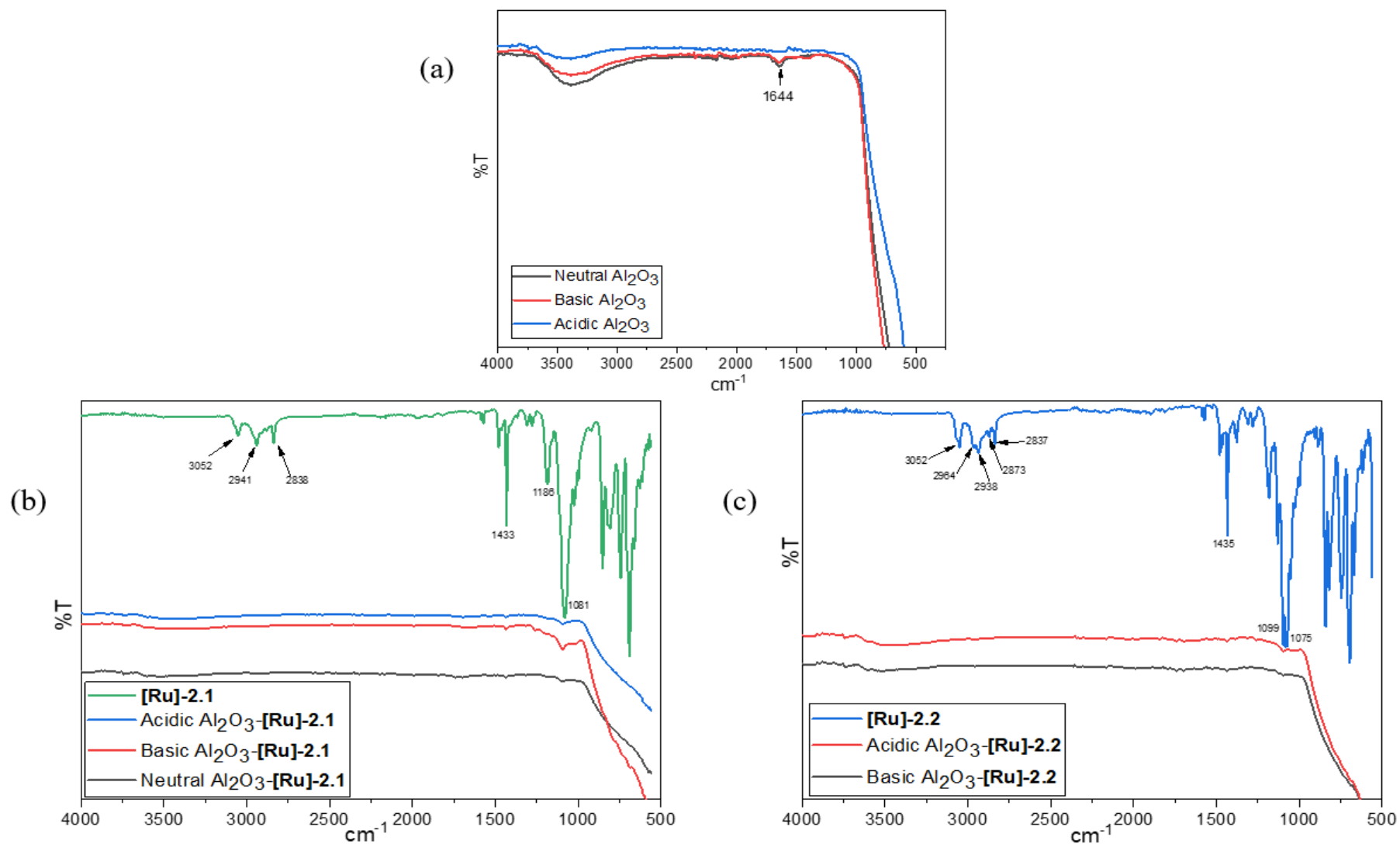


**Figure 4.3:** FTIR analysis of (a) unmodified aluminas (b) supported and unsupported [Ru]-2.1 and (c) supported and unsupported [Ru]-2.2

674 and 696°C evidenced on the DTG curve, probably due to the loss of other organic moieties (siloxyl, propyl and amino groups).<sup>15</sup> Due to the formation of Al-O-Si bonds on the supported catalysts, these peaks are unlikely to result from de-hydroxylation of the alumina surface hydroxides.

On the other hand, acidic and basic alumina-supported **[Ru]-2.2** showed three stages of weight loss (Figure 4.5d-e). The initial stage is related to the loss of adsorbed water molecules of about 2% between 30-200°C, followed by 3% weight loss at 200-330°C corresponding to the release of chlorine atoms. This agrees with the theoretical percentage weight loss of five chlorine atoms from the supported catalysts based on loadings (See experimental sections 6.3.4.5 and 6.3.4.8). The third stage occurred in the 330-470°C temperature range with ~4% weight, possibly due to loss of phenyl groups which is close to the theoretical percentage weight loss based on loadings (See experimental sections 6.3.4.6 and 6.3.4.9). According to the loading calculation, the decomposition process of alumina-supported **[Ru]-2.2** involves the release of all the five chlorine atoms present. Generally, the removal of catalyst components from alumina-supported **[Ru]-2.1** and **[Ru]-2.2** occurred under a similar temperature range of 200-500°C via single and double steps respectively due to different structural compositions and arrangement. Contrary to the work of Kang *et al*, the detachment of alkyl linker from the ruthenium complex via thermal degradation was undetected, however, phosphine loss was observed.<sup>16</sup>

In summary, the additional stages of degradation shown on the TG and DTG curves of the supported catalysts compared to that of pure alumina showed evidence of successful silylation on the alumina surfaces.

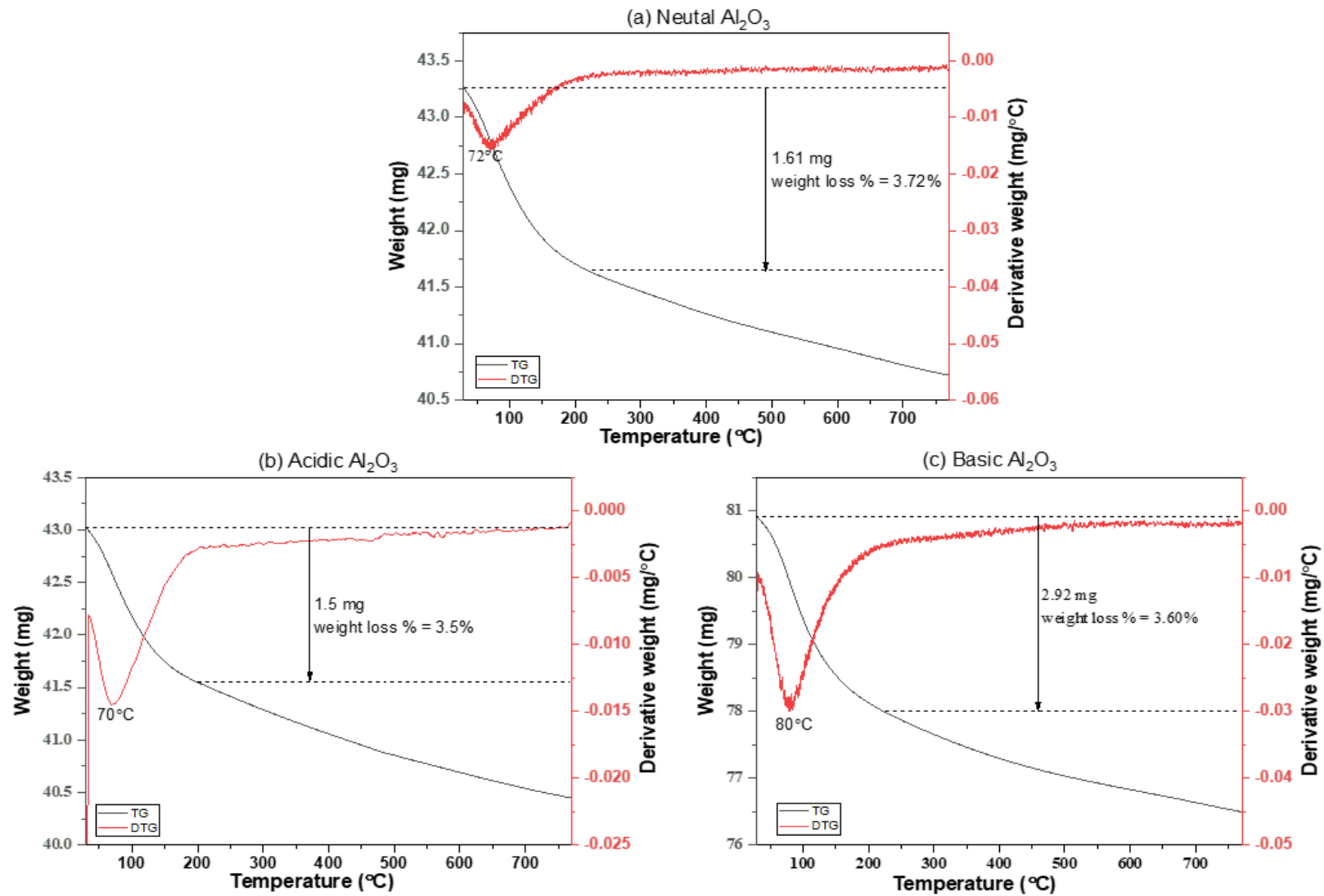


Figure 4.4: Thermal analysis of unmodified alumina (a) neutral (b) acidic (c) basic

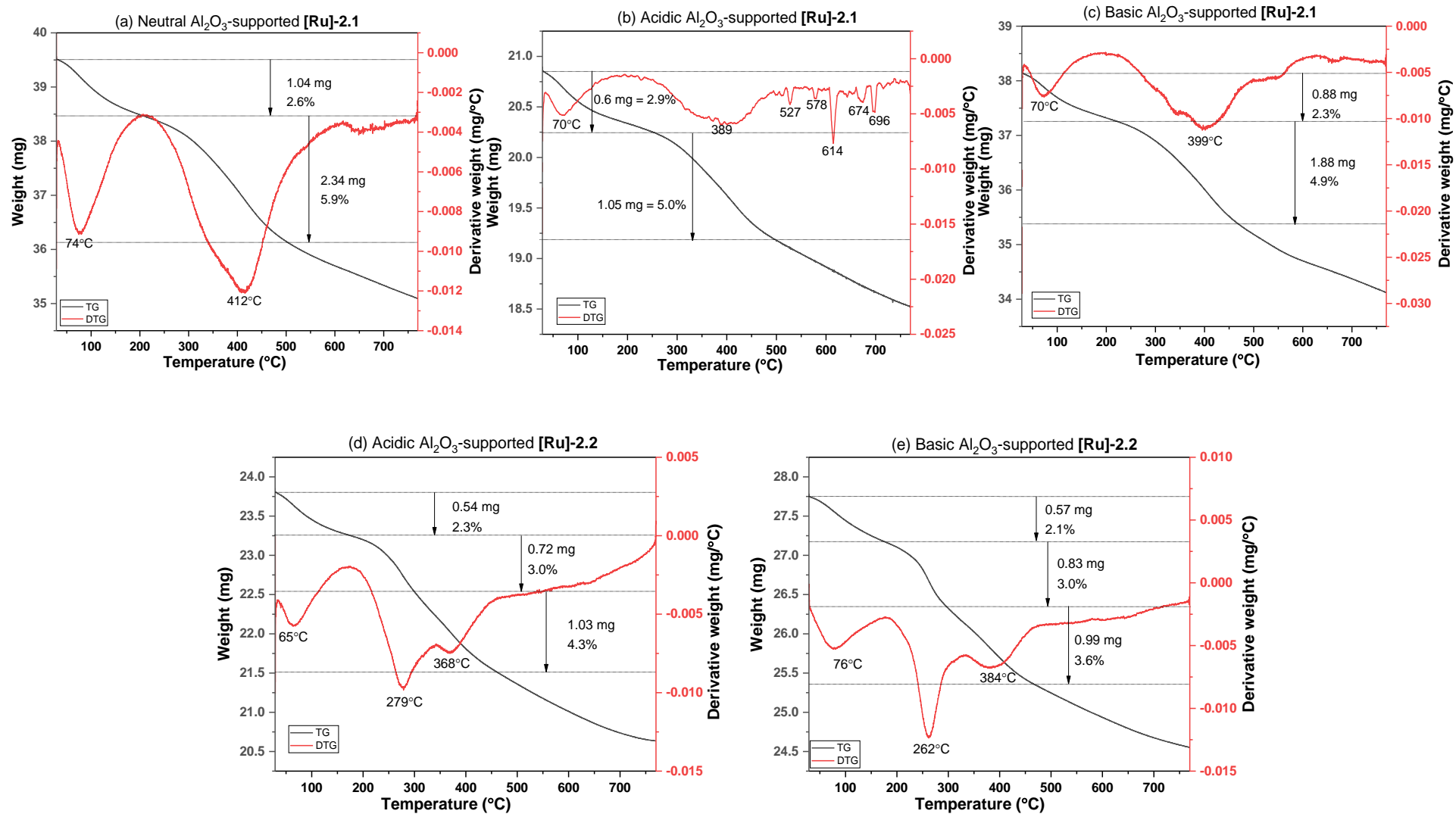
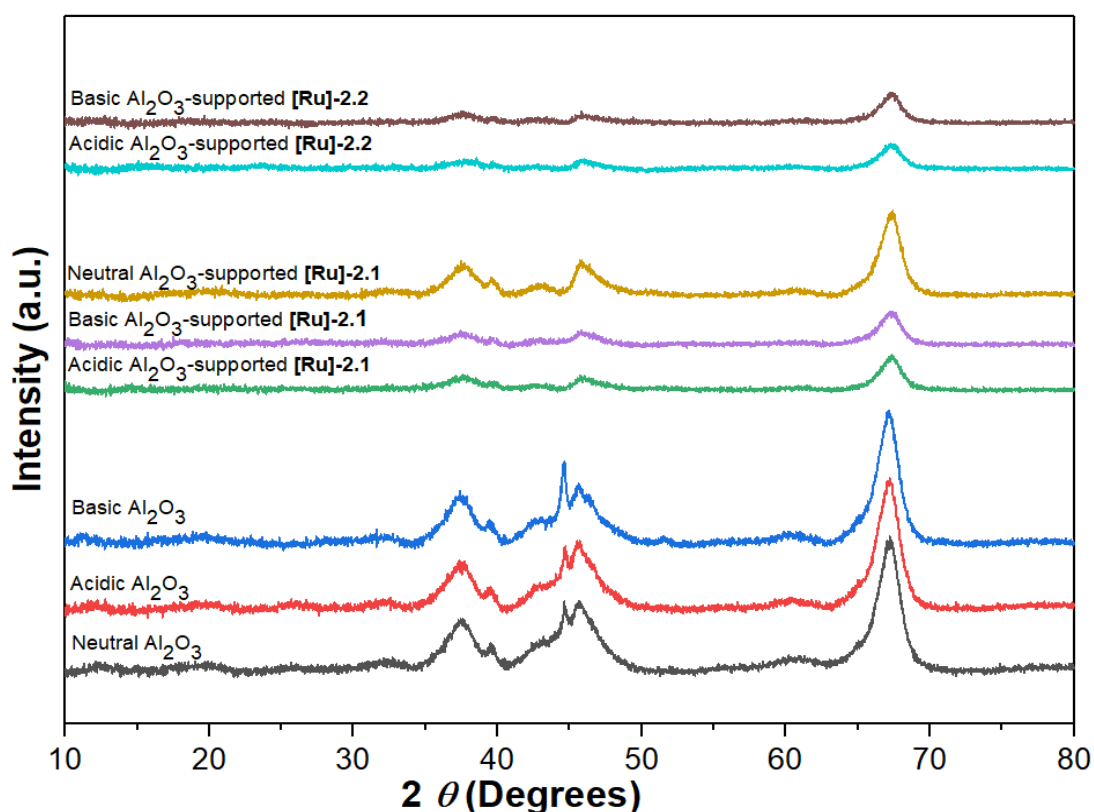


Figure 4.5: Thermal analysis of aluminas-supported [Ru]-2.1 and [Ru]-2.2

#### 4.3.2.3 X-ray diffraction (XRD) studies

To examine the structures of these aluminas and the effect of functionalisation, each sample was analysed by powder X-ray diffraction (XRD). XRD patterns for pre-treated pure neutral, acidic and basic alumina and the supported catalysts **[Ru]-2.1** and **[Ru]-2.2** are shown in Figure 4.6. The pattern of the peaks obtained for unmodified neutral, acidic, and basic alumina confirmed the samples are pure phase  $\gamma$ - $\text{Al}_2\text{O}_3$ .<sup>17-19</sup> As noticed on the XRD curves, the crystallographic phase of the aluminas was not altered upon functionalisation. However, the peak intensity of the aluminas decreased after modification, which suggests catalysts **[Ru]-2.1** and **[Ru]-2.2** are incorporated into the alumina channels at varied loadings. This is supported by ICP analysis which showed varied loadings. In fact, the similar XRD pattern displayed by these supported catalysts in relation to that of the unmodified aluminas showed that the crystal structures of the aluminas were retained after the silylation process. Therefore, the XRD results implied that adsorption of catalysts **[Ru]-2.1** and **[Ru]-2.2** on aluminas' surfaces did not result to phase alteration.



**Figure 4.6:** XRD patterns of pure alumina and alumina-supported catalysts **[Ru]-2.1** and **[Ru]-2.2**.

#### 4.3.2.4 Surface Area and Porosity (N<sub>2</sub> Adsorption/Desorption measurements)

Surface areas, total pore volumes, and average pore radius of acidic, and basic and neutral alumina and the supported catalysts are listed in Table 4.1. The surface areas and pore volume/radius were calculated using Brunauer-Emmett-Teller (BET)<sup>20-22</sup> and Barret-Joyner-Halenda (BJH)<sup>23</sup> methods, respectively. All of the pure pre-treated alumina samples studied have high surface area values and fall within the surface area range for  $\gamma$ -Al<sub>2</sub>O<sub>3</sub>.<sup>7</sup> On the other hand, they possess low pore volumes (0.34-0.37 cm<sup>3</sup>/g). Upon functionalisation with catalysts **[Ru]-2.1** and **[Ru]-2.2**, the surface areas, pore volumes and pore radius decreased accordingly, demonstrating the incorporation of catalyst inside the alumina channels. Additionally, the decrease in the surface area, pore volume and pore size varied for the type of alumina used,

**Table 4.1:** BET surface area, BJH pore volume, and pore diameter of pre-heated pure aluminas and alumina-supported **[Ru]-2.1** and **[Ru]-2.2**.

Samples	BET Surface Area (m <sup>2</sup> /g)	Pore Volume (cm <sup>3</sup> /g)	Pore Radius (Å)
Acidic Al <sub>2</sub> O <sub>3</sub>	202	0.37	23
Basic Al <sub>2</sub> O <sub>3</sub>	157	0.34	23
Neutral Al <sub>2</sub> O <sub>3</sub>	159	0.35	21
Acidic Al <sub>2</sub> O <sub>3</sub> -supported <b>[Ru]-2.1</b>	112	0.15	20
Basic Al <sub>2</sub> O <sub>3</sub> -supported <b>[Ru]-2.1</b>	129	0.24	18
Neutral Al <sub>2</sub> O <sub>3</sub> -supported <b>[Ru]-2.1</b>	98	0.13	20
Acidic Al <sub>2</sub> O <sub>3</sub> -supported <b>[Ru]-2.2</b>	53	0.18	18
Basic Al <sub>2</sub> O <sub>3</sub> -supported <b>[Ru]-2.2</b>	91	0.19	18

suggesting different catalyst loadings. This was supported by ICP results and XRD patterns obtained. Furthermore, the N<sub>2</sub> adsorption–desorption isotherms (Figure 4.7a-g) and the relative pore size distribution curves (Figure 4.7h) were obtained and are shown in Figure 4.7. All aluminas and supported catalysts displayed a type IV isotherm with H4-type hysteresis according to IUPAC classification (Figure 4.7a-g).<sup>21</sup> Mesoporous materials (pore diameter: 2 – 50 nm) typically exhibit a type IV isotherm whose hysteresis loops are relatable to the occurrence of capillary condensation in

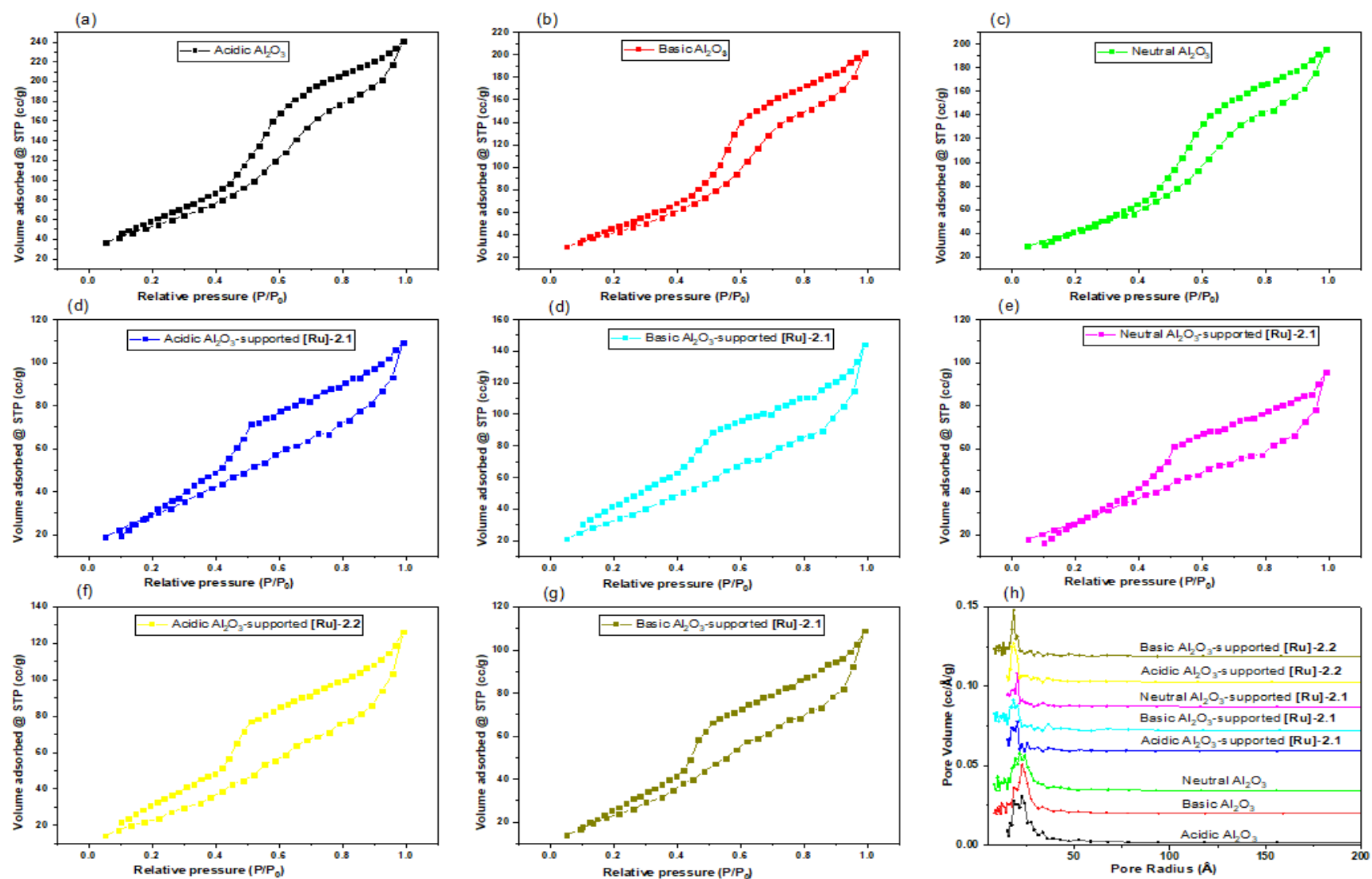


**Figure 4.7:** (a)-(g) N<sub>2</sub> adsorption-desorption isotherms and (h) pore size distribution curve for pure pre-heated Al<sub>2</sub>O<sub>3</sub> and supported catalysts (note cc = cm<sup>3</sup>).

mesopores.<sup>21</sup> This indicates that the aluminas used in the current study are all mesoporous in nature. Again, no micropore volume was determined by the t-plot method confirming that they were all mesoporous. Also, the pore size distributions were nearly monomodal for all unfunctionalised and functionalised aluminas in the 10-50 Å pore range.

In contrast, the average pore size of pure aluminas reduced after functionalisation. For example, the pore radius of acidic alumina (23 Å) decreased to 20 Å and 18 Å when impregnated with catalysts **[Ru]-2.1** and **[Ru]-2.2** respectively (Table 4.1). Similar reduction in pore radius was also observed in basic and neutral aluminas when loaded with catalysts **[Ru]-2.1** and **[Ru]-2.2**. This is evidenced with a shift in the aluminas peaks to lower values for supported catalysts in the pore size distribution plot (Figure 4.7 h), indicating that the size of the alumina mesopores have decreased after catalyst immobilisation.

#### 4.3.2.5 TEM/STEM/EDS

The morphology of pre-heated pure aluminas and functionalised aluminas (alumina-supported catalysts **[Ru]-2.1** and **[Ru]-2.2**) was examined by TEM/STEM/EDS techniques. All the samples exhibited non ordered mesoporous structures, common with  $\gamma$ -Al<sub>2</sub>O<sub>3</sub>. The monomodal porosity of these materials was likewise supported by TEM micrographs which showed just small interparticle mesopores (Figure 4.8 inset). Interestingly, TEM micrographs of the supported catalysts showed no visible Ru(0) nanoparticles, signifying that Ru(II) was atomically dispersed without the occurrence of agglomeration during the functionalisation process. TEM results of the aluminas and alumina-supported catalysts **[Ru]-2.1** and **[Ru]-2.2** displayed similar ordered mesoporous structures, demonstrating that mesostructures of the aluminas were unaltered by the impregnation process. This agrees with the results of XRD analysis. Similarly, with the combination of STEM-EDS techniques, the chemical mapping and spectra of pure aluminas and alumina-supported catalysts **[Ru]-2.1** and **[Ru]-2.2** was obtained as shown in Figure 4.8. Colour coding was used to indicate the presence of specific atom (Ru, P, Si, C, O, Cl) in the STEM micrographs. Ru(II) in conjunction with other atoms present in the organosilane moieties are shown to be atomically distributed over the alumina surfaces taking its shape. In fact, the retention of alumina shape post functionalisation process indicates no structural deformation to the support

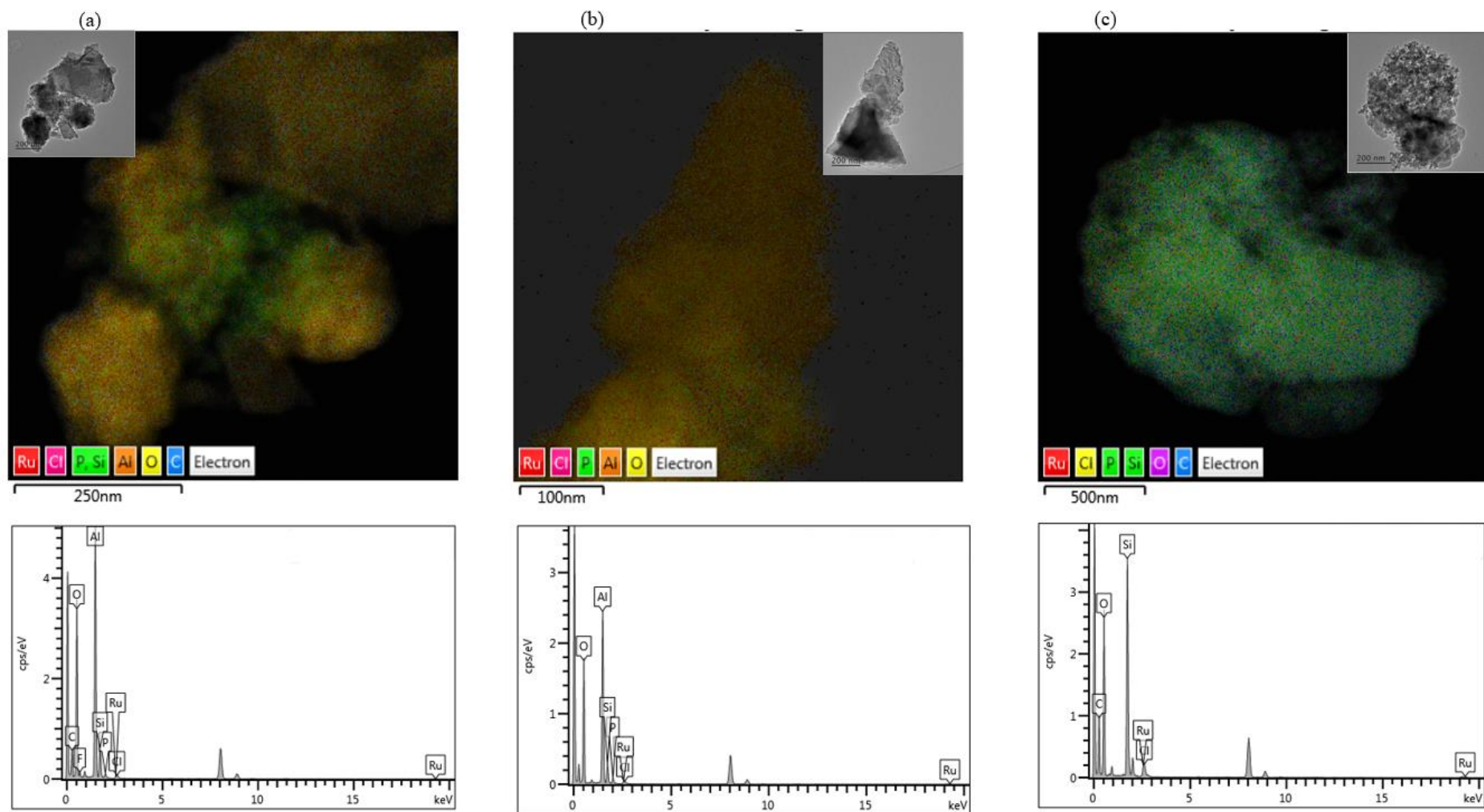


**Figure 4.8:** Representative TEM (inset), STEM (top) and EDS (bottom) of (a) acidic (b) basic (c) neutral  $\text{Al}_2\text{O}_3$ -supported [Ru]-2.1

material. Moreover, EDS spectra of the alumina-supported catalysts showed the presence of individual atoms of the supports and catalysts. Generally, STEM-EDS results confirmed the presence of the organosilane bound catalysts with uniform dispersion of all atoms in the supported catalysts.

#### 4.3.2.6 Solid-State NMR spectroscopy

The functionalisation of pure aluminas with catalysts **[Ru]-2.1** and **[Ru]-2.2** was investigated by  $^{31}\text{P}$ ,  $^{29}\text{Si}$ ,  $^{13}\text{C}$  and  $^{27}\text{Al}$  CP/MAS NMR spectroscopy.

##### 4.3.2.6.1 $^{31}\text{P}$ CP/MAS NMR spectroscopy

Recalling from Chapter two, the liquid state  $^{31}\text{P}\{^1\text{H}\}$  NMR spectra for homogeneous catalysts **[Ru]-2.1** and **[Ru]-2.2** gave signals at ca. 77 and 85 ppm respectively. The  $^{31}\text{P}$  CP/MAS NMR spectra of acidic, basic, and neutral alumina-supported catalysts **[Ru]-2.1** and **[Ru]-2.2** are shown in Figure 4.9. In the case of supported catalysts **[Ru]-2.1**, a broad resonance centered at ca. 77 ppm was obtained for the three alumina types (Figure 4.9a-c), justifying the anchorage of catalysts **[Ru]-2.1** to alumina. In short, the presence of this peak at ca. 77 ppm implied that the integrity of the homogeneous catalyst **[Ru]-2.1** was preserved in the supported catalysts. Fortunately, the presence of uncoordinated ligand (62.9 ppm) was not recorded, however, other phosphorus peaks at ca. 30, 40, and 43/58 ppm were observed for basic, acidic, and neutral alumina-supported catalyst **[Ru]-2.1** respectively corresponding to free  $\text{Ph}_3\text{P}=\text{O}$ ,  $\text{Ph}_2\text{P}-\text{P}(\text{O})\text{Ph}_2$  and alumina bound phosphine oxides.<sup>11</sup> On the other hand, acidic and basic alumina-supported catalysts **[Ru]-2.2** showed a characteristic well resolved peak at ca. 85 ppm (Figure 4.9d-c) relative to homogeneous catalyst **[Ru]-2.2** phosphorus peak. Contrary to alumina-supported catalyst **[Ru]-2.1**, other phosphine side products were not detected in alumina-supported catalyst **[Ru]-2.2**, demonstrating a clean immobilisation process. Besides the isotropic peaks recorded for these supported catalysts, spinning sidebands denoted by asterisks were observed.

##### 4.3.2.6.2 $^{13}\text{C}$ CP/MAS NMR spectroscopy

Comparing the liquid-state  $^{13}\text{C}\{^1\text{H}\}$  NMR spectra of catalysts **[Ru]-2.1** and **[Ru]-2.2** (Figure 4.10) with  $^{13}\text{C}$  CP/MAS NMR spectra of alumina-supported catalysts **[Ru]-2.1** and **[Ru]-2.2** (Figure 4.11), the majority of the expected organosilane catalysts carbon peaks were present in spectra of the supported catalysts. The most prominent

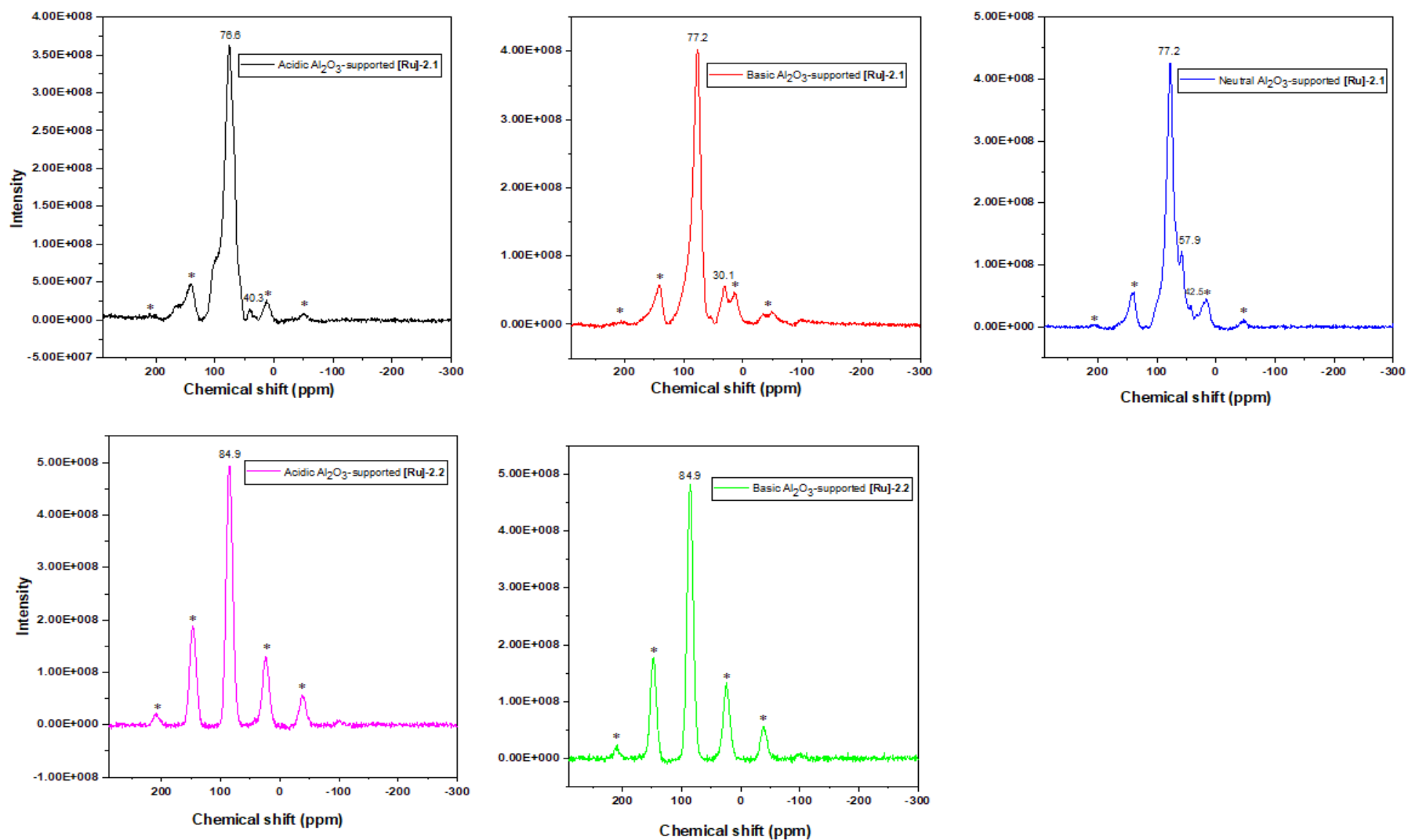


**Figure 4.9:**  $^{31}\text{P}$  CP/MAS NMR spectra (162 MHz, 10 kHz spinning speed) of  $\text{Al}_2\text{O}_3$ -supported [Ru]-2.1 and [Ru]-2.2 (\*spinning sidebands)

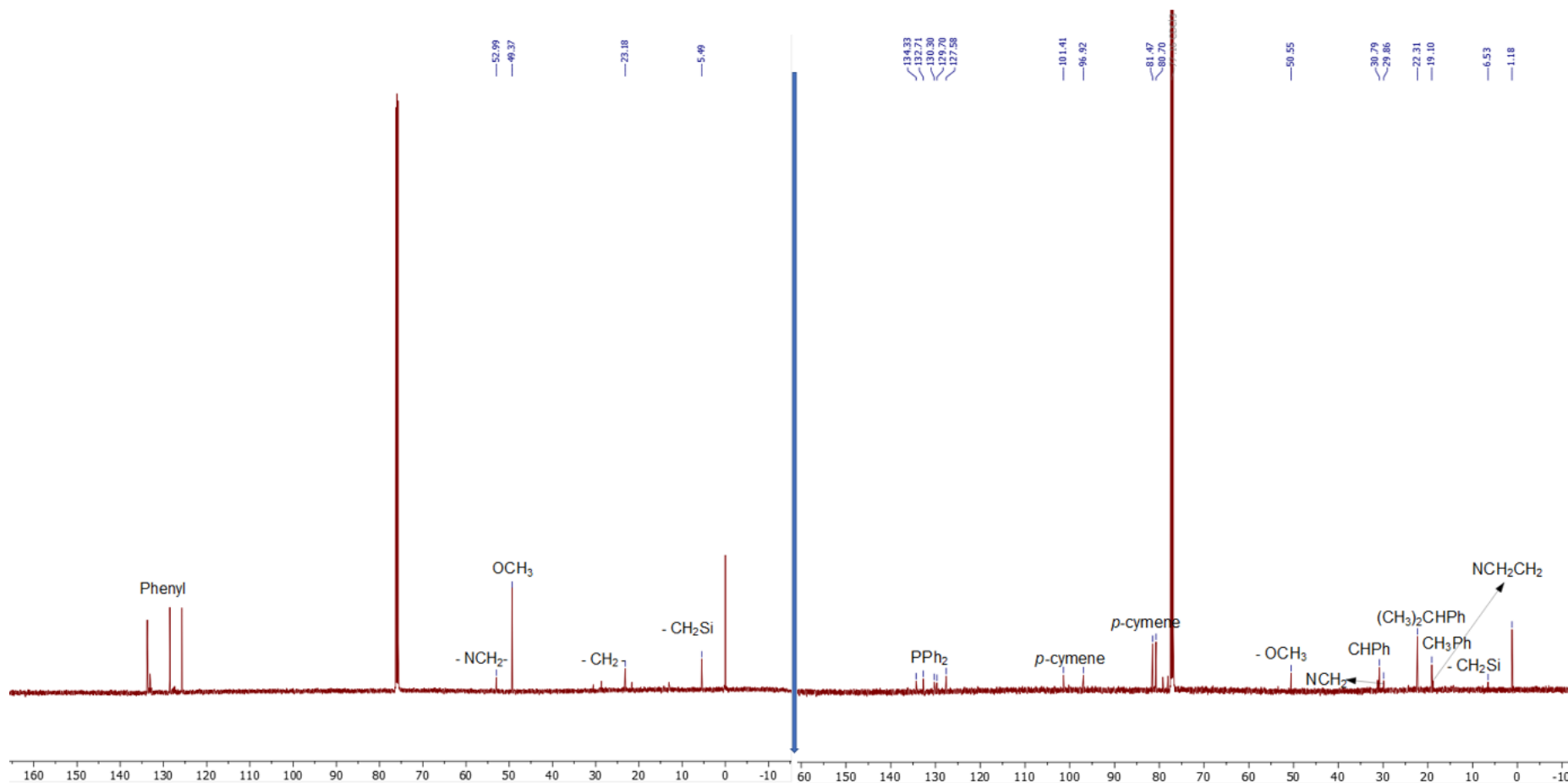


**Figure 4.10:** Liquid-state  $^{13}\text{C}\{^1\text{H}\}$  NMR spectra ( $\text{CDCl}_3$ , 126 MHz) of catalysts **[Ru]-2.1** (left) and **[Ru]-2.2** (right)

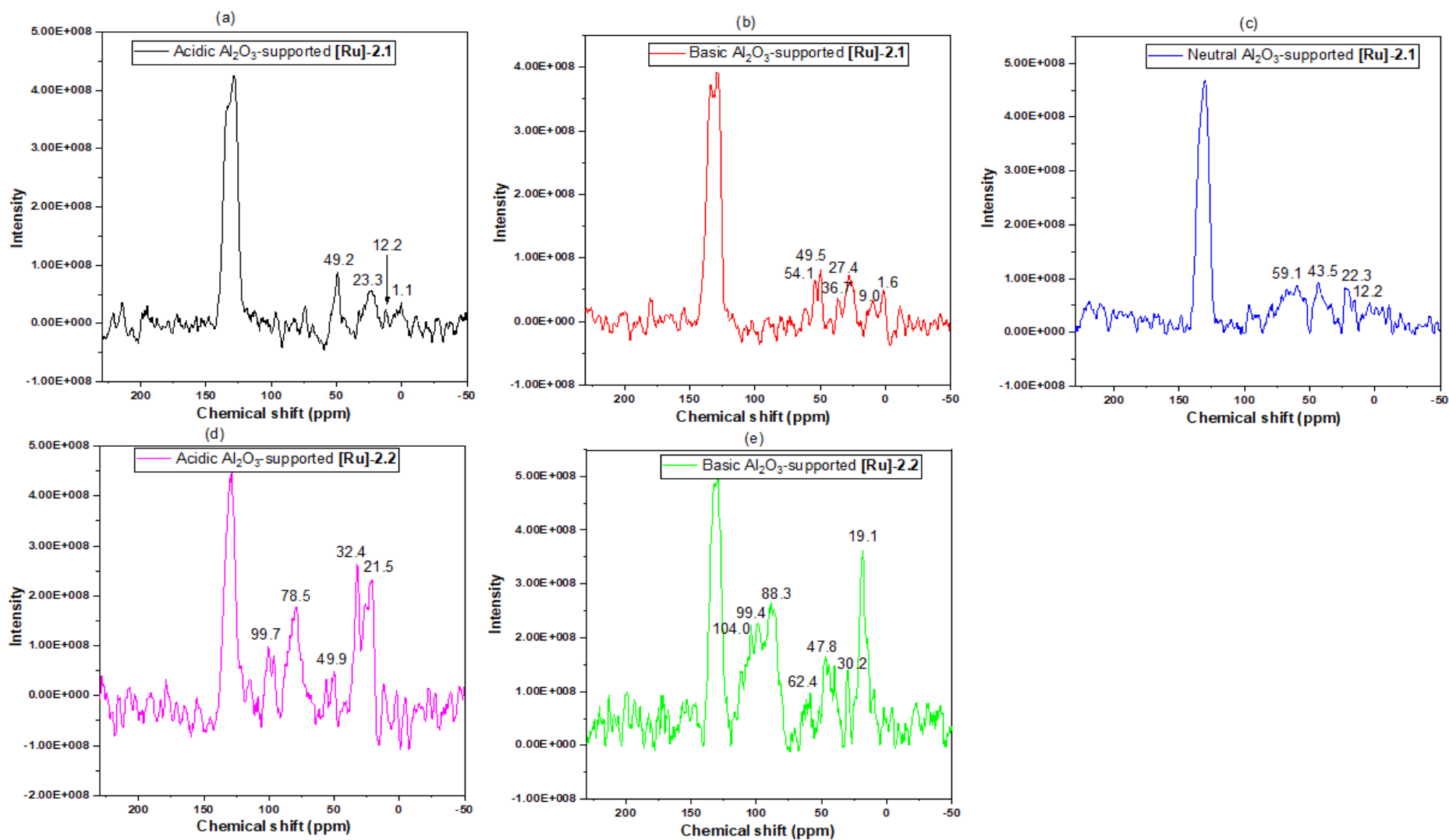
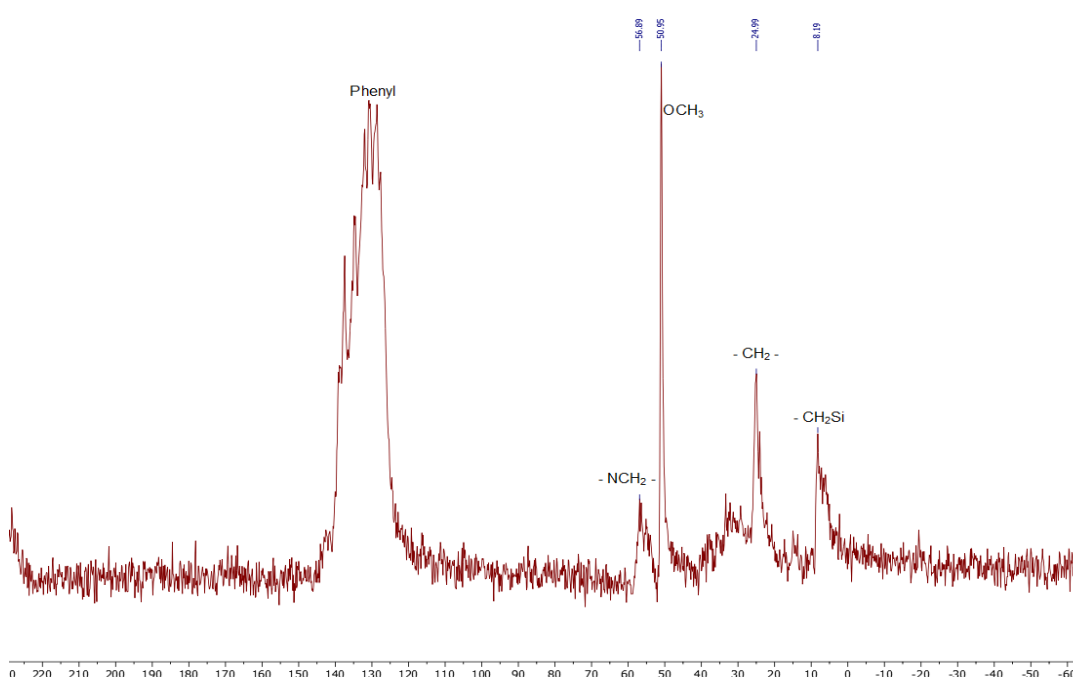


Figure 4.11:  $^{13}\text{C}$  CP/MAS NMR spectra (101 MHz, 10 kHz spinning speed) of  $\text{Al}_2\text{O}_3$ -supported [Ru]-2.1 and [Ru]-2.2

peak is a broad aromatic carbon peak due to PPh<sub>2</sub> groups between 100 – 150 ppm observed in all alumina-supported catalysts. Some other important peaks seen are due to propyl CH<sub>2</sub> groups recorded at ca. 12/23, 9/27, and 12/26 ppm for acidic, basic and neutral alumina-supported catalyst **[Ru]-2.1** respectively (Figure 4.11 a-c) similar to literature data.<sup>24</sup> Other notable peaks are due to the *p*-cymene methyl and phenyl carbon peaks observed in both acidic and basic alumina-supported catalyst **[Ru]-2.2** spectra (Figure 4.11d-e). The peaks due to propyl CH<sub>2</sub> groups in acidic and basic alumina-supported catalyst **[Ru]-2.2** are recorded at ca. 22 and 19 ppm respectively. Essentially, the presence of these peaks confirmed that catalysts **[Ru]-2.1** and **[Ru]-2.2** were successfully tethered to the alumina surface. However, complete condensation of the methoxy groups (OCH<sub>3</sub>) was not achieved as a peak at ca. 50 ppm due to OCH<sub>3</sub> is still observed on the spectra of all supported catalysts, suggesting the presence of free siloxyl (Si(OCH<sub>3</sub>)) group(s) in the supported catalyst.<sup>16, 24</sup> As can be seen in the liquid-state spectra, the intensity of the methoxy peak was found to be higher than those of the aromatic peaks but in the solid-state spectra, the reverse was the case which demonstrated partial consumption of methoxy groups during the functionalisation process. For close comparison, the <sup>13</sup>C CP/MAS NMR of unsupported catalyst **[Ru]-2.1** was analysed in the solid state and the spectrum is displayed in Figure 4.12.



**Figure 4.12:** <sup>13</sup>C CP/MAS NMR spectrum (101 MHz, 10kHz spinning speed) of unsupported catalyst **[Ru]-2.1**

Similarly, the methoxy signal showed higher intensity than the phenyl peak. This result is consistent with the result from  $^{29}\text{Si}$  CP/MAS NMR in which  $\text{T}^3$  silicon site ( $\text{RSiO}_{3/2}$ ) was undetected. Further evidence for the presence of free methoxy groups in the supported catalysts is the gradual colour change from brown to grey upon exposure to air (Figure 4.13). The examination of the grey-coloured basic alumina-supported catalyst **[Ru]-2.1** by  $^{31}\text{P}$  CP/MAS NMR spectroscopy showed no additional oxidised phosphine species, which suggests the colour change may result from the hydrolysis of the free methoxy groups with atmospheric water.



**Figure 4.13:** Exposed (left) and unexposed (right) basic alumina-supported catalyst **[Ru]-2.1** photograph

#### 4.3.2.6.3 $^{29}\text{Si}$ CP/MAS NMR spectroscopy

The  $^{29}\text{Si}$  CP/MAS NMR spectra of alumina-supported catalysts **[Ru]-2.1** and **[Ru]-2.2** was recorded to elucidate the silicon environment and degree of functionalisation. The spectra of all of the supported catalysts gave two prominent silicon peaks around -20 and -45 ppm attributed to  $\text{D}^2$  ( $\text{R}_2\text{SiO}_{2/2}$ ) and  $\text{T}^1$  ( $\text{RSi}(\text{OR})_2\text{O}_{1/2}$ ) silicon sites respectively (Figure 4.14).<sup>25-31</sup> A similar nickel catalyst was reported to give only one peak at -44.6 ppm.<sup>11</sup> It is quite unusual for a T silating agent ( $\text{RSi}(\text{OR})_3$ ) with a single R group to give  $\text{D}^n$  (0-2) species ( $\text{R}_2\text{SiO}_{n/2}$ ) with two R groups after the condensation process. Even with potential  $-\text{H}_2\text{C}-\text{Si}$  cleavage during functionalisation,<sup>16, 32</sup> it is unlikely for  $\text{D}^n$  species to occur. Assuming  $-\text{H}_2\text{C}-\text{Si}$  scission occurred,  $\text{Q}^n$  silicon sites between -90 to -120 ppm would be observed in the spectra of the supported catalysts.<sup>16, 32, 33</sup> The broad peaks between -83 to -136 ppm (Figure 4.14a, c-e, denoted  $\circ$ ) appeared to be due to noise as they disappeared when the number of scans was increased (Figure 4.14 b). As the intensity of the peak around -20 ppm was notably higher than that around -45 ppm in some of the supported catalysts (Figure 4.14 b, d & e), the former

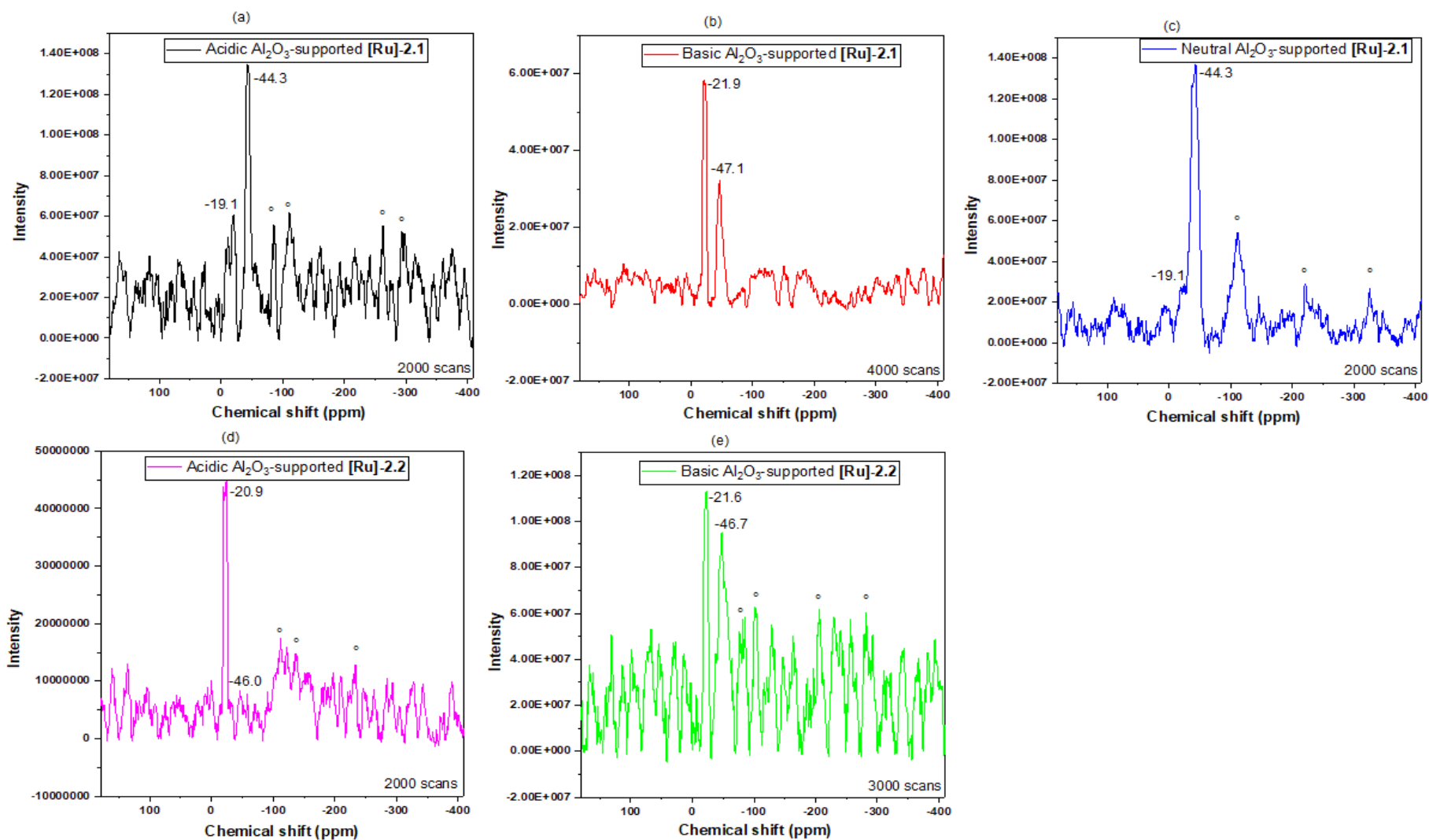
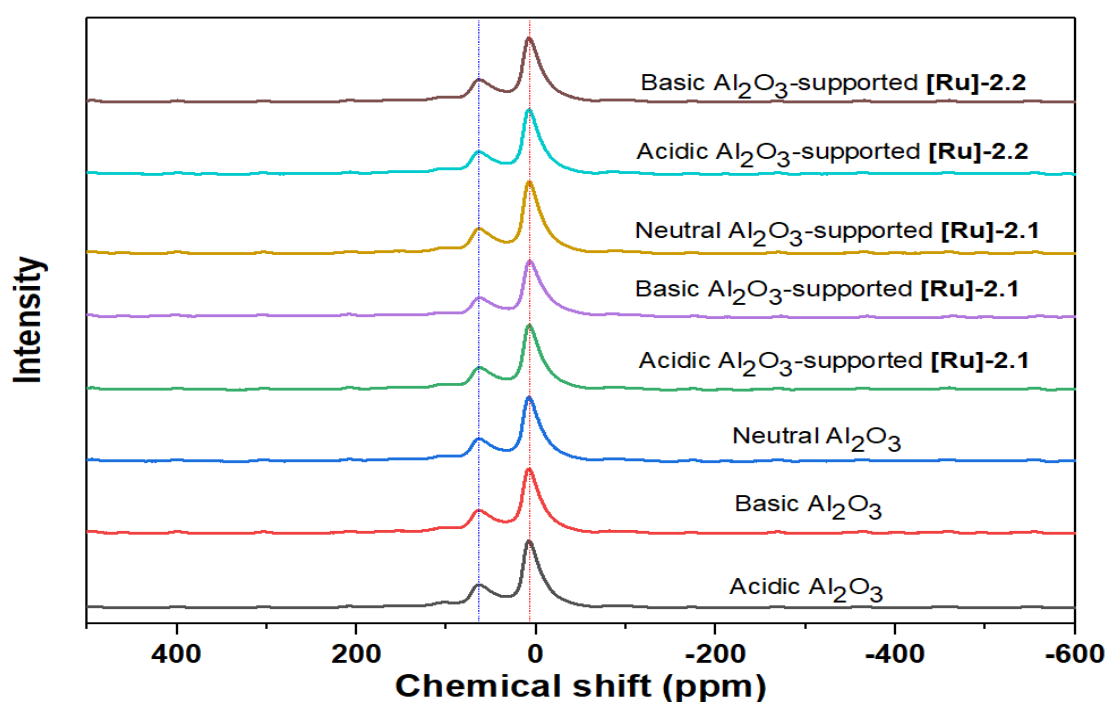


Figure 4.14:  $^{29}\text{Si}$  CP/MAS NMR spectra (79.5 MHz, 10 kHz spinning speed) of  $\text{Al}_2\text{O}_3$ -supported [Ru]-2.1 and [Ru]-2.2 (\*Spinning sidebands)

peak may be attributed to  $T^1$  ( $\text{RSi}(\text{OR})_2\text{O}_{1/2}$ ) and the latter to  $T^2$  ( $\text{RSi}(\text{OR})\text{O}_{2/2}$ ) sites based on the nature of the catalysts studied.

#### 4.3.2.6.4 $^{27}\text{Al}$ CP/MAS NMR spectroscopy

$^{27}\text{Al}$  CP/MAS NMR spectroscopy of unfunctionalised aluminas and alumina-supported catalysts **[Ru]-2.1** and **[Ru]-2.2** was carried out to reveal any structural changes to the alumina material due to the functionalisation process. Fortunately, the spectra of unfunctionalised and functionalised (i.e. supported catalysts) aluminas (Figure 4.15) showed no chemical shift differences in both octahedral ( $\text{Al}_{\text{oct}}$ , 7.2 ppm) and tetrahedral ( $\text{Al}_{\text{tet}}$ , 62.6 ppm) alumina sites post derivatisation.<sup>32</sup>



**Figure 4.15:**  $^{27}\text{Al}$  CP/MAS NMR spectra (104 MHz, 10kHz spinning speed) of pure  $\text{Al}_2\text{O}_3$  and  $\text{Al}_2\text{O}_3$ -supported **[Ru]-2.1** and **[Ru]-2.2**.

#### 4.3.2.7 Inductively Coupled Plasma-Mass Spectrometry (ICP-MS)

Analysis of the Ru content with atomic absorption spectroscopy (AAS) gave relatively low amounts due to incomplete digestion of the sample in aqua regia despite heating on a hot plate in a closed fumehood. Therefore, the exact Ru content in purportedly 2 wt% catalysts (assuming complete loading of homogeneous catalyst relative to alumina) was determined from ICP-MS via microwave-assisted digestion in aqua regia. The results are given in Table 4.2. As expected, the final catalyst loading of 0.86, 0.91 and 1.00 wt% for acidic, basic and neutral  $\text{Al}_2\text{O}_3$ -supported **[Ru]-2.1**

respectively were lower than the assumed 2 wt% incorporated into the alumina. Since the crystal structure of catalyst **[Ru]-2.2** revealed two Ru atoms per molecule, the initial 2 wt% loading, which had been based on a single Ru atom became 4 wt% using the correct number of Ru atoms (two) in the catalyst. The results from ICP support this latter calculation by giving 3.28 wt% and 3.21 wt% for acidic and basic Al<sub>2</sub>O<sub>3</sub>-supported **[Ru]-2.2** respectively, which are higher than the intended 2 wt% but lower than the corrected 4 wt% loading.

**Table 4.2:** Ru amount in supported catalysts determined by ICP

<b>Samples</b>	<b>Amounts of samples taken for ICP (g)</b>	<b>ICP Average Ru Conc. (ppb)</b>	<b>ICP Amount of Ru (mg/g)</b>	<b>ICP Actual Loading (wt %)</b>
Acidic Al <sub>2</sub> O <sub>3</sub> -supported <b>[Ru]-2.1</b>	0.05060	8657.94	8.56	0.86
Basic Al <sub>2</sub> O <sub>3</sub> -supported <b>[Ru]-2.1</b>	0.05066	9192.86	9.07	0.91
Neutral Al <sub>2</sub> O <sub>3</sub> -supported <b>[Ru]-2.1</b>	0.04950	9883.54	9.98	1.00
Acidic Al <sub>2</sub> O <sub>3</sub> -supported <b>[Ru]-2.2</b>	0.04630	30371.71	32.80	3.28 <sup>a</sup>
Basic Al <sub>2</sub> O <sub>3</sub> -supported <b>[Ru]-2.2</b>	0.04300	27639.79	32.14	3.21 <sup>a</sup>

<sup>a</sup>Initial 4 wt% catalyst loading based on two atoms of Ru in catalysts **[Ru]-2.2**

### 4.3.3 Catalytic activity

Testing of heterogeneous catalyst **[Ru]-2.1** was carried out in ethanol-methanol upgrading to *iso*-butanol under the same catalytic conditions used for the homogeneous catalyst; 1 mL ethanol (17.13 mmol), 10 mL methanol (246.88 mmol), 0.1 mol% catalyst loading (0.01713 mmol), 200 mol% NaOMe (34.26 mmol), 2 or 20 h at 180°C in a 100 mL Parr autoclave (mol% relative to ethanol). The 0.1 mol% supported catalyst was calculated based on the ruthenium loading as determined by ICP. The results of the catalysis are presented in Table 4.3. As illustrated in Table 4.3, all three alumina types displayed similar activity towards ethanol-methanol upgrading to *iso*-butanol by giving nearly the same ethanol conversion, *iso*-butanol yield and selectivity at 20 h (Runs 1-3). Nevertheless, acidic alumina gave the highest ethanol

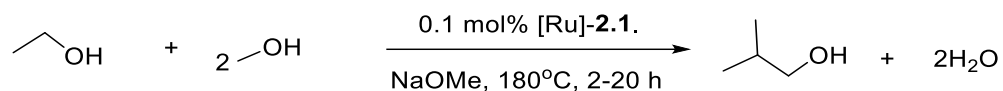


**Table 4.3:** Ruthenium catalysed conversion of ethanol and methanol to *iso*-butanol.

Run <sup>a</sup>	Catalyst	Time (h)	Base	Conversion <sup>b</sup> (%)	Total TON <sup>c</sup>	TON <sup>d</sup> (yield) <sup>e</sup> [selectivity] %				
						<i>iso</i> -Butanol	1-Propanol	1-Butanol	2-Methyl-1-butanol	Hexanol
1	Het[Ru]-2.1 <sup>f</sup>	20	NaOMe	66	660	210(21)[82]	30(3)[12]	-	20(2)[3]	20(2)[2]
2	Het[Ru]-2.1 <sup>g</sup>	20	NaOMe	64	640	200(20)[82]	30(3)[11]	-	20(2)[4]	20(2)[3]
3	Het[Ru]-2.1 <sup>h</sup>	20	NaOMe	64	640	200(20)[82]	30(3)[12]	-	20(2)[3]	20(2)[3]
4 <sup>i</sup>	Hom[Ru]-2.1	2	NaOMe	28	280	90(9)[72]	20(2)[18]	-	20(2)[9]	<1
5 <sup>i</sup>	Hom[Ru]-2.1	24	NaOMe	79	790	440(44)[87]	20(2)[4]	10(1)[1]	-	120(12)[8]
6 <sup>i</sup>	Hom[Ru]-2.1	48	NaOMe	78	780	580(58)[91]	30(3)[5]	-	-	90(9)[5]
7 <sup>j</sup>	Hom[Ru]-2.1	2	NaOMe	31	310	80(8)[67]	20(2)[20]	-	30(3)[10]	10(1)[1]

<sup>a</sup>Conditions: Ethanol (1 mL, 17.13 mmol), methanol (10 mL, 247.13 mmol), [Ru] catalyst (0.01713 mmol, 0.1 mol%), Base (34.26 mmol, 200 mol%), mol% is based on ethanol substrate, 180 °C. <sup>b</sup>Total conversion of ethanol to liquid products as determined by GC analysis of the liquid phase. <sup>c</sup>Total TON based on mmol of total ethanol converted to products per mmol of [Ru] catalyst (ethanol equivalent relative to mmol of catalysts x conversion = 1000 x conversion). <sup>d</sup>TON based on mmol of any product formed per mmol [Ru] catalyst (ethanol equivalent relative to mmol of catalysts x product yield = 1000 x product yield). <sup>e</sup>Total yield and selectivity of alcohol products in the liquid fraction as determined by GC. <sup>f</sup>Acidic Al<sub>2</sub>O<sub>3</sub>-supported [Ru]-2.1. <sup>g</sup>Basic Al<sub>2</sub>O<sub>3</sub>-supported [Ru]-2.1. <sup>h</sup>Neutral Al<sub>2</sub>O<sub>3</sub>-supported [Ru]-2.1 <sup>i</sup>From Chapter 2. <sup>j</sup>5 mol% acidic Al<sub>2</sub>O<sub>3</sub> added. (Het = Heterogeneous, Hom = Homogeneous).

conversion (66%) and *iso*-butanol yield (21%) among the three types of alumina used (Runs 1-3). Moreover, 82% *iso*-butanol selectivity was achieved with all the aluminas (Runs 1-3). Similarly, the three alumina types showed identical activity towards other Guerbet alcohol products (1-propanol, 2-methyl-1-butanol and 1-hexanol). Therefore, the pH of the alumina has no significant influence on the activity of the supported catalyst, as can be seen in Table 4.3. Though, homogeneous catalyst **[Ru]-2.1** was not tested using identical conditions, careful examination of the results from 2 – 48 h runs (Runs 4-6) suggested the activity at 20 h would likely be higher than those obtained for the heterogeneous catalyst **[Ru]-2.1** (Runs 1-3). The difference in activity may be due to the nature of the support used. The *in-situ* run with 5 mol% unfunctionalised acidic Al<sub>2</sub>O<sub>3</sub> in combination with 0.1 mol% homogeneous catalyst **[Ru]-2.1** at 2 h supports this finding, indicating that the presence of alumina shows no improvement on the activity of catalyst **[Ru]-2.1** (compare Runs 4 and 7). Unfortunately, due to time constraints, the activity of Al<sub>2</sub>O<sub>3</sub>-supported catalyst **[Ru]-2.2** or investigation into the recoverability and reusability of these immobilised catalysts were not performed but constitute the project future targets.

#### 4.4 Conclusion and Future work

In summary, the heterogenisation of homogeneous catalysts **[Ru]-2.1** and **[Ru]-2.2** was achieved. Complete characterisation of the supported catalysts was carried out using a variety of analytical tools, showing the presence of the catalysts inside alumina channels and evidence of aluminosiloxane (Al-O-Si) bond formation. Moreover, all catalysts displayed a combination of T<sup>1</sup> and T<sup>2</sup> silicon sites, indicating one and two degree(s) condensation reaction respectively. The presence of incomplete condensation of the three methoxy groups may be associated with the immobilisation period. Interestingly, acidic, basic and neutral Al<sub>2</sub>O<sub>3</sub>-supported catalysts **[Ru]-2.1** showed significant activity for ethanol-methanol upgrading to *iso*-butanol with the best ethanol conversion and *iso*-butanol yield obtained using acidic Al<sub>2</sub>O<sub>3</sub>-supported catalyst **[Ru]-2.1**. Albeit the catalytic activity of heterogeneous catalysts **[Ru]-2.1** seems lower than the homogeneous counterpart. Finally, the pH of the aluminas showed no significant effect on the activity of supported catalysts **[Ru]-2.1**.

In line with the findings from this chapter, the following future perspectives are of considerable interest.

- Recoverability, recyclability and leachability studies on all Al<sub>2</sub>O<sub>3</sub>-supported catalysts **[Ru]-2.1**.
- The effect of additionally water on the activity of Al<sub>2</sub>O<sub>3</sub>-supported catalysts **[Ru]-2.1**.
- Kinetics studies of the homogeneous and heterogeneous **[Ru]-2.1**.
- Catalytic activity of characterised acidic and basic Al<sub>2</sub>O<sub>3</sub>-supported catalysts **[Ru]-2.2**. and corresponding recoverability, reusability, leachability and water tolerance studies.
- Since incomplete condensation was achieved in the immobilisation of catalyst **[Ru]-2.1** and **[Ru]-2.2** with alumina within the 24 h refluxing time, longer reaction times may be required to drive the condensation process to completion.

## 4.5 References

1. C. Merckle and J. Blümel, *Chem. Mater.*, 2001, **13**, 3617-3623.
2. J. B. Peri and R. B. Hannan, *J. Phys. Chem.*, 1960, **64**, 1526-1530.
3. J. Peri, *J. Phys. Chem.*, 1965, **69**, 211-219.
4. J. Peri, *J. Phys. Chem.*, 1965, **69**, 220-230.
5. H. Knözinger and P. Ratnasamy, *Catal. Rev.: Sci. Eng.*, 1978, **17**, 31-70.
6. G. E. Maciel and P. D. Ellis, in *NMR Techniques in Catalysis*, ed. Alexis T. Bell and Alexander Pines, Marcel Dekker, Inc, New York, 1994, **Chemical industries**; **55**, ch. 5, pp. 231-245.
7. G. W. Kabalka and R. M. Pagni, *Tetrahedron*, 1997, **53**, 7999-8065.
8. J. J. Fitzgerald, G. Piedra, S. F. Dec, M. Seger and G. E. Maciel, *J. Am. Chem. Soc.*, 1997, **119**, 7832-7842.
9. A. T. Bell and A. Pines, in *NMR Techniques in Catalysis*, ed. Alexis T. Bell and Alexander Pines, Marcel Dekker, Inc, New York, 1994, **Chemical industries**; **55**, ch. 1, pp. 1-9.
10. P. Braunstein, H. P. Kormann, W. Meyer-Zaika, R. Pugin and G. Schmid, *Chem. Eur. J.*, 2000, **6**, 4637-4646.
11. T. Posset, F. Rominger and J. Blümel, *Chem. Mater.*, 2005, **17**, 586-595.
12. W. Mozgawa, *J. Mol. Struct.*, 2000, **555**, 299-304.
13. A. Kuznetsova, E. A. Wovchko and J. T. Yates, *Langmuir*, 1997, **13**, 5322-5328.
14. A. Ghorbani-Choghamarani, B. Tahmasbi, R. H. E. Hudson and A. Heidari, *Microporous Mesoporous Mater.*, 2019, **284**, 366-377.
15. H. W. Darwish, A. Barakat, A. Nafady, M. Suleiman, M. Al-Noaimi, B. Hammouti, S. Radi, T. B. Hadda, A. Abu-Obaid and M. S. Mubarak, *Molecules*, 2014, **19**, 5965-5980.
16. C. Kang, J. Huang, W. He and F. Zhang, *J. Organomet. Chem.*, 2010, **695**, 120-127.
17. Y. Lv, D. Li, P. Tang and Y. Feng, *Mater. Lett.*, 2015, **155**, 75-77.
18. A. Bazyari, Y. Mortazavi, A. A. Khodadadi, L. T. Thompson, R. Tafreshi, A. Zaker and O. T. Ajenifujah, *Appl. Catal., B*, 2016, **180**, 312-323.
19. J. J. Calvin, M. Asplund, Y. Zhang, B. Huang and B. F. Woodfield, *J. Chem. Thermodyn.*, 2017, **112**, 77-85.
20. S. Brunauer, P. H. Emmett and E. Teller, *J. Am. Chem. Soc.*, 1938, **60**, 309-319.
21. K. S. Sing, *Pure Appl. Chem.*, 1985, **57**, 603-619.
22. N. Hwang and A. R. Barron, *The Connexions project*, 2011, 1-11.
23. E. P. Barrett, L. G. Joyner and P. P. Halenda, *J. Am. Chem. Soc.*, 1951, **73**, 373-380.
24. K. D. Behringer and J. Blümel, *J. Liq. Chromatogr. Relat. Technol.*, 1996, **19**, 2753-2765.
25. G. Engelhardt, H. Jancke, E. Lippmaa and A. Samoson, *J. Organomet. Chem.*, 1981, **210**, 295-301.
26. D. W. Sindorf and G. E. Maciel, *J. Am. Chem. Soc.*, 1983, **105**, 3767-3776.
27. E. E. Vansant, P. V. D. Voort and K. C. Vrancken, in *Studies in Surface Science and Catalysis*, Ed. B. Delmon and J.T. Yates, Amsterdam, The Netherlands, 1995, **93**, ch. 9, pp. 203, 230, 258.
28. G. E. Maciel, C. E. Bronnimann, R. C. Zeigler, I.-S. Chuang, D. R. Kinney and E. A. Keiter, in *The Colloid Chemistry of Silica*, ed. Horacio E. Bergna, Dupont, American Chemical Society, Washington, DC, 1994, **Advances in chemistry series**, **234**, ch. 14, pp. 278.
29. G. E. Maciel and I.-S. Chuang, in *Colloidal Silica: Fundamentals and Applications*, ed. Horacio E. Bergna and William O. Roberts, CRC Press, Taylor & Francis Group, Boca Raton, FL, 2006, **Surfactant Science Series**, **131**, ch. 34, 445.

30. M. Itoh, F. Oka, M. Suto, S. D. Cook and N. Auner, *Int. J. Polym. Sci.*, 2012, **2012**, 1-17.
31. I. S. Protsak, Y. M. Morozov, W. Dong, Z. Le, D. Zhang and I. M. Henderson, *Nanoscale Res. Lett.*, 2019, **14**, 160.
32. L. A. S. A. Prado, M. Sriyai, M. Ghislandi, A. Barros-Timmons and K. Schulte, *J. Braz. Chem. Soc.*, 2010, **21**, 2238-2245.
33. D. Jiang, J. Gao, Q. Yang, J. Yang and C. Li, *Chem. Mater.*, 2006, **18**, 6012-6018.

## Chapter 5: Nucleophilic Addition to a Vinylidene Diphosphine Ru(II) Complex - Synthesis, Characterisation and Catalytic Activity towards Ethanol Upgrading to Advanced Biofuels

### 5.1 Introduction

Tertiary phosphines ( $\text{PR}_3$ ) are one of the most explored ligand types in the field of coordination and organometallic chemistry owing to the wide variety of electronic and steric effects that they can exhibit which can be altered in systematic and predictable ways by varying the R-groups. They are often easy to synthesis and, most importantly, provide stabilisation and solubilisation to transition-metal complexes in different oxidation states that is beneficial to many catalytic systems.<sup>1, 2</sup> Moreover, tertiary phosphines have an exceptional ability to control the reactivity and selectivity of transition metal promoted reactions. In light of this, the coordination chemistry of transition metals with bidentate tertiary phosphines ligands ( $\text{R}_2\text{P}^{\wedge}\text{PR}_2$ ) separated by carbon linker has been increasingly investigated. However, only a few studies on the complexes of functionalised analogues exist in literature. This may be due to the fact that most methods used to synthesise non-functionalised tertiary phosphines are ineffective when applied to the synthesis of functionalised tertiary phosphines.<sup>3, 4</sup> Customarily, functionalisation of these phosphines is either carried out independently prior to complexation or applicable after coordination to the metal centre.<sup>4-6</sup> Common examples of independent functionalisation of bidentate tertiary phosphines include the electrophilic attack on bis(diphenylphosphino)methane (dppm,  $\text{Ph}_2\text{PCH}_2\text{PPh}_2$ ) via deprotonation of a methylene hydrogen<sup>7, 8</sup> and the nucleophilic addition to the vinylidene group of 1,1-bis(diphenylphosphino)ethylene (dppen,  $(\text{Ph}_2\text{P})_2\text{C}=\text{CH}_2$ ).<sup>9-12</sup> The functionalisation of coordinated dppm<sup>3, 13-20</sup> and dppen<sup>3, 4, 6, 21-25</sup> metal complexes, in contrast to independent functionalisation, continues to receive much attraction because the metal acts as a protecting group against the oxidation of the phosphines coupled with the influence of the co-ligands. However, the deprotonation of metal-coordinated dppm takes place under forcing conditions with the use of very strong bases. On the other hand, nucleophilic addition to metal-coordinated dppen is relatively straightforward. Although, free dppen is seldomly susceptible to nucleophilic attack in the absence of a strong base like  $^t\text{BuOK}$ , coordination to a metal centre activates the double bond in a way that allows direct addition of nucleophiles via Michael addition reactions.<sup>4-6, 25</sup> Presumably, an additional induced polarisation of

the double bond in the complex precursor coupled with the angle strain relief at the  $\alpha$ -carbon following the addition reaction, are contributing factors to the ease of attack on the coordinated dppen.<sup>4, 6</sup> With the right choice of metal centre, oxidation state and co-ligands, the double bond of dppen becomes easily activated towards nucleophilic addition.<sup>5, 26</sup> Previous compounds include tetracarbonyl derivatives of group six,<sup>27, 28</sup> Fe(0),<sup>29</sup> Ru(II),<sup>22, 30</sup> Au(I),<sup>31</sup> Au(III),<sup>25</sup> Pd(II),<sup>32</sup> Pt(II)<sup>33, 34</sup> and Pt(IV)<sup>33</sup> coordinated dppen complexes.<sup>4</sup> Noteworthy, the P-C-P structural unit of dppen form part of the metallacycle where its chelation preferable favour Michael addition and, thus, increases the stability of the metal complex.<sup>5</sup>

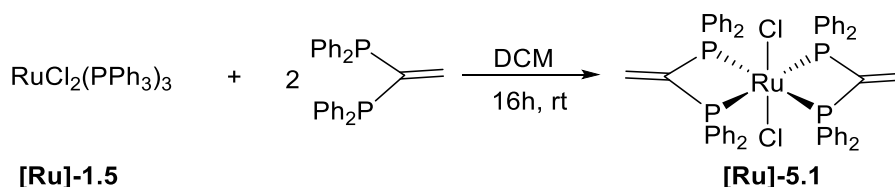
## 5.2 Aim and objectives

In the context of the projects continuing effort to investigate the catalytic activity of bidentate phosphine complexes for bioethanol upgrading, this chapter focuses on functionalising Ru(II) coordinated dppen with a variety of amines and thereafter explores their catalytic activity in this transformation. The reason for studying amines relies on the understanding of designing a catalyst with both acidic and basic sites that is required for such a catalytic system. Additionally, some of the amine moieties provide an additional potential binding motif for possible future heterogenisation to solid support materials.

## 5.3 Results and Discussion

### 5.3.1 Synthesis of [RuCl<sub>2</sub>{(PPh<sub>2</sub>)<sub>2</sub>CH=CH<sub>2</sub>}<sub>2</sub>] ([Ru]-5.1)

Complex precursor *trans*-[RuCl<sub>2</sub>(dppen)<sub>2</sub>] [Ru]-5.1 was prepared following a literature method<sup>21, 23</sup> by the addition of two equivalents of 1,1-Bis(diphenylphosphino)ethylene (dppen) to one equivalent of [Ru]-1.5 in dichloromethane (Scheme 5.1). A singlet at 15.3 ppm was observed in the <sup>31</sup>P{<sup>1</sup>H} NMR spectrum (Figure 5.1).



**Scheme 5.1:** Synthesis of complex [Ru]-5.1

In the <sup>1</sup>H NMR, a quintet at 6.1 ppm indicated the presence of terminal methylene protons in the complex. ESI mass spectrometry of complex [Ru]-5.1 in

dichloromethane solution shows four prominent peaks at 987 [M + Na]<sup>+</sup>, 964 [M]<sup>+</sup>, 929 [M - Cl]<sup>+</sup>, 4 and 47 [M - 2Cl]<sup>2+</sup>.

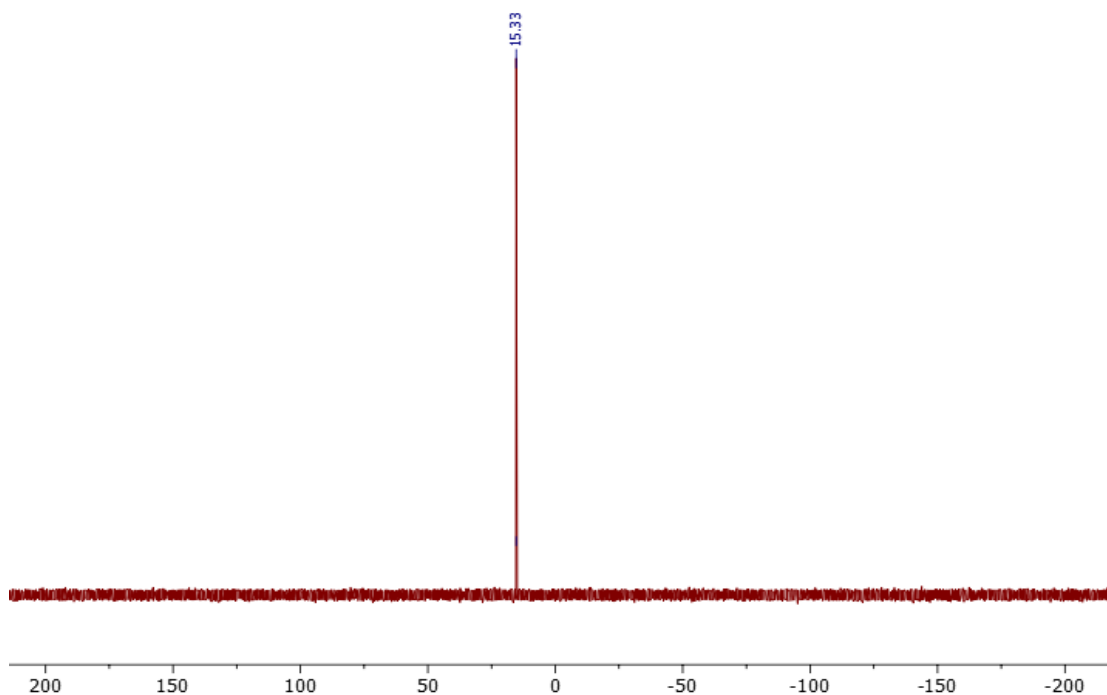
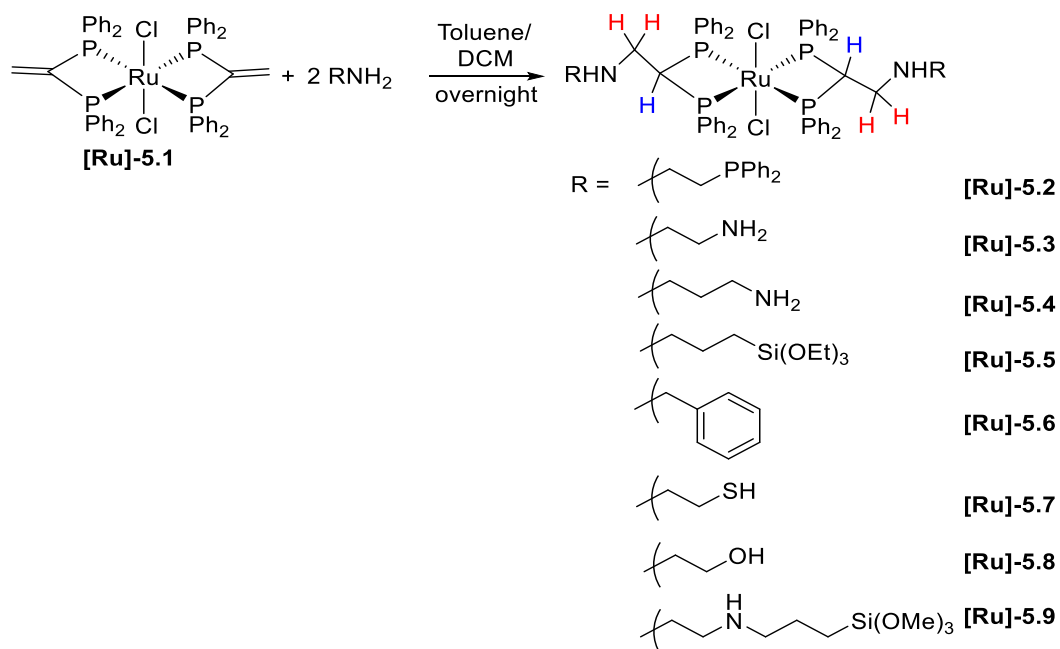


**Figure 5.1:** <sup>31</sup>P{<sup>1</sup>H} NMR spectrum (CDCl<sub>3</sub>, 162 MHz) of complex [Ru]-5.1

### 5.3.2 Functionalization of [Ru]-5.1 with Amines



**Scheme 5.2:** Synthesis of complexes [Ru]-5.2 to [Ru]-5.9

The complex precursor **[Ru]-5.1** was functionalised by the addition of a range of primary amines (RNH<sub>2</sub>) in dichloromethane or toluene solution to give complexes **[Ru]-5.2** to **[Ru]-5.9** (Scheme 5.2).

The functionalised complexes, except for **[Ru]-5.9**, were all isolated as yellow solids in good yields (87%) and characterised by <sup>31</sup>P{<sup>1</sup>H} and <sup>1</sup>H NMR spectroscopy and mass spectrometry. However, complex **[Ru]-5.9** was obtained as an oily product, several attempts to crystallise the product from methanol, ethanol, ether, hexane and pentane proved abortive. In complexes **[Ru]-5.2** to **[Ru]-5.9**, a new signal due to methylene protons appeared at ca. 3 ppm in the <sup>1</sup>H NMR spectra showing an upfield shift from those for the methyldene group of the pre-catalyst (complex **[Ru]-5.1**, 6.1 ppm). Additionally, a new methine proton (coloured blue in Scheme 5.2) was observed at ca. 5 ppm for all of the complexes. All other proton peaks matched those of the starting amines added to **[Ru]-5.1** to form complexes **[Ru]-5.2** to **[Ru]-5.9**. The <sup>31</sup>P{<sup>1</sup>H} NMR spectra for all the complexes showed a chemical shift at ca. 11 ppm except for complex **[Ru]-5.7** which exhibited a peak at 15.9 ppm, similar to that of the pre-catalyst (15.3 ppm). Complex **[Ru]-5.2** produced an additional peak at -20.8 ppm for the dangling PPh<sub>2</sub> groups (Figure 5.2 - 5.3). The ESI mass spectra of complexes **[Ru]-5.2** to **[Ru]-5.8** confirmed the

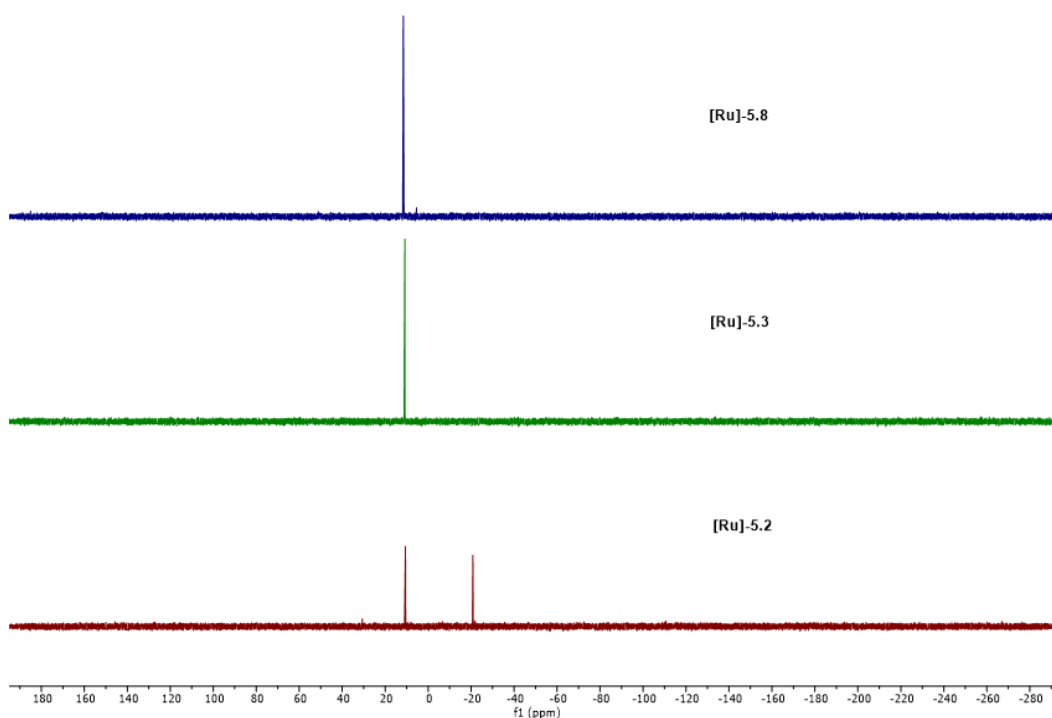


**Figure 5.2:** <sup>31</sup>P{<sup>1</sup>H} NMR spectra (CDCl<sub>3</sub>, 162 MHz) of complexes **[Ru]-5.2**, **[Ru]-5.3**, and **[Ru]-5.8**

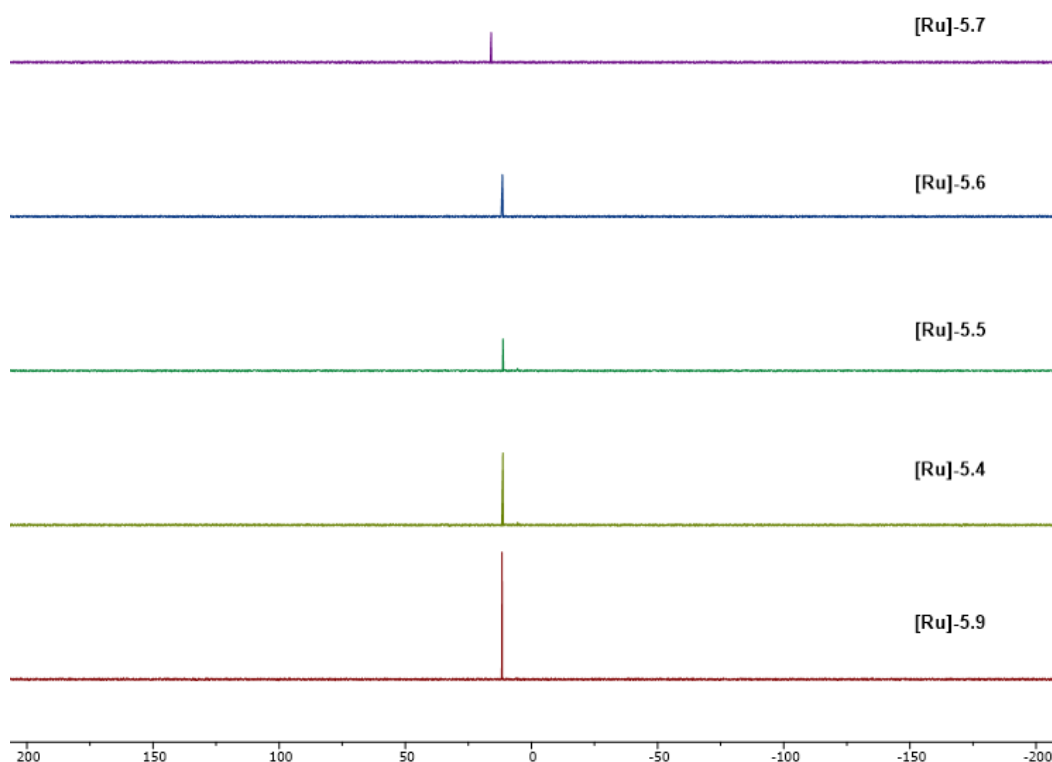


**Figure 5.3:**  $^{31}\text{P}\{^1\text{H}\}$  NMR spectra ( $\text{CDCl}_3$ , 162 MHz) of complexes **[Ru]-5.4** to **[Ru]-5.9**

proposed formulations. Nucleophilic addition with aniline, benzyl alcohol and other alcohols were unsuccessful. Though, a trace of products were noticed in crude  $^{31}\text{P}\{^1\text{H}\}$  NMR spectra of these reactions, however, complete reaction was not achieved even with addition of excess ligand, extended reaction time and refluxing in the reaction solvent. Additionally, unlike the successful reactions in which colour change was observed with 1 h or more, no colour change occurred in these reactions throughout the reaction period.

### 5.3.3 Crystal Structures

Single crystals of complexes **[Ru]-5.3**, **[Ru]-5.5**, **[Ru]-5.6** and **[Ru]-5.8** were obtained by slow evaporation of pentane into fluorobenzene/benzene solutions of the complexes. Recrystallisation of other complexes was unsuccessful. The molecular structures of **[Ru]-5.3**, **[Ru]-5.5**, **[Ru]-5.6** and **[Ru]-5.8** with selected bond lengths and angles are shown in Figure 5.4-5.7 respectively. All the structures show an octahedra geometry with *trans* chlorides. The crystal system of complexes **[Ru]-5.3**, **[Ru]-5.6** and **[Ru]-5.8** is triclinic with *P*-1 space group whereas complex **[Ru]-5.5** crystallise in the monoclinic space group *P*2<sub>1</sub>/*c*. The crystallographic data of these

complexes can be seen in the Appendix Section of Chapter 6. A crystallographically-imposed centre of symmetry exists at the ruthenium of complexes **[Ru]-5.5** and **[Ru]-5.6**. In short, complexes **[Ru]-5.5** and **[Ru]-5.6** are centrosymmetric. Therefore, each of the crystal structures of **[Ru]-5.5** and **[Ru]-5.6** has a half molecule in the asymmetric unit. Due to steric hindrance, these are likely the most thermodynamically stable stereoisomers of **[Ru]-5.5** and **[Ru]-5.6**.<sup>22</sup> Notably, complexes **[Ru]-5.3**, **[Ru]-5.6** and **[Ru]-5.8** crystallise as **[Ru]-5.3.2C<sub>7</sub>H<sub>8</sub>**, **[Ru]-5.6.2C<sub>6</sub>H<sub>5</sub>F** and **[Ru]-5.8.3CH<sub>2</sub>Cl<sub>2</sub>** per molecule in the crystal lattice. The coordination geometry of these complexes can be compared with that of  $[\text{RuCl}_2(\text{dppm})_2]$ ,<sup>35</sup>  $[\text{RuCl}_2(\text{dppen})_2]$ ,<sup>36</sup> and similar complex, *trans*- $[\text{RuCl}_2\{(\text{Ph}_2\text{P})_2\text{CHCH}_2\text{NH}(\text{CH}_2)_3\text{NH}_2\}_2]$ .<sup>22</sup> In all of the complexes, the P-Ru-P and P-C-P angles of the chelate ring are around 72° and 95° respectively, typical for dppm<sup>35</sup> and dppen<sup>22, 36</sup> complexes. Additionally, the complexes exhibit Cl-Ru-Cl angle of about 180°, similar to relative complexes. Nevertheless, the P-C-P angles (ca. 95°) of these complexes is small than those of  $[\text{RuCl}_2(\text{dppen})_2]$  (ca. 99°),<sup>36</sup> and uncomplexed dppen ligand (ca. 119°),<sup>37</sup> which is expected on going from *sp*<sup>2</sup> to *sp*<sup>3</sup> carbon. These functionalised complexes are probably forced to adopt these smaller values due to increasing strain effect of the four-membered chelate ring. Moreover, Ru-P and Ru-Cl distances in all complexes fall within 2.32-2.43 Å, which are within the expected range.<sup>22, 35, 36</sup>

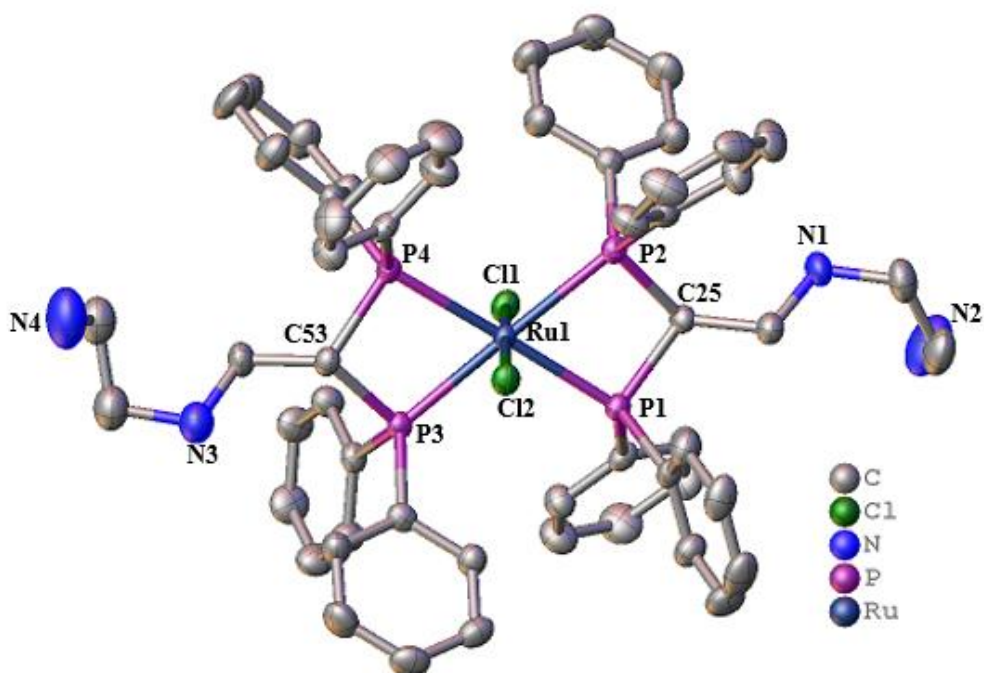


**Figure 5.4:** X-ray crystal structure of complex **[Ru]-5.3** showing *trans*-configuration. Hydrogen atoms and solvent molecules omitted for clarity. Complex **[Ru]-5.3** crystallise in the *P*-1 space group as a triclinic crystal system. **Selected bond lengths (Å):** Ru(1)-Cl(1) = 2.4266(12), Ru(1)-Cl(2) = 2.4263(11), Ru(1)-P(1) = 2.3351(12), Ru(1)-P(2) = 2.3722(12), Ru(1)-P(3) = 2.3296(12), Ru(1)-P(4) = 2.3887(12); **Selected bond angles (°):** P(1)-Ru(1)-P(2) = 71.81(4), P(3)-Ru(1)-P(4) = 72.08(4), P(1)-Ru(1)-P(4) = 178.72(4), P(2)-Ru(1)-P(4) = 109.04(4), P(3)-Ru(1)-P(1) = 107.08(4), P(3)-Ru(1)-P(2) = 178.66(4), Cl(1)-Ru(1)-Cl(2) = 176.35(4), P(3)-Ru(1)-Cl(1) = 95.15(4), P(1)-Ru(1)-Cl(1) = 81.25(4), P(2)-Ru(1)-Cl(1) = 83.96(4), P(4)-Ru(1)-Cl(1) = 99.75(4), P(3)-Ru(1)-Cl(2) = 82.92(4), P(1)-Ru(1)-Cl(2) = 96.33(4), P(2)-Ru(1)-Cl(2) = 97.92(4), P(4)-Ru(1)-Cl(2) = 82.63(4), P(1)-C(25)-P(2) = 95.5(2), P(3)-C(53)-P(4) = 96.0(2).

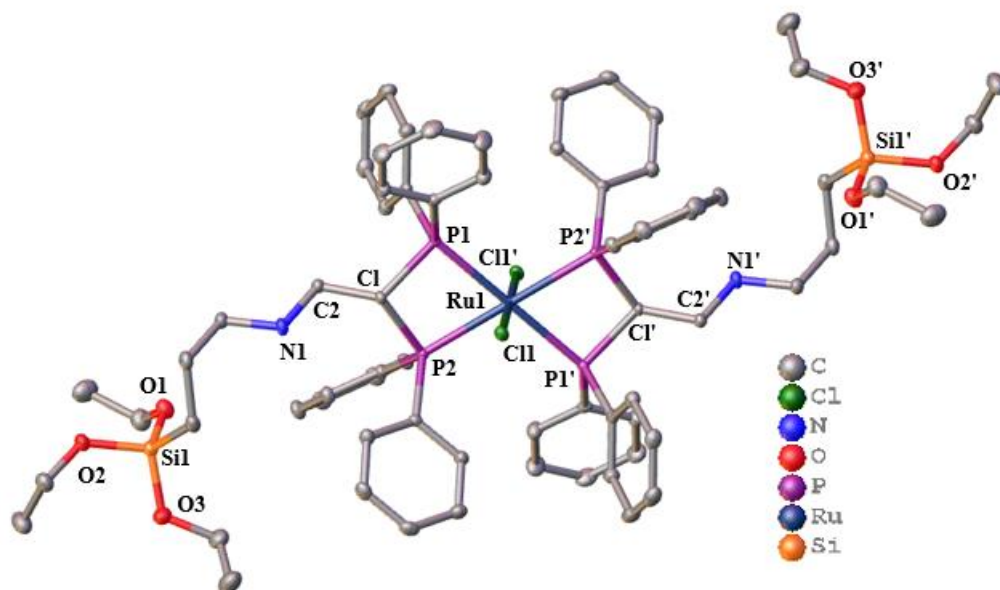


**Figure 5.5:** X-ray crystal structure of complex **[Ru]-5.5** showing *trans*-configuration. Hydrogen atoms omitted for clarity. Complex **[Ru]-5.5** crystallise in the  $P2_1/c$  space group as a monoclinic crystal system. **Selected bond lengths** (Å): Ru(1)-P(1) = Ru(1)-P(1)' = 2.3409(3), Ru(1)-P(2) = Ru(1)-P(2)' = 2.3604(3), Ru(1)-Cl(1) = Ru(1)-Cl(1)' = 2.4272(3), C(1)-P(1) = 1.8642(14), C(1)-P(2) = 1.8752(13). **Selected bond angles** (°): P(1)-Ru(1)-P(2) = 71.744(12), P(1)'-Ru(1)-P(2)' = 71.745(12), P(1)'-Ru(1)-P(2) = 108.255(12), P(1)-Ru(1)-P(2)' = 108.256(12), P(1)-Ru(1)-Cl(1) = P(1)'-Ru(1)-Cl(1)' = 84.523(11), P(1)-Ru(1)-Cl(1)' = 95.477(12), P(1)'-Ru(1)-Cl(1) = 95.477(11), Cl(1)-Ru(1)-Cl(1)' = 180.000(14), P(1)-Ru(1)-P(1)' = P(2)'-Ru(1)-P(2) = 180.0, P(2)-Ru(1)-Cl(1) = P(2)'-Ru(1)-Cl(1)' = 81.091(11), P(2)'-Ru(1)-Cl(1) = 98.908(11), P(2)-Ru(1)-Cl(1)' = 98.909(11), P(1)-C(1)-P(2) = 94.90(6).

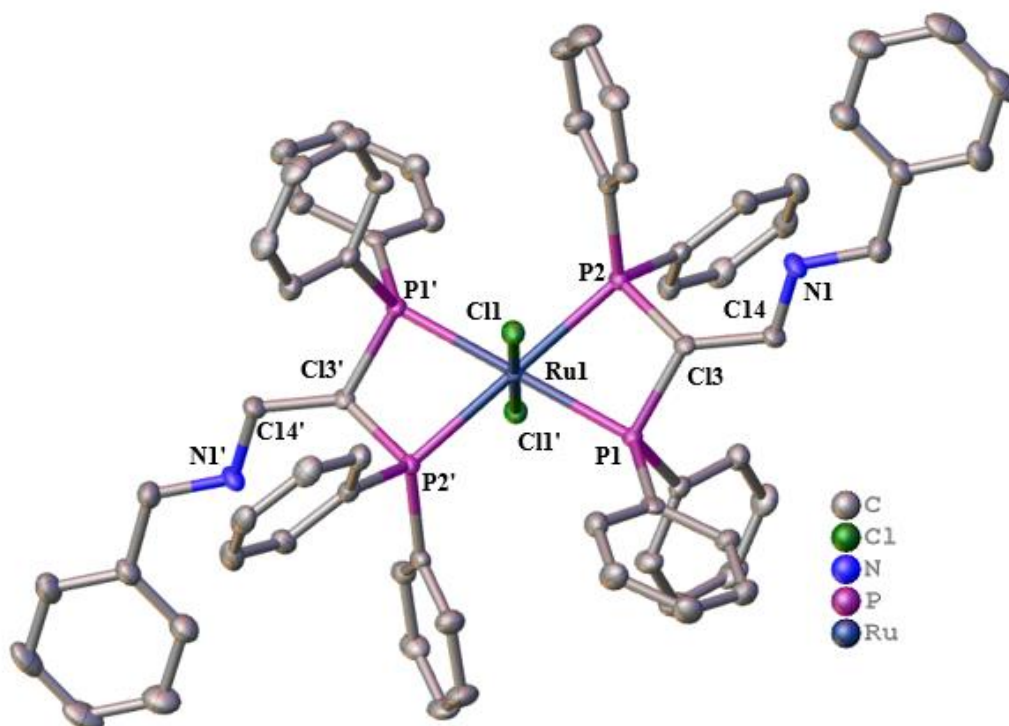


**Figure 5.6:** X-ray crystal structure of complex **[Ru]-5.6** showing *trans*-configuration. Hydrogen atoms and solvent molecules omitted for clarity. Complex **[Ru]-5.6** crystallise in the *P*-1 space group as a triclinic crystal system. **Selected bond lengths (Å):** Ru(1)-P(1) = Ru(1)-P(1)' = 2.3731(8), Ru(1)-P(2) = Ru(1)-P(2)' = 2.3350(8), Ru(1)-Cl(1) = Ru(1)-Cl(1)' = 2.4271(8), C(13)-P(1) = 1.866(3), C(13)-P(2) = 1.862(3). **Selected bond angles (°):** P(1)-Ru(1)-P(2) = P(1)′-Ru(1)-P(2)′ = 71.06(3), P(1)′-Ru(1)-P(2) = P(1)-Ru(1)-P(2)′ = 108.94(3), P(1)-Ru(1)-Cl(1) = P(1)′-Ru(1)-Cl(1)′ = 81.59(3), P(1)-Ru(1)-Cl(1)′ = P(1)′-Ru(1)-Cl(1) = 98.41(3), Cl(1)-Ru(1)-Cl(1)′ = P(1)-Ru(1)-P(1)′ = P(2)′-Ru(1)-P(2) = 180.0, P(2)-Ru(1)-Cl(1) = P(2)′-Ru(1)-Cl(1)′ = 86.95(3), P(2)′-Ru(1)-Cl(1) = P(2)-Ru(1)-Cl(1) = 93.05(3), P(1)-C(13)-P(2) = 94.44(15).

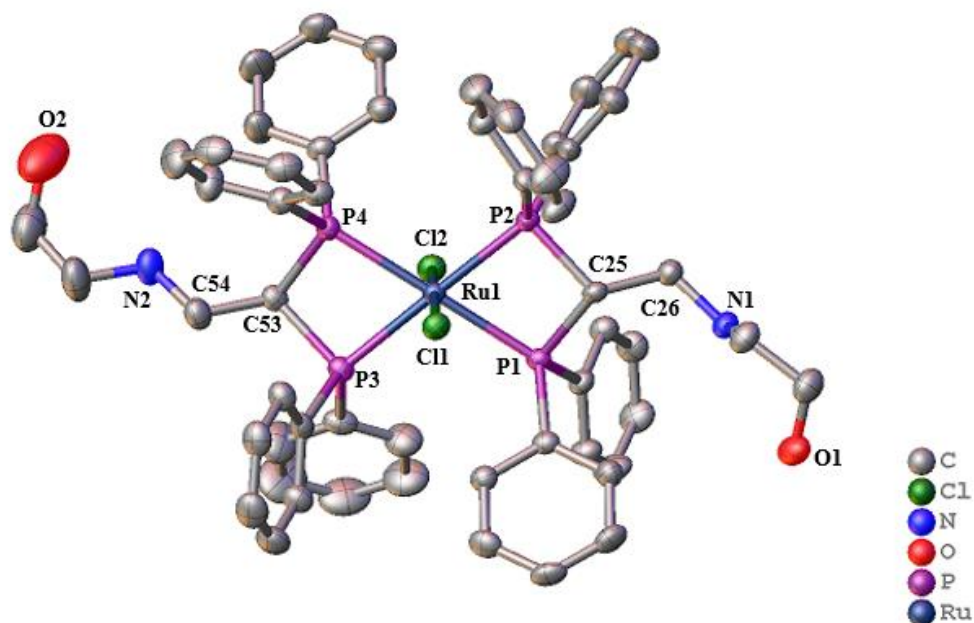
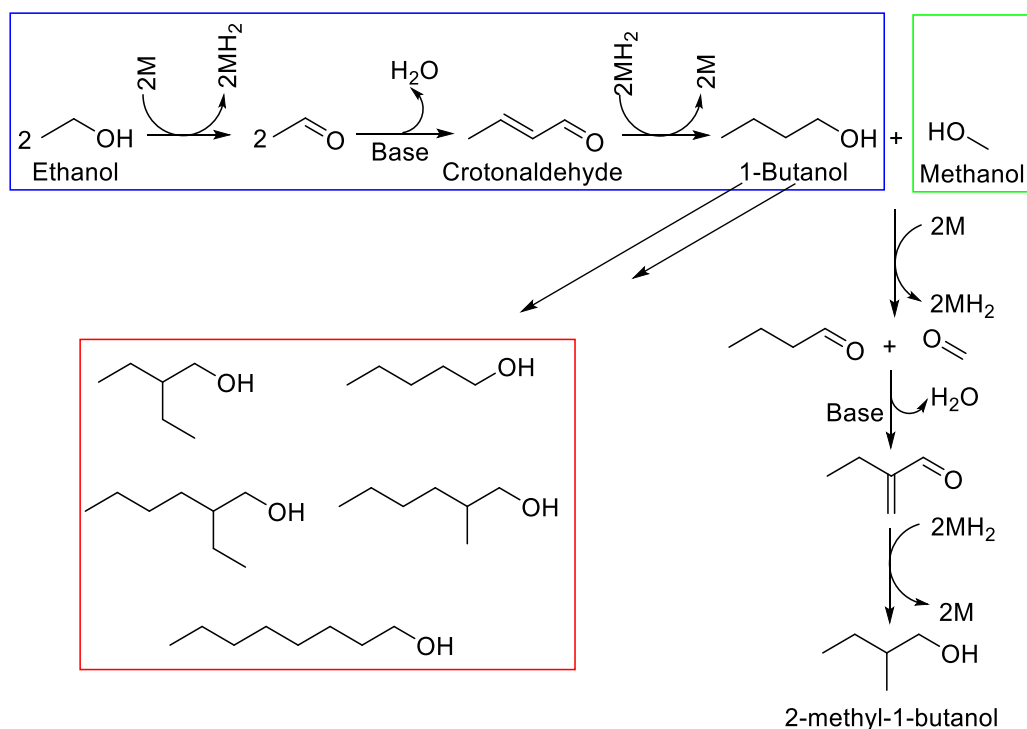


**Figure 5.7:** X-ray crystal structure of complex **[Ru]-5.8** showing *trans*-configuration. Hydrogen atoms and solvent molecules omitted for clarity. Complex **[Ru]-5.8** crystallise in the *P*-1 space group as a triclinic crystal system. **Selected bond lengths (Å):** P(1)-Ru(1) = 2.3504(9), P(2)-Ru(1) = 2.3654(9), P(3)-Ru(1) = 2.3445(9), P(4)-Ru(1) = 2.3717(9), Ru(1)-Cl(1) = 2.4232(8), Ru(1)-Cl(2) = 2.4290(8); **Selected bond angles (°):** P(1)-Ru(1)-P(2) = 72.02(3), P(3)-Ru(1)-P(4) = 71.48(3), P(3)-Ru(1)-P(1) = 107.70(3), P(3)-Ru(1)-P(2) = 176.51(3), P(1)-Ru(1)-P(4) = 177.94(3), P(2)-Ru(1)-P(4) = 108.92(3), P(3)-Ru(1)-Cl(1) = 94.46(3), P(1)-Ru(1)-Cl(1) = 84.05(3), P(2)-Ru(1)-Cl(1) = 82.05(3), P(4)-Ru(1)-Cl(1) = 97.87(3), P(3)-Ru(1)-Cl(2) = 83.01(3), P(1)-Ru(1)-Cl(2) = 94.40(3), P(2)-Ru(1)-Cl(2) = 100.47(3), P(4)-Ru(1)-Cl(2) = 83.64(3), Cl(1)-Ru(1)-Cl(2) = 176.51(3), P(2)-C(25)-P(1) = 95.25(15), P(3)-C(53)-P(4) = 94.74(15).

### 5.3.4 Catalytic Activity

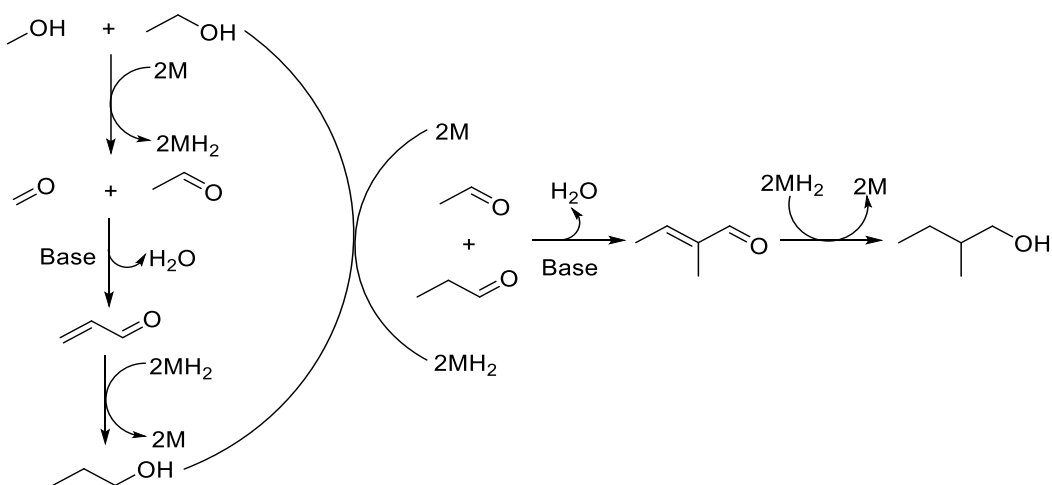
After the synthesis and characterisation of complexes **[Ru]-5.1** - **[Ru]-5.9**, catalytic screening was conducted to evaluate all complexes for ethanol upgrading to *iso*-butanol using catalytic conditions developed by Wass and co-workers; 1 mL ethanol (17.13 mmol), 10 mL methanol (246.88 mmol), 0.1 mol% catalyst loading (0.0171 mmol), 200 mol% NaOMe (34.26 mmol), 2 or 20 h at 180°C in a 100 mL Parr autoclave (mol% relative to ethanol).<sup>38, 39</sup> As established in Chapter 1, the conversion of ethanol alone to *iso*-butanol remains unknown. Unlike the catalytic production of 1-butanol from ethanol, the addition of methanol is required to obtain the branched isomer *iso*-butanol, via a cross condensation reaction. The catalytic formation of reactive formaldehyde from methanol promotes the high selectivity to *iso*-butanol in this system. Since ethanol can undergo a homocoupling reaction, excess methanol (246.88 mmol) is employed in the system to inhibit formation of the homocoupled product 1-butanol and further condensation products to favour formation of *iso*-butanol. Additionally, a large base loading is necessary to achieve good ethanol conversion. More so, methoxide base is chosen over ethoxide base to keep the system under continued excess methanol. The liquid products obtained after the catalytic period were analysed by GC with hexadecane as an internal standard. The presence of the liquid alcohol products was also confirmed by <sup>1</sup>H and <sup>13</sup>C{<sup>1</sup>H} NMR spectroscopy. Apart from the desired product *iso*-butanol, other products like 1-propanol, 1-butanol, 2-methyl-1-butanol, 2-ethyl-1-butanol, 1-hexanol, 2-ethyl-1-hexanol and 1-octanol may be present in very low yield. Recall in the Guerbet mechanism for *iso*-butanol discussed in Chapter 1 that 1-propanol is formed in the first catalytic coupling cycle as an intermediate product (ethanol/methanol coupling). Other higher alcohols are formed by coupling of alcohol products with alcohol substrates within the closed catalytic system. For example, 2-methyl-1-butanol results from 1-propanol/ethanol coupling or methanol/butanol coupling, 2-ethyl-1-butanol from ethanol/butanol coupling, 1-hexanol from ethanol-butanol coupling, 2-ethyl-1-hexanol from ethanol/hexanol coupling and 1-octanol from ethanol/hexanol coupling. The most commonly observed side products in *iso*-butanol synthesis are 1-propanol, 1-butanol, 2-methyl-1-butanol and 1-hexanol.<sup>38-41</sup> One possible pathway for 2-methyl-1-butanol formation is via condensation of 1-butanol and methanol via acetaldehyde and formaldehyde (Scheme 5.3). More importantly, the other longer chain alcohol side

products rely on the formation of 1-butanol (Scheme 5.3), which is rarely detected with the current catalysts presented here, suggesting that any formed is rapidly consumed to produce 1-hexanol and/or 2-methyl-1-butanol.



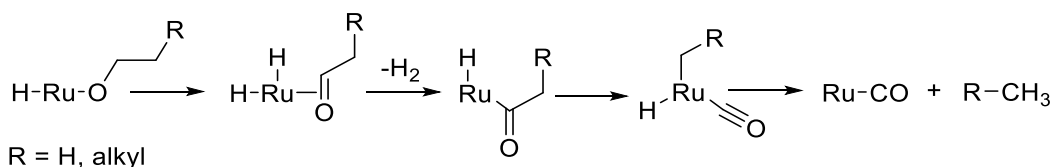
**Scheme 5.3:** Catalytic pathway for 2-methyl-1-butanol formation via 1-butanol/methanol coupling and 1-butanol to higher alcohols.<sup>40, 41</sup>

Another pathway to 2-methyl-1-butanol formation is by the coupling of 1-propanol and ethanol. The latter is likely the most favoured pathway as 1-propanol is the intermediate on route to *iso*-butanol and is detected in the majority of catalysts employed in the current study and those reported previously (Scheme 5.4).<sup>39</sup>



**Scheme 5.4:** Catalytic pathway for 2-methyl-1-butanol formation via propanol/ethanol coupling.

It is important to note that the ethanol conversion results reported here are based on all liquid products formed excluding solid and gaseous products. The solid products formed during the catalysis are carboxylate salts formed by competing Tishchenko or Cannizzaro mechanisms (Chapter 1, Section 1.6, Schemes 1.7 and 1.8) and carbonate formed by base mediated reforming of methanol. Wass<sup>39, 42</sup> and other authors<sup>43</sup> have reportedly observed the formation of large amounts of white solid post catalysis analysed as sodium acetate, sodium formate and sodium carbonate based on the base used. In the present work, the amount of solid products formed depends on the nature of the base used. Further to this, H<sub>2</sub>, CO, and C<sub>1</sub>-C<sub>4</sub> hydrocarbons have been reported as gaseous products of the catalytic reaction.<sup>42, 43</sup> Since the Guerbet reaction is typical of “hydrogen borrowing” processes, the hydrogen taken from the alcohol substrate to form the corresponding aldehyde is reused by the aldol product to give the final longer alcohol product. Therefore, the excess hydrogen gas is presumed to be generated from the formation of acetate, formate and carbonate via Tishchenko or Cannizzaro or methanol reforming reactions. Carbon monoxide released during the Guerbet reaction is suggested to result from dehydrogenation and decarbonylation of the primary alcohols by metal catalysts because related catalytic reactions are found in the literature (Scheme 5.5).<sup>44-47</sup> For metal catalysts with terminal carbonyl ligand(s), it is easy to assume that any carbon monoxide released is the product of catalyst decomposition, however, further evidence such as the presence of metal nanoparticles is required to support this claim.



**Scheme 5.5:** Catalytic dehydrogenation and decarbonylation of primary alcohols

Following on from Scheme 5.5, alkanes and hydrogen gas are concurrently formed with carbon monoxide. Due to the type of primary alcohol substrates employed in this work, C<sub>1</sub>-C<sub>4</sub> alkanes are possible products from the catalytic dehydrogenation-decarbonylation reaction. As a result of several competing side reactions in the Guerbet catalytic system, overall selectivity can be difficult to measure leading to many reports focussing on product selectivity and yield in the liquid phase. High conversion above conversion to liquids products is often observed and may be indicative of high yields of solid products. Furthermore, unlike the catalysts discussed in Chapter 2, that

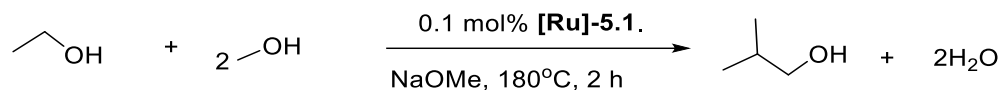


**Table 5.1:** Ruthenium catalysed conversion of ethanol and methanol to *iso*-butanol using different bases.

Run <sup>a</sup>	Catalysts	Time (h)	Base	Conversion <sup>b</sup> (%)	Total TON <sup>c</sup>	TON <sup>d</sup> (Yield) <sup>e</sup> [Selectivity] <sup>f</sup> %			
						<i>Iso</i> -butanol	1-propanol	2-methyl-1-butanol	1-hexanol
1	[Ru]-5.1	2	NaOMe	48	480	460(46)[97]	10(1)[2]	0(0)[0]	10(1)[1]
2	[Ru]-5.1	2	NaOEt	33	330	270(27)[87]	30(3)[10]	10(1)[1]	20(2)[2]
3	[Ru]-5.1	2	KOEt	35	350	290(29)[88]	30(3)[10]	0(0)[0]	30(3)[3]
4	[Ru]-5.1	2	<sup>t</sup> BuONa	56	560	520(52)[96]	20(2)[3]	0(0)[0]	20(2)[1]
5	[Ru]-5.1	2	<sup>t</sup> BuOK	42	420	400(40)[98]	10(1)[2]	0(0)[0]	10(1)[1]
6	[Ru]-5.1	2	NaOH	73	730	670(67)[93]	50(5)[7]	0(0)[0]	10(1)[*]
7	[Ru]-5.1	2	KOH	44	440	390(39)[89]	50(5)[10]	0(0)[0]	10(1)[1]
8	[Ru]-5.1	2	LiOH	13	130	110(11)[85]	20(2)[13]	0(0)[0]	10(1)[2]
9	[Ru]-5.1	2	NaH	39	390	370(37)[97]	10(1)[2]	0(0)[0]	<5(*)[*]
10	[Ru]-5.1	2	KH	61	610	580(58)[96]	20(2)[4]	0(0)[0]	10(1)[*]
11	[Ru]-5.1	2	LiH	3	30	30(3)[100]	0(0)[0]	0(0)[0]	0(0)[0]
12	[Ru]-5.1	2	Et <sub>3</sub> N	0	0	0(0)[0]	0(0)[0]	0(0)[0]	0(0)[0]
13	[Ru]-5.1	2	DBU	0	0	0(0)[0]	0(0)[0]	0(0)[0]	0(0)[0]
14	[Ru]-5.1	2	MgO	0	0	0(0)[0]	0(0)[0]	0(0)[0]	0(0)[0]
15 <sup>f</sup>	[Ru]-5.1	2	MgO	0	0	0(0)[0]	0(0)[0]	0(0)[0]	0(0)[0]

<sup>a</sup>Conditions: Ethanol (1 mL, 17.13 mmol), methanol (10 mL, 247.13 mmol), [Ru] catalyst (0.01713 mmol, 0.1 mol%), Base (34.26 mmol, 200 mol%), mol% is based on ethanol substrate, 180 °C. <sup>b</sup>Total conversion of ethanol to Guerbet products, *iso*-butanol, 1-propanol, 2-methyl-1-butanol, 1-hexanol. <sup>c</sup>Total TON based on mmol of total ethanol converted to products per mmol of [Ru] catalyst (ethanol equivalent relative to mmol of catalysts x conversion = 1000 x conversion). <sup>d</sup>TON based on mmol of any product formed per mmol [Ru] catalyst (ethanol equivalent relative to mmol of catalysts x product yield = 1000 x product yield). <sup>e</sup>Total yield and selectivity of alcohol products in the liquid fraction as determined by GC. <sup>f</sup>40 bar H<sub>2</sub>. \*Yield or selectivity less than 0.5%.

produced very dark post catalytic mixtures indicating ruthenium complex decomposition, the catalysts utilised here gave yellow/orange post-catalytic mixtures with no visible black deposit of ruthenium nanoparticles. Therefore, these catalysts appeared to maintain their homogeneous nature throughout the catalytic reaction. As a result, the complexes are presumed to be stable under the catalytic conditions used.

#### 5.3.4.1 Base Screening with Complex Precursor

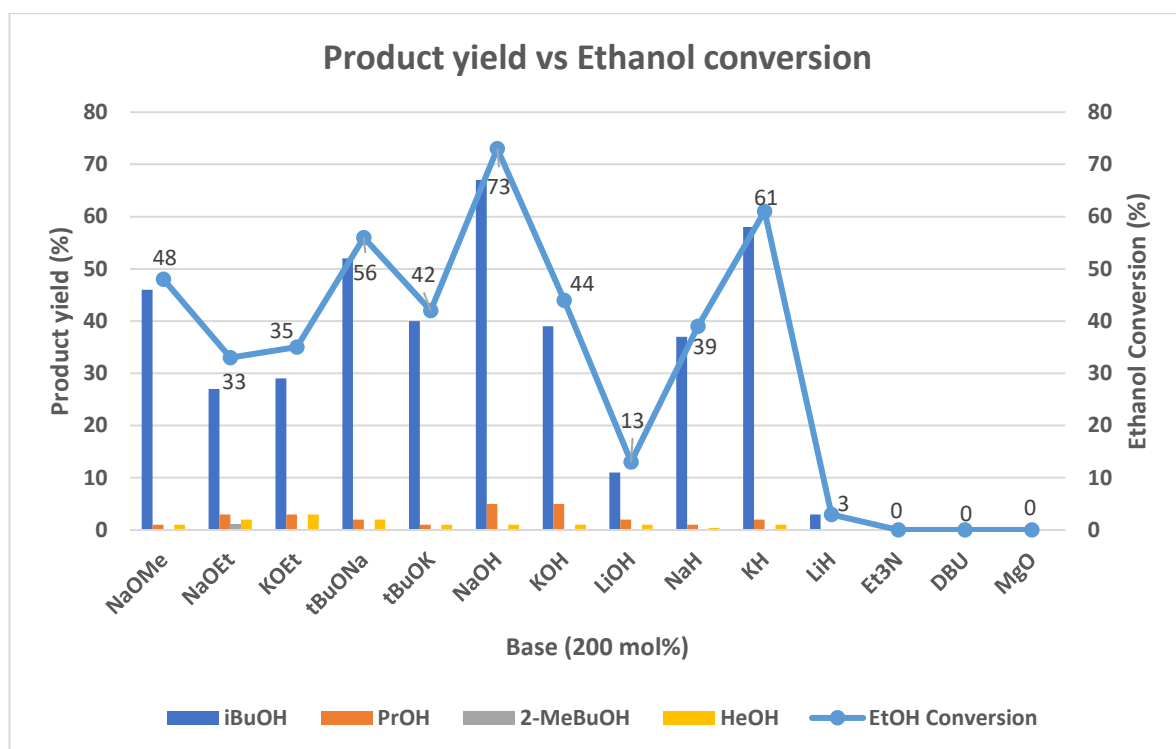


**Figure 5.8:** Yield of liquid products and ethanol conversion achieved with pre-catalyst **[Ru]-5.1** and different bases. Conditions: 1 mL ethanol, 10 mL methanol, 0.1 mol% **[Ru]-5.1**, 200 mol% base, 2 h, 180 °C, mol% relative to ethanol

In general, the Guerbet reaction requires a base co-catalyst for catalytic coupling of alcohols. So, different base co-catalysts were employed in the upgrading of ethanol/methanol to *iso*-butanol with the use of pre-catalyst **[Ru]-5.1**. The results for base screening are given in Table 5.1 and Figures 5.8 - 5.9. Catalyst **[Ru]-5.1** works well with a range of alkoxide, hydroxide and hydride bases with *iso*-butanol as major product and small amounts of 1-propanol, 2-methyl-1-butanol and 1-hexanol as alcohol side products. Sodium methoxide (NaOMe), the base most commonly used in ethanol/methanol upgrading, gave good results (48% conversion, 46% *iso*-butanol yield and 97% selectivity) with pre-catalyst **[Ru]-5.1** (Table 5.1, Run 1) albeit somewhat lower than those reported for *trans*-[RuCl<sub>2</sub>(dppm)<sub>2</sub>] (65% *iso*-butanol yield,

98% selectivity at 67% conversion).<sup>39</sup> Sodium ethoxide (NaOEt) and potassium ethoxide (KOEt) gave similar ethanol conversion and alcohol products yields/selectivity (Table 5.1, Runs 2 and 3). Notably, only the run with NaOEt generated 2-methyl-1-butanol (1% yield and 1% selectivity) of all the bases tested. Sodium tert-butoxide (<sup>t</sup>BuONa) and potassium tert-butoxide (<sup>t</sup>BuOK) gave 52% and 40% *iso*-butanol yield respectively (Table 5.1, Runs 4 and 5, Figure 5.8). Here, the sodium base of butoxide was found to be more efficient than the potassium congener (Figures 5.8), however, <sup>t</sup>BuOK gave the highest selectivity (98%) among all of the alkoxide bases (Figure 5.9).

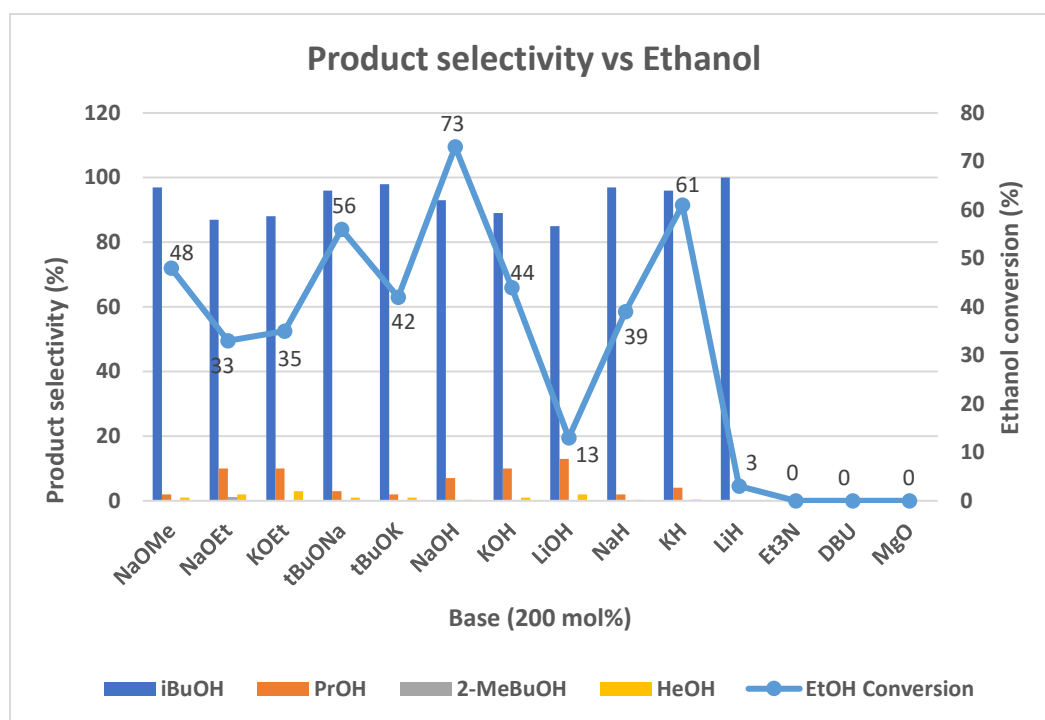


**Figure 5.9:** Selectivity of liquid products and ethanol conversion achieved with pre-catalyst **[Ru]-5.1** and different bases. Conditions: 1 mL ethanol, 10 mL methanol, 0.1 mol% **[Ru]-5.1**, 200 mol% base, 2 h, 180 °C, mol% relative to ethanol

For the hydroxide bases (Runs 6-8), the highest *iso*-butanol yield (67%), selectivity (93%) and ethanol conversion (73%) were achieved with sodium hydroxide (NaOH) (Figures 5.8 and 5.9). Additionally, an identical 1-propanol yield (5%) was obtained with NaOH and KOH, while lithium hydroxide (LiOH) gave only 2%. Also, the three hydroxide bases displayed identical activity towards 1-hexanol yield. Altogether, % ethanol conversion and % yield of *iso*-butanol using the hydroxide bases are in the order NaOH>KOH>LiOH. In comparison with previous catalysts reported by Wass group,<sup>39</sup> pre-catalyst **[Ru]-5.1** (73% conversion, 67% yield and 93% selectivity) was

comparable to *trans*-[RuCl<sub>2</sub>(dppm)<sub>2</sub>] (74% conversion, 71% yield and 96% selectivity) with NaOH and was of a considerable improvement over *trans*-[RuCl<sub>2</sub>(dppea)<sub>2</sub>] (dppea = 2-(Diphenylphosphino)ethylamine) (39% conversion, 28% yield and 74% selectivity) and commercially available Ru-MACHO® which was inactive with NaOH.

When the hydride bases were employed, the ethanol conversion and *iso*-butanol yield were in the order KH>NaH>LiH with high selectivity to *iso*-butanol observed for all three bases (Table 5.1, Runs 9-11). Potassium hydride (KH) gave the highest ethanol conversion (61%) and *iso*-butanol yield (58%) (Table 5.1, Runs 9-11). Sodium hydride gave moderate result (39% conversion and 37% yield) while lithium hydride gave very low activity to *iso*-butanol (3% conversion 3% yield), and no other Guerbet products were detected (Table 5.1, Run 11).

Organic bases like triethyl amine (Et<sub>3</sub>N) and 1,8-Diazabicyclo[5.4.0]undec-7-ene (DBU) were ineffective for *iso*-butanol, 1-propanol and 1-hexanol production (Figures 5.8 and 5.9). Though, DBU has been reported to produced very low yields of 1-butanol in ethanol homocoupling from Milsteins work,<sup>43</sup> here no Guerbet products were obtained. Also, with MgO solid base even in presence of 40 bar H<sub>2</sub> pressure, no activity was recorded (Figures 5.8 and 5.9).

In summary, pre-catalyst **[Ru]-5.1** is an effective catalyst for the ethanol/methanol upgrading reaction to *iso*-butanol with a range of alkoxide, hydroxide and hydride bases. When NaOH is used as the base co-catalyst catalytic activities approaching those observed with *trans*-[RuCl<sub>2</sub>(dppm)<sub>2</sub>] are achieved.

#### 5.3.4.2 Functionalised Complex Screening

The summary of all the catalytic results obtained from functionalised complexes **[Ru]-5.2** - **[Ru]-5.9** are presented in Table 5.2. The graphical presentation of the results at 2 and 20 h are shown in Figures 5.10 – 5.13. Generally, all of the amine functionalised complexes **[Ru]-5.2** - **[Ru]-5.9** performed well as catalysts for ethanol/methanol upgrading with over 50% *iso*-butanol yield obtained within 2 h (Figure 5.10). Not less than 90% *iso*-butanol selectivity was recorded with all the catalysts (Figure 5.11). Remarkably, the highest *iso*-butanol yield (74%) was achieved with catalyst **[Ru]-5.3** at 78% ethanol conversion in 2 h (Figures 5.10). Interestingly, the activity of catalyst **[Ru]-5.3** outperformed the best catalyst, [RuCl<sub>2</sub>(dppm)<sub>2</sub>] (65% yield, 98% selectivity

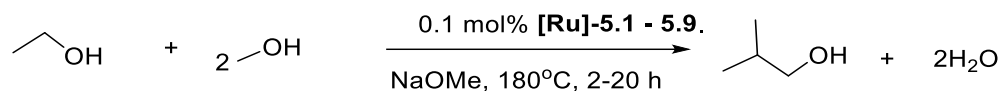


**Table 5.2:** Ruthenium catalysed conversion of ethanol and methanol to *iso*-butanol.

Run <sup>a</sup>	Catalysts	Time (h)	Base	Conversion <sup>b</sup> (%)	Total TON <sup>c</sup>	TON <sup>d</sup> (yield) <sup>e</sup> [selectivity] %			
						<i>iso</i> -butanol	1-Propanol	2-methyl-1-butanol	Hexanol
1	[Ru]-5.2	2	NaOMe	89	890	600(60)[94]	30(3)[5]	0(0)[0]	10(1)[1]
2	[Ru]-5.2	20	NaOMe	89	890	680(68)[94]	30(3)[4]	0(0)[0]	60(6)[3]
3	[Ru]-5.3	2	NaOMe	78	780	740(74)[94]	40(4)[5]	0(0)[0]	20(2)[1]
4	[Ru]-5.4	2	NaOMe	84	840	590(59)[97]	10(1)[2]	0(0)[0]	10(1)[1]
5	[Ru]-5.4	20	NaOMe	94	940	690(69)[94]	20(2)[2]	0(0)[0]	80(8)[4]
6	[Ru]-5.5	2	NaOMe	83	830	590(59)[97]	10(1)[2]	0(0)[0]	10(1)[1]
7	[Ru]-5.5	20	NaOMe	95	950	690(69)[96]	20(2)[2]	0(0)[0]	40(4)[2]
8	[Ru]-5.6	2	NaOMe	83	830	600(60)[98]	10(1)[2]	0(0)[0]	10(1)[1]
9	[Ru]-5.6	20	NaOMe	95	950	660(66)[96]	20(2)[2]	0(0)[0]	40(4)[2]
10	[Ru]-5.7	2	NaOMe	88	880	620(62)[100]	0(0)[0]	0(0)[0]	0(0)[0]
11	[Ru]-5.7	20	NaOMe	100	1000	790(79)[100]	0(0)[0]	0(0)[0]	0(0)[0]
12	[Ru]-5.8	2	NaOMe	79	790	520(52)[97]	20(2)[3]	0(0)[0]	10(1)[1]
13	[Ru]-5.8	20	NaOMe	94	940	720(72)[96]	20(2)[2]	0(0)[0]	40(4)[2]
14	[Ru]-5.9	2	NaOMe	77	770	510(51)[98]	10(1)[2]	0(0)[0]	10(1)[1]

<sup>a</sup>Conditions: Ethanol (1 mL, 17.13 mmol), methanol (10 mL, 247.13 mmol), [Ru] catalyst (0.01713 mmol, 0.1 mol%), Base (34.26 mmol, 200 mol%), mol% is based on ethanol substrate, 180 °C. <sup>b</sup>Total conversion of ethanol to liquid product as determined by GC analysis of the liquid phase. <sup>c</sup>Total TON based on mmol of total ethanol converted to products per mmol of [Ru] catalyst (ethanol equivalent relative to mmol of catalysts x conversion = 1000 x conversion). <sup>d</sup>TON based on mmol of any product formed per mmol [Ru] catalyst (ethanol equivalent relative to mmol of catalysts x product yield = 1000 x product yield). <sup>e</sup>Total yield and selectivity of alcohol products in the liquid fraction as determined by GC.

and 67% conversion), reported so far by Wass and co-workers at 2 h run time.<sup>39</sup> The exceptional performance of catalyst **[Ru]-5.3** may be due to increased basicity (that is the additional amine functionality) and shorter carbon link between the amine groups when compared to its analogue catalyst **[Ru]-5.4** (Figures 5.10, Table 5.2, Runs 3-4).

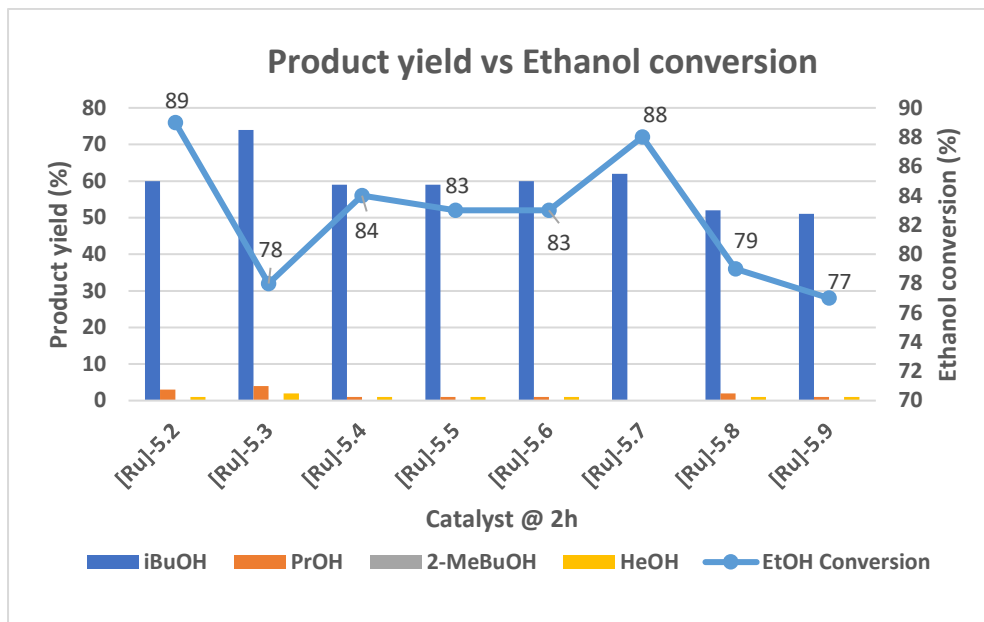


**Figure 5.10:** Yield of liquid products and ethanol conversion achieved with 0.1 mol% **[Ru]-5.2 - 5.9** with 200 mol% NaOMe. Conditions: 1 mL ethanol, 10 mL methanol, 2 h, 180 °C, mol% relative to ethanol.

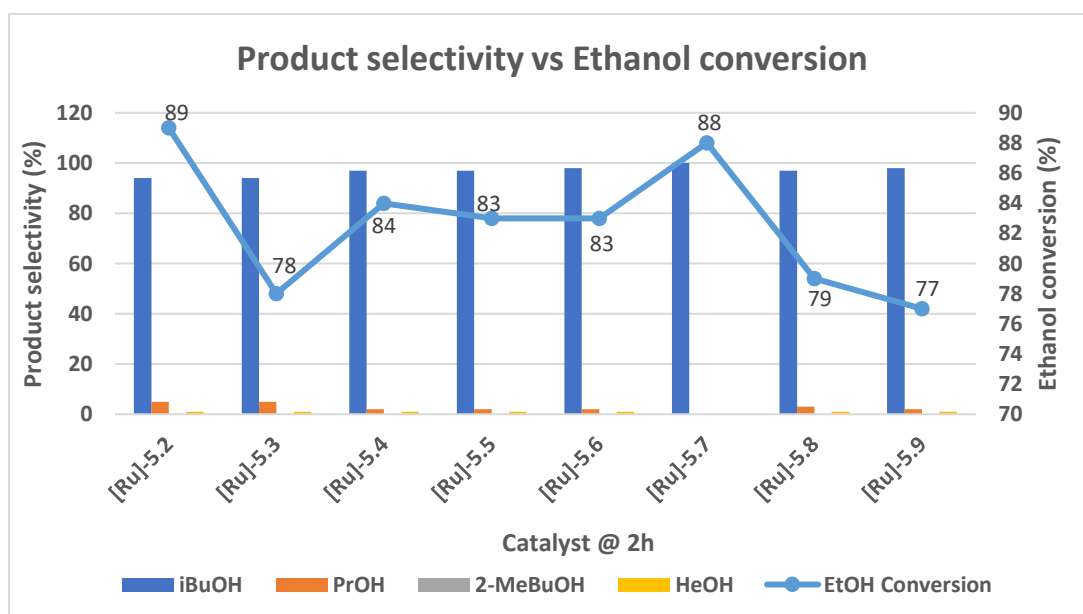


**Figure 5.11:** Selectivity of liquid products and ethanol conversion achieved with 0.1 mol% **[Ru]-5.2 - 5.9** with 200 mol% NaOMe. Conditions: 1 mL ethanol, 10 mL methanol, 2 h, 180 °C, mol% relative to ethanol.

There is also the possibility that the ligand structure provides additional coordination to the Ru centre. The formation of a 5-membered chelate to Ru centre is possible for all of the catalysts with of the presence of NH group between the two P atoms but the additional amine in **[Ru]-5.3** could make another 5-membered ring, hence the ligand acting as a tetradentate ligand, providing extra stability. Similarly, in **[Ru]-5.4**, the dangling amine could also make a 6-membered ring which is slightly less favoured. Furthermore, catalyst **[Ru]-5.7** at 20 h produced 79% *iso*-butanol yield at 100% selectivity with no competing liquid Guerbet alcohols formed even at 2 h (Figures 5.12 and 5.13). In fact, complete ethanol conversion (100%) was achieved at 20 h, with the missing ethanol presumably converted to solid and gaseous products. Again, this catalyst (**[Ru]-5.7**) efficiency is higher than that observed with  $[\text{RuCl}_2(\text{dppm})_2]$  (75% yield, 99% selectivity and 75% conversion) at 20 h.<sup>38</sup> On the whole, the activity of other functionalised catalysts utilised closely approached that of  $[\text{RuCl}_2(\text{dppm})_2]$  (Table 5.2).

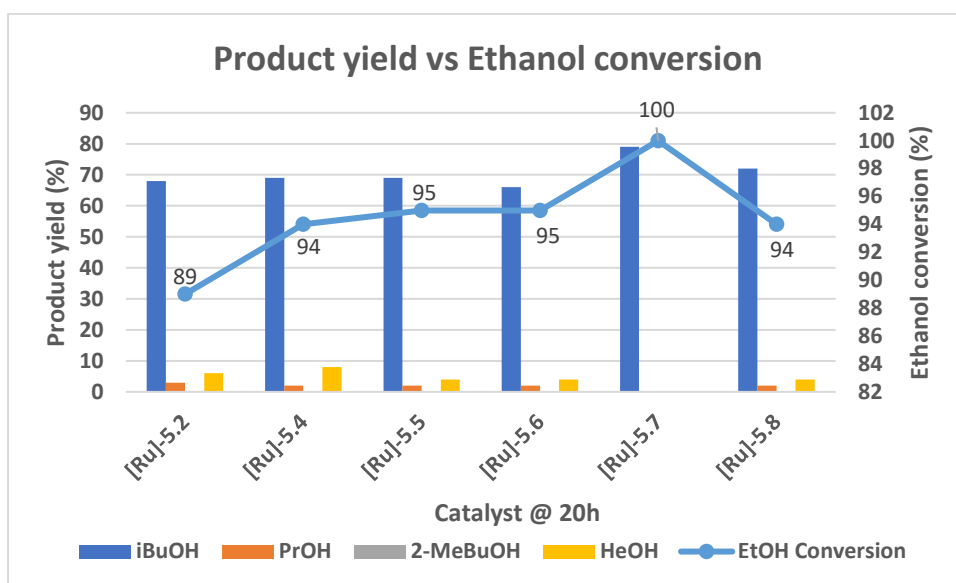


**Figure 5.12:** Yield of liquid products and ethanol conversion achieved with 0.1 mol% **[Ru]-5.2 - 5.9** with 200 mol% NaOMe. Conditions: 1 mL ethanol, 10 mL methanol, 20 h, 180 °C, mol% relative to ethanol.

Contrary to the P-N-P catalysts discussed in Chapter two, the acidic proton (coloured blue) of these functionalised complexes is presumably influential in this catalytic system in a similar way to  $[\text{RuCl}_2(\text{dppm})_2]$ . Successive replacement of the  $\text{CH}_2$  protons with methyl groups led to a poorer catalyst. In general, acidity and basicity tend to impact the reactivity of these functionalised catalysts. In summary, 1-propanol

and 1-hexanol were formed besides the desired *iso*-butanol main product with all functionalised catalysts except [Ru]-5.7 (Figures 5.12 and 5.13). Other Guerbet alcohols were undetected including 2-methyl-1-butanol.

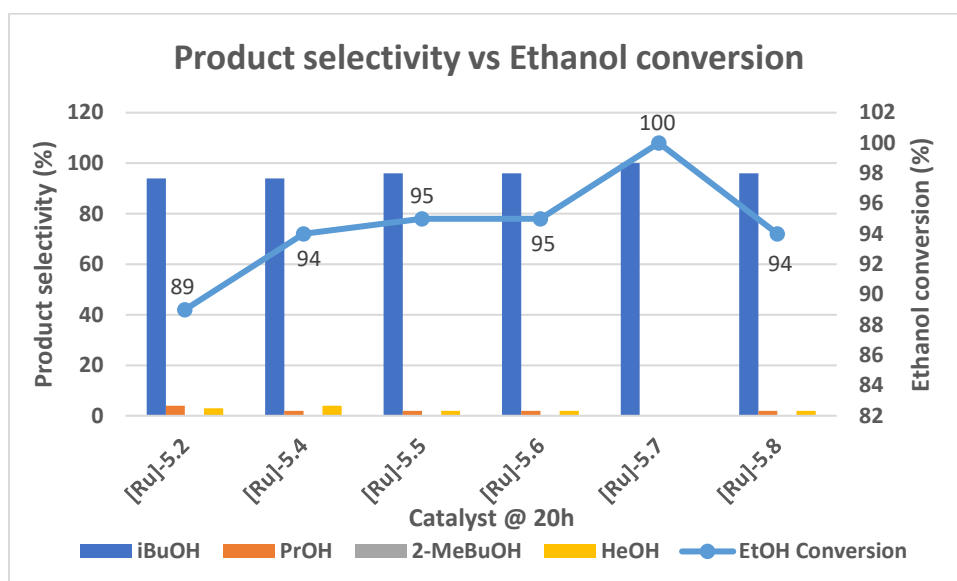


**Figure 5.13:** Selectivity of liquid products and ethanol conversion achieved with 0.1 mol% [Ru]-5.2 - 5.9 with 200 mol% NaOMe. Conditions: 1 mL ethanol, 10 mL methanol, 20 h, 180 °C, mol% relative to ethanol.

#### 5.4 Conclusion/Future Work

In this chapter, vinylidene diphosphine ruthenium(II) complex precursor  $[\text{RuCl}_2(\text{dppen})_2]$  ([Ru]-5.1) was synthesised and functionalised with several amines to obtain complexes [Ru]-5.2 - [Ru]-5.9. With the exception of complexes [Ru]-5.4 - [Ru]-5.6, all of the other complexes are novel. The amine-functionalised complexes were then utilised as catalysts for ethanol conversion to *iso*-butanol. All of the catalysts screened showed great effectiveness for upgrading methanol/ethanol to *iso*-butanol. Remarkable catalytic activity was achieved with novel catalysts [Ru]-5.3 and [Ru]-5.7. Additionally, the dual acidic and basic sites present in the functionalised catalysts greatly enhanced their catalytic activity when compared with the unfunctionalised complex precursor. In conclusion, the availability of acidic protons in these catalysts seems to be advantageous to the *iso*-butanol system. The following future work is considered to be of interest:

- Investigation of [Ru]-5.1 and KOMe in ethanol/methanol upgrading to *iso*-butanol.

- Studying the activity catalyst [**Ru**]-5.3 at 20 h in ethanol/methanol upgrading.
- Testing the catalysts herein in ethanol to 1-butanol catalytic system.
- Synthesise analogues of the functionalised catalysts without dangling amine groups to unveil the potential amine influence in this catalysis.
- Investigate the activity of other transition metal complexes (e.g. Mn, Fe etc) analogous to the complexes presented in this chapter.
- Examine the activity of these functionalised catalysts in other borrowed hydrogen chemistry.

## 5.5 References

1. A. Vogler and H. Kunkely, *Coord. Chem. Rev.*, 2002, **230**, 243-251.
2. J. Mathew, T. Thomas and C. H. Suresh, *Inorg. Chem.*, 2007, **46**, 10800-10809.
3. G. R. Cooper, D. M. Mcewan and B. L. Shaw, *Inorg. Chim. Acta*, 1986, **122**, 207-211.
4. R. Mosteiro, A. Fernández, M. López-Torres, D. Vázquez-García, A. Suárez, J. J. Fernández and J. M. Vila, *New J. Chem.*, 2002, **26**, 1425-1432.
5. E. J. Fernández, M. C. Gimeno, P. G. Jones, A. Laguna, J. M. López-de-Luzuriaga and E. Olmos, *Chem. Ber.*, 1997, **130**, 1513-1517.
6. R. Mosteiro, A. Fernández, M. López-Torres, D. Vázquez-García, L. Naya, J. M. Ortigueira, J. M. Vila and J. J. Fernández, *J. Organomet. Chem.*, 2012, **720**, 30-37.
7. F. Piestert, R. Fetouaki, M. Bogza, T. Oeser and J. Blümel, *Chem. Commun.*, 2005, 1481-1483.
8. S. Kabehie, M. Xue, A. Z. Stieg, M. Liong, K. L. Wang and J. I. Zink, *J. Am. Chem. Soc.*, 2010, **132**, 15987-15996.
9. J. L. Bookham, W. McFarlane and I. J. Colquhoun, *J. Chem. Soc., Chem. Commun.*, 1986, 1041-1042.
10. J. L. Bookham, W. McFarlane and I. J. Colquhoun, *J. Chem. Soc., Dalton Trans.*, 1988, 503-507.
11. J. L. Bookham and W. McFarlane, *Polyhedron*, 1991, **10**, 2381-2388.
12. J. L. Bookham, W. McFarlane and M. Thornton-Pett, *J. Chem. Soc., Dalton Trans.*, 1992, 2353-2360.
13. S. Al-Jibori and B. L. Shaw, *J. Chem. Soc., Chem. Commun.*, 1982, 286-287.
14. S. Al-Jibori and B. L. Shaw, *Inorg. Chim. Acta*, 1982, **65**, L123-L124.
15. S. Al-Jibori and B. L. Shaw, *Inorg. Chim. Acta*, 1983, **74**, 235-239.
16. S. Al-Jibori and B. L. Shaw, *J. Organomet. Chem.*, 1984, **273**, 213-219.
17. S. Al-Jibori, M. Hall, A. T. Hutton and B. L. Shaw, *J. Chem. Soc., Dalton Trans.*, 1984, 863-867.
18. J. Ruiz, V. Riera, M. Vivanco, M. Lanfranchi and A. Tiripicchio, *Organometallics*, 1998, **17**, 3835-3837.
19. J. Ruiz, V. Riera, M. Vivanco, S. García-Granda and M. Díaz, *Organometallics*, 1998, **17**, 4562-4567.
20. G. Hogarth and J. Kilmartin, *J. Organomet. Chem.*, 2007, **692**, 5655-5670.
21. S. J. Higgins, M. K. McCart, M. McElhinney, D. C. Nugent and T. J. Pounds, *J. Chem. Soc., Chem. Commun.*, 1995, 2129-2130.
22. J. V. Barkley, S. J. Higgins, M. K. McCart and T. J. Pounds, *Inorg. Chem.*, 1997, **36**, 6188-6196.
23. S. J. Higgins and H. L. Jones, *Chem. Commun.*, 1997, 1907-1908.
24. S. J. Higgins, C. A. Stuart and A. Mills, *Inorg. Chem. Commun.*, 2000, **3**, 208-210.
25. E. J. Fernández, M. C. Gimeno, P. G. Jones, A. Laguna and E. Olmos, *Organometallics*, 1997, **16**, 1130-1136.
26. S. J. Higgins, A. La Pensée, C. A. Stuart and J. M. Charnock, *J. Chem. Soc., Dalton Trans.*, 2001, 902-910.
27. A. M. Herring, S. H. Koskimies and B. L. Shaw, *J. Organomet. Chem.*, 1988, **338**, 13-17.
28. F. S. M. Hassan, B. L. Shaw and M. Thornton-Pett, *J. Chem. Soc., Dalton Trans.*, 1988, 89-92.

29. P. A. Dolby, M. M. Harding, N. Newar and A. K. Smith, *J. Chem. Soc., Dalton Trans.*, 1992, 2939-2942.
30. N. Nawar and A. K. Smith, *J. Organomet. Chem.*, 1995, **493**, 239-242.
31. H. Schmidbaur, R. Herr, G. Mueller and J. Riede, *Organometallics*, 1985, **4**, 1208-1213.
32. G. King, S. J. Higgins and A. Hopton, *J. Chem. Soc., Dalton Trans.*, 1992, 3403-3409.
33. F. S. M. Hassan, S. J. Higgins, G. B. Jacobsen, B. L. Shaw and M. Thornton-Pett, *J. Chem. Soc., Dalton Trans.*, 1988, 3011-3016.
34. S. J. Higgins and B. L. Shaw, *J. Chem. Soc., Dalton Trans.*, 1989, 1527.
35. A. R. Chakravarty, F. A. Cotton and W. Schwotzer, *Inorg. Chim. Acta.*, 1984, **84**, 179-185.
36. F. A. Cotton, M. P. Diebold and M. Matusz, *Polyhedron*, 1987, **6**, 1131-1134.
37. H. Schmidbaur, R. Herr and J. Riede, *Chem. Ber.*, 1984, **117**, 2322-2327.
38. R. L. Wingad, E. J. E. Bergstrom, M. Everett, K. J. Pellow and D. F. Wass, *Chem. Commun.*, 2016, **52**, 5202-5204.
39. K. J. Pellow, R. L. Wingad and D. F. Wass, *Catal. Sci. Technol.*, 2017, **7**, 5128-5134.
40. E. S. Olson, R. K. Sharma and T. R. Aulich, *Appl. Biochem. Biotechnol.*, 2004, **115**, 913-932.
41. Q. Liu, G. Xu, X. Wang and X. Mu, *Green Chem.*, 2016, **18**, 2811-2818.
42. K. J. Pellow, PhD Thesis, University of Bristol, 2018.
43. Y. Xie, Y. Ben-David, L. J. Shimon and D. Milstein, *Journal of the American Chemical Society*, 2016, **138**, 9077-9080.
44. H. A. Ho, K. Manna and A. D. Sadow, *Angew. Chem., Int. Ed.*, 2012, **51**, 8607-8610.
45. E. P. Olsen and R. Madsen, *Chem. Eur. J.*, 2012, **18**, 16023-16029.
46. E. P. Olsen, T. Singh, P. Harris, P. G. Andersson and R. Madsen, *J. Am. Chem. Soc.*, 2015, **137**, 834-842.
47. A. Mazziotta and R. Madsen, *Eur. J. Org. Chem.*, 2017, **2017**, 5417-5420.

## Chapter 6: Experimental

### 6.1. General Experimental Information

#### 6.1.1 General Experimental Considerations

All reagents were purchased from commercial suppliers without further purification, unless otherwise stated. All reactions were carried out under an inert atmosphere of N<sub>2</sub> using conventional Schlenk glassware or glovebox techniques. Hexane, toluene, diethyl ether, dichloromethane, and tetrahydrofuran were purified using Anhydrous Engineering Grubbs-type solvent system except anhydrous ethanol and methanol which were purchased from Sigma-Aldrich and used as received. Pentane and deuterated solvents were dried using established procedures and further degassed under nitrogen. Jeol ECS 300, Jeol ECS 400, Varian 400 or Bruker 400/500 NMR spectrometers were used to record <sup>1</sup>H and <sup>31</sup>P{<sup>1</sup>H} NMR spectra. Proton chemical shifts ( $\delta$ ) are reported in ppm relative to the deuterated solvent. Data is reported as follows: chemical shift, integration, multiplicity (s = singlet, d = doublet, t = triplet, q = quintet, m = multiplet), coupling constant (Hz) and assignment. <sup>31</sup>P{<sup>1</sup>H} NMR spectra were referenced relative to 85% H<sub>3</sub>PO<sub>4</sub> external standard. Mass spectra (ESI) were recorded on a Bruker Daltonics micrOTOF II. IR spectra of samples in their solid state were recorded using a Perkin Elmer Spectrum FT-IR spectrometer. All liquid products of catalysis were analysed by GC-FID using (1) **Bristol University**: Agilent 7820A GC, fitted with a DB-WAX column (30m x 320 $\mu$ m, I.D. 0.25 $\mu$ m). Method: column oven temperature programme starts at 35 °C for 5 minutes, heat to 250 °C at 50 °C min<sup>-1</sup> then hold at 250 °C for 5 minutes (2) **Cardiff University**: Agilent 7820A GC, fitted with a DB-WAX column (30m x 320 $\mu$ m, I.D. 0.25  $\mu$ m). Method: column oven temperature programme starts at 60 °C for 5 minutes, heat to 220 °C at 40 °C min<sup>-1</sup> then hold at 220 °C for 5 minutes; helium carrier gas (flow rate of 2.5 mL min<sup>-1</sup>); 1  $\mu$ L injection volume; 1:100 split ratio.

#### 6.1.2 General Catalytic Procedure

Catalytic reactions were carried out in a 100 mL Parr stainless steel autoclave with aluminium heating mantle and a magnetic stirrer. The previously published procedure used is as follows:<sup>1-3</sup> Catalyst (0.1 mol%) and NaOMe (200 mol%) or NaOEt (5 mol%) were measured into an oven-dried autoclave in a glovebox (other bases such as NaOEt, KOEt, NaOtBu, KOtBu, NaOH, KOH, LiOH, NaH, KH, LiH, Et<sub>3</sub>N, DBU, MgO (200

mol%) were also used). A magnetic stirrer bead was added, and the autoclave was sealed and transferred to the Schlenk line. Ethanol (1.0 mL) and methanol (10 mL) (or 10 mL ethanol only for ethanol homocoupling) were injected into the autoclave under a nitrogen flow (note; for the run with additional H<sub>2</sub>O, degassed deionised H<sub>2</sub>O (1.0 mL) was injected after the addition of alcohol substrate and for the run with external H<sub>2</sub>, the autoclave was pressurised with 40 bar H<sub>2</sub> post alcohol substrate addition). The autoclave was sealed and placed on a pre-heated (180°C or 150°C) aluminium heating mantle for a specified period. Agitation was achieved by using a magnetic stirrer (500 rpm). After the run time, the autoclave was cooled to room temperature in an ice bath. It was vented to remove any gas generated during the reaction. The product mixture was collected, filtered through an alumina column and analysed by <sup>1</sup>H NMR spectroscopy and GC-MS (100 µL of sample, 25 (or 10) µL of hexadecane as a standard, and 1 (or 1.7) mL of diethyl ether). In situ runs were carried out similarly with addition of the pre-catalysts, followed by the ligand and the base. Most importantly, the PTFE autoclave sleeve was cleaned with bleach (soak overnight), followed by washing with soap and water and finally with acetone and deionised water. In some cases, the sleeve was soaked in aqua regia to dissolve any residue metal catalysts.

### **6.1.3 GC Calibration Methods and Calculation of Conversion, Yield and Selectivity.**

The standard solutions of varying amounts of ethanol, methanol and all Guerbet alcohols products (1-butanol, 2-butanol, 1-propanol, 2-methyl-1-propanol, 2-ethyl-1-butanol, 1-hexanol, 2-ethyl-1-hexanol, 1-octanol) were prepared by diluting the required amount of alcohol (e.g., ethanol) with 10 µL hexadecane and 1.7 mL diethyl ether in a GC vial. Then, the solutions were analysed by GC and the peak area of the alcohol and hexadecane recorded. The peak area ratio and the mole ratio of the alcohol and hexadecane were calculated and the calibration curve between the ratios was drawn. The representative calibration data and curves of ethanol and 1-butanol are shown in Tables 6.1 – 6.2 and Figures 6.1 – 6.2. Other alcohol calibration curves were generated in similar way.

**Table 6.1:** GC Calibration Data for Ethanol (EtOH density = 0.789 g/mL, M.W = 46.07 g/mol)

Volume (μL)	Amount (mmol)	Amount hexadecane (mmol)	Peak EtOH	Peak hexadecane	Amt EtOH/Amt hexadecane	Peak EtOH/ Peak hexadecane
20	0.342522249	0.034137078	714.2	884	10.03373074	0.807918552
40	0.685044498	0.034137078	1482.1	964.1	20.06746147	1.537288663
60	1.027566746	0.034137078	1838.4	802.3	30.10119221	2.29141219
80	1.370088995	0.034137078	3912.5	1296.9	40.13492294	3.016809315
100	1.712611244	0.034137078	4388	1189.1	50.16865368	3.690185855

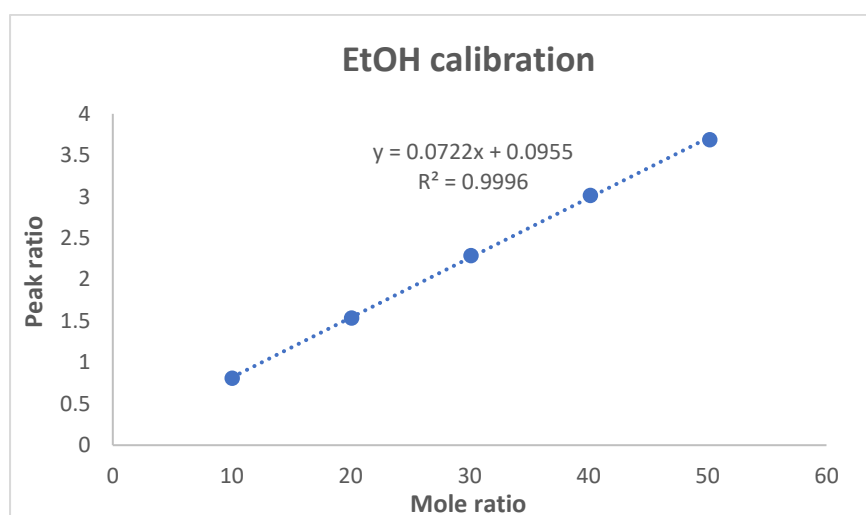


**Figure 6.1:** Ethanol Calibration Curve (Slope = 0.0722)

**Table 6.2:** GC Calibration Data for 1-butanol (1-BuOH density = 0.81 g/mL, M.W = 74.12 g/mol)

Volume (μL)	Amount (mmol)	Amount hexdecane (mmol)	Peak BuOH	Peak hexdecane	Amt BuOH/Amt hexadecane	Peak BuOH/ Peak hexadecane
20	0.21856449	0.034137078	989.3	838.2	6.402554138	1.180267239
40	0.43712898	0.034137078	1834.2	774.8	12.80510828	2.367320599
60	0.65569347	0.034137078	3238.9	866	19.20766241	3.740069284
80	0.87425796	0.034137078	4123.4	834.4	25.61021655	4.941754554
100	1.09282245	0.034137078	4379.9	689.3	32.01277069	6.354127376

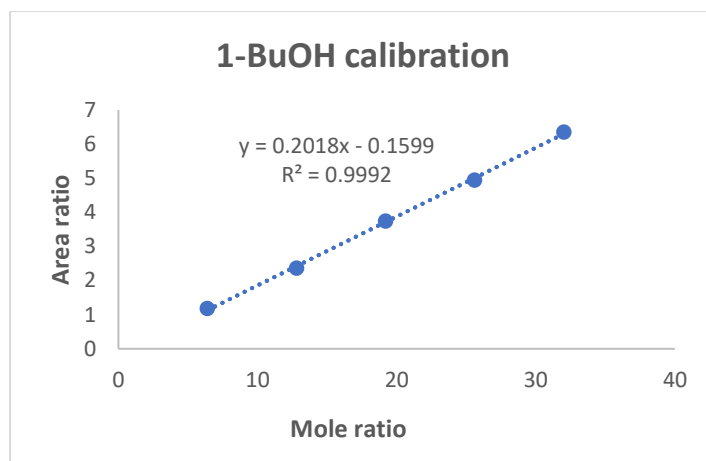


**Figure 6.2:** 1-Butanol Calibration Curve (Slope = 0.2018)

Using the internal standard equation method (Equation 6.1),<sup>4</sup> the moles of each alcohol present in the liquid product was calculated.

$$\frac{\text{Peak Area of analyte}}{\text{Peak Area of internal standard}} = \text{Slope} \times \frac{\text{mmol of analyte}}{\text{mmol of internal standard}} \quad \text{Eq. (6.1)}^4$$

It should be noted that only liquid products analysis was carried out by the GC. The ethanol conversion, product yield and selectivity were calculated based on Equations (6.2) - (6.4), respectively, as used in previous report.<sup>5</sup>

$$\text{Ethanol conversion (\%)} = \frac{(\text{mmol of EtOH introduced} - \text{mmol of unreacted EtOH})}{\text{mmols of EtOH introduced}} \times 100 \quad \text{Eq. (6.2)}$$

**Taking 1-butanol run for example:**

In the 100  $\mu\text{L}$  liquid product analysed by GC, the peak area of the ethanol present was obtained and using Equation 6.1, the mmol of the unreacted ethanol was calculated. Since this is only the amount present in 100  $\mu\text{L}$ , the value was multiplied by 100 to get an equivalent amount in 10 mL (i.e., volume of EtOH introduced)

$$\text{Ethanol conversion (\%)} = \frac{100 - \left( \frac{\text{mmols of EtOH in vial}}{\text{mmols of EtOH introduced}} \times 100 \right)}{100} \times 100 \quad \text{Eq. (6.3)}$$

**To obtain the result in Chapter 2, Table 2.2, entry 7 for example, the follow calculations were performed,**

➤ *Ethanol conversion calculation*

10 mL EtOH = 171.26 mmol (density = 0.789 g/mL, M.W = 46.07 g/mol)

100  $\mu\text{L}$  EtOH = 1.7126 mmol

10  $\mu\text{L}$  hexadecane = 0.03414 mmol (0.773 g/mL, M.W = 226.44 g/mol)

Peak area of hexadecane = 801.1

Peak area of ethanol = 2445.9

Ethanol calibration Slope = 0.0722

Using equation 6.1,

$$\text{Amount of ethanol} = \frac{0.03414 \times 2445.9}{0.0722 \times 801.1} = 1.4437044 \text{ mmol}$$

Using equation 6.3,

$$\text{Ethanol conversion (\%)} = \frac{100 - \left(\frac{1.44370}{1.7126} \times 100\right)}{100} \times 100 = 16\%$$

➤ ***Yield calculation***

The yield of each Guerbet alcohol product was calculated using equation 6.4.

$$\text{Yield (\%)} = \frac{(X \times n\text{Product})}{n\text{EtOH}} \times 100 \quad \text{Eq. (6.4)}$$

$n$  = number of mmol and  $X$  = number of ethanol equivalents of product (for butanol,  $X = 2$ )

10  $\mu\text{L}$  hexadecane = 0.03414 mmol

Peak area of hexadecane = 801.1

Peak area of butanol = 379.4

1-Butanol calibration Slope = 0.2018

Using equation 6.1,

$$\text{Amount of 1-butanol} = \frac{0.03414 \times 379.4}{0.2018 \times 801.1} = 0.0801222 \text{ mmol in } 100 \mu\text{L of liquid products}$$

$$\begin{aligned} \text{Amount of 1-butanol} &= 100 \times 0.0801222 \text{ mmol in } 10 \text{ mL (10,000 } \mu\text{L) of liquid} \\ &= 8.01222 \text{ mmol} \end{aligned}$$

Using equation 6.4,

$$\text{1-Butanol yield (\%)} = \frac{2 \times 8.01222}{171.26} \times 100 = 9\%$$

➤ **Selectivity calculation**

The selectivity of each Guerbet alcohol product was calculated using equation 6.5.

$$\text{Selectivity (\%)} = \frac{(n_{\text{Product}})}{n_{\text{All liquid products}}} \times 100 \quad \text{Eq. (6.5)}$$

Turnover number (TON) was calculated based on the mmol of total ethanol converted to products per mmol of [Ru] catalyst. (Ethanol equivalent relative to mmol of catalysts)

**For ethanol only upgrading (10 mL ethanol = 171.3 mmol)**

$$\text{Catalyst (0.1 mol\%)} = 0.001 \times 171.3 = 0.1713 \text{ mmol}$$

$$\text{Equivalent} = \frac{171.3}{0.1713} = 1000$$

**For ethanol/methanol mixture upgrading (1 mL ethanol = 17.13 mmol)**

$$\text{Catalyst (0.1 mol\%)} = 0.001 \times 17.13 = 0.01713 \text{ mmol}$$

$$\text{Equivalent} = \frac{17.13}{0.01713} = 1000$$

$$\text{TON} = \text{Equivalent} \times \text{conversion value} = 1000 \times \text{conversion value}$$

## 6.2 Chapter 2 Experimental

### 6.2.1 Ligand Synthesis

#### 6.2.1.1 Synthesis of $(\text{Ph}_2\text{P})_2\text{N}(\text{CH}_2)_3\text{Si}(\text{OMe})_3$ (**L2.1**)

**L2.1** was synthesised using a published procedure.<sup>6</sup> 3-aminopropyltrimethoxysilane (2.65 mL, 15.18 mmol) and  $\text{NEt}_3$  (4.60 mL, 32.98 mmol) were dissolved in toluene (60 mL) in a two-neck round bottom flask. The mixture was cooled to  $-40^\circ\text{C}$ , followed by addition of  $\text{Ph}_2\text{PCl}$  (5.70 mL, 31.75 mmol) dropwise under vigorous stirring until room temperature was reached. Stirring continued for an additional 2 h. A light yellowish gel-like product was obtained. The resulting solution was filtered through a cannula. Toluene was used to wash the precipitated ammonium salt formed and the solvent was removed *in vacuo*. A slight yellowish oil was obtained. Yield, 74% (6.16 g).  $^1\text{H}$  NMR (500 MHz,  $\text{CDCl}_3$ )  $\delta$  7.37 – 7.32 (m, 8H, **Ph**), 7.27 – 7.23 (m, 12H, **Ph**), 3.33 (s, 9H,  $\text{Si}(\text{OCH}_3)_3$ ), 3.22 – 3.12 (m, 2H,  $-\text{N}-\text{CH}_2$ ), 1.21 – 1.10 (m, 2H,  $-\text{C}-\text{CH}_2-\text{C}-$ ), 0.20 – 0.13 (m, 2H,  $-\text{Si}-\text{CH}_2-$ ).  $^{31}\text{P}\{^1\text{H}\}$  NMR (202 MHz,  $\text{CDCl}_3$ )  $\delta$  62.2. IR:  $\tilde{\nu}$  = 3052 (w,  $\nu_{\text{sym}}$  C-H arom.), 2940 (m,  $\nu(\text{C}-\text{H})$ ,  $\text{CH}_2$ ), 2838 (m,  $\nu_{\text{sym}}$  (C-H),  $\text{SiO}(\text{CH}_3)_3$ ), 1585 (w,  $\nu_{\text{sym}}$  C=C-C, aromatic ring stretching), 1478 (m,  $\nu_{\text{sym}}$  C=C-C, aromatic stretching), 1434 (s,  $\nu_{\text{sym}}$  (P-phenyl)), 1307 (m,  $\nu_{\text{sym}}$  (P-N- $\text{CH}_2$ )), 1280 (sym. Bending Si-C), 1187 (s, rocking  $\text{CH}_3$ ,  $\text{SiO}(\text{CH}_3)_3$ ), 1082 (br & vs,  $\nu_{\text{asym}}$  (Si-O-C)), 861 (s,  $\nu_{\text{sym}}$ , P-N), 743 (s,  $\nu_{\text{sym}}$   $\text{C}_6\text{H}_5$ ),  $695\text{ cm}^{-1}$  ( $\nu_{\text{sym}}$  P- $\text{C}_6\text{H}_5$ ). Mainly organic siloxane or silicone Si-O-C observed between  $1110\text{-}1080\text{ cm}^{-1}$ .

### 6.2.2 Catalysts Synthesis

#### 6.2.2.1 Synthesis of dichlorotris(triphenylphosphine)ruthenium(II) - $[\text{RuCl}_2(\text{PPh}_3)_3]$ (**[Ru]-1.5**)

$[\text{RuCl}_2(\text{PPh}_3)_3]$  (**[Ru]-1.5**) was synthesized using a published procedure.<sup>7, 8</sup>  $[\text{RuCl}_2(\text{PPh}_3)_3]$  was prepared by refluxing  $\text{RuCl}_3 \cdot 3\text{H}_2\text{O}$  (1.00 g, 3.82 mmol) with  $\text{PPh}_3$  (4.00 g, 15.25 mmol) in degassed ethanol (30 mL) for 1 h under a nitrogen atmosphere. The resulting mixture was cooled, filtered, and the collected solid was washed with ether (3 x 10 mL) and dried *in vacuo* to a dark brown powder. Yield, 93% (3.43 g).  $^1\text{H}$  NMR (500 MHz,  $\text{CDCl}_3$ ):  $\delta$  7.29 – 7.18 (m, 25H, **Ph**), 7.02 – 6.94 (m, 15H, **Ph**).  $^{31}\text{P}\{^1\text{H}\}$  NMR (162 MHz,  $\text{CDCl}_3$ )  $\delta$  41.02 (s, br), 29.02 (s, ( $\text{PPh}_3=\text{O}$ )), -5.4 (s, free  $\text{PPh}_3$ ).

### 6.2.2.2 Dichloro(*p*-cymene)ruthenium(II) dimer - [RuCl<sub>2</sub>(*p*-cymene)]<sub>2</sub> ([Ru]-1.7)

[RuCl<sub>2</sub>(*p*-cymene)]<sub>2</sub> ([Ru]-1.7) was synthesised using a modified procedure.<sup>9-12</sup> To a solution of hydrated ruthenium(III) chloride (5.00 g, 19.1 mmol) in 250 mL of ethanol was added  $\alpha$ -terpinene (25 mL, 20.93 g, 153.6 mmol) and the solution was heated under reflux for 4 h. The solution was cooled and left to stand overnight. The resultant dark orange solution was filtered through a sinter funnel to collect the almost black crystals, which were washed with cold ethanol (5 x 20 mL) and dried *in vacuo* to a brown solid. Yield, 37% (4.37 g). <sup>1</sup>H NMR (400 MHz, CDCl<sub>3</sub>)  $\delta$  5.47 (d,  $J$  = 5.9 Hz, 4H, *m*-Ph), 5.34 (d,  $J$  = 5.9 Hz, 4H, *o*-Ph), 2.92 (septet,  $J$  = 7.0 Hz, 2H, Ph-CH), 2.15 (s, 6H, Ph-CH<sub>3</sub>), 1.28 ppm (d,  $J$  = 6.9 Hz, 12H, Ph-CH(CH<sub>3</sub>)<sub>2</sub>).

### 6.2.2.3 Synthesis of trans-[RuCl<sub>2</sub>{(PPh<sub>2</sub>)<sub>2</sub>N(CH<sub>2</sub>)<sub>3</sub>Si(OCH<sub>3</sub>)<sub>3</sub>}<sub>2</sub>] ([Ru]-2.1)

[Ru]-2.1 was synthesised using a modified literature procedure.<sup>13</sup> Complex [Ru]-2.1 was synthesised by dropwise addition of ligand L2.1 (1.10 g, 2.00 mmol) in DCM (10 mL) to a continuously stirred solution of complex [Ru]-1.5 (0.96 g, 1.00 mmol) in DCM (10 mL). The mixture was stirred for 1 h at room temperature and thereafter, filtered to remove any impurities. The resulting filtrate was concentrated *in vacuo* and then precipitated by addition of hexane to obtain a yellow crystalline powder. This product was purified by washing with hexane (3 x 10 mL) before drying overnight *in vacuo* to give yellow solid. Yield, 77% (0.98 g). ESI-MS:  $m/z$  calc. 1231.2462 {M-Cl}<sup>+</sup>. Selected <sup>1</sup>H NMR (500 MHz, CDCl<sub>3</sub>)  $\delta$  3.35 (s, 18H, Si(OCH<sub>3</sub>)<sub>3</sub>), 1.71 (dt,  $J$  = 12.9, 8.8 Hz, 4H, -N-CH<sub>2</sub>), 1.26 (s, 4H, -C-CH<sub>2</sub>-C-), 0.34 (t,  $J$  = 8.0 Hz, 4H, -C-CH<sub>2</sub>-Si-). <sup>31</sup>P{<sup>1</sup>H} NMR (162 MHz, CDCl<sub>3</sub>)  $\delta$  76.5. IR:  $\tilde{\nu}$  = 3053 (w,  $\nu_{\text{sym}}$  C-H arom.), 2941 (m,  $\nu$ (C-H), CH<sub>2</sub>), 2839 (m,  $\nu_{\text{sym}}$  (C-H), SiO(CH<sub>3</sub>)<sub>3</sub>), 1586 (w,  $\nu_{\text{sym}}$  C=C-C, aromatic ring stretching), 1572 (w,  $\nu_{\text{sym}}$  C=C-C, aromatic ring stretching), 1481 (m,  $\nu_{\text{sym}}$  C=C-C, aromatic stretching), 1434 (s,  $\nu_{\text{sym}}$  (P-phenyl)), 1310 (m,  $\nu_{\text{sym}}$  (P-N-CH<sub>2</sub>)), 1263-1279 (sym. Bending Si-C), 1187 (s, rocking CH<sub>3</sub>, SiO(CH<sub>3</sub>)<sub>3</sub>), 1086 (br & vs,  $\nu_{\text{asym}}$  (Si-O-C)), 854 (s,  $\nu_{\text{sym}}$ , P-N), 745 (s,  $\nu_{\text{sym}}$  monosubstituted Ar), 698 cm<sup>-1</sup> ( $\nu_{\text{sym}}$  P-C<sub>6</sub>H<sub>5</sub>).

#### 6.2.2.4 Synthesis of $[(\eta^6\text{-p-cymene})\text{Ru}(\mu\text{-Cl})_3\text{RuCl}\{\text{PPh}_2\}_2\text{N}(\text{CH}_2)_3\text{Si}(\text{OMe})_3]\text{Cl}$ ([Ru]-2.2)

[Ru]-2.2 was synthesised using a modified literature procedure.<sup>6, 13</sup> A solution of complex [Ru]-1.7 (0.524 g, 0.856 mmol) in DCM (20 mL) was added to a solution of ligand L2.1 (0.938 g, 1.713 mmol) in DCM (55 mL). The resulting reaction mixture was left to proceed under vigorous stirring at room temperature for 1 h. The solution was filtered off and the filtrate was reduced *in vacuo*. An orange solid was obtained by precipitation with pentane. This solid was purified by washing with diethyl ether (3 x 10 mL) and dried *in vacuo* overnight to obtain an orange solid. Yield, 51% (0.37 g). ESI-MS:  $m/z$  calc. 1020.95  $[\text{M} - \text{Cl} - 4\text{H}]^+$ .  $^1\text{H}$  NMR (400 MHz,  $\text{CDCl}_3$ ):  $\delta$  7.74 – 7.65 (m, 4H, Ph), 7.57 – 7.50 (m, 4H, Ph), 7.39 – 7.27 (m, 12H, Ph), 5.42 (d,  $J = 6.0$  Hz, 2H,  $m\text{-Ph}^{cym}$ ), 5.25 (d,  $J = 6.0$  Hz, 2H,  $o\text{-Ph}^{cym}$ ), 3.34 (s, 9H,  $\text{Si}(\text{OCH}_3)_3$ ), 3.19 – 3.09 (m, 2H,  $-\text{N}-\text{CH}_2$ ), 2.87 – 2.67 (m, 1H,  $\text{Ar}-\text{CH}^{cym}$ ), 2.25 (s, 3H,  $\text{Ar}-\text{CH}_3^{cym}$ ), 1.20 (d,  $J = 6.9$  Hz, 6H,  $\text{Ph}-\text{CH}(\text{CH}_3)_2^{cym}$ ), 0.90 – 0.83 (m, 2H,  $-\text{C}-\text{CH}_2-\text{C}-$ ), 0.27 (t,  $J = 7.9$  Hz, 2H,  $\text{Si}-\text{CH}_2-$ ).  $^{31}\text{P}\{^1\text{H}\}$  NMR (162 MHz,  $\text{CDCl}_3$ )  $\delta$  85.1. IR:  $\tilde{\nu} = 3052$  (w,  $\nu_{\text{sym}}$  C-H arom.), 2962 (sh,  $\nu(\text{C}-\text{H})$ ,  $\text{CH}_3$ ), 2938 (m,  $\nu(\text{C}-\text{H})$ ,  $\text{CH}_2$ ), 2873 (w,  $\nu(\text{C}-\text{H})$ ,  $-\text{CH}-$ ), 2838 (m,  $\nu_{\text{sym}}$  (C-H),  $\text{SiO}(\text{CH}_3)_3$ ), 1727 (m & br), 1587 (w,  $\nu_{\text{sym}}$  C=C-C, aromatic ring stretching), 1481 (m,  $\nu_{\text{sym}}$  C=C-C, aromatic stretching), 1435 (s,  $\nu_{\text{sym}}$  (P-phenyl)), 1308 (m,  $\nu_{\text{sym}}$  (P-N- $\text{CH}_2$ )), 1280 (sym. Bending Si-C), 1184 (s, rocking  $\text{CH}_3$ ,  $\text{SiO}(\text{CH}_3)_3$ ), 1083 (b & vs, ( $\nu_{\text{asym}}$  (Si-O-C)), 842 (s,  $\nu_{\text{sym}}$ , P-N), 746 (s,  $\nu_{\text{sym}}$  monosubstituted Ar), 693 ( $\nu_{\text{sym}}$  P- $\text{C}_6\text{H}_5$ ).

#### 6.2.2.5 Synthesis of $[\text{RuCl}_2(\text{PPh}_3)_2\{\text{NH}_2(\text{CH}_2)_2\text{NH}(\text{CH}_2)_3\text{Si}(\text{OCH}_3)_3\}_2]$ ([Ru]-2.5)

According to literature method,<sup>14</sup> 0.5 mL of N-[3-(trimethoxysilyl)propyl]ethane-1,2-diamine in DCM (5 mL) was added dropwise (within 2 min) to  $\text{RuCl}_2(\text{PPh}_3)_3$  (0.1 g, 0.104 mmol) in 10 mL and left to stir at room temperature for 2 h. A colour change from dark brown to yellow was observed. Solution mixture was concentrated under reduced pressure, followed by the addition of ether (40 mL) and kept in the freezer over the weekend. Thereafter, solution was filtered (filtrate 1), residue dried and redissolved in 40 mL DCM, then, left to stir for 1 h. Product mixture reduced to 2 mL *in vacuo*, precipitated with hexane (80 mL) and kept in the freezer. Yellow product filtered, washed with hexane to obtain yellow solid and dried overnight *in vacuo*. Yield, 50% (0.0481 g).  $^{31}\text{P}\{^1\text{H}\}$  NMR (162 MHz,  $\text{CDCl}_3$ ) at  $\delta_{\text{p}} = 39.4$  and 43.5 and their coupling constant is 31.95 Hz.  $^1\text{H}$  NMR (400 MHz,  $\text{CDCl}_3$ )  $\delta$  7.58 - 7.01 (m,

30H, **Ph**), 3.49 (s, 9H,  $\text{Si}(\text{OCH}_3)_3$ ), 3.28 (s, 2H,  $-\text{HNCH}_2\text{CH}_2\text{NH}_2$ ), 3.08 (s, 2H,  $-\text{HNCH}_2\text{CH}_2\text{NH}_2$ ), 2.86 (s, 3H,  $-\text{HNCH}_2\text{CH}_2\text{NH}_2$ ), 1.27 (s, 2H,  $-\text{NCH}_2\text{CH}_2\text{CH}_2\text{Si}$ ), 0.86 (s, 3H,  $-\text{NCH}_2\text{CH}_2\text{CH}_2\text{Si}$ ), 0.15 (s, 1H,  $-\text{NCH}_2\text{CH}_2\text{CH}_2\text{Si}$ ).

## **6.3 Chapter 3 and 4 Experimental**

### **6.3.1 Experimental Procedure**

#### **6.3.1.1 Chemicals**

Fumed silica, MCM-41, neutral alumina, acidic alumina and basic alumina were supplied by Aldrich and they were used after pre-treatment process.

#### **6.3.1.2 Pre-treatment procedure for alumina and silica**

To remove the presence of adsorbed water on the surface of the aluminas used in this study, the samples were subjected to a pre-treatment process. Each sample was weighed into a dried round bottom Schlenk flask and connected to a Schlenkline. After three cycles of vacuum-N<sub>2</sub> filling, the flask was heated at between 180-250°C for 24 h under vacuum. At this temperature range, physisorbed water molecules were liberated from the surface of alumina, leaving chemically bound water. On the following day, the flask was left to cool to room temperature and transferred to a vial inside the glovebox under an argon environment with oxygen and water less than 1 ppm respectively to prevent adsorption of atmospheric water prior to use.<sup>15</sup>

#### **6.3.1.3 Immobilisation method**

A method adapted from the literature was used.<sup>6</sup> The preheated alumina was first washed with hexane, dried at 120°C in vacuo overnight, cooled to room temperature and then taken back to the glovebox. 1.00 g of dried solid support and 2% by weight of [Ru]-2.1 or 4% [Ru]-2.2 were placed in a two-neck round bottom flask in the glovebox. The flask was transferred to the Schlenk line and toluene (20 mL) was added under nitrogen flow. The solution mixture was heated to reflux temperature for 24 h under continuous stirring. The next day, the solution was cooled under N<sub>2</sub> and the supported catalyst was washed several times with toluene to remove any uncoordinated catalyst. Washing with toluene was stopped when a clear filtrate was observed. This was confirmed by <sup>31</sup>P{<sup>1</sup>H} NMR spectroscopy which showed no peaks after the third to seventh washings depending on the catalyst. Finally, the supported catalysts were dried under vacuum for 24 h. After drying, they were stored in the glovebox under argon atmosphere with less than 1 ppm O<sub>2</sub> and H<sub>2</sub>O to prevent adsorption of additional water before they were characterised and used. Supported catalysts were characterised by FTIR, TGA, XRD, BET, TEM/STEM/EDX, SS NMR, and ICP-MS situated at the School of Chemistry, Cardiff University, UK.

## **6.3.2 Instrument Methods**

### **6.3.2.1 Thermal analysis**

A PerkinElmer TGA 4000 thermogravimetric analyzer (TGA) was used. A ceramic sample boat was used with samples weighing between 3 - 100 mg. Data was recorded upon heating from 30 - 800°C at 5-10°C min<sup>-1</sup> in N<sub>2</sub> atmosphere with a purging rate of 20 mL min<sup>-1</sup>.

### **6.3.2.2 Fourier-transform infra-red (FTIR) method**

FTIR spectroscopy for the test materials was carried out using KBr disc technique using a Perkin Elmer Fourier transform infrared spectrometer in the range 4000 – 400 cm<sup>-1</sup>, with 40 scans and a resolution of 4 cm<sup>-1</sup>.

### **6.3.2.3 X-ray diffraction (XRD)**

To confirm the crystal structures of these aluminas and effect of modification on the crystallographic phase of the alumina, each sample was examined by powder X-ray diffraction (XRD) using Panalytical X'Pert Pro X-ray diffractometer with Ni-filtered Cu-K<sub>α</sub> radiation ( $\lambda = 0.15418$  nm) at a scanning rate of 0.016°s<sup>-1</sup> in the  $2\theta$  ranges from 5° to 80°. A power source of 40 kV, 40 mA was applied.<sup>15</sup> After complete analysis, using Highscore software, the peaks were matched with standard data for crystallographic phase identification purpose.<sup>16</sup>

### **6.3.2.4 Electron microscopy**

Transmission electron microscopy (TEM) images were obtained using JOEL 2010 LaB<sub>6</sub> microscope operated at 200 kV. Images were captured using a high resolution Gatan 1000XP digital camera. Samples for TEM analysis were prepared by dry dispersion of the powders onto a holey carbon film coated 300 mech Cu grid. Energy-dispersive X-ray spectroscopy was carried out using an Oxford Instruments X-Max<sup>80N</sup> detector.

### **6.3.2.5 Nitrogen adsorption and desorption measurement**

The physical properties of aluminas and functionalised aluminas were examined through N<sub>2</sub> adsorption and desorption measurement. Then, the surface area and pore size distribution were calculated by BET and BJH methods respectively.<sup>17-19</sup> The calculations were done using Quantachrome® quadraWin software. Prior to analysis, all samples were subjected to degassing process for 3 h at 150°C to < 1 mmHg. For

the degassing method, an empty sample cell was first weighed and reweighed after ~0.05 g sample was added. The sample cell was thereafter fixed to the vacuum line of the degasser where heat and vacuum were applied to evacuate dissolved vapours. After 3 h, the sample cell was removed, allowed to cool to room temperature and weighed. Hence, the final weight of the sample was taken by subtracting the weight of the sample cell. Finally, the sample cell was fixed to the Micrometrics surface area analyser (Quantachrome, USA) and N<sub>2</sub> adsorption/desorption measurements at 77 K carried out standard analytical conditions.

#### **6.3.2.6 NMR spectroscopy**

Solid-state NMR experiments were conducted on a Bruker Avance 400 III HD spectrometer (Bruker, USA magnetic field strength of 9.4 T), operating at the frequency of 162 MHz for <sup>31</sup>P, 101 MHz for <sup>13</sup>C, 104 MHz for <sup>27</sup>Al, and 79.5 MHz for <sup>29</sup>Si, using a wide bore probe with a 4 -mm double air-bearing magic-angle spinning (MAS) assembly. The powder samples were loaded in ceramic sample holder (rotor) of 4 mm o.d. and spun at 10 kHz spinning frequency (4 μs, 90° pulses). All spectra were obtained using cross-polarisation (CP), magic-angle spinning (MAS) and a high-power <sup>1</sup>H decoupling. However, it was not necessary to use high-power decoupling for to obtained silicon spectra because at high magnetic field applied, the little chemical-shift anisotropy and dipolar coupling with proton were able to be removed by MAS only. The number of accumulated free induction decays (FIDs) per spectrum ranged within 200 and 4000, depending on the system being investigated. Phosphoric acid, glycine, kaolin and aluminium nitrate solution were used as reference standard for <sup>31</sup>P, <sup>13</sup>C, <sup>29</sup>Si and <sup>27</sup>Al respectively.

#### **6.3.2.7 Inductively coupled plasma-mass spectroscopy (ICP-MS)**

The amount of Ru was obtained using Agilent 7900 ICP-MS integrated with I-AS autosampler situated in School of Chemistry, Cardiff University. Weighed amount of sample was dissolved in 5 mL aqua regia (3 HCl : 1 HNO<sub>3</sub>) via microwave digestion and thereafter diluted to 50 mL mark with deionised water. The white solid obtained was filtered off prior to analysis.

### 6.3.3 Catalyst Compositions Weight % based on Loadings (Chapter 3)

**Table 6.3:** Ru amount in immobilised complexes determined by ICP-MS

Samples	Amounts of samples taken for ICP (g)	ICP Average Ru Conc. (ppb)	ICP Amount of Ru (mg/g)	ICP Actual Loading (wt %)
Fumed silica-supported [Ru]-2.1	0.05077	12091.95	11.91	1.19
MCM-41-supported [Ru]-2.1	0.05057	11878.16	11.74	1.17
Fumed silica-supported [Ru]-2.2	0.04880	39391.35	40.36	4.04 <sup>a</sup>
MCM-41-supported [Ru]-2.2	0.05070	50717.43	50.02	5.00 <sup>a</sup>

<sup>a</sup>Initial 4 wt% catalyst loading based on two atoms of Ru in catalysts [Ru]-2.2

#### 6.3.3.1 Weight % PPh<sub>2</sub> for fumed silica-supported [Ru]-2.1

Amount of Ru = 11.91 mg/g

11.91 mg Ru = 1 g of fumed silica-supported [Ru]-2.1

That is, 11.91 mg Ru = 1000 mg supported catalyst

12.044 mg of this supported catalyst was analysed by TGA

Therefore, amount of Ru in TGA sample =  $\frac{11.91 \times 12.044}{1000} = 0.1434$  mg

0.1434 mg Ru =  $1.434 \times 10^{-4}$  g =  $1.419 \times 10^{-6}$  mol (M.W of Ru = 101.07 g/mol)

For every 1 mol Ru = 4 mol PPh<sub>2</sub> in the catalyst

Thus, mol PPh<sub>2</sub> =  $4 \times 1.419 \times 10^{-6}$  mol =  $5.676 \times 10^{-6}$  mol =  $1.051 \times 10^{-3}$  g = 1.051 mg (M.W of PPh<sub>2</sub> = 185.19 g/mol)

Finally, wt% =  $\frac{1.051 \text{ mg}}{12.044 \text{ mg}} \times 100 = 9\%$

#### 6.3.3.2 Weight % PPh<sub>2</sub> for MCM-41-supported [Ru]-2.1

Amount of Ru = 11.74 mg/g

11.74 mg Ru = 1 g of MCM-41-supported [Ru]-2.1

That is, 11.74 mg Ru = 1000 mg supported catalyst

6.948 mg of this supported catalyst was analysed by TGA

$$\text{Therefore, amount of Ru in TGA sample} = \frac{11.74 \times 6.948}{1000} = 0.0816 \text{ mg}$$

$$0.0816 \text{ mg Ru} = 8.16 \times 10^{-5} \text{ g} = 8.074 \times 10^{-7} \text{ mol (M.W of Ru} = 101.07 \text{ g/mol)}$$

For every 1 mol Ru = 4 mol PPh<sub>2</sub> in the catalyst

$$\text{Thus, mol PPh}_2 = 4 \times 8.074 \times 10^{-7} \text{ mol} = 3.230 \times 10^{-6} \text{ mol} = 5.982 \times 10^{-4} \text{ g} = 0.598 \text{ mg}$$

(M.W of PPh<sub>2</sub> = 185.19 g/mol)

$$\text{Finally, wt\%} = \frac{0.598 \text{ mg}}{6.948 \text{ mg}} \times 100 = 9\%$$

### 6.3.3.3 Weight % Cl for fumed silica-supported [Ru]-2.2

Amount of Ru = 40.36 mg/g

40.36 mg Ru = 1 g of fumed silica-supported [Ru]-2.2

That is, 40.36 mg Ru = 1000 mg supported catalyst

6.761 mg of this supported catalyst was analysed by TGA

$$\text{Therefore, amount of Ru in TGA sample} = \frac{40.36 \times 6.761}{1000} = 0.273 \text{ mg}$$

$$0.273 \text{ mg Ru} = 2.73 \times 10^{-4} \text{ g} = 2.701 \times 10^{-6} \text{ mol (M.W of Ru} = 101.07 \text{ g/mol)}$$

For every 2 mol Ru = 5 mol Cl in the catalyst

$$\text{Thus, mol Cl} = \frac{5}{2} \times 2.701 \times 10^{-6} \text{ mol} = 6.753 \times 10^{-6} \text{ mol} = 2.397 \times 10^{-3} \text{ g} = 2.397 \text{ mg}$$

(M.W of Cl = 35.5 g/mol)

$$\text{Finally, wt\%} = \frac{2.397 \text{ mg}}{6.761 \text{ mg}} \times 100 = 4\%$$

### 6.3.3.4 Weight % Cl for MCM-41-supported [Ru]-2.2

Amount of Ru = 50.02 mg/g

50.02 mg Ru = 1 g of MCM-41-supported [Ru]-2.2

That is, 50.02 mg Ru = 1000 mg supported catalyst

14.563 mg of this supported catalyst was analysed by TGA

$$\text{Therefore, amount of Ru in TGA sample} = \frac{50.02 \times 14.563}{1000} = 0.728 \text{ mg}$$

$$0.728 \text{ mg Ru} = 7.28 \times 10^{-4} \text{ g} = 7.203 \times 10^{-6} \text{ mol (M.W of Ru} = 101.07 \text{ g/mol)}$$

For every 2 mol Ru = 5 mol Cl in the catalyst

Thus, mol Cl =  $\frac{5}{2} \times 7.203 \times 10^{-6} \text{ mol} = 1.801 \times 10^{-5} \text{ mol} = 6.394 \times 10^{-4} \text{ g} = 0.639 \text{ mg}$   
(M.W of Cl = 35.5 g/mol)

Finally, wt% =  $\frac{0.639 \text{ mg}}{14.563 \text{ mg}} \times 100 = 4\%$

### 6.3.3.5 Weight % Ph for fumed silica-supported [Ru]-2.2

Amount of Ru = 40.36 mg/g

40.36 mg Ru = 1 g of fumed silica-supported [Ru]-2.2

That is, 40.36 mg Ru = 1000 mg supported catalyst

6.761 mg of this supported catalyst was analysed by TGA

Therefore, amount of Ru in TGA sample =  $\frac{40.36 \times 6.761}{1000} = 0.273 \text{ mg}$

0.273 mg Ru =  $2.73 \times 10^{-4} \text{ g} = 2.701 \times 10^{-6} \text{ mol}$  (M.W of Ru = 101.07 g/mol)

For every 2 mol Ru = 4 mol Ph in the catalyst

Thus, mol Ph =  $2 \times 2.701 \times 10^{-6} \text{ mol} = 5.402 \times 10^{-6} \text{ mol} = 4.165 \times 10^{-4} \text{ g} = 0.417 \text{ mg}$   
(M.W of Ph = 77.11 g/mol)

Finally, wt% =  $\frac{0.417 \text{ mg}}{6.761 \text{ mg}} \times 100 = 6\%$

### 6.3.3.6 Weight % Ph for MCM-41-supported [Ru]-2.2

Amount of Ru = 50.02 mg/g

50.02 mg Ru = 1 g of MCM-41-supported [Ru]-2.2

That is, 50.02 mg Ru = 1000 mg supported catalyst

14.563 mg of this supported catalyst was analysed by TGA

Therefore, amount of Ru in TGA sample =  $\frac{50.02 \times 14.563}{1000} = 0.728 \text{ mg}$

0.728 mg Ru =  $7.28 \times 10^{-4} \text{ g} = 7.203 \times 10^{-6} \text{ mol}$  (M.W of Ru = 101.07 g/mol)

For every 2 mol Ru = 4 mol Ph in the catalyst

Thus, mol Ph =  $2 \times 7.203 \times 10^{-6} \text{ mol} = 1.441 \times 10^{-5} \text{ mol} = 1.111 \times 10^{-3} \text{ g} = 1.111 \text{ mg}$   
(M.W of Ph = 77.11 g/mol)

Finally, wt% =  $\frac{1.111 \text{ mg}}{14.563 \text{ mg}} \times 100 = 8\%$

### 6.3.3.7 Weight % Cy for fumed silica-supported [Ru]-2.2

Amount of Ru = 40.36 mg/g

40.36 mg Ru = 1 g of fumed silica-supported [Ru]-2.2

That is, 40.36 mg Ru = 1000 mg supported catalyst

6.761 mg of this supported catalyst was analysed by TGA

Therefore, amount of Ru in TGA sample =  $\frac{40.36 \times 6.761}{1000} = 0.273 \text{ mg}$

0.273 mg Ru =  $2.73 \times 10^{-4} \text{ g} = 2.701 \times 10^{-6} \text{ mol}$  (M.W of Ru = 101.07 g/mol)

For every 2 mol Ru = 1 mol *p*-cymene (Cy) in the catalyst

Thus, mol Cy =  $\frac{1}{2} \times 2.701 \times 10^{-6} \text{ mol} = 1.351 \times 10^{-6} \text{ mol} = 1.813 \times 10^{-4} \text{ g} = 0.181 \text{ mg}$   
(M.W of Cy = 134.22 g/mol)

Finally, wt% =  $\frac{0.181 \text{ mg}}{6.761 \text{ mg}} \times 100 = 3\%$

### 6.3.3.8 Weight % Cy for MCM-41-supported [Ru]-2.2

Amount of Ru = 50.02 mg/g

50.02 mg Ru = 1 g of MCM-41-supported [Ru]-2.2

That is, 50.02 mg Ru = 1000 mg supported catalyst

14.563 mg of this supported catalyst was analysed by TGA

Therefore, amount of Ru in TGA sample =  $\frac{50.02 \times 14.563}{1000} = 0.728 \text{ mg}$

0.728 mg Ru =  $7.28 \times 10^{-4} \text{ g} = 7.203 \times 10^{-6} \text{ mol}$  (M.W of Ru = 101.07 g/mol)

For every 2 mol Ru = 1 mol *p*-cymene (Cy) in the catalyst

Thus, mol Cy =  $\frac{1}{2} \times 7.203 \times 10^{-6} \text{ mol} = 3.602 \times 10^{-6} \text{ mol} = 4.835 \times 10^{-4} \text{ g} = 0.484 \text{ mg}$   
(M.W of Cy = 134.22 g/mol)

Finally, wt% =  $\frac{0.484 \text{ mg}}{14.563 \text{ mg}} \times 100 = 3\%$

### 6.3.4 Catalyst Compositions Weight % based on Loadings (Chapter 4)

**Table 6.4:** Ru amount in immobilised complexes determined by ICP-MS

Samples	Amounts of samples taken for ICP (g)	ICP Average Ru Conc. (ppb)	ICP Amount of Ru (mg/g)	ICP Actual Loading (wt %)
Acidic Al <sub>2</sub> O <sub>3</sub> -supported [Ru]-2.1	0.05060	8657.94	8.56	0.86
Basic Al <sub>2</sub> O <sub>3</sub> -supported [Ru]-2.1	0.05066	9192.86	9.07	0.91
Neutral Al <sub>2</sub> O <sub>3</sub> -supported [Ru]-2.1	0.04950	9883.54	9.98	1.00
Acidic Al <sub>2</sub> O <sub>3</sub> -supported [Ru]-2.2	0.04630	30371.71	32.80	3.28 <sup>a</sup>
Basic Al <sub>2</sub> O <sub>3</sub> -supported [Ru]-2.2	0.04300	27639.79	32.14	3.21 <sup>a</sup>

<sup>a</sup>Initial 4 wt% catalyst loading based on two atoms of Ru in catalysts [Ru]-2.2

#### 6.3.4.1 Weight % PPh<sub>2</sub> for acidic alumina-supported [Ru]-2.1

Amount of Ru = 8.56 mg/g

8.56 mg Ru = 1 g of acidic alumina-supported [Ru]-2.1

That is, 8.56 mg Ru = 1000 mg supported catalyst

20.896 mg of this supported catalyst was analysed by TGA

Therefore, amount of Ru in TGA sample =  $\frac{8.56 \times 20.896}{1000} = 0.179$  mg

0.179 mg Ru =  $1.790 \times 10^{-4}$  g =  $1.771 \times 10^{-6}$  mol (M.W of Ru = 101.07 g/mol)

For every 1 mol Ru = 4 mol PPh<sub>2</sub> in the catalyst

Thus, mol PPh<sub>2</sub> =  $4 \times 1.771 \times 10^{-6}$  mol =  $7.084 \times 10^{-6}$  mol =  $1.312 \times 10^{-3}$  g = 1.312 mg (M.W of PPh<sub>2</sub> = 185.19 g/mol)

Finally, wt% =  $\frac{1.312 \text{ mg}}{20.896 \text{ mg}} \times 100 = 6\%$

#### 6.3.4.2 Weight % PPh<sub>2</sub> for basic alumina-supported [Ru]-2.1

Amount of Ru = 9.07 mg/g

9.07 mg Ru = 1 g of basic alumina-supported [Ru]-2.1

That is, 9.07 mg Ru = 1000 mg supported catalyst

38.192 mg of this supported catalyst was analysed by TGA

$$\text{Therefore, amount of Ru in TGA sample} = \frac{9.07 \times 38.192}{1000} = 0.346 \text{ mg}$$

$$0.346 \text{ mg Ru} = 3.460 \times 10^{-4} \text{ g} = 3.423 \times 10^{-6} \text{ mol (M.W of Ru} = 101.07 \text{ g/mol)}$$

For every 1 mol Ru = 4 mol PPh<sub>2</sub> in the catalyst

$$\text{Thus, mol PPh}_2 = 4 \times 3.423 \times 10^{-6} \text{ mol} = 1.369 \times 10^{-5} \text{ mol} = 2.535 \times 10^{-3} \text{ g} = 2.535 \text{ mg}$$

(M.W of PPh<sub>2</sub> = 185.19 g/mol)

$$\text{Finally, wt\%} = \frac{2.535 \text{ mg}}{38.192 \text{ mg}} \times 100 = 7\%$$

#### **6.3.4.3 Weight % PPh<sub>2</sub> for neutral alumina-supported [Ru]-2.1**

Amount of Ru = 9.98 mg/g

9.98 mg Ru = 1 g of neutral alumina-supported **[Ru]-2.1**

That is, 9.98 mg Ru = 1000 mg supported catalyst

39.570 mg of this supported catalyst was analysed by TGA

$$\text{Therefore, amount of Ru in TGA sample} = \frac{9.98 \times 39.570}{1000} = 0.395 \text{ mg}$$

$$0.395 \text{ mg Ru} = 3.95 \times 10^{-4} \text{ g} = 3.908 \times 10^{-6} \text{ mol (M.W of Ru} = 101.07 \text{ g/mol)}$$

For every 1 mol Ru = 4 mol PPh<sub>2</sub> in the catalyst

$$\text{Thus, mol PPh}_2 = 4 \times 3.908 \times 10^{-6} \text{ mol} = 1.563 \times 10^{-5} \text{ mol} = 2.895 \times 10^{-3} \text{ g} = 2.895 \text{ mg}$$

(M.W of PPh<sub>2</sub> = 185.19 g/mol)

$$\text{Finally, wt\%} = \frac{2.895 \text{ mg}}{39.570 \text{ mg}} \times 100 = 7\%$$

#### **6.3.4.4 Weight % Cy for acidic alumina-supported [Ru]-2.2**

Amount of Ru = 32.80 mg/g

32.80 mg Ru = 1 g of acidic alumina-supported **[Ru]-2.2**

That is, 32.80 mg Ru = 1000 mg supported catalyst

23.856 mg of this supported catalyst was analysed by TGA

$$\text{Therefore, amount of Ru in TGA sample} = \frac{32.80 \times 23.856}{1000} = 0.782 \text{ mg}$$

$$0.782 \text{ mg Ru} = 7.820 \times 10^{-4} \text{ g} = 7.737 \times 10^{-6} \text{ mol (M.W of Ru} = 101.07 \text{ g/mol)}$$

For every 2 mol Ru = 1 mol *p*-cymene (Cy) in the catalyst

Thus, mol Cy =  $\frac{1}{2} \times 7.737 \times 10^{-6} \text{ mol} = 3.869 \times 10^{-6} \text{ mol} = 5.193 \times 10^{-4} \text{ g} = 0.519 \text{ mg}$   
(M.W of Cy = 134.22 g/mol)

Finally, wt% =  $\frac{0.519 \text{ mg}}{23.856 \text{ mg}} \times 100 = 2\%$

#### **6.3.4.5 Weight % Cl for acidic alumina-supported [Ru]-2.2**

Amount of Ru = 32.80 mg/g

32.80 mg Ru = 1 g of acidic alumina-supported **[Ru]-2.2**

That is, 32.80 mg Ru = 1000 mg supported catalyst

23.856 mg of this supported catalyst was analysed by TGA

Therefore, amount of Ru in TGA sample =  $\frac{32.80 \times 23.856}{1000} = 0.782 \text{ mg}$

0.782 mg Ru =  $7.820 \times 10^{-4} \text{ g} = 7.737 \times 10^{-6} \text{ mol}$  (M.W of Ru = 101.07 g/mol)

For every 2 mol Ru = 5 mol Cl in the catalyst

Thus, mol Cl =  $\frac{5}{2} \times 7.737 \times 10^{-6} \text{ mol} = 1.934 \times 10^{-5} \text{ mol} = 6.866 \times 10^{-4} \text{ g} = 0.687 \text{ mg}$   
(M.W of Cl = 35.5 g/mol)

Finally, wt% =  $\frac{0.687 \text{ mg}}{23.856 \text{ mg}} \times 100 = 3\%$

#### **6.3.4.6 Weight % Ph for acidic alumina-supported [Ru]-2.2**

Amount of Ru = 32.80 mg/g

32.80 mg Ru = 1 g of acidic alumina-supported **[Ru]-2.2**

That is, 32.80 mg Ru = 1000 mg supported catalyst

23.856 mg of this supported catalyst was analysed by TGA

Therefore, amount of Ru in TGA sample =  $\frac{32.80 \times 23.856}{1000} = 0.782 \text{ mg}$

0.782 mg Ru =  $7.820 \times 10^{-4} \text{ g} = 7.737 \times 10^{-6} \text{ mol}$  (M.W of Ru = 101.07 g/mol)

For every 2 mol Ru = 4 mol Ph in the catalyst

Thus, mol Ph =  $2 \times 7.737 \times 10^{-6} \text{ mol} = 1.547 \times 10^{-5} \text{ mol} = 1.193 \times 10^{-4} \text{ g} = 1.193 \text{ mg}$   
(M.W of Ph = 77.11 g/mol)

Finally, wt% =  $\frac{1.193 \text{ mg}}{23.856 \text{ mg}} \times 100 = 5\%$

#### 6.3.4.7 Weight % Cy for basic alumina-supported [Ru]-2.2

Amount of Ru = 32.14 mg/g

32.14 mg Ru = 1 g of basic alumina-supported [Ru]-2.2

That is, 32.14 mg Ru = 1000 mg supported catalyst

27.781 mg of this supported catalyst was analysed by TGA

Therefore, amount of Ru in TGA sample =  $\frac{32.14 \times 27.781}{1000} = 0.893$  mg

0.893 mg Ru =  $8.930 \times 10^{-4}$  g =  $8.835 \times 10^{-6}$  mol (M.W of Ru = 101.07 g/mol)

For every 2 mol Ru = 1 mol *p*-cymene (Cy) in the catalyst

Thus, mol Cy =  $\frac{1}{2} \times 8.835 \times 10^{-6}$  mol =  $4.418 \times 10^{-6}$  mol =  $5.930 \times 10^{-4}$  g = 0.593 mg  
(M.W of Cy = 134.22 g/mol)

Finally, wt% =  $\frac{0.593 \text{ mg}}{27.781 \text{ mg}} \times 100 = 2\%$

#### 6.3.4.8 Weight % Cl for basic-supported [Ru]-2.2

Amount of Ru = 32.14 mg/g

32.14 mg Ru = 1 g of basic alumina-supported [Ru]-2.2

That is, 32.14 mg Ru = 1000 mg supported catalyst

27.781 mg of this supported catalyst was analysed by TGA

Therefore, amount of Ru in TGA sample =  $\frac{32.14 \times 27.781}{1000} = 0.893$  mg

0.893 mg Ru =  $8.930 \times 10^{-4}$  g =  $8.835 \times 10^{-6}$  mol (M.W of Ru = 101.07 g/mol)

For every 2 mol Ru = 5 mol Cl in the catalyst

Thus, mol Cl =  $\frac{5}{2} \times 8.835 \times 10^{-6}$  mol =  $2.209 \times 10^{-5}$  mol =  $7.842 \times 10^{-4}$  g = 0.784 mg  
(M.W of Cl = 35.5 g/mol)

Finally, wt% =  $\frac{0.784 \text{ mg}}{27.781 \text{ mg}} \times 100 = 3\%$

#### 6.3.4.9 Weight % Ph for basic alumina-supported [Ru]-2.2

Amount of Ru = 32.14 mg/g

32.14 mg Ru = 1 g of basic alumina-supported [Ru]-2.2

That is, 32.14 mg Ru = 1000 mg supported catalyst

27.781 mg of this supported catalyst was analysed by TGA

$$\text{Therefore, amount of Ru in TGA sample} = \frac{32.14 \times 27.781}{1000} = 0.893 \text{ mg}$$

$$0.893 \text{ mg Ru} = 8.930 \times 10^{-4} \text{ g} = 8.835 \times 10^{-6} \text{ mol (M.W of Ru} = 101.07 \text{ g/mol)}$$

For every 2 mol Ru = 4 mol Ph in the catalyst

$$\text{Thus, mol Ph} = 2 \times 8.835 \times 10^{-6} \text{ mol} = 1.767 \times 10^{-5} \text{ mol} = 1.363 \times 10^{-3} \text{ g} = 1.363 \text{ mg}$$

(M.W of Ph = 77.11 g/mol)

$$\text{Finally, wt\%} = \frac{1.363 \text{ mg}}{27.781 \text{ mg}} \times 100 = 5\%$$

## 6.5 Chapter 5 Experimental

### 6.5.1 Catalysts Synthesis

#### 6.5.1.1 Synthesis of $\text{RuCl}_2\{(\text{PPh}_2)_2\text{CH}=\text{CH}_2\}_2$ ([Ru]-5.1)

Following a literature method,<sup>20-22</sup> dppen (0.82 g, 2.07 mmol) in 10 mL DCM was added to a solution of  $\text{RuCl}_2(\text{PPh}_3)_3$  (0.96 g, 1.0 mmol) in 10 mL DCM under a flow of nitrogen. The resulting blackish brown mixture was left to stir for 16 h at room temperature. On the following day, a red coloured solution was observed. The product mixture was filtered, washed with DCM (2 x 10 mL) and  $\text{Et}_2\text{O}$  (2 x 10 mL). The red powder product was left to dry overnight under vacuo. Additional product was obtained by reducing DCM filtrate under vacuo and thereafter precipitated with  $\text{Et}_2\text{O}$ . The product mixture was kept in the freezer overnight, then filtered, washed with  $\text{Et}_2\text{O}$  (3 x 10 mL) and dried overnight under vacuo. Total product yield 87% (0.8401 g). ESI-MS:  $m/z$  calc. 987  $[\text{M} + \text{Na}]^+$ ; 964  $[\text{M}]^+$ ; 929  $[\text{M} - \text{Cl}]^+$ , 447  $[\text{M} - 2\text{Cl}]^{2+}$ .  $^1\text{H}$  NMR (400 MHz,  $\text{CDCl}_3$ )  $\delta$  7.48 – 7.08 (m, 40H, **Ph**), 6.14 (p,  $^3J_{\text{HP}} = 12.6$  Hz, 4H, **C=CH<sub>2</sub>**).  $^{31}\text{P}\{^1\text{H}\}$  NMR (162 MHz,  $\text{CDCl}_3$ ):  $\delta$  15.35 (s)  $^{13}\text{C}\{^1\text{H}\}$  NMR (126 MHz,  $\text{CDCl}_3$ )  $\delta$  134.73 – 134.51 (m, **o-Ph**), 132.42 (s, 2C, **C=CH<sub>2</sub>**), 132.09 – 131.59 (m, 2C, **C=CH<sub>2</sub>**), 129.43 (s, **p-Ph**), 127.62 – 127.30 (m, **m-Ph**).

#### 6.5.1.2 Synthesis of $[\text{RuCl}_2\{(\text{Ph}_2\text{P})_2\text{CHCH}_2\text{NH}(\text{CH}_2)_2\text{PPh}_2\}_2]$ ([Ru]-5.2)

2-(diphenylphosphino)ethylamine (3 mL) was added to a suspension of ([Ru]-5.1) (0.10 g, 0.10 mmol) in toluene (10 mL) under a nitrogen flow with continuous stirring overnight. No colour change was observed. Crude  $^{31}\text{P}\{^1\text{H}\}$  NMR of the mixture was recorded with no traces of product formed. An additional 0.3 mL of the ligand was added and allowed to stir overnight. The solution changed from red to yellow. The solvent was removed in vacuo to give a yellow oily product. The oily product was triturated with MeOH to give a yellow product. The product was filtered, washed with MeOH (3 x 10 mL) and dried *in vacuo*. Yield, 47% (0.0699 g.). ESI-MS:  $m/z$  calc. 1423  $[\text{M} + \text{H}]^+$ ; 712  $[\text{M} + 2\text{H}]^{2+}$ . Selected  $^1\text{H}$  NMR (400 MHz,  $\text{CDCl}_3$ )  $\delta$  5.43 – 5.32 (m, 2H, **P<sub>2</sub>CHCH<sub>2</sub>**), 2.95 (d,  $J = 6.7$  Hz, 4H, **P<sub>2</sub>CHCH<sub>2</sub>**), 2.56 (q,  $J = 8.0$  Hz, 4H, **NHCH<sub>2</sub>CH<sub>2</sub>PPh<sub>2</sub>**), 2.12 – 2.02 (m, 4H, **NHCH<sub>2</sub>CH<sub>2</sub>PPh<sub>2</sub>**), 0.88 (s, 2H, **NH**).  $^{31}\text{P}\{^1\text{H}\}$  NMR (162 MHz,  $\text{CDCl}_3$ ):  $\delta$  10.64 (s), -20.81 (s). Selected  $^{13}\text{C}\{^1\text{H}\}$  NMR (126 MHz,  $\text{CDCl}_3$ ) 131.42 (s, **p-Ph**), 128.48 (s, **m-Ph**, **(PPh<sub>2</sub>)<sub>2</sub>CH**), 127.20 (s, **m-Ph**, **NHCH<sub>2</sub>CH<sub>2</sub>PPh<sub>2</sub>**).

### 6.5.1.3 Synthesis of [RuCl<sub>2</sub>{(Ph<sub>2</sub>P)<sub>2</sub>CHCH<sub>2</sub>NH(CH<sub>2</sub>)<sub>2</sub>NH<sub>2</sub>}<sub>2</sub>] ([Ru]-5.3)

To a solution of [Ru]-5.1 (0.10 g, 0.10 mmol) in toluene (10 mL) was added ethylenediamine (1.0 mL, 14.96 mmol) and the resulting mixture was stirred for 2 h during which the colour changed to yellow. The solvent was reduced in vacuo to ca. 4 mL and the product was crystallised with pentane (10 mL). The yellow crystals obtained were washed with pentane and dried *in vacuo*. Single crystals suitable for X-ray diffraction studies were obtained from a fluorobenzene/pentane mixture. Yield, 47% (0.0528 g). ESI-MS: *m/z* calc. 1085 [M + H]<sup>+</sup>; 1048 [M - Cl]<sup>+</sup>; 593 [M - Cl - L<sub>1</sub>]<sup>+</sup>; 457 [L<sub>1</sub> + H]<sup>+</sup> (L<sub>1</sub> = (Ph<sub>2</sub>P)<sub>2</sub>CHCH<sub>2</sub>NH(CH<sub>2</sub>)<sub>2</sub>NH<sub>2</sub>); 385 [(Ph<sub>2</sub>P)<sub>2</sub>CH<sub>2</sub> + H]<sup>+</sup>. <sup>1</sup>H NMR (500 MHz, CDCl<sub>3</sub>) δ 7.67 – 7.60 (m, 8H, *o*-Ph), 7.54 – 7.48 (m, 8H, *o*-Ph), 7.29 – 7.23 (m, 12H, *m*, *p*-Ph), 7.10 (t, *J*<sub>HH</sub> = 7.8, 1.8 Hz, 16H, *m*, *p*-Ph), 5.46 (sept, *J*<sub>PH</sub> = 6.6 Hz, 2H, P<sub>2</sub>CHCH<sub>2</sub>), 3.10 – 3.00 (m, 4H, P<sub>2</sub>CHCH<sub>2</sub>), 2.61 (t, *J* = 5.7 Hz, 4H, NHCH<sub>2</sub>CH<sub>2</sub>NH<sub>2</sub>), 2.52 – 2.45 (m, 4H, NHCH<sub>2</sub>CH<sub>2</sub>NH<sub>2</sub>), 0.93 (s, br, 6H, NH). <sup>31</sup>P{<sup>1</sup>H} NMR (202 MHz, CDCl<sub>3</sub>): δ 10.82 (s). <sup>13</sup>C{<sup>1</sup>H} NMR (126 MHz, CDCl<sub>3</sub>) δ 136.22 (s, 8C, *C*<sub>i</sub>-Ph), 134.59 – 134.18 (m, 8C *o*-Ph), 129.90 (s, 4C, *p*-Ph), 129.44 (s, 4C, *p*-Ph), 127.61 (s, 16C, *m*-Ph), 61.34 – 60.75 (m, 2C, NHCH<sub>2</sub>CH<sub>2</sub>NH<sub>2</sub>), 52.68 (s, 2C, P<sub>2</sub>CHCH<sub>2</sub>NH), 51.09 (s, 2C, P<sub>2</sub>CHCH<sub>2</sub>), 42.07 (s, 2C, NHCH<sub>2</sub>CH<sub>2</sub>NH<sub>2</sub>).

### 6.5.1.4 Synthesis of [RuCl<sub>2</sub>{(Ph<sub>2</sub>P)<sub>2</sub>CHCH<sub>2</sub>NH(CH<sub>2</sub>)<sub>3</sub>NH<sub>2</sub>}<sub>2</sub>] ([Ru]-5.4)

Adapting a literature procedure,<sup>20, 22</sup> 1, 3-diaminopropane (0.4 mL, 4.79 mmol) was added to a suspension of [Ru]-5.1 (0.20 g, 0.2 mmol) in toluene (10 mL) under a nitrogen flow with continuous stirring. The colour of the solution changed from red to cloudy yellow after 4 h. The solution mixture was left to stir overnight. The product mixture was filtered and the resulting yellow residue was triturated with MeOH (3 x 10 mL). After filtration, the yellow product was dried *in vacuo*. Yield, 46% (0.1060 g.). ESI-MS: *m/z* calc. 1113 [M + H]<sup>+</sup>; 557 [M + 2H]<sup>2+</sup>. <sup>1</sup>H NMR (400 MHz, CDCl<sub>3</sub>) δ 7.66 – 7.59 (m, 7H, Ph), 7.54 – 7.47 (m, 7H, Ph), 7.29 – 7.22 (m, 11H, Ph), 7.14 – 7.05 (m, 15H, Ph), 5.45 (p, <sup>1</sup>*J*<sub>PH</sub> = 6.5 Hz, 2H, P<sub>2</sub>CHCH<sub>2</sub>), 3.07 – 2.97 (m, 4H, P<sub>2</sub>CHCH<sub>2</sub>), 2.60 (t, *J*<sub>HH</sub> = 6.8 Hz, 4H, -NHCH<sub>2</sub>CH<sub>2</sub>CH<sub>2</sub>NH<sub>2</sub>), 2.48 (t, *J*<sub>HH</sub> = 6.7 Hz, 4H, -NHCH<sub>2</sub>CH<sub>2</sub>CH<sub>2</sub>NH<sub>2</sub>), 1.46 (p, *J*<sub>HH</sub> = 6.7 Hz, 4H, -NHCH<sub>2</sub>CH<sub>2</sub>CH<sub>2</sub>NH<sub>2</sub>), 0.95 (br, s, 6H, amine H). <sup>31</sup>P{<sup>1</sup>H} NMR ((162 MHz, CDCl<sub>3</sub>): δ 11.35 (s). <sup>13</sup>C{<sup>1</sup>H} NMR (126 MHz, CDCl<sub>3</sub>) δ 135.96 (8C, *C*<sub>i</sub>-Ph), 134.31 – 133.99 (m, *o*-Ph), 131.62 – 131.19 (m, P<sub>2</sub>CHCH<sub>2</sub>), 129.62-129.16 (s, *p*-Ph), 127.36 (d, *J* = 3.0 Hz, *m*-Ph), 61.03-60.52

(m,  $P_2CHCH_2$ ), 51.15 (s,  $CHCOH_2$ ), 47.74 (s,  $-NHCH_2CH_2CH_2NH_2$ ), 40.72 (s,  $-NHCH_2CH_2CH_2NH_2$ ), 33.77 (s,  $-NHCH_2CH_2CH_2NH_2$ ).

#### 6.5.1.5 Synthesis of $[RuCl_2\{(Ph_2P)_2CHCH_2NH(CH_2)_3Si(OEt)_3\}_2]$ ([Ru]-5.5)

Adapting a literature procedure,<sup>20, 22</sup> 3-(aminopropyl) triethoxysilane (1.0 mL, 4.27 mmol) was added under a nitrogen flow to a suspension of [Ru]-5.1 (0.2 g, 0.2 mmol) in toluene (10 mL). The mixture was left to stir overnight. The red suspension dissolved gradually to give a yellow solution. The next day, the mixture was filtered to remove any solid impurities. The filtrate was reduced under vacuo to ca. 4 mL and the product precipitated with  $Et_2O$ . The product mixture was kept in the freezer overnight. Thereafter, the product was filtered, washed with  $Et_2O$  (3 x 10 mL) and dried *in vacuo*. Yield, 40% (0.1166 g). ESI-MS:  $m/z$  calc. 1407  $[M + H]^+$ , 705  $[M + 2H]^{2+}$ . Selected  $^1H$  NMR (400 MHz,  $CDCl_3$ ): 5.49 – 5.39 (m, 2H,  $P_2CHCH_2$ ), 3.74 (q,  $J_{HH} = 7.0$  Hz, 12H,  $Si(OCH_2CH_3)_3$ ), 3.48 (q,  $J = 7.0$  Hz, 2H,  $-NHCH_2CH_2CH_2Si$ ), 3.01 (br, s, 4H,  $P_2CHCH_2$ ), 1.42 (p,  $J_{HH} = 8.3$  Hz, 4H,  $-NHCH_2CH_2CH_2Si$ ), 1.17 (t,  $J_{HH} = 7.0$  Hz, 18H,  $Si(OCH_2CH_3)_3$ ), 0.85 (br, s, 4H,  $-NHCH_2CH_2CH_2Si$ ), 0.51 – 0.43 (m, 4H,  $-NHCH_2CH_2CH_2Si$ ).  $^{31}P\{^1H\}$  NMR (162 MHz,  $CDCl_3$ ):  $\delta$  11.31 (s). Selected  $^{13}C\{^1H\}$  NMR (126 MHz,  $CDCl_3$ )  $\delta$  135.99 (s,  $C_i-Ph$ ), 134.31 – 134.03 (m,  $o-Ph$ ), 129.57 (s,  $p-Ph$ ), 129.09 (s,  $p-Ph$ ), 127.32 (s,  $m-Ph$ ), 60.85 (s,  $PCHCH_2$ ), 58.45 (s,  $-SiOCH_2CH_3$ ), 52.32 (s,  $-NCH_2CH_2CH_2Si$ ), 50.87 (s,  $PCHCH_2$ ), 23.24 (s,  $-NCH_2CH_2CH_2Si$ ), 18.45 (s,  $-SiOCH_2CH_3$ ), 7.98 (s,  $-NCH_2CH_2CH_2Si$ ).  $Et_2O$  impurity was present in the spectrum.

#### 6.5.1.6 Synthesis of $[RuCl_2\{(Ph_2P)_2CHCH_2NH(CH_2)C_6H_5\}_2]$ ([Ru]-5.6)

Complex [Ru]-5.6 was synthesised by adapting a literature procedure.<sup>20, 22</sup> To a suspension of [Ru]-5.1 (0.20 g, 0.20 mmol) in toluene (10 mL) was added benzylamine (1.0 mL, 9.16 mmol) under nitrogen and left to stir overnight. The suspension dissolved to give a yellow precipitate. The product mixture was filtered and washed with toluene (10 mL). The yellow residue was triturated with MeOH (10 mL). The final product was washed with MeOH (2 x 10 mL) to obtain a yellow solid product which was dried *in vacuo*. Yield, 55% (0.1348 g). ESI-MS:  $m/z$  calc. 1178  $[M]^+$ , 1143  $[M - Cl]^+$ , 590  $[M + 2H]^{2+}$ .  $^1H$  NMR (400 MHz,  $CDCl_3$ )  $\delta$  7.64 - 7.04 (m, 50H,  $Ph$ ), 5.50 (p,  $J = 6.5$  Hz, 2H,  $P_2CHCH_2$ ), 3.62 (s, 4H,  $NHCH_2Ph$ ), 3.09 (s, 4H,  $P_2CHCH_2$ ), 0.84 (br, s, 2H,  $NH$ ).  $^{31}P\{^1H\}$  NMR (162 MHz,  $CDCl_3$ ):  $\delta$  11.52 (s).

Selected  $^{13}\text{C}\{^1\text{H}\}$  NMR (126 MHz,  $\text{CDCl}_3$ ):  $\delta$  140.07 (s, 2H, *Ci*-Bz), 135.97 (s, 8H, *Ci*-Ph), 134.28 – 134.08 (m, 16H, *o*-Ph), 129.62 -129.15 (s, 8H, *p*-Ph), 128.45 (s, 4H, *o*-Bz), 128.03 (s, 4H, *m*-Bz), 127.37 (s, 16H, *m*-Ph), 127.02 (s, 2H, *o*-Bz), 53.57 – 53.32 (m, 4H,  $\text{NHCH}_2\text{Bz}$ ), 50.46 (s, 2H,  $\text{PCHCH}_2$ ).

#### 6.5.1.7 Synthesis of $[\text{RuCl}_2\{(\text{Ph}_2\text{P})_2\text{CHCH}_2\text{NH}(\text{CH}_2)_2\text{SH}\}]$ ([Ru]-5.7)

Cysteamine (0.016 g, 0.207 mmol) was dissolved in DCM (5 mL) overnight and was added to a suspension of [Ru]-5.1 (0.10 g, 0.10 mmol) in DCM (10 mL) and left to stir overnight. The product mixture concentrated under reduce pressure to ca. 4 mL and crystallised with pentane (10 mL) and kept in the freezer. The product was filtered, washed with pentane and dried *in vacuo* to obtain a yellow solid. Yield, 58% (0.0670 g). ESI-MS:  $m/z$  calc. 1083  $[\text{M} - \text{Cl}]^+$ , 1047  $[\text{M} - 2\text{Cl}]^+$ , 542  $[\text{M} - \text{Cl}]^{2+}$ .  $^1\text{H}$  NMR (400 MHz,  $\text{CDCl}_3$ )  $\delta$  7.55 – 7.11 (m, 30H, Ph), 5.50 (p,  $J = 6.4$  Hz, 2H,  $\text{P}_2\text{CHCH}_2$ ), 2.96 (q,  $J = 5.9$  Hz, 4H,  $\text{P}_2\text{CHCH}_2$ ), 2.70 (t,  $J_{\text{HH}} = 6.4$  Hz, 4H,  $\text{HNCH}_2\text{CH}_2\text{SH}$ ), 2.47 (t,  $J_{\text{HH}} = 6.4$  Hz, 4H,  $\text{HNCH}_2\text{CH}_2\text{SH}$ ).  $^{31}\text{P}\{^1\text{H}\}$  NMR (162 MHz,  $\text{CDCl}_3$ ):  $\delta$  15.95 (s).

#### 6.5.1.8 Synthesis of $[\text{RuCl}_2\{(\text{Ph}_2\text{P})_2\text{CHCH}_2\text{NH}(\text{CH}_2)_2\text{OH}\}_2]$ ([Ru]-5.8)

To a suspension of [Ru]-5.1 (0.20 g, 0.10 mmol) in DCM (15 mL) was added ethanolamine (2.0 mL, 33.14 mmol) under a flow of nitrogen. A yellow colour was observed within 1 h. The solution was concentrated under reduce pressure to ca. 4 mL and the resulting oil was triturated with MeOH (10 mL) to give yellow precipitate. The mixture was kept in the freezer overnight. The product was filtered, washed with MeOH (3 x 10 mL) and dried *in vacuo* to give a yellow powder. Yield, 93% (0.1006 g). ESI-MS:  $m/z$  calc. 1087  $[\text{M} + \text{H}]^+$ , 630  $[\text{M} + \text{H} - \text{L}]^+$ , 629  $[\text{M} - \text{L}]^+$ , 458  $[\text{L} + \text{H}]^+$ , 273  $[\text{L} + \text{PPh}_2]^+$ , 385  $[(\text{PPh}_2)_2\text{CH} + \text{H}]^+$ , ( $\text{L} = (\text{Ph}_2\text{P})_2\text{CHCH}_2\text{NH}(\text{CH}_2)_2\text{OH}$ ). Selected  $^1\text{H}$  NMR (400 MHz,  $\text{CDCl}_3$ ):  $\delta$  5.47 (p,  $J = 6.6$  Hz, 2H,  $\text{P}_2\text{CHCH}_2$ ), 3.46 (t,  $J = 5.1$  Hz, 4H,  $\text{HNCH}_2\text{CH}_2\text{OH}$ ), 3.08 (q,  $J = 5.7$  Hz, 4H,  $\text{P}_2\text{CHCH}_2$ ), 2.63 – 2.57 (m, 4H,  $\text{HNCH}_2\text{CH}_2\text{OH}$ ).  $^{31}\text{P}\{^1\text{H}\}$  NMR (162 MHz,  $\text{CDCl}_3$ ):  $\delta$  10.93 (s). Selected  $^{13}\text{C}\{^1\text{H}\}$  NMR (126 MHz,  $\text{CDCl}_3$ ): 131.09 (s, *p*-Ph), 127.78 (s, *m*-Ph,  $\text{NHCH}_2\text{CH}_2\text{PPh}_2$ ).

#### 6.5.1.9 Synthesis of $[\text{RuCl}_2\{(\text{Ph}_2\text{P})_2\text{CHCH}_2\text{NH}(\text{CH}_2)_2\text{NH}(\text{CH}_2)_3\text{Si}(\text{OMe})_3\}_2]$ ([Ru]-5.9)

N-[3-(trimethoxysilyl)propyl]ethane-1,2-diamine (2.0 mL, 9.25 mmol) was added under a nitrogen flow to a suspension of [Ru]-5.1 (0.2 g, 0.2 mmol) in toluene (10 mL). The orange-red mixture was left to stir overnight and the colour changed to

yellow. The solvent was removed under reduced pressure to give a yellow oil. Hexane (10 mL) was added to triturate the oil, but no precipitate was formed. Other solvents like pentane, Et<sub>2</sub>O, MeOH and EtOH were also used to attempt to crystallise the oily product but no crystal was formed. The solvent was removed under reduced pressure and the product was analysed as an oil. ESI-MS: *m/z* calc. 1087 [M + H]<sup>+</sup>, 544 [M + 2H]<sup>2+</sup>. <sup>1</sup>H NMR (400 MHz, CDCl<sub>3</sub>): δ 7.62 (m, 7H, **Ph**), 7.48 (m, 7H, **Ph**), 7.09 (m, 16H, **Ph**), 5.44 (m, 2H, *PCHCH*<sub>2</sub>), 3.52 (s, 18H, *Si(OCH*<sub>3</sub>*)*<sub>3</sub>), 3.04 (s, br, 4H, *PCHCH*<sub>2</sub>), 2.53 (s, 8H, *HNCH*<sub>2</sub>*CH*<sub>2</sub>), 2.46 (m, 4H, *CH*<sub>2</sub>*CH*<sub>2</sub>*CH*<sub>2</sub>*Si*), 1.45 (m, 4H, *CH*<sub>2</sub>*CH*<sub>2</sub>*CH*<sub>2</sub>*Si*), 0.56 (s, 4H, *CH*<sub>2</sub>*CH*<sub>2</sub>*CH*<sub>2</sub>*Si*). <sup>31</sup>P{<sup>1</sup>H} NMR (162 MHz, CDCl<sub>3</sub>): δ 11.64 (s).

## 6.6 Appendix

### 6.6.1 Chapter 2 Crystallographic data

#### 6.6.1.1 Crystallographic data of *cis*-[Ru]-2.1

**Table 6.5:** Crystallographic data of *cis*-[Ru]-2.1

Identification code	dw2001d
Empirical formula	C <sub>72</sub> H <sub>82</sub> Cl <sub>2</sub> N <sub>2</sub> O <sub>6</sub> P <sub>4</sub> RuSi <sub>2</sub>
Formula weight	1423.42
Temperature/K	293(2)
Crystal system	monoclinic
Space group	P2 <sub>1</sub> /n
a/Å	17.7295(8)
b/Å	11.3722(4)
c/Å	34.9258(9)
α/°	90
β/°	91.185(3)
γ/°	90
Volume/Å <sup>3</sup>	7040.4(4)
Z	4
ρ <sub>calc</sub> /g/cm <sup>3</sup>	1.343
μ/mm <sup>-1</sup>	0.476
F(000)	2968.0
Crystal size/mm <sup>3</sup>	0.558 × 0.177 × 0.057
Radiation	MoKα (λ = 0.71073)
2θ range for data collection/°	6.618 to 59.68
Index ranges	-24 ≤ h ≤ 24, -15 ≤ k ≤ 15, -47 ≤ l ≤ 48
Reflections collected	76621
Independent reflections	17781 [R <sub>int</sub> = 0.0964, R <sub>sigma</sub> = 0.1365]
Data/restraints/parameters	17781/201/778
Goodness-of-fit on F <sup>2</sup>	1.016
Final R indexes [I ≥ 2σ (I)]	R <sub>1</sub> = 0.0924, wR <sub>2</sub> = 0.2524
Final R indexes [all data]	R <sub>1</sub> = 0.2140, wR <sub>2</sub> = 0.3319
Largest diff. peak/hole / e Å <sup>-3</sup>	1.29/-1.38

### 6.6.1.2 Crystallographic data of dinuclear complex [Ru]-2.2

**Table 6.6:** Crystallographic data of dinuclear complex [Ru]-2.2

Identification code	SFJ27A (8)
Empirical formula	C <sub>41</sub> H <sub>51</sub> Cl <sub>7</sub> NO <sub>3</sub> P <sub>2</sub> Ru <sub>2</sub> Si
Formula weight	1146.14
Temperature/K	100(2)
Crystal system	triclinic
Space group	P-1
a/Å	10.9396(8)
b/Å	12.0869(9)
c/Å	18.7440(14)
$\alpha$ /°	79.743(4)
$\beta$ /°	82.674(4)
$\gamma$ /°	74.279(4)
Volume/Å <sup>3</sup>	2339.4(3)
Z	2
$\rho_{\text{calc}}$ /g/cm <sup>3</sup>	1.627
$\mu$ /mm <sup>-1</sup>	1.178
F(000)	1158.0
Crystal size/mm <sup>3</sup>	0.608 × 0.275 × 0.218
Radiation	MoK $\alpha$ ( $\lambda$ = 0.71073)
2 $\theta$ range for data collection/°	3.54 to 55.88
Index ranges	-14 ≤ h ≤ 14, -15 ≤ k ≤ 15, -24 ≤ l ≤ 24
Reflections collected	42849
Independent reflections	11128 [ $R_{\text{int}}$ = 0.0334, $R_{\text{sigma}}$ = 0.0309]
Data/restraints/parameters	11128/448/647
Goodness-of-fit on F <sup>2</sup>	1.112
Final R indexes [ $I \geq 2\sigma(I)$ ]	$R_1$ = 0.0435, $wR_2$ = 0.0957
Final R indexes [all data]	$R_1$ = 0.0513, $wR_2$ = 0.0990
Largest diff. peak/hole / e Å <sup>-3</sup>	1.61/-1.41

## 6.6.2 Chapter 5 Crystallographic data

### 6.6.2.1 Crystallographic data of *trans*-[Ru]-5.3

**Table 6.7:** Crystallographic data of *trans*-[Ru]-5.3

Identification code	fs1902c_1 (2)
Empirical formula	C <sub>63</sub> H <sub>66</sub> Cl <sub>2</sub> N <sub>4</sub> P <sub>4</sub> Ru
Formula weight	1175.04
Temperature/K	200(2)
Crystal system	triclinic
Space group	P-1
a/Å	10.4353(3)
b/Å	16.5511(6)
c/Å	17.3827(6)
α/°	85.285(3)
β/°	86.600(2)
γ/°	77.255(3)
Volume/Å <sup>3</sup>	2915.77(17)
Z	2
ρ <sub>calc</sub> /cm <sup>3</sup>	1.338
μ/mm <sup>-1</sup>	0.513
F(000)	1220.0
Crystal size/mm <sup>3</sup>	0.277 × 0.237 × 0.033
Radiation	MoKα (λ = 0.71073)
2θ range for data collection/°	2.352 to 59.722
Index ranges	-13 ≤ h ≤ 12, -20 ≤ k ≤ 21, -22 ≤ l ≤ 20
Reflections collected	25358
Independent reflections	13851 [R <sub>int</sub> = 0.0386, R <sub>sigma</sub> = 0.0822]
Data/restraints/parameters	13851/461/756
Goodness-of-fit on F <sup>2</sup>	1.049
Final R indexes [I ≥ 2σ (I)]	R <sub>1</sub> = 0.0663, wR <sub>2</sub> = 0.1590
Final R indexes [all data]	R <sub>1</sub> = 0.1177, wR <sub>2</sub> = 0.1980

### 6.6.2.2 Crystallographic data of *trans*-[Ru]-5.5

**Table 6.8:** Crystallographic data of *trans*-[Ru]-5.5

Identification code	SFJ51
Empirical formula	C <sub>70</sub> H <sub>90</sub> Cl <sub>2</sub> N <sub>2</sub> O <sub>6</sub> P <sub>4</sub> RuSi <sub>2</sub>
Formula weight	1407.46
Temperature/K	100
Crystal system	monoclinic
Space group	P2 <sub>1</sub> /c
a/Å	13.1386(3)
b/Å	10.9694(3)
c/Å	23.2017(6)
α/°	90
β/°	92.5001(15)
γ/°	90
Volume/Å <sup>3</sup>	3340.71(15)
Z	2
ρ <sub>calc</sub> /cm <sup>3</sup>	1.399
μ/mm <sup>-1</sup>	0.500
F(000)	1476.0
Crystal size/mm <sup>3</sup>	0.499 × 0.419 × 0.204
Radiation	MoKα (λ = 0.71073)
2θ range for data collection/°	3.102 to 60.228
Index ranges	-18 ≤ h ≤ 18, -15 ≤ k ≤ 15, -32 ≤ l ≤ 32
Reflections collected	73176
Independent reflections	9837 [R <sub>int</sub> = 0.0382, R <sub>sigma</sub> = 0.0223]
Data/restraints/parameters	9837/2/406
Goodness-of-fit on F <sup>2</sup>	1.036
Final R indexes [I ≥ 2σ (I)]	R <sub>1</sub> = 0.0289, wR <sub>2</sub> = 0.0653
Final R indexes [all data]	R <sub>1</sub> = 0.0371, wR <sub>2</sub> = 0.0687
Largest diff. peak/hole / e Å <sup>-3</sup>	0.85/-0.43

### 6.6.2.3 Crystallographic data of trans-[Ru]-5.6

**Table 6.9:** Crystallographic data of *trans*-[Ru]-5.6

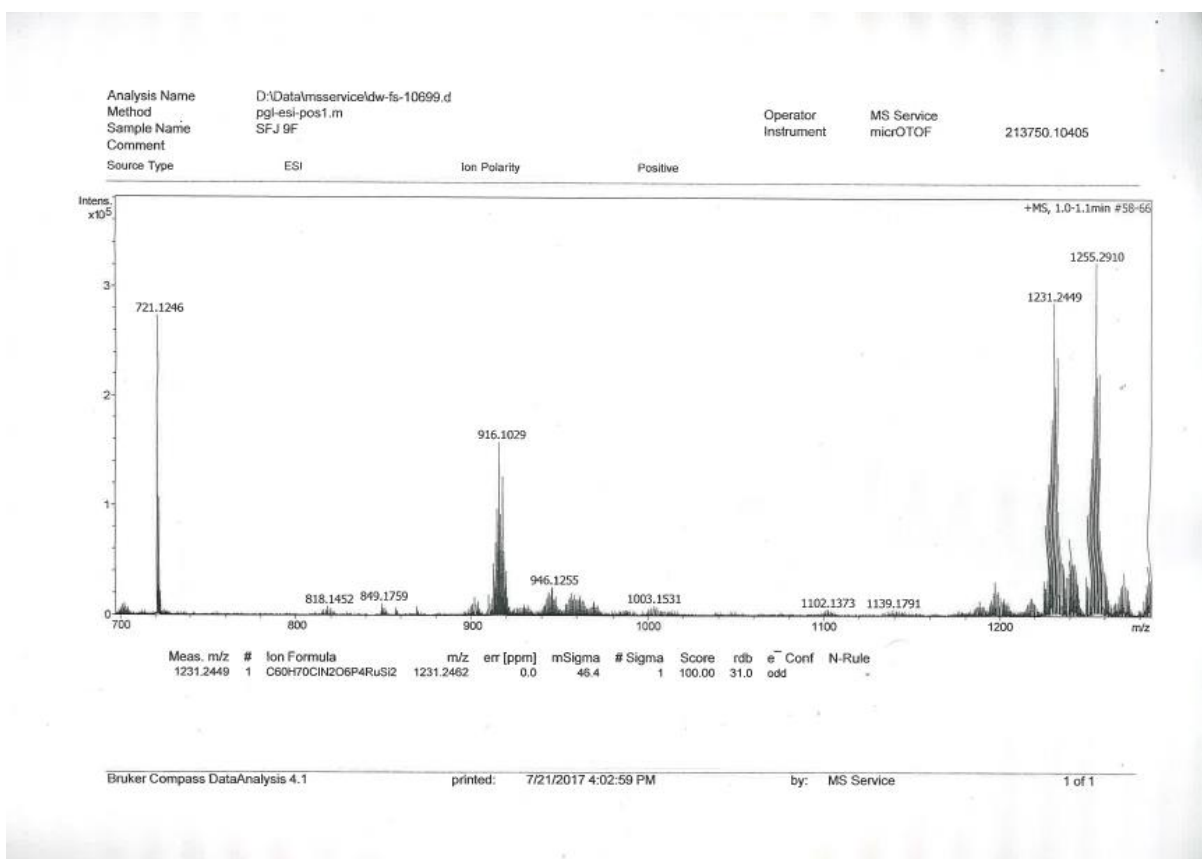
Identification code	SFJ50
Empirical formula	C <sub>74.03</sub> H <sub>73.39</sub> Cl <sub>2</sub> F <sub>0.84</sub> N <sub>2</sub> P <sub>4</sub> Ru
Formula weight	1302.90
Temperature/K	100(2)
Crystal system	triclinic
Space group	P-1
a/Å	10.3517(3)
b/Å	11.7890(3)
c/Å	14.7461(4)
α/°	86.830(2)
β/°	82.892(2)
γ/°	66.874(2)
Volume/Å <sup>3</sup>	1642.19(8)
Z	1
ρ <sub>calc</sub> /g/cm <sup>3</sup>	1.317
μ/mm <sup>-1</sup>	0.464
F(000)	677.0
Crystal size/mm <sup>3</sup>	0.277 × 0.179 × 0.168
Radiation	MoKα (λ = 0.71073)
2θ range for data collection/°	3.756 to 52.734
Index ranges	-12 ≤ h ≤ 12, -14 ≤ k ≤ 14, -18 ≤ l ≤ 18
Reflections collected	27125
Independent reflections	6706 [R <sub>int</sub> = 0.0738, R <sub>sigma</sub> = 0.0666]
Data/restraints/parameters	6706/339/476
Goodness-of-fit on F <sup>2</sup>	1.003
Final R indexes [I ≥ 2σ (I)]	R <sub>1</sub> = 0.0452, wR <sub>2</sub> = 0.1082
Final R indexes [all data]	R <sub>1</sub> = 0.0668, wR <sub>2</sub> = 0.1190
Largest diff. peak/hole / e Å <sup>-3</sup>	0.79/-0.83

#### 6.6.2.4 Crystallographic data of trans-[Ru]-5.8

**Table 6.10:** Crystallographic data of *trans*-[Ru]-5.8

Identification code	dw1903d_1
Empirical formula	C <sub>58.5</sub> H <sub>63</sub> Cl <sub>7</sub> N <sub>2</sub> O <sub>2</sub> P <sub>4</sub> Ru
Formula weight	1299.21
Temperature/K	200(2)
Crystal system	triclinic
Space group	P-1
a/Å	10.6436(3)
b/Å	11.7714(3)
c/Å	24.4707(8)
α/°	82.484(3)
β/°	88.161(3)
γ/°	75.155(3)
Volume/Å <sup>3</sup>	2938.14(15)
Z	2
ρ <sub>calc</sub> /cm <sup>3</sup>	1.469
μ/mm <sup>-1</sup>	0.738
F(000)	1334.0
Crystal size/mm <sup>3</sup>	0.380 × 0.120 × 0.056
Radiation	MoKα (λ = 0.71073)
2θ range for data collection/°	1.678 to 59.44
Index ranges	-12 ≤ h ≤ 14, -15 ≤ k ≤ 16, -28 ≤ l ≤ 33
Reflections collected	27259
Independent reflections	13872 [R <sub>int</sub> = 0.0291, R <sub>sigma</sub> = 0.0544]
Data/restraints/parameters	13872/21/686
Goodness-of-fit on F <sup>2</sup>	1.057
Final R indexes [I ≥ 2σ (I)]	R <sub>1</sub> = 0.0532, wR <sub>2</sub> = 0.1168
Final R indexes [all data]	R <sub>1</sub> = 0.0747, wR <sub>2</sub> = 0.1284
Largest diff. peak/hole / e Å <sup>-3</sup>	1.17/-1.11

### 6.6.3 Mass Spectrum of [Ru]-2.1



## 6.7 References

1. R. L. Wingad, E. J. E. Bergstrom, M. Everett, K. J. Pellow and D. F. Wass, *Chem. Commun.*, 2016, **52**, 5202-5204.
2. R. L. Wingad, P. J. Gates, S. T. G. Street and D. F. Wass, *ACS Catal.*, 2015, **5**, 5822-5826.
3. G. R. M. Dowson, M. F. Haddow, J. Lee, R. L. Wingad and D. F. Wass, *Angew. Chem. Int. Ed.*, 2013, **52**, 9005-9008.
4. R. L. Grob and M. A. Kaiser, in *Modern Practice of Gas Chromatography*, ed. Robert L. Grob and Eugene. F. Barry, Wiley Online Library, Hoboken, New Jersey, 4<sup>th</sup> edn, 2004, vol. 2, ch. 8, pp. 449-450.
5. K. J. Pellow, PhD Thesis, University of Bristol, 2018.
6. P. Braunstein, H. P. Kormann, W. Meyer-Zaika, R. Pugin and G. Schmid, *Chem. Eur. J.*, 2000, **6**, 4637-4646.
7. A. P. Shaw, B. L. Ryland, J. R. Norton, D. Buccella and A. Moscatelli, *Inorg. Chem.*, 2007, **46**, 5805-5812.
8. L. A. Ortiz-Frade, L. Ruiz-Ramírez, I. González, A. Marín-Becerra, M. Alcarazo, J. G. Alvarado-Rodriguez and R. Moreno-Esparza, *Inorg. Chem.*, 2003, **42**, 1825-1834.
9. R. Mitra, S. Das, S. V. Shinde, S. Sinha, K. Somasundaram and A. G. Samuelson, *Chem. Eur. J.*, 2012, **18**, 12278-12291.
10. M. A. Bennett and A. K. Smith, *J. Chem. Soc., Dalton Trans.*, 1974, 233-241.
11. G. T. Giuffredi, S. Purser, M. Sawicki, A. L. Thompson and V. Gouverneur, *Tetrahedron: Asymmetry*, 2009, **20**, 910-920.
12. R. Sáez, J. Lorenzo, M. J. Prieto, M. Font-Bardia, T. Calvet, N. Omeñaca, M. Vilaseca and V. Moreno, *J. Inorg. Biochem.*, 2014, **136**, 1-12.
13. M. Aydemir, A. Baysal, S. Özkar and L. T. Yildirim, *Inorg. Chim. Acta*, 2011, **367**, 166-172.
14. I. Warad, *Molecules*, 2010, **15**, 4652-4669.
15. J. J. Calvin, M. Asplund, Y. Zhang, B. Huang and B. F. Woodfield, *J. Chem. Thermodyn.*, 2017, **112**, 77-85.
16. K. M. S. Khalil, *J. Colloid Interface Sci.*, 2007, **307**, 172-180.
17. S. Brunauer, P. H. Emmett and E. Teller, *J. Am. Chem. Soc.*, 1938, **60**, 309-319.
18. E. P. Barrett, L. G. Joyner and P. P. Halenda, *J. Am. Chem. Soc.*, 1951, **73**, 373-380.
19. K. S. Sing, *Pure Appl. Chem.*, 1985, **57**, 603-619.
20. S. J. Higgins, M. K. McCart, M. McElhinney, D. C. Nugent and T. J. Pounds, *J. Chem. Soc., Chem. Commun.*, 1995, 2129-2130.
21. S. J. Higgins and H. L. Jones, *Chem. Commun.*, 1997, 1907-1908.
22. J. V. Barkley, S. J. Higgins, M. K. McCart and T. J. Pounds, *Inorg. Chem.*, 1997, **36**, 6188-6196.